# AN INVESTIGATION INTO CURRENT AND VIBRATION SIGNATURES OF THREE PHASE INDUCTION MOTORS

RMDAN ABDUSSALM ASHNIBHA

A thesis submitted in partial fulfilment of the requirements of the Manchester Metropolitan University for the degree of Doctor of Philosophy

School of Engineering, Manchester Metropolitan University

September 2012

**Abstract**

This research aimed at investigating the relationship between three phase induction motors vibration (MVS) and current signatures (MCS). This is essential due to the cost of vibration measuring equipment and in cases where vibration of interest point is not accessible; such as electrical submersible pumps (ESP) used in oil industry.

A mathematical model was developed to understand the effects of two types of induction motors common faults; rotor bar imperfections and phase imbalance on the motor vibration and current signatures.

An automated test facility was developed in which 1.1 kW three phase motor could be tested under varying shaft rotation speeds and loads for validating the developed model. Time and frequency domains statistical parameters of the measured signals were calculated for fault detection and assessing its severity. The measured signals were also processed using the short time Fourier transform (STFT), the Wigner-Ville distribution (WVD), the continuous wavelet transform (CWT) and discrete wavelet transform (DWT) and wavelet multi-resolution analysis (MRA).

The non-stationary components, representing faults within induction motor measured vibration and current signals, were successfully detected using wavelet decomposition technique.

An effective alternative to direct vibration measurement scheme, based on radial basis function networks, was developed to the reconstruction of motor vibration using measurements of one phase of the motor current. It was found that this method captured the features of induction motor faults with reasonable degrees of accuracy.

Another method was also developed for the early detection and diagnosis of faults using an enhanced power factor method. Experimental results confirmed that the power factor can be used successfully for induction motor fault diagnosis and is also promising in assessing fault severity.

The suggested two methods offer inexpensive, reliable and non-intrusive condition monitoring tools that suits real-time applications. Directions for further work were also outlined.

**Declaration**

---

No section of the work referred to in this thesis has been submitted for use of any another degree or qualification of this university or any other institute of learning.

Signature: _____

**Acknowledgements**

---

It would not have been possible to write this doctoral thesis without the help and support of the generous people around me, of which only certain individuals have been given a distinctive mention here.

I give my sincere thanks to my wonderful supervisor Dr. Alhussein Albarbar who accepted me as his PhD student without any hesitation when I presented my research proposal. Throughout my research, he offered me an abundance of advice, as well as patiently supervising me, and guiding me in the right direction. I have learned a vast amount of knowledge thanks to his support, and without him I could not have completed my dissertation successfully.

I would also like to thank all my friends, particularly Abdelnasser, Ghalib and Emad for the encouragement and assistance they gave me to complete my work.

Finally, I would like to dedicate this to my family for all their love and support, and providing me with the motivation to achieve. Special thanks to my wife and children for their care, patience and inspiration during my project.

**Table of Content**

**Table of Figures**

**Table of Tables**

**Nomenclature**

| | |
|---|---|
| T | Torque |
| *I* | Motor current |
| Ψ | magnetic flux |
| FFT | Fast Fourier Transform |
| *f1* | the electrical power supply frequency |
| *Nr* | rotational speed |
| S | slip frequency Hz |
| CM | Condition monitoring |
| MCSA | Motor Current Signature analysis |
| RMS | Root Mean Square |
| DFT | Discrete Fourier Transform |
| STFT | Short Time Fourier Transform |
| WVD | Wigner-Ville Distribution |
| WT | Wavelet Transform |
| ANNS | Artificial neural networks |
| ESP | Electrical submersible pumps |
| MCS | motor current signature |
| MVS | motor vibration signature |
| RBF | radial basis function |
| IM | Induction motor |
| PW | power factor |
| CBM | Condition Based Maintenance |
| AE | acoustic emission |
| NN | neural network |
| AC | alternating current |
| FEM | finite element model |
| DWT | discrete wavelet transform |
| CWT | continuous wavelet transform |
| PSD | Power Spectral Density |
| AI | Artificial Intelligent |
| BPNN | Back Propagation neural network |
| SOM | Self-Organizing Map |
| MLP | multi-layer perceptron |

| | |
|---|---|
| $J_m$ | moment of inertia of the motor |
| $J_L$ | moment of inertia of the load |
| $T_{em}$ | electromechanical torque |
| $\ddot{\theta_\iota}, \dot{\theta_\iota}\ \theta$ | angular acceleration, velocity and displacement, respectively |
| $T_L$ | torque due to the load |
| $\psi^s$ | flux linkage |
| $X^s$ | Reactances |
| $\omega_b$ | angular frequency |
| *frated* | rated frequency of the machine in Hertz |
| $P$ | number of pair-poles |
| $V_{rated}$ | Voltage rated |
| $P_{rated}$ | Power rated |
| $\omega_{bm}$ | base mechanical frequency |
| dq0 | direct-quadrature-zero axes |
| $\omega$ | an angular speed rad/s |
| $v$ | phase voltage |
| $V_{as}$, $V_{bs}$,$V_{cs}$ | three-phase balanced symmetrical voltages applied to the stator terminals |
| $V_{ar}$, $V_{br}$,$V_{cr}$ | three-phase balanced symmetrical voltages applied to the rotor terminals |
| $v'_{rn}$ | voltage between points r and n |
| E | unbalanced voltage drop |
| M | Mass |
| $M_0$ | unbalanced eccentric mass |
| R | radial distance |
| $F_f$ | centrifugal force |
| $f_{r1}, f_{r2}$ | Frequencies of rotation of motor shaft and loader shaft respectively. |
| $f_0$ | is the frequency (Hz) of the current |
| $\varphi$ | the phase angle |
| $I_0$ | RMS amplitude of the current (A) |
| $f_{rn}$ | nth modulating frequency (Hz) |
| $m_{rn}$ | nth modulation index |
| $B_s$ | amplitude of the modulating signal |
| $N$ | $n^{th}$ harmonic |
| K | number of rotating shafts |
| $m_{r1}$ $m_{r2}$ $m_{r3}$ | modulation indices |
| $Ft$ | tangential transmitted force |

| | |
|---|---|
| $V_m$ | Peak supply voltage (volt) |
| $i_s(t)$ | Where = total current (A) |
| $i_0(t)$ | magnetization current(A) |
| $i(t)$ | stator current producing the torque (A) |
| Z | magnetising impedance (Ω) |
| *Fc* | oscillation frequency |
| *B* | magnetic flux density (in Tesla, T) |
| *A* | cross-sectional area ($m^2$) of the poles |
| *M* | permeability of the medium between the poles |
| *F* | force (in Newton) experienced by between two magnetic poles |
| IAS | instantaneous angular speed |
| DAQ | data acquisition |
| LSB | least significant bit |
| GUI | Graphical User Interface |
| CF | Crest Factor |
| K | Kurtosis |
| *N* | number of samples |
| *x(n)* | amplitude of the nth sample |
| $X_{pp}$ | peak-to-peak value of the signal |
| S/N | signal to noise ratio |
| MRA | multi-resolution analysis |
| *x(t)* | main signal |
| *w(t)* | window function |
| $x_w(t)$ | windowed signal |
| R(τ) | auto-correlation function |
| $\Psi(t)$ | mother wavelet |
| B | translation factor |
| A | dilation factor |
| $\Psi_{ab}(t)$ | the daughter wavelet |
| Ø[n] | scale function |
| $a_{j0,k}$ | coefficients of approximation at scale s= 2j0 |
| $a_{j,k}$ | coefficients of approximation at scale s= 2j |
| *Pxy* | cross power spectral density |
| *Cx(a,b), Cy(a,b)* | continuous wavelet transforms of *x* and *y* |
| *UMP* | unbalanced magnetic pull |

| | |
|---|---|
| *VAR* | *Reactive Power* |
| *AV* | *Apparent Power* |
| *W* | *Real Power* |

**List of publications:**

1. **R. Shnibha, G. Ibahim**, **A. Albarbar, A. Abouhnik** (2012), *A More Reliable Method for Monitoring the Condition of Three-Phase Induction Motors Based on Their Vibrations* ISRN Mechanical Engineering Volume 2012 (2012), Article ID 230314, 9 pages doi:10.5402/2012/230314
2. **R. Shnibha, A. Albarbar** (2012) *Smart Technique for Induction Motor Diagnosis by Monitoring the Power Factor Using Only the Measured Current* Journal of Physics: Conf. Ser. 364 012062
3. **A. Abouhnik, G. Ibrahim, R. Shnibha, A. Albarbar,** (2012), *Novel Approach to Rotating Machinery Diagnostics Based on Principal Component and Residual Matrix Analysis*, ISRN Mechanical Engineering, doi:10.5402/2012/715893.
4. **A. Abouhnik, Ghalib R. Ibrahim, R. Shnibha, A. Albarbar.** *Wind Turbine Blade Fault Detection Using the Empirical Mode Decomposition Method; Numerical Simulation And Experimental Testing*, The Third International Renewable Energy Congress, Hammamet, Tunisia. 498- 503, 2011.
5. **R. Shnibha, A. Albarbar, J. Gu,** *A Step Towards 3-Phase Induction Machines Intelligent Diagnostic Systems*. COMADEM, Stavenger, Norway. 2011.
6. **R. Shnibha**, **A. Albarbar**, **G R. Ibrahim**, **A. Badri**. *Three Phase Induction Motors: Phase Imbalance Severity Evaluation Based on Acoustic Measurements and Energy Calculations*, The Libyan Arab International Conference on Electrical and Electronic Engineering LAICEEE, Tripoli/Libya, 2010, pp. 32-37.

7. **R. Shnibha** and **A. Albarbar.** *Induction Motor Condition Monitoring Based on Acoustic Measurements and Energy Calculation.* In First Faculty of Science and Engineering Research and Development Day at Manchester Metropolitan University, Manchester, 2010.
8. **R. Shnibha** and **A. Albarbar.** *Petroleum Pumps Monitoring Based on Wavelet Coherence Analysis of Driver's Current and Vibration Signatures.* In Second Faculty of Science and Engineering Research and Development Day at Manchester Metropolitan University, Manchester, 2011.

# CHAPTER 1

# INTRODUCTION

*This chapter describes the main purposes of maintenance strategies. It also introduces condition monitoring and describes the different types of condition monitoring systems and techniques. The basics of signal modulation and aspects of statistical processing are presented in this chapter. Finally, the research aims and objectives are given, as is a description of the thesis structure.*

## 1.1 Background

Machine condition monitoring (CM) plays a vital task in guaranteeing both the reliability and low-cost operation of industrial facilities [1]. CM permits detection of machine faults at an early stage and offers the opportunity for appropriate action to be taken before the fault causes secondary damage and, possibly, a disastrous accident. In addition, CM permits a machine to be controlled and monitored during its operation and repaired according to a planned schedule which will give economical operation and decrease possible production losses. As a result, many technologies and techniques have been studied and applied to improve the reliability, applicability, and accuracy of CM systems[1, 2] .

These days, run-to-failure is an unwanted approach for most processes and manufacturing operations. Alternative CM systems that depend on the continuous collection and analysis of machine data have proved more acceptable and desirable because of their capability to offer early stage detection of machinery faults [2]. Selecting a suitable CM system is a significant part of guaranteeing increased machine availability, performance and life span, in addition to a reduction of spare parts stocks and break-down maintenance [3].

## 1.2 Maintenance Strategies and Condition Based Maintenance of Electrical Machines

Companies search continuously to find the best methods to reduce maintenance costs mitigate possible injuries to personnel or damage to the local environment. However, the main objective of maintenance is to prevent machine and/or production failure and production losses. Maintenance strategies can be divided into three different categories:

- *Breakdown maintenance***:** Machines are run until they fail, and are then repaired; a crude method of operation that can be very expensive in terms of lost output and machine damage, it may also lead to dangerous occurrences[4].
- *Preventive maintenance*: Also called time-based maintenance, machines are thoroughly inspected and tested at set intervals and any necessary maintenance carried out to remedy faults present within the system[5] .
- *Predictive maintenance*: This strategy requires continuous monitoring of equipment to detect and diagnose defects. Only when a defect is detected, is maintenance work planned and executed [1].

The main objectives for maintenance can be summarised as follows [1]

- To improve/maintain productivity.
- To minimize the number of repairs and replacement routines.
- To extend the life of the machine.
- To ensure a high quality of products.

For maintenance, the plant equipment can be classified into three categories [1].

1. *Critical equipment*: expensive to repair, or takes a long time to repair.
2. *Essential equipment*: affects the next stage of the process.
3. *General equipment*: is not critical to the process and does not affect plant operations when it is broken.

Electrical machinery supports a vast range of economic activity in almost every industrial sector, with the majority of prime movers being electric motors. Electric motors as shown in Figure 1.1 are the most general drivers for industrial gearboxes, compressors, pumps, and machines. Many types of these motors are used in

commercial, industrial, and residential applications[6]. Nowadays, the leading motor technology is in induction motors, the majority of the installed motor capability world-wide, which consume between 40-50% of all the generated power in the world [7]. Moreover, the induction motor is simple device that consists of two basic electrical assemblies: the wound stator and the rotor assembly. The name of the induction motor is derived from the fact that currents do not directly flow in the secondary member (rotor), but are induced by the alternating currents flowing in the primary member (stator).

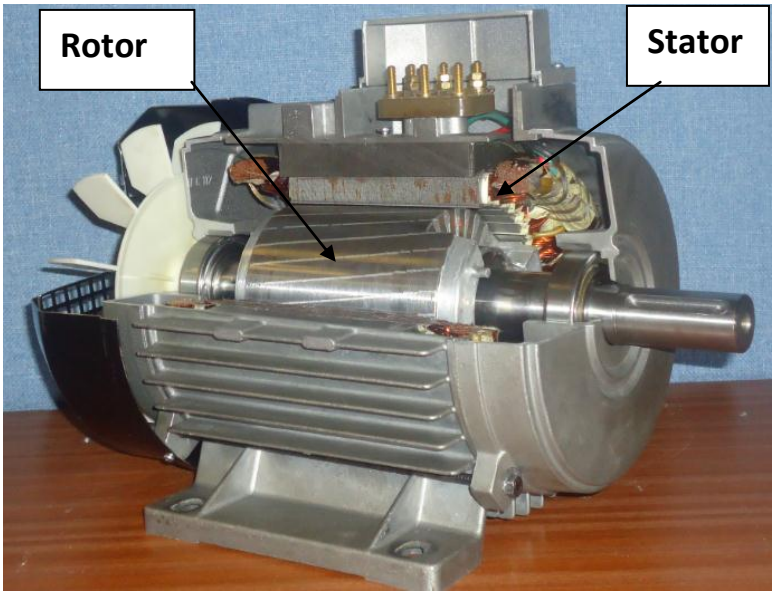


**Figure 1-1** typical small induction motor

Despite the economic importance of electrical machines relatively few operators apply CM to their electrical machinery even though the consequential damage due to the failure of electric motors can be considerable, particularly in terms of lost production. Electrical faults can be very simple and lead not only to inefficiencies but disastrous consequences, a loose electrical connection can cause overheating and a fire which can result in the destruction of an entire plant.

Electrical faults commonly develop to failure very rapidly. Thus too high a current (over current) or current leakage to earth, for example, are protected against using a trip, which is a form of detection but one which allows the system to fail to prevent permanent damage. These very simple techniques and alternative measures which act to prevent failure through strategies which modify machine or system operation are discussed below. Then more advanced techniques which diagnose faults in motors and systems are considered.

### 1.4 Induction Motor Failure Modes

The squirrel-cage induction motor is the most common motor in use in industry. The smallest typical motor will be about 0.5 kW and the biggest will be about 30 kW, but much larger motors can be found.

Amongst the factors that may lead to a fault are [8]:

1. eccentricity in rotor motion of the rotor will result in a variation in the air gap separating the stator and rotor, with a consequent large proportional change in the magnetic flux,
2. defects in the rotor cage due to poor assembly, cracks and/or gaps, variation in material properties, etc.,
3. excessive currents during starting,
4. excessive winding forces during starting, and
5. bracing problems with the stator end winding.

Additional faults which can be found in slip or wound motors are:

- defects in the rotor windings, brush gear and/or slip rings,
- motor resistances unbalanced, and
- excessive stress on the overhangs of the rotor windings.

Adverse operating conditions can also generate failure. For example, the load might itself be subject to an external oscillating force or may not be aligned correctly. Repeated and frequent starting of the motor will lead to winding and/or bearing failure. Excessive stress whether of mechanical or electromagnetic origin can lead to premature bearing failure, possibly the most common cause of failure with induction motors. Fluctuations in one or more of the phases of the voltage supply can cause stalling or even insulation failure. Adverse environmental conditions (high humidity, high temperature, corrosive contamination) can also cause insulation breakdown. Motor faults are usually classified into electrical, thermal or mechanical, see table 1.1

**Table 1-1** Examples of motor failures[9]

| | |
|---|---|
| **Mechanical** | Shock loads, Bearing failure, Misalignment ,Mechanical unbalance, Loss of lubricant |
| **Thermal** | Overload, Stall, Single phasing, Loss of coolant/inadequate cooling ,Harmonic heating |
| **Electrical** | Insulation breakdown due to: Contamination, Vibration/mechanical damage, Thermal cycling, Overvoltage Broken rotor bars/rotor windings due to: Overspeed, Frequent starts, Harmonic heating, Lamination damage |
| **Commutator, slip rings and brush gear (DC motors)** | Overheating, Contamination, Excessive sparking |

### 1.5 Condition Monitoring (Static Techniques)

Many simple CM techniques which do not require large expenditure or staff expertise are readily available. These include motor current measurement, temperature of the motor, electrical resistance of the winding, observation of the state

of the lubricating oil, all of which give useful information. These methods are described below [8]:

### 1.5.1 Motor Current

With an induction motor the stator coils produce a rotating magnetic field such that the torque, T, developed is proportional to the product of the motor current (I) and magnetic flux (ψ):

$$T \propto \psi . I \qquad (1.1)$$

The current can be measured directly but will usually be used to compare the currents in the three phases, which will identify problems in a specific phase. This is more usually performed as a comparative test between identical machines. While it can give immediate results it is more common to find the current recorded at regular intervals to mark any trend towards failure.

Normally the motor does not reduce its speed to less than about 95% of synchronous speed and for such a "constant speed" motor under constant load, a change in current may suggest the presence of a fault but is unlikely to indicate the cause of the fault. If the applied load is subject to change the signs of incipient failure will be lost in normal current variation.

### 1.5.2 Temperature Monitoring

Current flowing through the stator and rotor generates heat and many motors are cooled by a fan mounted on the drive shaft which blows ambient air across fins attached to the stator. Excess heat from the rotor is radiated and convected across the air gap to the stator, and conducted away through the motor housing and shaft. A significant reduction in motor speed will mean that heat is generated faster than it is

removed (the most extreme case is if the motor stalls) and the motor temperature rises rapidly activating temperature trips to avoid serious damage.

The temperature monitoring is not a sensitive monitoring mechanism and suffers from three obvious drawbacks: the local temperature will change during the course of a day and in some regions of the world this can be by more than $20^0$C; if the motor is subject to changing load then a corresponding change in temperature would be expected as part of the normal operation of the motor; the temperature is likely to be monitored at or near the surface while the source of the excessive heat may well be deep within the motor. Once a fault has developed then the rate of increase in temperature is likely to be rapid so that the monitoring system must sample at low frequency intervals.

In practice thermal imaging is the most widely used thermal monitoring system, though it is usually performed by a trained operative according to a set schedule rather than continuously. Thermal imaging has proved effective in diagnosing overheating due to many causes: loose connections, short circuits and bearing friction.

Motor brush and holder temperature are related to the degree of sparking so that it is desirable to keep the number of brushes to a minimum. Monitoring the temperature will give an indication when sparking is a problem and when the brushes should be changed.

### 1.5.3 Electrical Resistance

Low winding resistance is an indication of a short circuit due to leakage currents which leads to local high temperatures. The higher the temperature, the greater the extent and rapidity of further degradation in the insulation, and failure soon follows.

The electrical resistances of the stator windings are simple to measure but the resistance of the rotor windings, or between rotor and earth, can only be measured if the rotor is wound and connected to slip rings. Maximum information will be obtained only if all six winding connections are available.

During a direct start a motor will experience maximum current and this is why many if not most failures occur at start-up. Motors which are being started, especially in the morning, are likely to be significantly cooler than the surrounding air with the consequent likelihood of condensation. A combination of condensation and dirt from any source are the major cause of flashover. The flashover is the voltage at which an electric discharge occurs between two electrodes that are separated by an insulator; the value depends on whether the insulator surface is dry or wet, further enhanced if there is any terminal damage. Thus it is very sensible to test the motor prior to starting [8].

### 1.5.4 Lubrication Inspection

The bearings in an electric motor are designed to cope with the large loads they will experience, provided that adequate lubrication is supplied. Indeed, inadequate lubrication is a frequent cause of premature bearing failure. Most electric motors are not sufficiently large to have pressurised oil lubrication so spectrographic oil analysis and similar advanced techniques are not appropriate[8]. Instead shock pulse methods which monitor metal-to-metal impacts can be used to determine whether lubrication levels are sufficiently low as to need topping-up[8]

The presence of contaminants can seriously adversely affect the performance of insulation materials, so regular and effective cleaning of electrical machines is important. Similarly bearing life will be reduced if abrasive particles have entered.

Cleaning on a regular basis combined with a general inspection is a quick, relatively cheap and cost effective method that can uncover such faults as:

- Lubricant leakage (oil on floor),
- Excessive noise and vibration,
- Excessive temperatures (surfaces hot to the touch, smell of burning)
- Ambient conditions too hot, too wet, etc.,
- Loose (rattling) bolts.

### 1.6 Condition Monitoring (Dynamic Techniques)

Many techniques are available for the detection of faults in large electrical machines such as turbine generators.

Two techniques are worth describing in some detail because they are used commercially and in research. Both are applicable to a wide range of machinery and use similar technology [8].

#### 1.6.1 Motor Vibration Signature

Vibration monitoring is widely used for the detection and diagnosis of mechanical faults in rotating machinery. In electrical motors where main sources of vibration are:

- The stator core response to the attractive force developed between rotor and stator;
- The response of the stator end windings to electromagnetic force on the conductors;
- The dynamic behaviour of the rotor;
- The response of the shaft bearing to vibration transmitted from the rotor.

Because bearing failures account for more than half of all motor failures this last point is important[9]. The forces between stator and rotor will impact on the bearings

so any problems in or between the stator and rotor which generates excessive forces will increase the likelihood of bearing failure and reduce its working life. Because of their position and function the bearings are where the system forces will impact and so this is the best place to position vibration transducers. Ideally the transducers should be sited on the bearing housing, but with small motors this may not be possible and placing them on the end caps should suffice. Usually time-domain signals (typically root mean square (RMS) value) are used for trending. The vibration transducer (usually an accelerometer) is best fixed by screwing the sensor to a screw-threaded brass stud attaching to the casing by drilling and tapping or suitable super glue.

All machines vibrate so vibration itself is not a fault. However, excessive vibration can be a symptom of a developing fault and an early warning of machine failure. Bearings most often fail as a result of lengthy exposure to forces greater than those for which they were designed, or poor installation such as a mis-aligned drive shaft, or from inadequate lubrication. All these will generate excessive vibration which can be compared to a standard and taken as an indication of a developing problem. However, spectral analysis (based on the Fast Fourier Transform - FFT) of the signal is necessary for a more precise diagnosis. Table 1-2 shows characteristic fault features and associated symptomatic frequencies in the vibration spectra of rotating machines, where *f1* is the electrical power supply frequency, *Nr* is rotational speed and s is the slip frequency in Hz [10].

Figure 1-2 shows time- and frequency-domain vibration signals obtained from an induction motor using an accelerometer

**Table 1-2** Characteristic Fault Features in Vibration Spectra [10]

| **Fault Condition** | **Symptomatic Frequencies (in Hz) in Vibration** | **Notes** |
|---|---|---|
| Stator Electrical Asymmetry | 2×*f1* | Fault may be caused by a stator winding problem or weakness of stator winding support. |
| Rotor Electrical Asymmetry | 1×*Nr* with 2×*s* sidebands | Fault may be caused by cracked or broken rotor bars, or shorted rotor laminations. |
| Mechanical Imbalance | 1×*Nr* | The change in the frequency component is usually most dominant in the radial direction. |
| Bent Shaft or Misalignment (Angular or Parallel) | 1×*Nr* and 2×*Nr* | A high 2×*Nr* component can be expected if the problem is severe and the system is sufficiently mobile. |
| Mechanical Looseness | 1×*Nr* and 2×*Nr* | Higher harmonics and also inter-harmonics of 1×Nr may also be caused by signal truncation. |
| Bearing Defects | Impact Excitation Resonance (IER) | Indication of the fault occurs in the high frequency range |

With electrical motors, information useful for the diagnosis of faults is found in the form of sidebands either side of the power supply frequency ($f_1 \pm s$) so the frequency analysis must be performed to a high degree of precision. Motors also generate vibrations at frequencies related to the rotor slot passing frequency and its harmonics, the number of poles and the slip frequency.

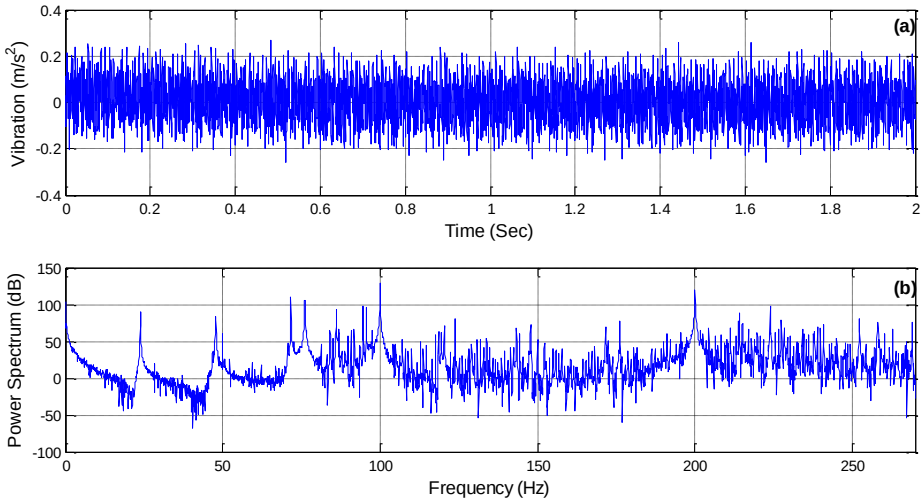


**Figure 1-2** Time- and frequency-domain vibration signals from an induction motor using an accelerometer as transducer (a) time domain (b) frequency domain

### 1.6.2 Motor Current Signature Analysis (MCSA)

The current through the stator can be used to identify variations in the magnetic flux[8]. These variations in supply current are measurable at any suitable point, even some distance away from the motor, e.g. in a control cubicle, and this is the main advantage of MCSA. Because MCSA can monitor the motor from a remote point then problems of access due to hazardous environments or where non-intrusive techniques are required, it has proved a very useful CM technique. MCSA is relatively inexpensive, can monitor the efficiency of motors and improve their reliability by providing on-line diagnostics for critical equipment. Spectral analysis can be an integral part of this method. Figure 1-3 shows time- and frequency-domain current signals obtained from an induction motor using MCSA.

Advantages that can be gained from applying the MCSA analysis compared to other CM techniques have been summarized as [8]:

- Economic, reliable and easy to use,

- Non-intrusive monitoring capability at a location remote from the equipment and, can be used in hostile environments,
- Rapid measurement can be performed as frequently as desired by relatively unskilled personnel,
- Motor current spectrum is not affected by current transducer or probe location,
- Improved plant management and saving of money and staff time,
- Can be used in places where conventional methods are inapplicable such as deep wells in the oil industry,
- No risk involved in data collection, hence safety improved,
- Increased machine availability, reduced down time,
- Maintenance man-hours saved, and
- Improved ability to manage and plan maintenance.

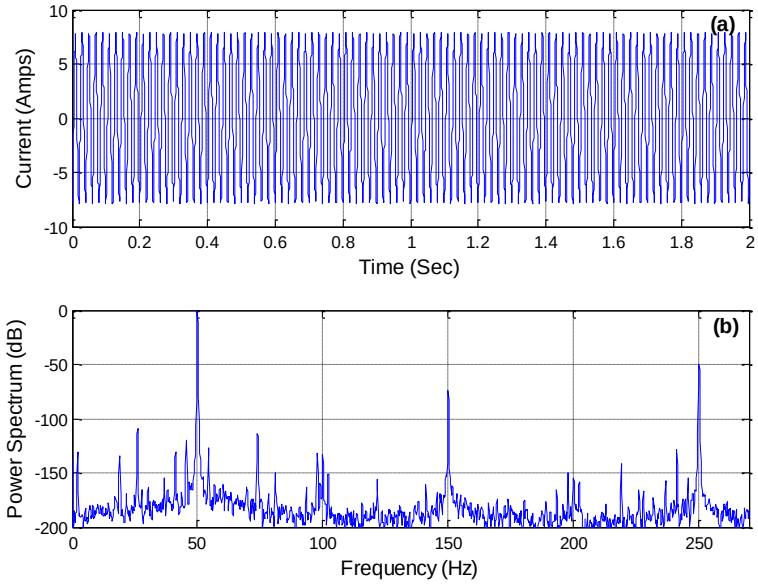


**Figure 1-3** shows time- and frequency-domain current signals obtained from an induction motor using MCSA (a) time domain (b) frequency domain

## 1.7 Data Processing

### 1.7.1 Time-Domain

Time-domain digital data records of transducer signals consist of individual values representing the energy content of the signal when the samples were taken. With more sophisticated digital systems the sampling rate will vary, increasing with increasing frequency content of the signal, but it is still more common today to sample at a fixed rate. With analogue measurement, time-domain signals are continuous. Statistical measures used in industry to represent the time-domain signal are usually the RMS value, and occasionally the maximum amplitude and mean value. Industry values simplicity and thus tends to use single-value assessments of the time-domain signal which can be easily compared with accepted standards. For vibration signals from electric motors the RMS vibration value is by far the most common such measure and is used for trending, with action being required when prescribed levels are reached [10]. However, the setting of trending criteria is not

simple since the differences between individual motors may exceed - in some cases - the difference between a healthy and a faulty motor.

The time-domain signal data is often very sensitive to small changes in speed or load and valuable features such as transients will show up. However, in practice, analysis of the raw time-domain signal is less common than that of a corresponding frequency spectrum.

### 1.7.2 Frequency-Domain

The frequency content of vibration signals are always directly related to the mechanical condition of the machine components. The frequency-domain allows identification and tracking of individual frequency components, and identification of frequency and amplitude modulation, distortion and also noise levels. It therefore permits close correlation with physical machine characteristics.

Fourier transformations are based on Fourier series analysis of continuous and infinite functions. With digital sampling the Discrete Fourier Transform (DFT) is used. The Fourier transform is particularly important for condition monitoring and therefore this section provides details on its practical application.

#### *1.7.2.1 Frequency Spectrum Amplitude Scales*

In Figures 1-2 and 1-3 the spectral plots were plotted on a logarithmic scale. However, it is more common in condition monitoring to create a *power spectrum* by multiplying the result of the FFT with its complex conjugate. Furthermore, this is often transformed to a logarithmic (ie decibel) scale which is made with respect to some reference value[11] .

The power spectrum presents an indication of the energy in the signal [10] and the logarithmic scale has the effect of emphasising relatively low amplitude components.

Figure 1-4 presents different amplitude scales using the simulated time data. In real applications, the choice of the scale used will depend on the features of interest.

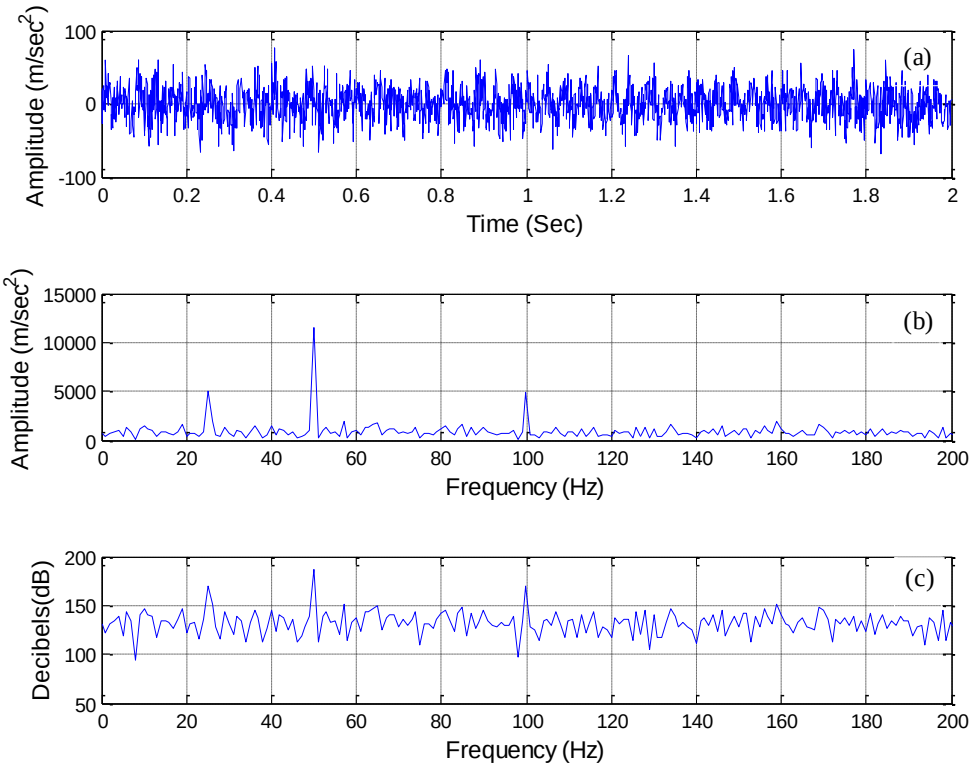


**Figure 1-4** Illustrations of different spectra amplitude scales for simulated signal (a) time domain- (b) power spectrum linear scale (c) power spectrum log scale

### *1.7.2.2 Differentiation and Integration of Time-domain Signal: Effect on Frequency Spectra*

It is interesting to consider differentiation and integration of the time-domain signal and subsequent effects on the FFT. This is particularly relevant as vibration is the most popular measurement parameter for machinery condition monitoring that are linked by differentiation/integration – as shown in Figure 1-5.

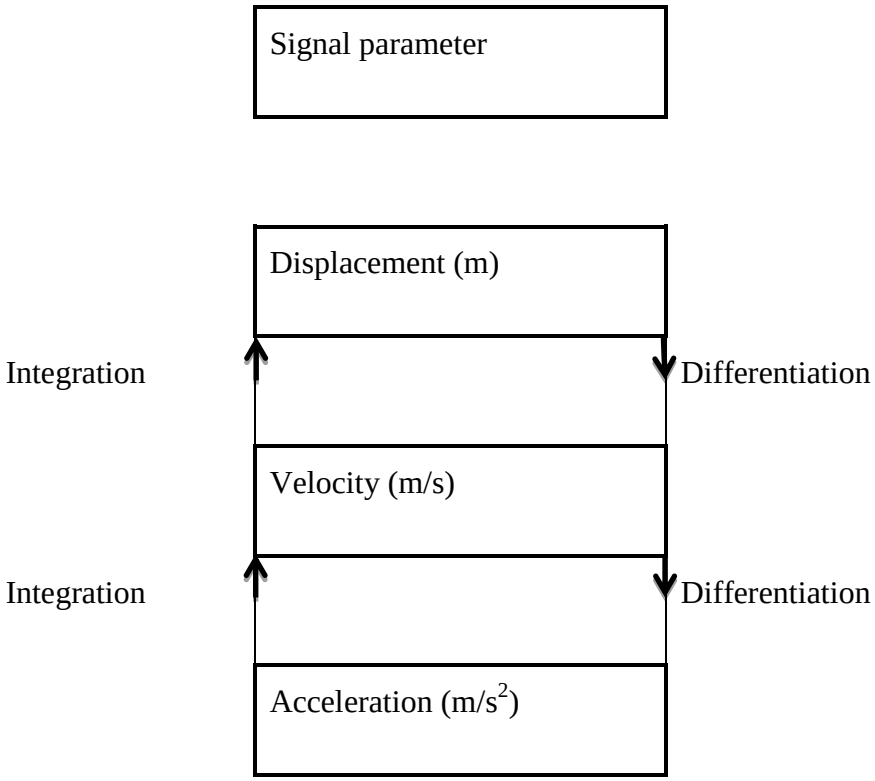


**Figure 1-5** Relation between vibration parameters

A displacement signal was simulated by summation of sine-waves of frequencies 50Hz, 97.2Hz, 800Hz and 1200Hz, and random noise and their amplitude are one (Figure 1-6(a)). The two lower frequency sinusoids predominate in the FFT of the displacement signal, and the two higher frequencies are not seen (Figure 1-6(b)). When the time signal is differentiated twice, first to obtain velocity and then acceleration, the higher frequency components increase in relative magnitude, see Figure 1-6(d) and 1-6(f). This is because for simple sine waves differentiation is the same as multiplying each component by its frequency, acceleration = $\omega$ x velocity = $\omega^2$ x displacement.

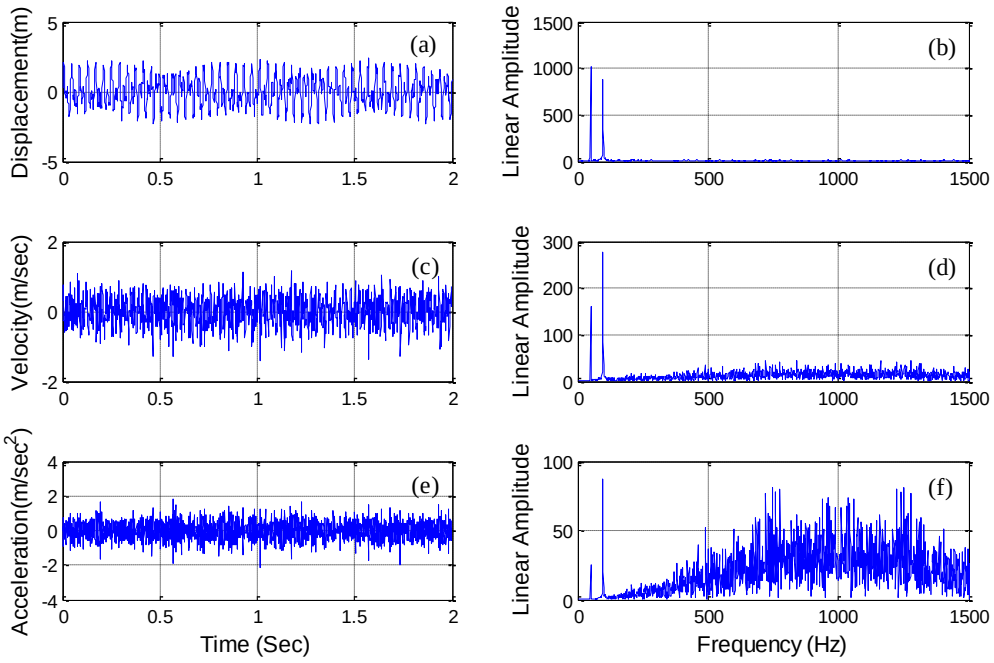


**Figure 1-6** Differentiation of a simulated signal (a) displacement signal- (b) FFT of displacement signal - (c) Velocity signal –(d) FFT of velocity signal –(e) Acceleration signal –(f) FFT of acceleration signal

### *1.7.2.4 Signal Distortion and Modulation*

Two highly important factors in transformation from the time-domain to frequency-domain are signal distortion and frequency modulation, features which are often met during fault diagnosis. As shown in Figure 1-7, a sine-wave of 50 Hz with an integer number of periods yields a single component in the frequency domain located at the frequency of the sine-wave. Figure 1-7 shows various types of distortion and the resulting effect in the frequency domain.

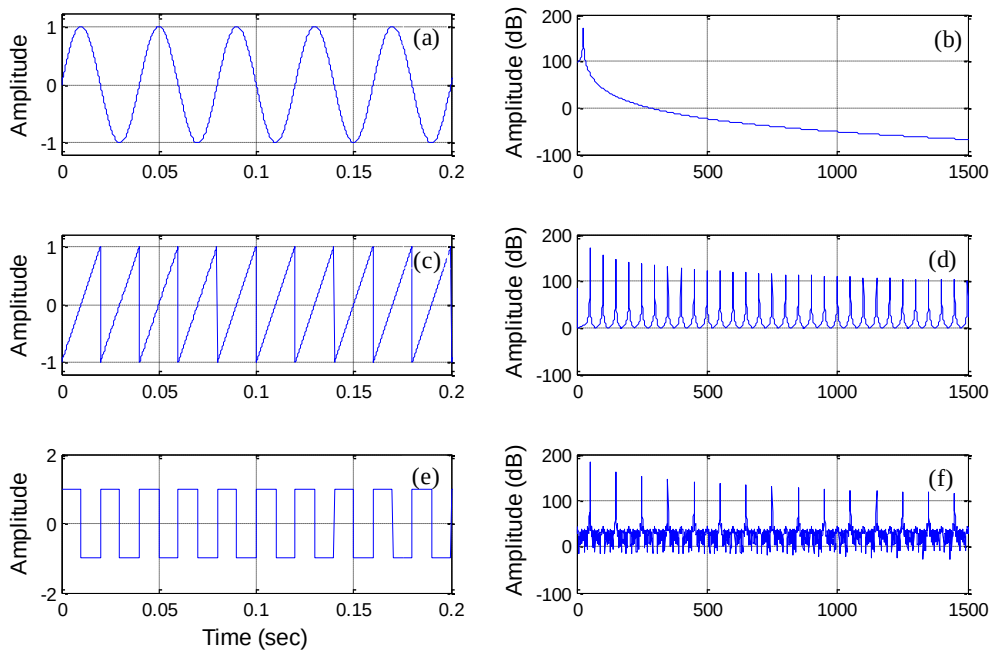


**Figure 1-7** Sine-wave distortion and effect in the frequency-domain (a) sine wave- (b) FFT of sine wave (c) Sawtooth wave – (d) FFT of sawtooth wave- (e) Square wave – (f) FFT of square wave

Truncated sine waves do not have the same spectrum as sine waves of infinite duration. It can be seen that when the 50 Hz sine wave is of finite duration a number of additional peaks appear in the spectrum. The frequencies of these peaks will be a function of the duration of the signal and the frequency of the truncated sine wave. The transforms of a square wave and a triangular wave are also shown in Figure 1-7.

A signal may be modulated by amplitude, phase or both. The result of modulation in the frequency domain is the appearance of sidebands spaced either side of the fundamental frequency. The spacing of the sidebands is equal to that of the modulating frequency.

Figure 1-8 (a) shows the time-domain signals of a 50Hz sine wave with and without amplitude modulation of ± 50%. Figure 1-8 (b) shows that even a relatively large amount of amplitude modulation leads to relatively low-level sidebands.

Figure 1-8(c) shows the time-domain signals of a 50 Hz sine wave with and without frequency modulation of 200 Hz. Figure 1-8 (d) shows that the effect is to produce significant sidebands.

In both cases the amplitudes of the sidebands are symmetrical about the fundamental frequency (ie the carrier) and it is difficult to see more than the immediate sidebands using the linear ordinate scale in Figure 1-8. A real signal is likely to have both amplitude and frequency modulation and each modulating frequency will yield two sets of sideband families in the frequency domain.

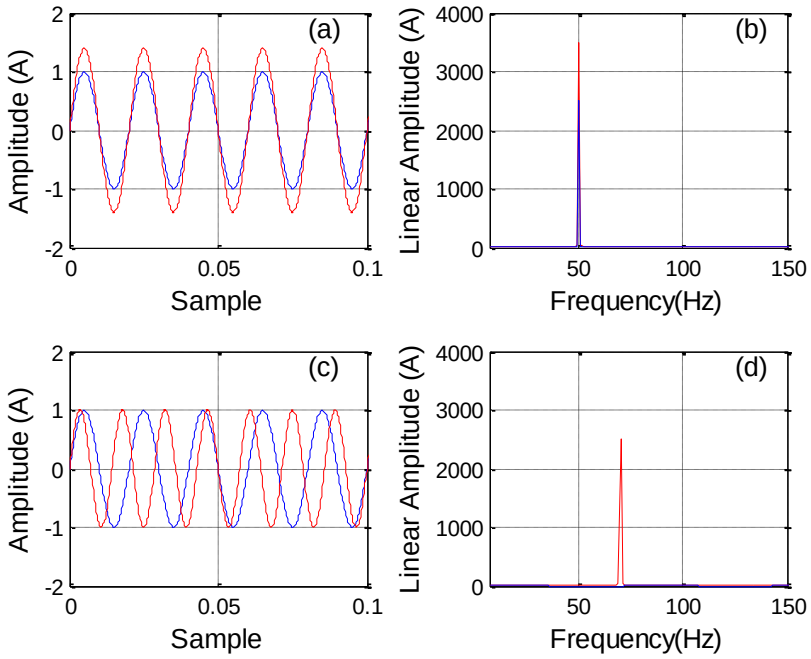


**Figure 1-8** Sine-wave modulation and effect in the frequency-domain

### *1.7.2.5 Averaging of Frequency Spectra*

Averaging is also an important process of data manipulation in the frequency-domain. It is used to reduce the effect of random noise. Averaging is easier to achieve in this domain than for a raw time signal, as the latter requires a reference mark to align periodic data (usually a once per revolution marker). Figure 1-9 shows that for recorded induction motor vibration data even using only a small number of

tests to obtain an average gives a significant improvement in signal quality. In comparison to Figure 1-9 in which no averaging was performed in blue one; and red one shows the result of averaging across 5 sequentially recorded data files. Alternatively, averaging could have been carried out with just one data file by splitting it (in the time-domain) into a number of segments and averaging the spectra from each segment. However, for the same file sizes as those used in Figure 1-6, this would have led to a reduction in the frequency resolution.

**1-9**

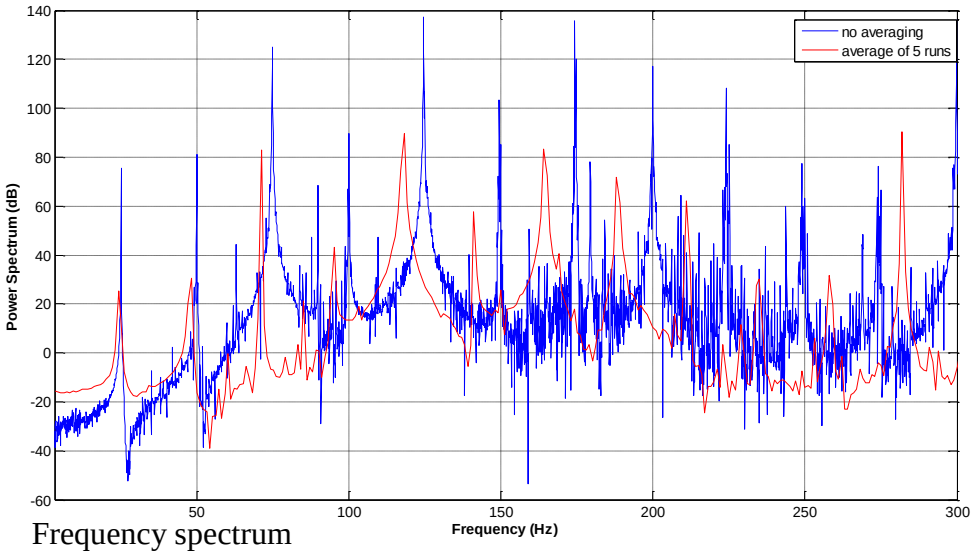


Frequency spectrum

### 1.7.3 Time-Frequency Domain

It is possible to view both time and frequency information simultaneously in a three or two-dimensional time-frequency plot. Here the changes in particular frequency components may be related to particular instances in time, allowing the possibility of improved fault location.

There are many algorithms for achieving a time-frequency plot, such as:

• Short Time Fourier Transform (STFT),

• Wigner-Ville Distribution (WVD), and

• Wavelet Transform (WT).

Each of these has its own advantages/disadvantages, but they all require the setting of a number of parameters such as window type (e.g. Hanning), length and overlap (to minimise loss of information the length of the windows is such that each window overlaps to a degree with its neighnor) and all lead to very similar time-frequency results. Examples of time-frequency plot is given in Figures 1-10, for which the MatLab WVD function was used on simulated time data containing predominantly frequencies shaft frequency of 23.53 Hz, the power supply frequency at 50 Hz, twice power supply frequency 100 Hz, rotor oscillation frequency at 190.64 Hz with sidebands around the 1st shaft frequency

Figure 1-10 highlights an example of the problems which can occur with this type of representation – that is the interference between the two components 23Hz and 50Hz

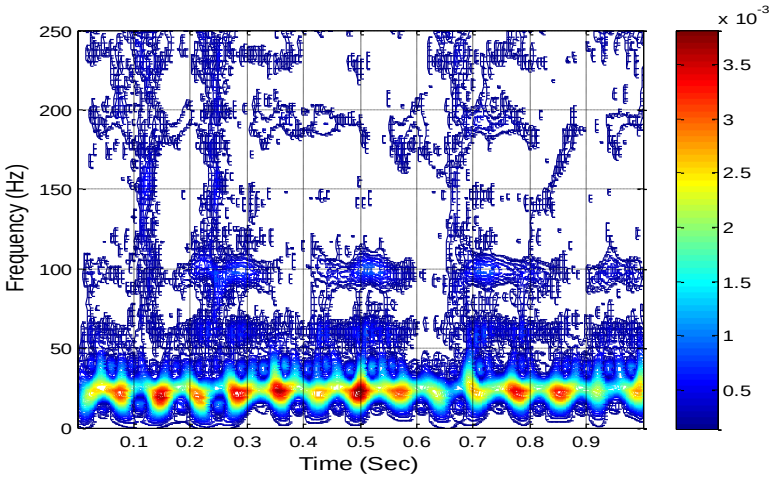


**Figure 1-10** 2-D Time-Frequency Plot

### 1.8 Neural Networks (NN)

Artificial neural networks (ANNs) are used for statistical processing of data and applied to fault detection and diagnosis. Generally these networks are divided into

two main types - *supervised* and *unsupervised*. The difference is the method used to train the network.

In supervised learning a "teacher" is present during the learning process, the ANN has a given input and the error is the difference between ANN output and the target. The network weightings are adjusted using a back-propagation algorithm to reduce the difference between the actual and desired outputs. In this way the ANN is trained to learn specific behaviour and desired outputs for each input. It is the presence of the training pattern which makes this learning supervised.

With unsupervised learning there is no target available to the ANN, only the input is present. This type of ANN learns by discovering and adapting to structural features in the input pattern. This is achieved by adapting to statistical regularities or clustering patterns in the training samples.

In unsupervised training the input patterns are applied to the network but there is no specified output from the training process. Here the network organises itself to develop properties of the training data set that emerge as the process proceeds.

ANNs are often supplied with input variables extracted from the raw data using more conventional signal processing techniques. Jacob [11] report applications of ANNs to incipient fault detection in induction motors where the input variables were taken from the relative phases of the power supply current. Filippetti [12] has suggested that the ANN inputs could be the phase current and the induction motor slip. Paya et al[13] detected motor bearing faults using vibration data pre-processed by a wavelet transform as the input to the ANN.

## 1.9 Research Aim and Objectives

### 1.9.1 Research Aims

The aim of research is to investigate and recommend a condition monitoring (Motor current signature or Vibration signature) approach for three phase induction motors. Moreover, reconstruction vibrations signal from phase current signal.

The specific aims are:

Vibration measurement is widely used for diagnosing the condition of rotating machinery; but sometimes direct measurement can be difficult and expensive in remote or locations that are challenging to access, in harsh environments and where it is expensive to install sensors close to the machine. These conditions apply to electrical submersible pumps (ESPs) in deep-well oil and gas extraction, or deep within nuclear power stations. The current driving the pump has a signature which has been shown to provide information on the condition of the pump without requiring direct access to the pump itself

The first aim of research is to investigate and recommend a condition monitoring (motor current signature (MCS) or motor vibration signature (MVS)) approach for three phase induction motors.

The secondary purpose was to develop a technique for detecting and locating faults (assessing condition and performance) in inaccessible equipment using radial basis function (RBF) networks to reconstruct the vibration waveform from the measured power (one phase current)

The third purpose was to present the new an innovative, non-intrusive, accurate and reliable method for the early detection and diagnosis of faults in an induction motor (IM) using an enhanced power parameter measurement technique. It is argued, and

initial results suggest that it is more effective to monitor the operating power factor (PF) of the IM using only measured current and supplied manufacturer's data.

### 1.9.2 Research objectives

The objectives are as listed below:

- Explore induction motors failure modes and understand condition monitoring techniques e.g. vibration and motor current signature analysis.
- Develop a mathematical model for induction motor operations and effect of faults on the measured performance.
- Design and construct a test rig with associated instrumentation for fault simulation namely phase imbalance and rotor bar broken, data collection and subsequent data analysis.
- Investigate the use of conventional signal processing techniques such as time-domain and frequency-domain for detection and diagnosing of the seeded faults.
- Apply advanced signal processing methods such as time-frequency-domain using the short time Fourier transform (STFT), Wigner Ville distribution (WVD) ,continuous wavelet transform (CWT) and discrete wavelet transform (DWT) for detecting and diagnosing quantified faults.
- Compare the capabilities of the techniques investigated for fault detection and diagnosis.
- Apply Radial Basis Function networks to the reconstruction of motor vibration using measurements of one phase of the motor current.
- Apply a method of determining the operating PF of the IM using only the measured current and the manufacturer's data available from the nameplate

and/or datasheet to detect, diagnose and assess the relative fault severity of the seeded faults

### 1.10 Organisation of the Thesis

This thesis is organised in the following way: the literature review is given in Chapter Two. Chapter Three provides a mathematical model for the induction motor. The test rig, transducers, data acquisition system and fault simulation are presented in Chapter Four.

Chapter Five describes fundamental signal processing techniques and their use in collecting and processing data.

Chapter Six compares the performance of the short time Fourier transform (STFT), the Wigner-Ville distribution (WVD), the continuous wavelet transform (CWT), the discrete wavelet transform (DWT) and wavelet multi-resolution analysis (MRA) using a simulated signal and measured data from an induction motor with seeded faults.

Chapter seven investigates the relationship between phase current and vibration using coherence technique as a measure of the relationship and proposes a novel method of applying Radial Basis Function networks to the reconstruction of motor vibration using measurements of one phase of the motor current.

Chapter Eight provides an innovative, non-intrusive, accurate and reliable method for the early detection and diagnosis of faults in an induction motor using a power factor measurement technique.

Conclusions, contributions, and recommendations for future work are discussed in Chapter Nine.

# CHAPTER 2

# LITERATURE REVIEW

*This chapter begins by reviewing the current literature on fault finding and monitoring of, specifically, three phase induction motors with emphasis on modern techniques and methods.*

*This chapter then summarises the investigations into the type of faults found in an induction motor and techniques for detecting and identifying them.*

## 2.1 Introduction

Induction motors are low cost, reasonably sized, and are powered by an easily available power supply. This results in them being widely used as critical components in many industries and a common component in much commercially available equipment. Often the induction motor will operate in hostile conditions and both the method of installation and the type of duty may seriously accelerate failure. **Nandi et. al.,** [14, 15] have provided a useful classification of major failure modes in electrical machines:

- "Stator faults resulting in the opening or shorting of one or more stator coils or phase windings,
- Abnormal connection of the stator winding,
- Broken rotor bars or cracked end rings,
- Static and/or dynamic air-gap eccentricities,
- Bent shaft,
- Shorted rotor field winding, and
- Bearing and gearbox failures."

**In [16]** on the reliability of induction motors classifies faults in order of likelihood of occurrence: bearing failure (51%), external faults such as a hostile environment (16%) stator winding faults (16%), unknown 10%, broken or damaged rotor bars (5%) and damage to shafts and/or couplings (2%).

The above faults produce one or more of the following symptoms: noise and vibration, excessive heating, unbalanced line currents and voltages, torque pulsations and flux leakage. Other symptoms are, of course, also possible.

It is the location that categorizes bearing faults, e.g., inner or outer race. Common causes of bearing faults are an inadequate supply of lubricant, foreign material contaminating the lubricant, over-loading and over-heating. If untreated these lead to seizure of the bearing or violent vibration and catastrophic failure.

Failure of winding insulation is the most common cause of stator faults due to over-heating, mechanical vibration, excessive voltages or possibly abrasion between the rotor and stator. The immediate result will tend to be turn-to-turn short circuits but these can build to a winding-to-ground short circuit.

There are two common rotor faults. The first is related to air gap eccentricity which commonly arises from such mechanical problems as shaft misalignment or load unbalance. With shaft misalignment, the rotor can be displaced from its normal position because of an error in construction or a constant radial force. Load unbalance over a long period can cause bearing damage, which will adversely affect air gap symmetry.

The second common faults are with the rotor itself, i.e. a bar defect or even breakage, usually due to thermal or fatigue stresses during start-up, especially in large motors. A broken bar changes torque significantly and is dangerous for the safe operation of the motor.

### 2.2 Condition Monitoring Technologies

To monitor the condition of a machine, Condition Based Maintenance (CBM), or Predictive Maintenance, uses a wide range of measurements including vibration, acoustic emission (AE), oil debris analysis, thermography and phase current (motor current signature analysis - MCSA). For the CBM system to be effective and efficient the measured parameters must accurately reflect the condition of the

machine, must be obtained on a regular and frequent basis and the system should be cost-effective and practical. Today, vibration acceleration is widely used parameter for detection of faults in machines particularly with artificial intelligence and neural network (NN) based techniques

To study static rotor eccentricity **Toliyat, et. al.** [17] considered the geometry and physical layout of the windings to develop a model of the induction motor which could simulate performance during transients as well as the steady state. The mechanical equations of the model allowed any arbitrary time function of load torque to be specified and the resulting stator current calculated. Simulations gave results which were in good agreement with the experimental results of previous studies.

**Henao, et. al. [18]** developed an analytic expression for the equivalent internal circuit of a three-phase squirrel-cage induction motor and validated it experimentally. The proposed model allowed for simulation of induction motor state variables, both stator and rotor, under normal or faulty operation. It was found that the model was very good at predicting the effects of fault on the behaviour of the induction motor.

A comparative study of the use of different physical parameters for condition monitoring (CM) using both measured and simulated data was undertaken by **Negrea, et. al. [19].** They found the best indicators of faults to be axial flux and electromagnetic forces acting between rotor and stator. This work included a comprehensive study of electromagnetic flux patterns in the presence of faults and it was claimed that useful insights were obtained into the use of particular configurations of search coils.

**Legowski, et. al. [20]** demonstrated that instantaneous electric power has significant advantages when used for signature analysis of induction motors because its

characteristic spectral component is at the frequency of the disturbance, independent of the motor speed. This is important for diagnostics because irrelevant components at multiples of the supply frequency are screened out.

**Ellison and Yang [21]** used the airborne sound generated by air gap eccentricity in induction motors to detect the presence of this fault, and confirmed that harmonics found in the acoustic noise spectrum from an induction motor were generated by static eccentricity. However, it has long been known that noise measurements in industrial plant are rarely practical because of the high levels of background noise from nearby machines **[22], [23]**.

Nearly all motor faults generate harmonics in the torque which exists in the air gap, at specific frequencies but this is not a simple parameter to measure, for example, the instantaneous power is not a direct measure of the instantaneous torque. The mechanical load, the shaft and the rotor of a rotating machine combine to form a spring system with its own resonant frequencies, so the air gap torque transmitted via this spring system will be modified and will not be the same as that measured at the shaft **[24],[25].** Nevertheless Hsu **[24]** has suggested a method using the air gap torque for the detection of stator unbalance and cracked rotor bars.

Because the flux in the air gap of an induction motor is rich in harmonics it can be used to give reliable information concerning the electrical condition of the motor. Any change in a relevant parameter such as voltage and/or current will generate changes in the spectrum. **Xianghui, et. al. [26]** studied the effect of static rotor eccentricity on air gap flux .**Trutt, et. al. [27]** measured air gap flux and motor vibration and concluded that both signals provided useful information for machine CM. But both **[26]** and **[27]** identified only parameters that were functions of eccentricity of the air gap, rather than useful for on-line diagnostics.

In practical terms the most interesting technique for CM was based on monitoring of vibration and electrical parameters because these are readily available for motor drive systems and in a form suitable for signal processing.

### 2.2.1 Motor Vibration Signature.

Rotating electrical machines generating mechanical power operate under variable or even dynamic loads and are thus vulnerable to forced vibrations leading to dynamic stresses should the mechanical condition of the machine change.

**Dorrell and Smith [28]** produced an analytical model of an induction motor subject to static eccentricity. Their approach was to use air-gap permeance with rotor and stator magneto-motive forces producing unbalanced magnetic pull. The model was tested and confirmed by experiment and good agreement was found at low slip. They concluded that rotor skew effects and higher order winding harmonics can affect the magnitude of the unbalanced magnetic pull.

**Finley, et. al. [29]** compiled a table of electrically and mechanically excited vibration patterns for induction motors and analysed the important electromagnetic force components between rotor and stator. These reached their peak when the magnetising current flowing in the stator is a maximum, so there are two force peaks during each power cycle and the vibration frequency will be twice the line frequency. This phenomenon is sensitive to (and hence a possible measure of) problems in eccentricity, and motor frame and base stiffness.

**Trutt, et. al. [30]** made a theoretical study of the relationships between mechanical vibration and electrical winding deterioration in AC synchronous machine elements for different operating conditions**.** They found significant quantifiable correlation

between mechanical vibration and electrical deterioration which was thus a possible basis for the CM of AC synchronous machines.

**Müller and Landy [31]** made an experimental and theoretical study of broken rotor bars and their impact on axial forces. They developed a mathematical model of the interaction of inter-bar current with stator flux and the resultant force in the axial direction. The results were confirmed by experiment. The drawback of this research is that it is solely applicable to the condition where there are inter-bar currents, e.g. as in some copper cage rotors.

An induction motor fed from a Pulse Width Modulation Inverter, was investigated by **Villada, et. al. [32]** and the measured vibration and current from healthy and faulty (stator faults) machines were compared. The vibration spectrum underwent measurable changes at a number of frequencies and these can be used as early indicators of stator winding faults. It was recommended that to obtain a full picture, the results should be part of a predictive program and the commencement of any change be established and initial cause identified. Trending was considered vital as attempting to establish motor condition from one set of data alone was considered undesirable and possibly unachievable.

**Vandevelde and Melkebeek [33]** developed a finite element model (FEM) for numerical analysis and prediction of vibration and noise from induction motors based on electro-mechanical analysis of magnetic equivalent circuits. These researchers claimed their method overcame the drawbacks inherent in such analytical models but analysis was not made of lower-order forces and vibrations generated by electro-mechanical faults. However, such effects might be studied using this approach.

**Ishibashi, et. al. [34]** were concerned to reduce the noise radiated from induction motors. Most electromagnetic noise occurs when the natural frequencies of the stator coincide with or are close to the frequencies of the magneto-motive forces and they used FEMs to assess electromagnetic force associated with the Maxwell stress tensor the stator's natural frequencies assuming spring elements between stator frame and stacked core. Good accuracy was claimed between the calculated and experimental results.

**Jang and Park [35]** simulated electro-mechanical faults (rotor eccentricities and broken bars) in a single-phase induction motor. Characteristic magnetic, mechanical and electrical equations were solved using finite element method to obtain the resulting characteristic frequencies of the magnetic forces and rotor vibrations. Faults were introduced into the model and the model showed that the faults could be clearly identified by the changes they made to the vibration spectrum.

**More and Ishiskawa [36]** using a 2-D non-linear FEM to analyse the radial electromagnetic forces in an induction motor. They considered the coupling of the motion of the rotor with the voltage. Steady-state characteristics were analysed and the influence of stator winding and slip on the radial force at the teeth and slots was clarified.

### 2.2.2 Motor Current Signature

Electrical current monitoring includes current signature analysis, zero-sequence and negative-sequence current monitoring and Park's vector. The Park's vector transforms three quantities (direct axis, quadratic axis, and zero-sequence components) expressed in a two-axis reference frame back to phase quantities. It is used in power systems models and functions. All these methods (and more) are used

to analyse stator current in order to detect machine and inverter faults. Usually with induction motors, monitoring of the stator current is already used to protect the machines from troublesome over-currents, ground leakage current, etc. Thus, current monitoring can be a sensor-less detection method, implemented without any extra hardware.

Numerous applications of MCSA for CM of equipment have been published and in most of the applications, the stator current was monitored for detection and diagnosis of the faults. **Schoen, et. al. [37]** used MCSA to detect damage of induction motor rolling-element bearings. The investigation considered the relationship between motor current and induced vibration due to incipient bearing failure. The study reviewed and defined bearing characteristic frequencies and failure modes associated with the physical construction of the bearings. The effects on the stator current spectrum were derived for different bearing faults and experimental results verified the predicted relationship between the vibration and current frequencies. The test results confirmed that the stator current signature could be used to detect the presence of a bearing fault.

**Schoen and Habetler [38]** presented an analysis of the effects on the current harmonic spectrum of oscillation of the flux density in the air gap due to position-varying loads. When the load torque varies with rotor position, the current will possess spectral components with load induced harmonics and the induced rotor fault harmonics coinciding. Furthermore, since the effect of the load and fault on a single stator current harmonic component is spatially dependent, the fault induced portion cannot be separated from the load portion. Thus on-line detection systems which measure and analyse the spectrum of a single phase of the stator current must

monitor those spectral components which are not affected by the oscillation of the load.

**Benbouzid [39]** investigated fault detection using MCSA (spectral analysis of the stator current). This study examined the impact of air-gap eccentricity, bearing damage and broken rotor bars on the stator current. Of particular interest were the sidebands in the current spectrum produced by the various faults. It was shown that the sidebands could coincide with others resulting different faults, for example, stator current harmonics follow due to torque oscillation could obscure those created by the induced fault condition.

**Thomson and W.T [40]** used MCSA for induction motor faults, particularly air-gap eccentricity, broken rotor bars and shorted turns The broken rotor bars caused current components, the so-called twice-slip frequency side bands, to be induced in the stator winding. These researchers pointed out that any successful diagnostic strategy must be able to account for at least the following: different rotor designs, different load conditions, varying mechanical load characteristics, a range of mechanical components and power ratings in the drive train. Thomson and Fenger reviewed four selected industrial case histories and showed MCSA could be a powerful mechanism to monitor the health of induction motors.

**Benbouzied, M.E.H and Kliman [41]** investigated motor current for fault detection in induction motors, in particular rotor fault detection (broken bars and bearing deterioration) with special emphasis on the signal processing techniques used. They pointed out that in many cases, conventional techniques are sufficient for the steady state situation, but for the most difficult cases (i.e., non-stationary), time-frequency and time-scale transformations, such as wavelets, are necessary for the detection and diagnosis of the rotors faults.

**Dimitrov, et. al. [42]** experimentally diagnosed a broken rotor bar fault using (MCSA). The experiment used a 0.5 kW induction motor where the rotor bar was damaged by having a hole drilled onto it. The spectra produced by the health and the faulty motors were compared. The presence of the faulty rotor bar produced sidebands in the stator current spectrum at certain frequencies. It was concluded that MCSA was a reliable technique for diagnosis of broken rotor bar faults.

**Frosini, and Bassi [43]** have recently proposed a new use for MCSA, combining it with and motor efficiency as an indicators of faults in rolling bearings. This study investigated experimentally four bearing defects: a crack in the outer race, a hole in the outer race, deformation of the seal, and corrosion. The use of decrease in efficiency of the induction motor as a warning of incipient fault was a novel feature of this study.

**Faiz, et. al. [44]** recognized that variation in the load quite apart from changes in static and dynamic eccentricities is a major factor affecting the changes in dynamic behaviour which are used for fault diagnosis. Without taking load variation into account faults are inaccurately diagnosed. For example load variation will have noticeable effects on side-bands that are used as fault detection indices. Faiz, et. al. therefore proposed a "unified framework" an approach that determines the degrees of static and dynamic eccentricities at different load levels. The researchers proposed a systematic relation with which to evaluate the impact of load-dependent indices on eccentricity detection and fault-severity estimation. Correlation techniques were used to assess the quality of the indices obtained for detection in terms of their relation to static and dynamic eccentricities, their degrees and dependency on the load of motor. It was claimed that the results obtained determined the type of eccentricity and degree exactly.

## 2.3 Signal Processing Techniques

The condition of the induction motor can be estimated from the time domain signal using signal processing techniques which vary from the simple to the sophisticated. This section provides a brief summary of the common fault detection techniques; time domain analysis, frequency domain analysis, cepstrum analysis and time-frequency analysis applied to measured signals obtained from induction motor.

The most direct approach has been is to extract statistical properties from the time domain signals; the most common were *RMS, standard deviation, Kurtosis, mean, skewness, crest factor and impulse factor*.

**Benbouzid [39]** when he reviewed MCSA as a mechanism for fault detection also reviewed advanced data processing techniques for monitoring of induction motors. Possibly the most powerful of the time-domain techniques uses characteristic values (such as RMS) and trends them to see how the condition of the motor changes with time. Spectrum analysis examines characteristic frequencies and this can allow discrimination between faults and even detection of incipient faults. Cepstrum analysis is a powerful method for detecting periodical components in the spectra and is sometimes used as an evaluation tool.

Benbouzid also described some of the traditional stator current signature analysis methods: the Fast Fourier Transform (FFT), the Digital Transform (DFT), the instantaneous power spectrum, the bispectrum, high-resolution spectral analysis and wavelet analysis. He concluded that Fourier analysis is generally the most useful where the signals are stationary, but is not appropriate for signals with a transitory characteristic such as rapid drifts, abrupt changes in amplitude and/or frequency, or impulses. The Short Time FFT (STFT) was developed to overcome such problems

and can be considered as a compromise between time- and frequency-based analyses of a signal. However, Benbouzid recommends wavelet analysis for CM and fault diagnosis because it can cope with transients in the stator current. The Wavelet Transform (WT) analysis places a window over a portion of the signal and analyses the signal within that window, subject to certain mathematical conditions. The window moves along the signal and by continuously varying the duration of the window analyses the original signal in terms of time and frequency. Longer windows give more precise low-frequency information and shorter windows give more precise high-frequency information.

**Yi-Ching, et. al. [45]** focused on developing a non-intrusive monitoring of power system signatures, using the WT and STFT. They found that the WT was superior to the STFT. The paper presented two case studies to demonstrate that choice of power signature can greatly influence the accuracy of load identifications.

**Eren and Devaney [46]** used wavelet packet decomposition to analyze stator current and detect bearing defects. The advantage over the FFT for MCSA is the non-stationary nature of the stator current, and the WT provides better analysis for varying load conditions. The WT also allows the frequency bands to be tailored to better cover the range of frequencies induced by the bearing-defect and rotor speed variations.

**Antonino-Daviu, et. al. [47]** used the discrete wavelet transform (DWT) to diagnose rotor bar failure in induction motors based on stator current during start-up. With bar breakage, the higher level components of the DWT of the startup stator current showed a characteristic pattern. Experiments were carried out for different machine conditions (healthy machine and machine with different faults) and different operating conditions (zero load, full load, pulsating load and fluctuating voltage). In

each case, the results were compared with those obtained using the FFT. As might be expected if the startup time was not very short, the DWT and the FFT gave similar results for the diagnosis of a broken bar in the case of loaded motors. However, the DWT can detect a broken bar in the unloaded condition (rapid transient), and it provides a correct diagnosis in particular cases where FFT gave an incorrect diagnosis.

**Patel, et. al. [48]** presented a method for identification of bearing defects of an induction motor at full load, making use of the advantage of the DWT and Hilbert Transform to extract the necessary features from the vibration signal of the bearing. The experimental results show this method can be successfully used for bearing fault detection and diagnosis.

**Obaid, et. al. [49]** have demonstrated that detecting the characteristic frequencies of a bearing fault using the motor current was especially difficult for inner race faults, even when the fault frequencies were prominent in the motor vibration signal. To overcome this problem they suggested that a wider frequency range be used for current-based fault detection. It was shown that disassembling and remounting the bearings can significantly alter the vibration characteristics and conceal some fault signatures.

**Gritli, et. al. [50]**, improved the performance of the DWT in detecting a broken rotor bar by simply pre-processing the stator phase current, even for speed-varying conditions. Once the fault was detected, a cyclic time-frequency indicator was used to quantify the extent of the fault. It was obvious that the method was advantageous even when the fault characteristic frequency is very close to those of other faults or even a fundamental frequency of the motor or system. The approach allows the extraction of each frequency component separately and with high precision. Both

experimental and simulated results confirmed the effectiveness of this method for detecting a broken rotor bar even under time varying conditions.

**Cusido, et. al. [51]** developed a methodology for the detection of faults in induction-motors combining the Power Spectral Density (PSD) with using wavelet analysis of the stator current. It is claimed that this method is particularly useful for online diagnosis and industrial applications. The MCSA gives good results for the detection of motor faults under constant load torque, but improvement is required in the case of variable load torque, and also of variable speed. Cusido, et. al. demonstrated that their method can detect and diagnose shorted turns and broken rotor bars in induction motors in the cases where the load-torque is not constant, and achieved good fault diagnosis results for every operating point reported. However, this method requires good prior knowledge of the signals to determine the best sampling frequency and wavelet type to achieve detection of the faults.

The authors introduce a so-called "merit factor" which is found by adding the squares of the detail corresponding to the frequency band where the fault harmonic is situated and show that this is a powerful tool in enabling the process of diagnosis to be automated and applied to practical industrial systems under both constant torque and variable load torque.

### 2.4 Fault classification

**Fillippetti [52]** comprehensively reviewed the application of AI to machine monitoring and fault diagnosis. He demonstrated the validity of using NNs together with fuzzy logic for fault identification and fault severity evaluation. In recent years the CM and fault diagnosis of induction motors has moved towards Artificial Intelligent (AI) techniques **[52]** such Artificial Neural Network (ANN) and Support

Vector Machine (SVM) which have been applied in fault diagnosis of complex time varying and non-linear system. AI techniques use association, reasoning and decision making processes to solve diagnostic problems in a similar way to the human brain.

A major advantage of AI techniques is that they are good candidates for automation of diagnostic procedures [53]. ANNs have many advantages over conventional diagnostic techniques, the most important being their learning flexibility and that their design does not need a rigorous model of the motor. ANNs have demonstrated their ability to in the field of CM and fault diagnosis of induction motors. ANNs can represent highly nonlinear functions and are capable of performing multi-input, multi-output mappings.

Several research activities used ANN for CM and fault diagnosis of electric motors using different approaches and setting different tasks, **Chow, et. al. [54]** have listed these as:

(1) "Pattern recognition, parameter estimation, and nonlinear mapping applied to CM,

(2) Training based on both time and frequency domain signals obtained via simulation and experimental results,

(3) Real time and online unsupervised diagnosis,

(4) Dynamic updating of the structure with no need to retrain the whole network;

(5) Filtering out transients, disturbances and noise,

(6) Fault prediction in incipient stages owing to operation anomalies, and

(7) Operating conditions clustering based on fault types."

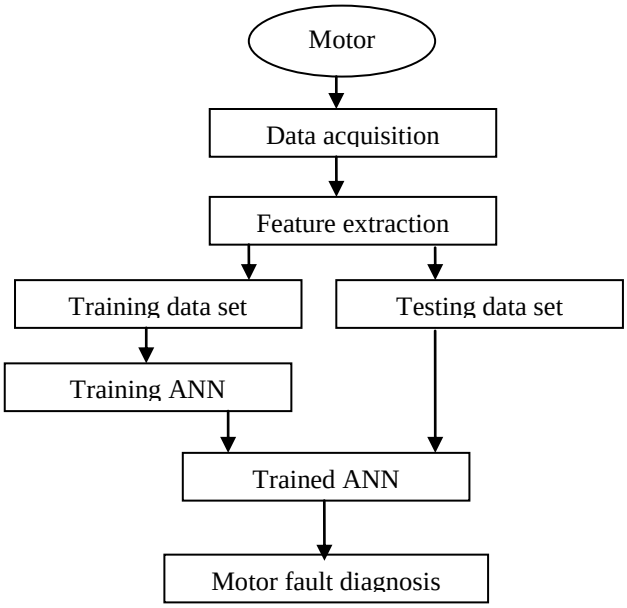


**Figure 2-1** Block diagram of an ANN-based fault diagnosis system [54]

The ANN flow chart for fault diagnosis of induction motor faults based is shown in Figure 2.1. In [54], successful results were obtained using a Back Propagation neural network (BPNN) on motor winding short circuit and bearing fault detection. **Merwe and Hoffman [55]** showed if the classification problems are well defined, the Radial Basis Function (RBF) neural network can identify the degree of fault severity. **Penman and Yin [56]**, applied a Self-Organizing Feature Map (SOM) to CM of electrical drives and reported practical advantages including the ability to learn and produce classifications without supervision.

**Du and Wolfe [57]** proposed an approach for diagnosis of faults in rolling bearing using neural networks and time-frequency-domain analysis of bearing vibration. In **[32],** the attempt was made model the non-linear steady state conditions of rotor speed and stator current versus damping factor and main winding equivalent turns using a multi-layer perceptron (MLP) approach by suitable training of the ANN. In **[12]**, a supervised MLP structure detected broken rotor bars based on the spectrum of

the motor current; experiment and simulation was used to obtain a hybrid training set. In **[58]**, an algorithm based on an unsupervised NN was proposed for online diagnosis of faults in the stators of induction motors. A fully automated and unsupervised method was applied in which a Hebbian-based unsupervised NN was used to extract the principal components of the stator current data. A very useful feature of this method is that it does not need *a priori* identification of system characteristics.

**Nejjari and Benbouzid [59]** have used the Park's vector for detecting different supply faults, including voltage imbalance in a single phase. A NN based on a back-propagation algorithm was used to determine the condition of the machine by examining the patterns and shapes of the Park's vector. Both classical and decentralized NNs were used and the generality of the method was tested experimentally. The authors claim that the results provide a "satisfactory level" of accuracy.

**Abiyev and Kaynak [60]** integrated fuzzy logic systems with a wavelet NN for identification and control of an uncertain system. In his paper he used the well-known gradient decent algorithm to update parameters. It was claimed that the fuzzy wavelet NN networks can converge faster and are more adaptive to new data.

**Bouzid, et. al.[61]** Suggested a NN approach for the automatic detection and location of an inter-turn short circuit in the stator of an induction motor. In his paper he used a feed-forward MLP NN trained using the back-propagation technique. The difference in phase between the phase voltage and line current of the induction motor was used as the input to the NN. The output is set to either 'zero or 'one. If a short circuit is detected in one of the three phases, the corresponding NN output is 'one'; otherwise, it is 'zero'.

**Hua et. al [62]** successfully demonstrated a system for monitoring induction motor vibrations based on a NN which used analytical redundancy. The STFT was adopted for processing quasi-steady vibration signals for NN model training and faults were identified using changes in the vibration modelling error expectation. The main feature of this system was its attempts to account for the spread and random nature of the vibration signals.

Vibration monitoring for diagnosis of rolling bearing faults via a NN was undertaken by **Li, et. al. [63]**. The research contained both experimental and simulated vibration. It was shown that the application of a NN to the interpretation of measured bearing vibration signals can effectively diagnose a range of faults. Li, et. al. obtained the vibration spectrum using the FFT. Vibration signatures were generated from the power spectrum of the vibration signal, these contained specific frequencies based on the prevailing defects, with a range of amplitudes. Time domain parameters such as kurtosis and mean and maximum amplitudes of the vibration waveform were also considered by the NN.

**Jack and Nandi [64]** claimed superior results were obtained when they used genetic algorithm assists the ANN. The genetic algorithm used statistical estimates of the vibration signal to select the most important aspects for machine condition monitoring. A subset of six features was selected from a large set of possible features, and these gave a claimed classification accuracy of 99.8 %.

It is possible that similar approach to that of **Li et al. [63]** and **Jack and Nandi [64]** could be adopted using mechanical vibration pattern analysis to detect when an induction motor operates with an electrical fault.

A radial-basis-function NN for fault detection in induction motors was developed by **Wu and Chow [65]**. The inputs to the system are represented by four-feature vectors extracted from the power spectrum of the vibration signals of the machine. This system was able to detect both mechanical and electrical faults, and also the subsequent development of the mechanical faults. Here, the four-feature vectors were total power average frequency **,** and normalised variance and skewness of vibration measurements. Good rates of detection were claimed by the authors for frequencies in the range 40 – 60 Hz. The seeded electrical fault was a stator inter-turn short circuit created by the addition of a resistor across one phase which changed the electromagnetic force on the stator. Unfortunately the simulated fault differed considerably from the actual vibration signals produced by real stator winding inter-turn short circuits.

Wu and Chow also investigated detection of mechanical faults within induction motors. The mechanical fault investigated was simply a loose screw used to hold the motor. This experiment was to highlight the high degree of accuracy that can be achieved with suitable feature extraction. It was found that the proposed NN diagnostic system was effective at identifying machine faults over a range of rotation speeds.

Good results for detection of rotor faults in induction motors using RBF NNs were claimed by **Kaminski, et. al. [66]**. the presence of the load changes and converter supply harmonics, for the relatively short input vector of NN. The possibility of detection of the severity of the fault is a major attraction of the proposed RBF-based detectors. Other valuable advantages are the relatively simplicity of the design of the RBF network and that RBF-based detectors can be an alternative to the well-known MLP-based fault detectors.

**Matic, et. al. [67]** recently presented an overview of rotor condition classification using single perceptron NNs. They concluded that a well-trained ANN should be capable of providing an accurate classification of rotor condition. They also argued that this approach is suitable for online classification because of the simplicity of implementation of ANNs. They also suggest classification based on experimental data provides a more accurate and flexible approach than simulation and analytical models.

**Bouzid, et. al. [68]**, presented an efficient method for the automatic quantification of the number of the broken rotor bars in an induction motor. The method was based on a feed-forward MLP NN which continuously monitored the amplitude and frequency of a low frequency sideband of res-ids. Experimental validation showed that the proposed NN system gave accurate diagnosis of broken bars with a satisfactory robustness under different load conditions, and was insensitive to background noise.

**Santos and Costa [69]** have presented an application of ANNs to detection of bearing faults. A feed-forward network trained using real vibration data collected from a test rig was used to detect a very small fault in the shield of a bearing. The results show proposed network can efficiently detect the incipient fault.

**Dash, et. al. [70]** presented a comparison of MLP NN and RBF NN. techniques for detecting inter-turn faults in the stator of a three phase induction motor. The data base for the inter-turn fault was obtained from a model of the induction motor. They observed that the errors in RBF NN were very much less than for the MLP NN and concluded that the RBF NN was the more accurate as a fault detector.

At present a new comprehensive and indirect diagnostic method is being developed for mechanical equipment driven by AC induction motors. This method of sensorless

detection and diagnosis and monitors the state of the motor (and system driven by the motor) by analysing motor's stator current (**Xianjiang, et. al. [71]**). Because it does not use additional sensors such as accelerometers or microphones it is called sensorless detection and diagnosis. It is possible because the power spectrum of the stator current contains large amounts of information relevant to faults in the mechanical system.

The relationship between the magnitudes of the harmonics of current and vibration signals and specific machine faults has been studied closely **[72],[73]**. **In [72] Riley**, **et. al**. investigated the relationship between magnitudes of the vibration and stator current for a specific frequency of vibration to determine the feasibility of setting a limit on the mechanical vibrations by setting a limit the current harmonics generated by the vibrations. They concluded that for a given vibration frequency, the *RMS* vibration level and *RMS* current level for the individual harmonics are monotonically related. In **[73] Riley, et. al**. proposed a sensorless on-line vibration monitoring using the motor current and carried out a laboratory evaluation. They showed that vibration information can be gained in this way by utilizing the nearly linear relation between a particular harmonic in the current spectrum with its corresponding vibration component and as an indicator of motor vibration. A series of experiments using an accelerometer determined the constant of proportionality between the current and vibration harmonics. It was claimed that the experimental results showed this method was applicable to a wide range of vibrations.

Cause and effect between two signals is often estimated using the coherence function. **Xianjian, et. al. [71]** studied motor bearing degradation caused by accelerated electrical discharge machining. In an attempt to identify bearing damage using the motor current, the coherence function between vibration signal and motor

current was determined and the largest values of the coherence, i.e. where vibration signals and motor current are best correlated, are the locations of the bearing defect and dynamic eccentricity.

While the literature review shows that thermal monitoring, vibration monitoring, and electrical monitoring, noise monitoring, torque monitoring and flux monitoring are the some important techniques of condition monitoring and fault diagnosis of three phase induction motors. Now days, electric monitoring or current monitoring is increasingly popular. In current monitoring, no additional sensors are necessary. This is because the basic electrical quantities associated with electromechanical plants such as currents and voltages are readily measured by tapping into the existing voltage and current transformers that are always installed as part of the protection system. As a result, current monitoring is non-intrusive and can even be remotely implemented in the motor control center of monitored motor

In the literature review it has been shown to correspond to a relationship between the mechanical vibration of a machine and the amplitude of the harmonic component of the stator current. For increased vibration, the amplitude of harmonic components of the stator currents are also increased. This is because the mechanical vibration modulates the air gap at that particular frequency. These frequency components then show up in the stator inductance, and finally in the stator current. For this reason, the MCSA is the most commonly used method in the detection of common faults of three phase induction motors.

Wavelet Transform can be used for the diagnosis of the failure of the three induction motor. It works on principle that all signals can be reconstructed from sets of local signals of varying scale and amplitude, but constant shape. It is an easy and fast to implement data processing technique. It analyses the signal at different frequency

bands with different resolution by decomposing the signal into coarse approximation and detail information.

From the literature cited, the following observations can be made:

(i) The biggest drawback of the vibration measurement is cost. A vibration sensor costs several hundred dollars. A high product cost can be incurred just by employing the necessary vibration sensors for a large number of electric machines. Another disadvantage of the vibration measurement is that it requires access to the machine. For accurate measurements, sensors should be mounted tightly on the induction motor, and expertise is required in the assembly. On other hand, there is no physical contact between the current sensor and motor-driven equipment in electric monitoring so an electric monitoring is especially attractive for applications where safety is of major concern.

(ii) It has been a broadly accepted requirement that a diagnostic scheme should be non-invasive and capable of detecting faults accurately at low cost. Therefore, Motor Current Signature Analysis (MCSA) has become a widely used method because its monitoring parameter is a motor terminal quantity that is easily accessible.

(iii) The effectiveness of signal processing techniques for non-stationary signals has not been addressed appropriately in the literature. Therefore, more experiments need to be carried out with different signal processing techniques so that it may be examined which technique is best suited for non-stationary signals.

(iv) It is observed that no experimental studies have been published which may diagnose the fault of induction motors using an enhanced power

factor measurement technique. Therefore, an experimental study must be conducted to diagnose the fault with the power factor method.

(v) Numerous applications of using electric monitoring in motor health monitoring have been published among the nuclear-generation, industrial, oil industries. In published work, researchers used the variety of motors of different rating to diagnose the faults. But no work has been done to diagnose the all possible common fault of induction motor by using reconstruction vibration signal from phase current signal so, there is a need to apply Radial Basis Function networks to the reconstruction of motor vibration using measurements of one phase of the motor current.

**2.5 Summary and Motivation**

Effective maintenance of induction motors is a serious problem faced by many utilities and industries because the initial cost of buying and installing the motor is usually cost less than half of the total life cycle cost. Maintenance can present between 15 to 40 % of the total cost and in some cases can rise to 80% .

As the author has more then twelve years working in oil field with Veba oil Operations Company Libya branch the average installation period for Electrical Submersible Pumps (ESP) takes around 7 to 10 days in the normal conditions, that costs within the range between 50,000 to 100,000 US$ depends on the well depth, pump size, production rate, this cost does not include any suddenly influence in the operation of the pump repair. The most likely reasons causing ESP failures are due to: cable shorted, motor burn, pump sealed.

Having reviewed techniques used for fault diagnosis of induction motors it is concluded that accurate models of the faulty machine are necessary for efficient and

effective fault diagnosis. Sometimes it is difficult to accurately model the faulty machine and to apply model based techniques. On the other hand, soft computing approaches such as NNs and wavelet techniques can provide a good analysis of a system even if accurate models are not available.

For these reasons, focus has turned to alternative methods of vibration estimation based on easy-to measure variables. Advances in both sensors and adaptive computing technology together with increased availability of high performance signal processing, has made the use of advanced diagnostic systems possible in industrial applications. Such approaches include the use of non-parametric models such as RBF NNs.

The purpose here is to develop a technique for detecting and locating faults (assessing condition and performance) in inaccessible equipment using RBF NNs to reconstruct the vibration waveform from the measured power (single phase current). The aim of this research is to develop an innovative, non-intrusive, accurate and reliable method for the early detection and diagnosis of faults in an induction motor using an enhanced power parameter measurement technique. It is argued, and initial results suggest that it is more effective to monitor the operating power factor of the induction motor using only measured current and supplied manufacturer's data. This may help in induction motor design and development

# CHAPTER 3

# MODELLING AND SIMULATION FOR INDUCTION MOTOR FAULT DETECTION

*This chapter presents mathematical equations to describe the behaviour of the motor-driven system, and uses them to predict vibration and current in a motor driven system using the parameters for a healthy three phase induction motor, coupling and a load machine. The model's equations are solved numerically using a MatLab program to simulate the effects of rotor bar imperfections on the motor current including phase imbalance. The simulation predictions were tested against actual test rig results and found to be in good qualitative agreement.*

## 3.1 Introduction

Despite the extensive research devoted to induction motor research there still does not exist a general numerical approach capable of predicting the effect of variation in faults arising within the motor. The main objective of this chapter is to use electromechanical models to:

1. Gain a better understanding of how the induction motor train system works and to be able to observe its performance under different loading and fault conditions

2. Gain a better understanding of how motor structure and dynamics affect the vibration and motor current signatures for healthy and faulty rotor bar or power supply.

3. Compare experimental and simulation results for healthy and faulty induction motors and make an assessment of the accuracy of the simulation.

## 3.2 Modelling a Motor Driving System

Typically motor driving industrial systems consist of: an induction motor (3-phase), some form of transmission (coupling or gearbox) and a load which may be a machine, see Figure 3.1. Any model of such a system should consist of three corresponding sub-systems. Here we assume the load system to have constant torque, so that only the model of the motor requires further development.

Modelling can be seen as developing a mathematical representation of a system where the functional relationships between components of the real system can be solved for given boundary conditions and used for prediction and control [74]. Any model must be realistic, and should be simple to understand and easy to manipulate.

Electromechanical systems are usually complex and their modelling is rarely straightforward. The numerical solution of the set of equation modelling the real

system by computer ("computer simulation") is now almost universally applied to gain insight into the dynamic behaviour of electromechanical systems and has produced results that were unexpected from the available experimental or theoretical results. Using a suitable model it should be possible to simulate and predict fault development behaviour in an induction motor before ever running any experiment. Such models allow a better understanding of the system and individual component behaviour. Every model contains parameters that have to be estimated; in this case most will be based on the manufacturer's data.

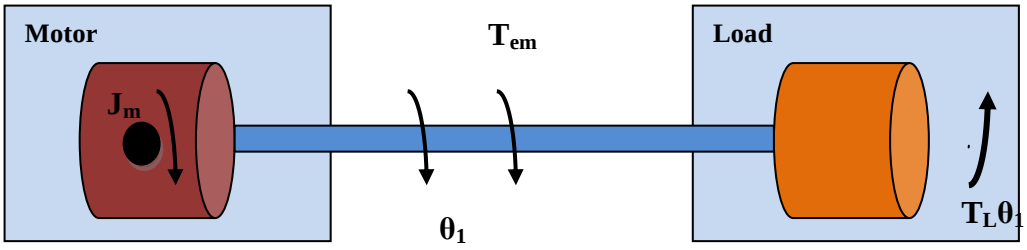


**Figure 3-1** A schematic of a motor driven system

### 3.3. Review of the Modelling of an Induction Machine

#### 3.3.1 Modelling parameters

Each system component is examined and validated separately before being integrated into the set of equations modelling all components.

To simplify the complexity of the model six initial assumptions were made[74] :

(i) the induction motor is assumed ideal and linear which means a number of factors can be ignored. These are eddy current, friction and iron losses, saturation, skin effect and windage losses,

(ii) the mains source power supply is also assumed ideal,

(iii) A stationary reference frame (see Section 3.3.3),

(iv) The three phase induction machine has a symmetrical air-gap,

(v) The mutual inductances between the stator and rotor windings are functions of the rotor position,

(vi) The self and mutual inductances between stator phases or rotor phases are constant, and (vi) the motor has uniformly distributed cage bars and the rotor bars are insulated.

A three-phase balanced system, each phase sine wave shaped, and all voltages symmetrical. The basis for the model to simulate a three-phase, P-pole, symmetrical induction machine is the winding connection induction machine shown in Figure 3.2. The values of the parameters used in the model are those of the equivalent circuit of the 3-phase asynchronous induction motor used in the real test rig.

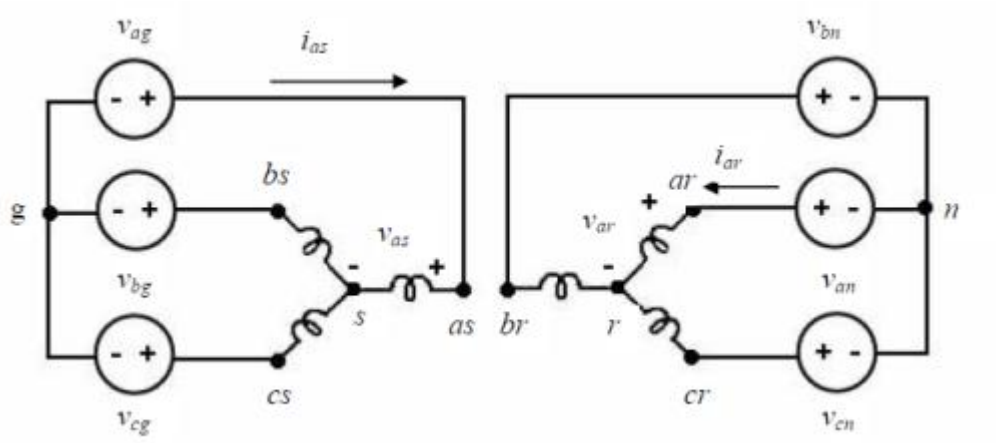


**Figure 3-2** three -phase winding connection circuit used in the model

### 3.3.2 Base quantities equations

Variables and parameters used in the model were normalized to the relevant base quantity.

Machine equations are often described in terms rate of change of flux linkage, $\psi^s$, and reactances, $X^s$, which are related by the angular frequency, $\omega_b$ , where $\omega_b = 2\pi f_{rated}$ and $f_{rated}$ is the rated frequency of the machine in Hertz[74]. For a three-phase, P-pole induction machine with rated line-to-line voltage the base quantities are peak rather than RMS values. The base voltage, impedance, electrical frequency and voltage are:

1. Base voltage

$$V_b = (\sqrt{2})(V_{rated}) \quad (3.1)$$

2. Base impedance

$$Z_b = \frac{(V_{rated})^2}{P_{rated}} \quad (3.2)$$

3. Base electrical frequency

$$\omega_b = 2\pi f_{rated} \quad (3.3)$$

4. Base torque

$$T_b = \frac{P_{rated}}{\omega_{bm}} \quad (3.4)$$

Where $\omega_{bm}$ = base mechanical frequency (Hz),

$P_{rated}$ = rated power (W),

$V_{rated}$ = rated voltage (V),

$P$ = number of pair-poles and

$f_{rated}$= machine rated frequency (Hz).

### 3.3.3 The dq0 reference frame transformation in induction motor modelling

A core concern in the development of mathematical models of electrical machines is how to represent variables such as current, voltages, and flux. Usually this is done by space vectors expressed in a particular reference frame [75]. The common approach when modelling a three-phase electric machine is to transform all variables and equations of the model from Cartesian (*abc*) axes to direct-quadrature-zero (dq0) axes, see Figure 3-3. The dq0 reference frame rotates at the frequency of the system and so this transformation is a single reference frame transformation. Thus simulations in the dq0 reference frame will be particularly efficient at or around the system frequency [75]. Figure 3-3 shows the relationship between the *abc* and the dq0 quantities of a reference frame rotating at an angular speed $\omega$ rad/s [74].

An advantage of using the dq0 reference frame for expressing three-phase equations for AC induction machine is that stator quantities are constants for balanced steady-state operation. For other modes of operation the stator quantities vary slowly with time (2-3Hz). This means faster simulation times for balanced conditions with much slower variation of other parameters than in the original Cartesian reference frame.

It is usual to begin by deriving relevant stator and rotor voltage equation in a dq0 reference frame when modelling induction motors. The chosen rotational speed will be $\omega$ rad/s in the direction of the rotor rotation. The dq0 reference frame for the induction machine stationery is obtained by setting $\omega$ to zero. The *abc* to dq0 transformation computes the direct axis, quadratic axis, and zero sequence quantities in a two-axis rotating reference frame for a three-phase sinusoidal signal.

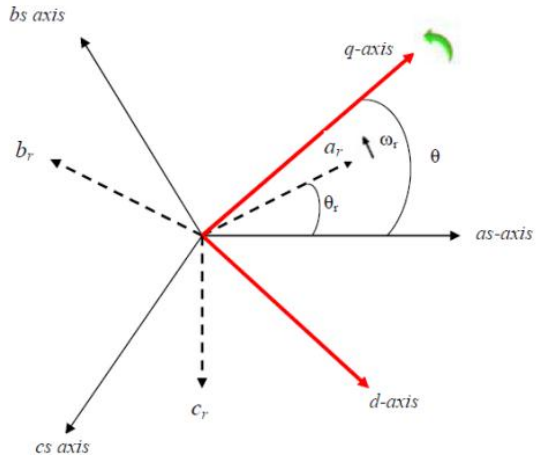


**Figure 3-3** Relation between abc and dq0 frames of reference

Equation 5 shows the transformation equations from the *abc* into the dq0 reference frame.

$$\begin{bmatrix} v_q \\ v_d \\ v_0 \end{bmatrix} = \left[T_{dq0}(\theta)\right] \begin{bmatrix} v_a \\ v_b \\ v_c \end{bmatrix} \tag{3.5}$$

Where $v$ is the phase voltage (or current or flux linkage) of the machine and the dq0 transformation matrix is given by [74]:

$$\left[T_{qd0}(\theta)\right] = \frac{2}{3}\begin{bmatrix} cos\theta & cos\left(\theta - \frac{2\pi}{3}\right) & cos\left(\theta + \frac{2\pi}{3}\right) \\ sin\theta & sin\left(\theta - \frac{2\pi}{3}\right) & sin\left(\theta + \frac{2\pi}{3}\right) \\ \frac{1}{2} & \frac{1}{2} & \frac{1}{2} \end{bmatrix} \tag{3.6}$$

### 3.3.4 Induction motor electric dynamic equations

This section presents the equations used to develop the model of a three-phase, P-pole symmetrical induction machine and explains how they were derived. The model will be used to simulate the behaviour of the given induction machine in the qd0 reference frame with winding connections as shown in Figure 3.2 [74]. We begin by

deriving the input voltage equations for neutral connections of the rotor and stator windings.

First, we write down the equations for the three-phase balanced symmetrical voltages applied to the stator terminals, see Figure 3.2 [74]:

$$v_{as} = \sqrt{2}V_{rated}cos\theta$$

$$v_{bs} = \sqrt{2}V_{rated}cos\left(\theta - \frac{2\pi}{3}\right) \quad (3.7)$$

$$v_{cs} = \sqrt{2}V_{rated}cos\left(\theta + \frac{2\pi}{3}\right)$$

Next Equation (3.7) need to be re-written in with respect to the system reference point 'g' in Figure 3.2, as follows [74]:

$$v_{as} = v_{ag} - v_{sg}$$

$$v_{bs} = v_{bg} - v_{sg} \quad (3.8)$$

$$v_{cs} = v_{cg} - v_{sg}$$

From Equation 3.8, the dq0 stationery voltages $v_{qs}^{s}$ , $v_{ds}^{s}$ , $v_{os}^{s}$ can be expressed as

$$v_{qs}^{s} = \frac{2}{3}v_{ag} - \frac{1}{3}v_{bg} - \frac{1}{3}v_{cg} - v_{sg}$$

$$v_{ds}^{s} = \frac{1}{\sqrt{3}}(v_{cg} - v_{bg}) \quad (3.9)$$

$$v_{0s}^{s} = \frac{1}{3}\left(v_{ag} + v_{bg} + v_{cg}\right) - v_{sg}$$

Given symmetrical, sinusoidal and balanced applied voltages $v_{sg}$ can be considered zero because the neutral current will be zero [74].

Correspond transformation of the rotor winding voltages from the *abc* frame to the stationary dq0 reference frame stator quantities gives Equation 3.10 [74] where the prime denotes values referred to the stator:

$$v_{qr}^{\prime r} = \frac{2}{3}v_{an}^{\prime} - \frac{1}{3}v_{bn}^{\prime} - \frac{1}{3}v_{cn}^{\prime} - v_{rn}^{\prime}$$

$$v_{dr}^{\prime r} = {}^{1}/_{\sqrt{3}}(v_{cn}^{\prime} - v_{bn}^{\prime}) \quad (3.10)$$

$$v_{0r}^{\prime} = \frac{1}{3}\left(v_{an}^{\prime} + v_{bn}^{\prime} + v_{cn}^{\prime}\right) - v_{rn}^{\prime}$$

Where $v_{rn}^{\prime}$ is the voltage between points r and n in Figure 3.2.

The dq0 rotor quantities in Equation 3.10 can be transformed rotationally into the same stationary dq0 frame for the stator quantities using Equation 3.11[74] .

$$v_{qr}^{\prime s} = v_{qr}^{\prime r}cos\theta_r(t) + v_{dr}^{\prime r}sin\theta_r(t)$$

$$v_{dr}^{\prime s} = -v_{qr}^{\prime r}sin\theta_r(t) + v_{dr}^{\prime r}cos\theta_r(t) \quad (3.11)$$

Using Equations 3.10 and 3.11 gives the first transformation of the rotor voltages in the dq0 reference frame. It can be seen that these voltage are similar to those of the stator voltages.

To link rotor and stator voltages in the dq0 stationary reference frame to the current in the induction motor - which is the parameter of most concern in this thesis - Equations 3.10 and 3.11 are re-written in term of the rate of change of flux linkage at the base frequency (see Equation 3.3), and all zero sequence equations are disabled since the operation condition is balanced [74]. Equations 3.12 – 3.15 give rotor and stator voltages as a function of the rate of change of flux linkage and current. The dq0 voltages at both rotor and the stator terminals are referred to the same stationery dq0 reference frame.

$$v_{qs}^{s} = \frac{P}{\omega_b}\psi_{qs}^{s} + r_s i_{qs}^{s} \quad (3.12)$$

$$v_{ds}^{s} = \frac{P}{\omega_b}\psi_{ds}^{s} + r_s i_{ds}^{s} \quad (3.13)$$

$$v_{qr}^{'s} = \frac{P}{\omega_b}\psi_{qr}^{'s} - \frac{\omega_r}{\omega_b}\psi_{dr}^{'s} + r_r^{'} i_{qr}^{'s} \tag{3.14}$$

$$v_{dr}^{'s} = \frac{P}{\omega_b}\psi_{dr}^{'s} + \frac{\omega_r}{\omega_b}\psi_{qr}^{'s} + r_r^{'} i_{dr}^{'s} \tag{3.15}$$

The electromechanical torque is given by Equations 3.16 and 3.17:

$$T_{em} = \frac{3}{2}\frac{P}{2\omega_b}\left(\psi_{ds}^{s} i_{qs}^{s} - \psi_{qs}^{s} i_{ds}^{s}\right) \tag{3.16}$$

$$T_{em} = \frac{3}{2}\frac{P}{2\omega_b} x_m\left(i_{dr}^{'s} i_{qs}^{s} - i_{qr}^{'s} i_{ds}^{s}\right) \tag{3.17}$$

Equations 3.18 – 3.25 give rotor and stator currents and flux linkage in the dq0 reference frame for the case of a symmetrical induction motor [74]:

$$\psi_{qs}^{s} = x_{ls} i_{qs}^{s} + \psi_{mq}^{s} \tag{3.18}$$

$$\psi_{ds}^{s} = x_{ls} i_{ds}^{s} + \psi_{md}^{s} \tag{3.19}$$

$$\psi_{qr}^{'s} = x_{lr}^{'} i_{qr}^{'s} + \psi_{mq}^{s} \tag{3.20}$$

$$\psi_{dr}^{'} = x_{lr}^{'} i_{dr}^{'} + \psi_{mq} \tag{3.21}$$

$$i_{qs}^{s} = \frac{1}{X_{ls}}(\psi_{qs}^{s} - \psi_{mq}^{s}) \tag{3.22}$$

$$i_{ds}^{s} = \frac{1}{X_{ls}}(\psi_{ds}^{s} - \psi_{mq}^{s}) \tag{3.23}$$

$$i_{ds}^{'s} = \frac{1}{X_{lr}^{'}}(\psi_{qs}^{'s} - \psi_{mq}^{s}) \tag{3.24}$$

$$i_{dr}^{'s} = \frac{1}{X_{lr}^{'}}(\psi_{qr}^{'s} - \psi_{mq}^{s}) \tag{3.25}$$

Equations 3.12 – 3.25 can all be used as inputs to the simulation equations for the induction motor to obtain the corresponding dq0 currents [74].

### 3.4 Mechanical dynamic equations

The equations of motion of the mechanical system can be written with two degrees of freedom. The dynamic characteristics of the rotor and the load can be written as function of the electromechanical torque supplied by the induction motor ($T_{em}$), the torque due to the load ($T_L$) as in in Equations 3.26 – 3.27:

$$J_m\ddot{\theta_1} + k(\theta 1 - \theta 2) = T_{em} \quad (3.26)$$

$$J_L\ddot{\theta_2} + k(\theta 2 - \theta 1) = T_L \quad (3.27)$$

Where $J_m$ is the moment of inertia of the motor and associated components and $J_L$ is the total moment of inertia of the load, and $\ddot{\theta_\iota}, \dot{\theta_\iota}\ \theta$ are the angular acceleration, velocity and displacement respectively for the two rotational shafts of motor and load It can be seen from Equations 3.16, 3.17, 3.22 – 3.25, 3.26 and 3.27 that torque and speed govern the connection between the motor current and the mechanical behaviour of the system.

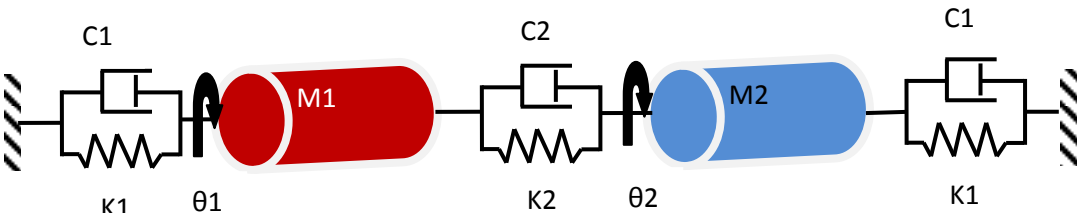


**Figure 3-4** Schematic diagram of model

## 3.5 Simulation of stator and rotor faults

### 3.5.1 Simulation of asymmetric stator fault in a 3-phase induction motor

The seeded asymmetric stator faults are unbalanced stator phase voltages. This is simulated in Equation 3.7 where an unbalanced voltage drop E is input to one phase:

$$v_{as} = \sqrt{2}(V_{rated} - E)cos\theta$$

$$v_{bs} = \sqrt{2}V_{rated}cos\left(\theta - \frac{2\pi}{3}\right) \quad (3.28)$$

$$v_{cs} = \sqrt{2}V_{rated}cos\left(\theta + \frac{2\pi}{3}\right)$$

The vibration response due to resulting variation in the electromechanical torque will be given by Equations 3.26 and 3.27.

### 3.5.2 Simulation of a broken rotor bar in a 3-phase induction motor

To simulate a broken rotor bar fault in a three-phase induction motor, the relevant simulation equations for unbalanced stator phase voltage were modified by changing each rotor bar's inductance and resistance.

#### *3.5.2.1 Vibration system response*

The mass, M, of the healthy rotor is assumed concentrated on the central axis between the supported bearings, the unhealthy bearing with a hole drilled in one or more rotor bars will have an unbalanced eccentric mass ($m_0$) located at a radial distance *r* rotating at the same angular speed, $\omega$, as the rotor.

The centrifugal force ($F_f$) due to $m_o$ which causes the vertical vibration force measured by the accelerometer at the base is simulated in Equation 3.29

$$F_f = m_0 r\omega^2 \sin(\omega t) \quad (3.29)$$

### 3.6 Induction Motor Simulation and Model Validation

The numerical simulation was run using a MatLab software package and the results are presented in Figures 3.5 to 3.10 which show rotor speed, variation in motor speed, motor stator phase currents, stator phase A current, stator phase B current and stator phase C current respectively. The motor starts from standstill and reaches a steady maximum speed of about 1475 rev/min when the load torque is 1.1 kW.

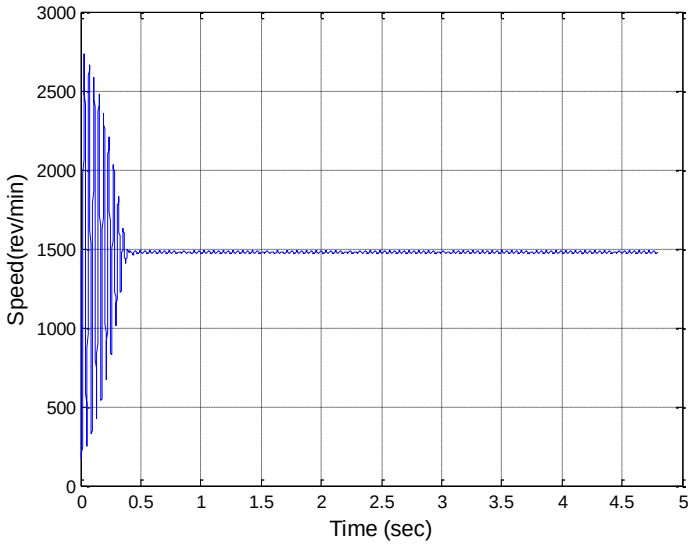


**Figure 3-5** Simulated rotor speed during start-up and steady-state for a healthy motor

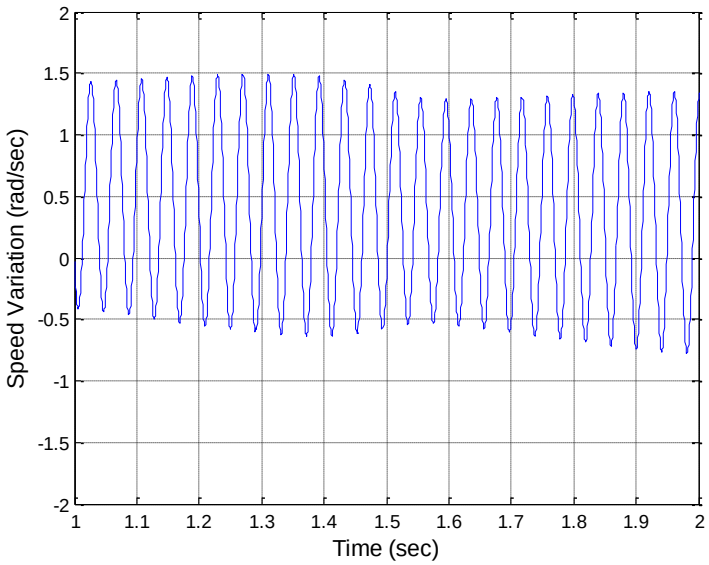


**Figure 3-6** Simulated variation speed of healthy induction motor

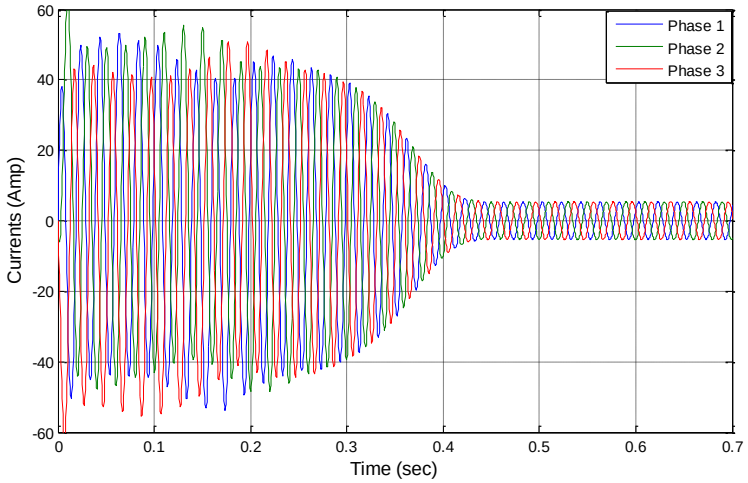


**Figure 3-7** Simulated stator phases current during start-up and steady-state for a healthy motor

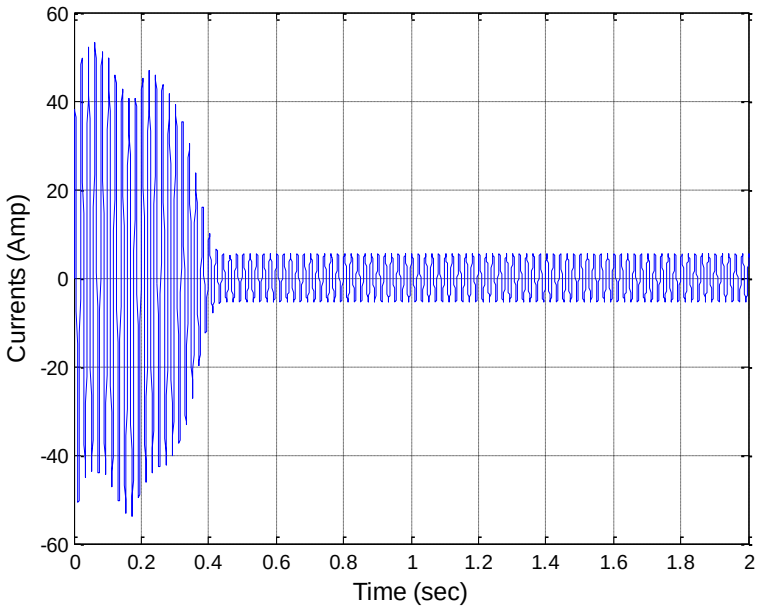


**Figure 3-8** Simulated stator phase A current during start-up and steady-state for a healthy motor

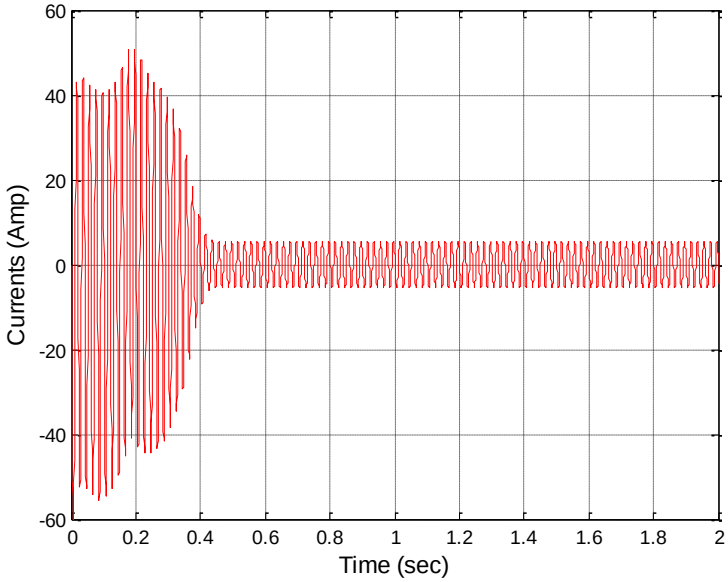


**Figure 3-9** Simulated stator phase B current during start-up and steady-state for a healthy motor

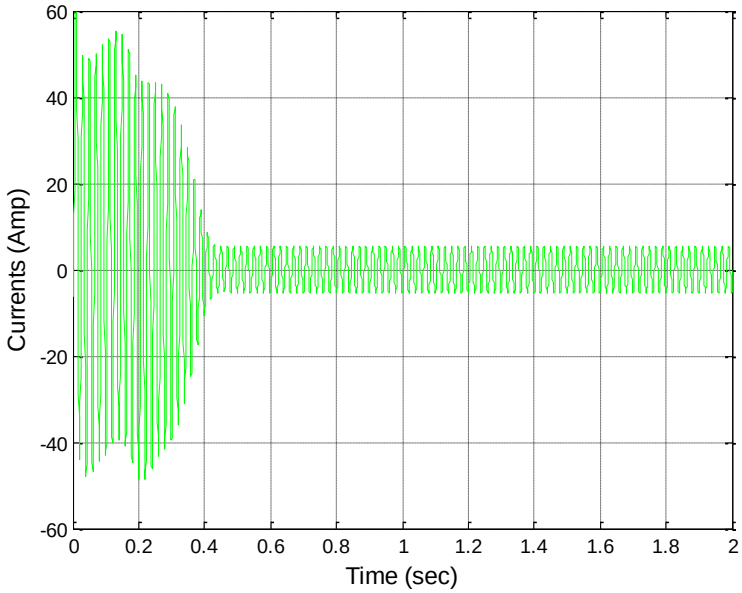


**Figure 3-10** Simulated stator phase C current during start-up and steady-state for a healthy motor

Figure 3.7 shows the three stator phase currents as a function of time during start up under full load for the induction motor. Initially the amplitude of the current is much larger than the final (rated) current until the machine reaches its normal speed. This is because the inertial of the machine has to be overcome and the rotor accelerated to

its operating speed. At synchronous speed the motor draws only sufficient current to overcome frictional and electrical power losses in the windings [75]. Their frequencies are essentially constant at 24.6 Hz (rotational speed) and 50 Hz (power supply frequency) as shown in Figures 3.11 and 3.12.

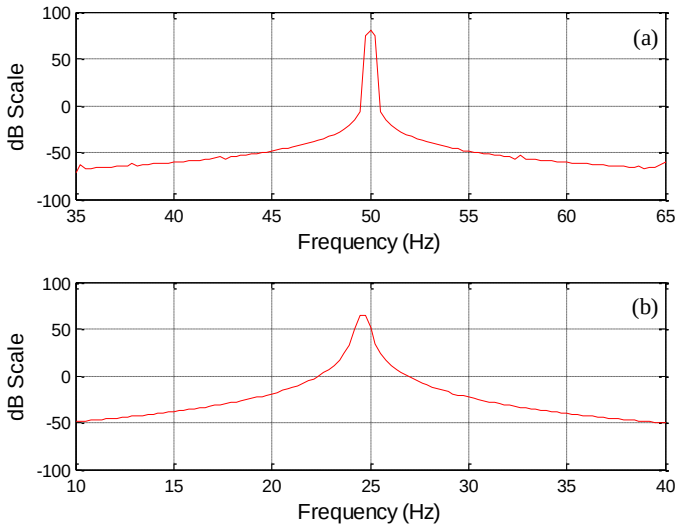


**Figure 3-11** Frequency domain of simulated healthy stator phase A current during start-up (a) steady-state (b) at full load

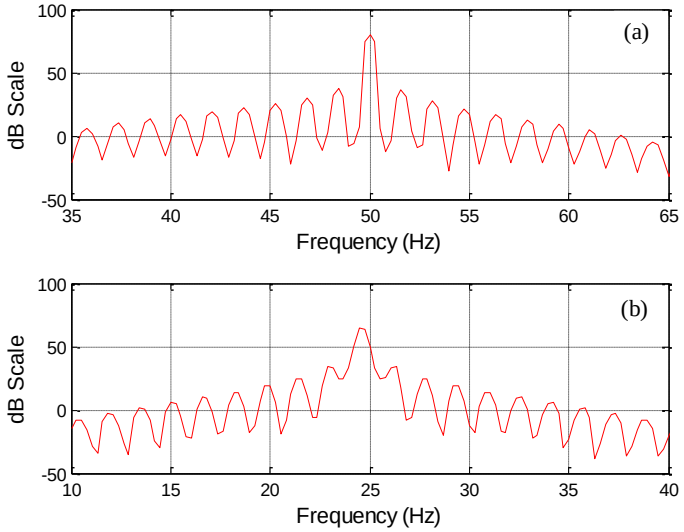


**Figure 3-12** Frequency domain of simulated one rotor bar broken stator phase A current during start-up (a) steady-state (b) at full load

The graph in Figure 3.13 shows the electromagnetic torque from initial power-up to steady state. Initially the torque is oscillatory, very similar to that for a system with near critical damping, even with a balanced three phase supply.

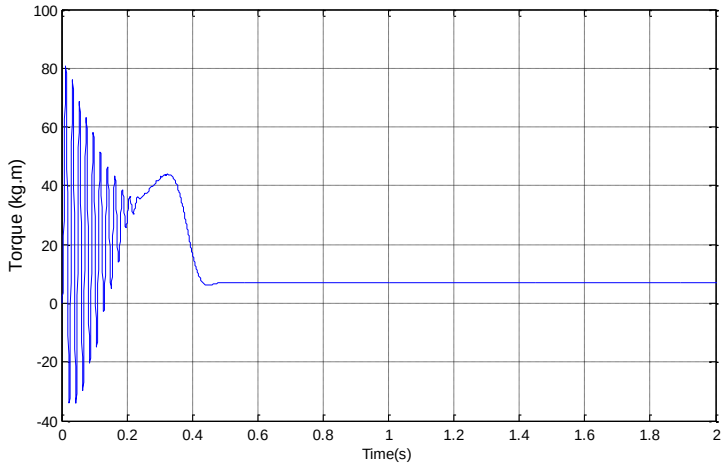


**Figure 3-13** Simulated electromagnetic torque for a healthy motor

To investigate the dynamic mechanical characteristics of the model of the induction motor, a sinusoidal load fluctuation was introduced:

$$T_L = T_b(0.79 + \mathrm{a}\sin(2\pi f_{r1}t + \varphi_1) + b\sin(2\pi f_{r2}t + \varphi_2)) \qquad (3.30)$$

Where $f_{r1}$ and $f_{r2}$ are the frequencies of rotation of motor shaft and loader shaft respectively. The factor of 0.79 is introduced so that the simulated torque remains less than the actual value of the motor torque. The constants *a* and *b* allow the degree of fluctuation of $T_L$ to be to whatever percentage of the full load ($T_b$) is required. The load fluctuations are introduced to both shafts because the fluctuation of the load shaft is always transmitted to the motor shaft.

Figure 3.14 shows the simulated motor current spectrum when the load was kept constant at near full load with no load fluctuation. Obviously the spectrum is dominated by a peak at the 50 Hz main supply frequency.

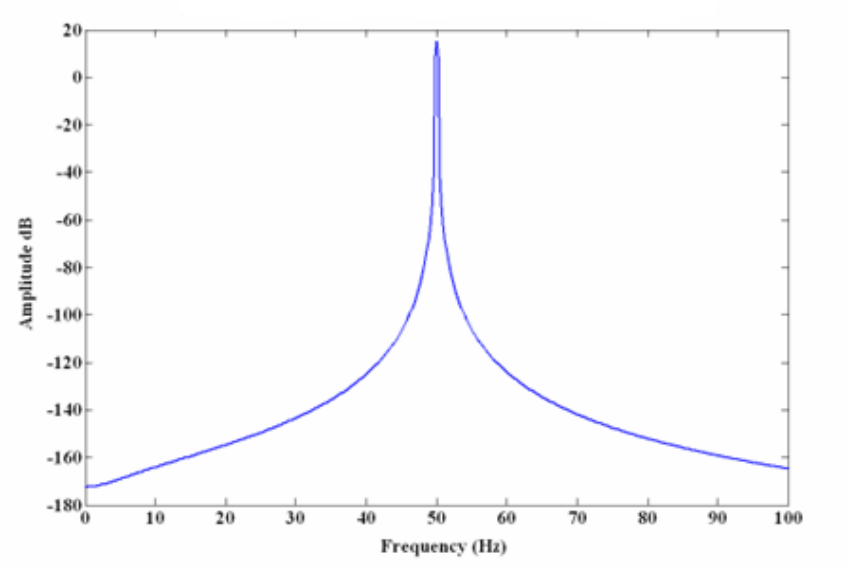


**Figure 3-14** Simulated ideal current spectrum with no load fluctuation healthy motor

However, when a load fluctuation is introduced the current spectrum undergoes a dramatic change and sidebands appear both sides of the 50Hz peak, see Figure 3.15. These sidebands clearly demonstrate that the current is being modulated by the load fluctuation. The spectrum in Figure 3.15 exhibits symmetrical sidebands at motor and load shaft rotational speeds and their harmonics at 12 Hz**,** 24.60 Hz, 50 Hz, 72.80 Hz and 98.40 Hz. This shows that the modulation of motor current signal is not only from the individual rotation speed but also from the speed combination of the two shafts.

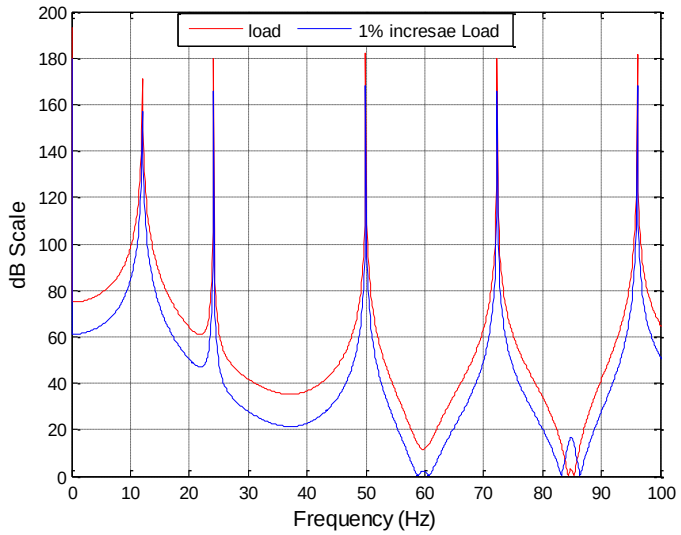


**Figure 3-15** Simulated stator current spectrum with load fluctuation healthy motor

Figure 3.15 shows clearly the effect of different values of the amplitude parameter $T_b$ on the motor current spectrum as the load fluctuates (Equation 3.30). An increase in the fluctuating load equivalent to 1% of the full load (*Tb*) of the fluctuating produces an increase of approximately 20 dB in the amplitude of the sidebands (red dashed lines) in Figure 3.15. In addition higher harmonic sidebands are also generated in the spectrum (1.21 Hz, 98.80 Hz) as a result of this increase in the load fluctuation.

## 3.7 Effect of Vibration Signal Modulation on the Motor Current Spectrum

This section investigates the effect of radial and torsional vibration on the motor current spectrum, and examines the suggestion that the main sources of the induced sidebands in the motor current spectrum are amplitude and frequency modulation [75].

### 3.7.1 The effect of radial motor vibration

This sub-section explores the modulation of motor current due to dynamic changes in the radial forces caused by rotor bar faults. The carrier and the modulation signals are assumed to be initially sinusoidal, and the instantaneous motor current is:

$$i(t) = \sqrt{2}I_0[\cos(2\pi f_0)\, t - \varphi] \quad (3.31)$$

Where $f_0$ is the frequency (Hz) of the current $\varphi$ is the phase angle **3** and $I_0$ RMS amplitude of the current (A).

If only the signal amplitude is considered, the author may assume that the phase of the carrier signal is zero, hence $\varphi$ in Equation 3.31 can be neglected and *i(t)* can be written as:

$$i(t) = \sqrt{2}I_0[\cos(2\pi f_0)\, t] \quad (3.32)$$

Due to dynamic changes in the radial forces caused by abnormal conditions Equation 3.32 will be modulated by a signal *m(t)* which may contain more than one modulating frequency and may be described mathematically as:

$$m(t) = B_s \sum_{n=1}^{k} m_{rn} \cos(2\pi f_{rn})\, t \quad (3.33)$$

Where $f_{rn}$ is the nth modulating frequency (Hz), $m_{rn}$ is the nth modulation index, $B_s$ is the amplitude of the modulating signal, *n* is the $n^{th}$ harmonic, and k is the number of rotating shafts.

The amplitude of the modulated motor current signal can be written as:

$$i(t)_{Am} = i(t)[1 + B_s \sum_{n=1}^{k} m_{rn} \cos(2\pi f_{rn})\, t] \quad (3.34)$$

Equation 3.34 may be separated into two parts; the first part consisting only of the main carrier frequency *f0*, and the second part representing the amplitude modulated motor current signal:

$$i(t)_{Am} = \sqrt{2}I_0[\cos(2\pi f_0)\, t] + \sqrt{2}I_0[\cos(2\pi f_0)\, t][B_s \sum_{n=1}^{k} m_{rn} \cos(2\pi f_{rn})\, t] \quad (3.35)$$

Using the elementary trigonometric identity $cosA\ cosB = \frac{1}{2}[\cos(A+B) + \cos(A-B)]$ Equation 3.35 may be written as:

$$i(t)_{Am} =$$

$$(B_s[m_{r1}\cos(2\pi f_{r1})\,t + m_{r2}\cos(2\pi f_{r2})\,t + m_{r3}\cos(2\pi f_{r3})\,t])\sqrt{2}I_0\cos(2\pi f_0)\,t \quad (3.36)$$

$$i(t)_{Am} = \frac{B_s I_0 m_{r1}}{\sqrt{2}}[cos2\pi(f_0 + f_{r1})t + cos2\pi(f_0 - f_{r1})t] + \frac{B_s I_0 m_{r2}}{\sqrt{2}}[cos2\pi(f_0 + f_{r2})t + cos2\pi(f_0 - f_{r2})t] + \frac{B_s I_0 m_{r3}}{\sqrt{2}}[cos2\pi(f_0 + f_{r3})t + cos2\pi(f_0 - f_{r3})t] \quad (3.37)$$

Where $m_{r1} = \frac{I_{mr1}}{I_0}$ , $m_{r2} = \frac{I_{mr2}}{I_0}$ and $m_{r3} = \frac{I_{mr3}}{I_0}$ are the modulation indices.

Equation 3.37 shows the presence of six sidebands at sum and differences of the main line frequency, $f_0$, and the three different rotational speed frequencies $f_{r1}$, $f_{r2}$ and $f_{r3}$). These frequency components are:

$$(f_0 + f_{r1})\,, (f_0 - f_{r1}), (f_0 + f_{r2}), (f_0 - f_{r2}), (f_0 + f_{r3}), \text{and } (f_0 - f_{r3})$$

Additional sidebands will be induced in the motor current spectrum due to rotor oscillations of the broken bar. If S is the motor slip frequency.

$$f_{2s} = f_0(1 \pm 2S) \quad (3.38)$$

### 3.7.2 The effect of the motor torsional vibration

Under normal operating conditions the shaft speed is assumed constant. A fault in a rotor bar will, however, initiate a change in the tangential transmitted force, *Ft*, for that individual bar. This will appear as a load fluctuation that produces torsional vibration of the rotor as a whole, which leads to a cyclic change in the shaft rotational speed and creates a shaft oscillation [75]. The stator current is modulated at this oscillation frequency to a degree which determined by the inter-relations within the electro-mechanical system, and the induction motor's electrical and electromagnetic characteristics [75]. A steady state equivalent circuit for the

induction motor was assumed and the stator current spectrum predicted for broken rotor bar faults [75].

In this section the steady state assumption for the equivalent circuit of the induction motor has been used to derive the motor current spectrum with variation of motor speed. It is assumed that the supply is sinusoidal at frequency 50 Hz and the motor runs under steady state conditions. The equivalent circuit is simplified and includes only the slip dependent rotor resistance. Under healthy operation the rotor shaft speed is considered constant and of an average value, but with introduction of the fault the instantaneous speed will be the sum of the average value plus an oscillating component [75].

Figure 3.16 shows the simplified equivalent circuit of the induction motor. For the induction motor running at constant speed supplied with a purely sinusoidal voltage in the form:

$$v(t) = V_m sin\omega_0(t) \qquad (3.39)$$

Where $V_m$ = Peak supply voltage (volt), $\omega_0 = 2\pi f_0$ angular frequency (rad/s) and $f_0$ = frequency of the main supply (Hz).

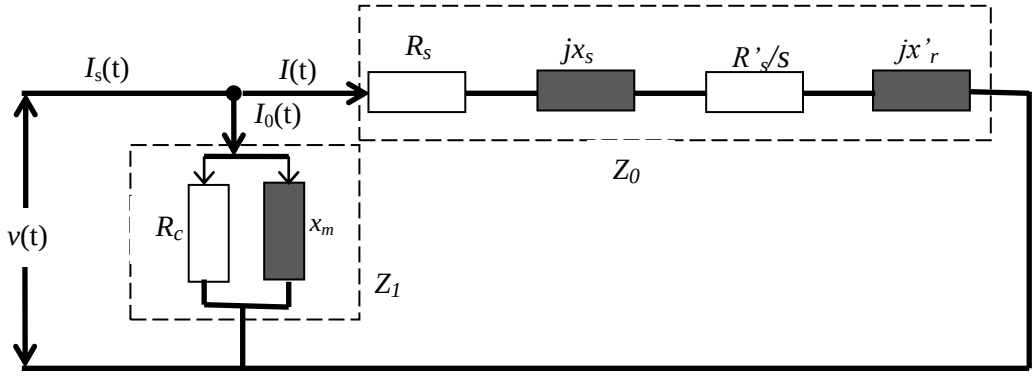


**Figure 3-16** Simplified equivalent circuit of the induction motor

The aim here is to investigate the effect of rotor speed variation on the motor current spectrum in the presence of a motor fault, so the stator current is given in terms of the motor rotor slip. Applying Kirchhoff's laws to the circuit node A:

$$i_s(t) = i_0(t) + i(t) \tag{3.40}$$

Where $i_s(t)$ = total current (A), $i_0(t)$ = magnetization current (A) and $i(t)$ = stator current producing the torque (A).

Applying Ohm's law to the circuit in Figure 3.16, with the assumption that all higher harmonic are negligible we obtain: $i_0(t) = \frac{v(t)}{Z_1}$ and i$(t) = \frac{v(t)}{Z_0}$ . The stator current Equation 3.40 can now be expressed as:

$$i_s(t) = \frac{v(t)}{\frac{(R_c)(jx_m)}{(R_c + jx_m)}} + \frac{v(t)}{\left(R_s + \frac{R'_r}{s}\right) + j(x_s + x'_r)} \tag{3.41}$$

Where Z = $R_m$ // $jx_m$ is the magnetising impedance (Ω)

Substituting $v(t) = V_m sin\omega_0(t)$ in Equation 3.41 and expressing rotor impedance as $j(x_s + x'_r)$ and stator impedance as $\left(R_s + \frac{R'_r}{s}\right)$ gives:

$$i_s(t) = \frac{V_m sin\omega_0(t)}{\frac{(R_c)(jx_m)}{(R_c + jx_m)}} + \frac{V_m sin\omega_0(t)}{\left(R_s + \frac{R'_r}{s}\right) + j(x_s + x'_r)} \tag{3.42}$$

### 3.7.3 Angular Speed Oscillation

For the healthy motor we assume the rotational frequency of the rotor, $\omega_0(t)$, is constant, and $\omega_r = \omega_a$. Hence the motor slip, S, is constant:

$$S = \frac{\omega_s - \omega_r}{\omega_s} \tag{3.43}$$

However, the presence of a faulty rotor bar will cause the angular speed of the drive shaft to oscillate and thus induction motor slip becomes time varying, and the shaft rotational frequency will consist of an average value $\omega_a$ plus a superimposed

oscillation, $V_c sin\omega_c t$. More precisely this superimposed oscillation will have an impulsive component which occurs once per revolution, thus the sinusoidal terms is only an approximation for the purpose of this investigation. The superimposed oscillation will induce specific components into the stator current spectrum.

Given the sinusoidal approximation the rotor speed, $\omega_r(t), is$ be expressed as:

$$\omega_r(t) = \omega_a + V_c sin\omega_c t \tag{3.44}$$

The shaft speed is now a function of time with an oscillating component of frequency, fc. Substituting Equation 3.44 into Equation 3.43 gives S as a function of time

$$S(t) = \frac{\omega_s - (\omega_a + V_c sin\omega_c t)}{\omega_s} \tag{3.45}$$

Substituting Equation 3.45 into Equation 3.41 gives the stator current $i_s(t)$ as function of $\omega_a$, $\omega_c$, $\omega_0$ and $\omega_s$ :

$$i_s(t) = \frac{V_m sin\omega_0 t}{Z_1} + \frac{V_m sin\omega_0 t}{\left(R_s + \frac{\omega_s R'_r}{(\omega_s - (\omega_a + V_c sin\omega_c))}\right) + j(x_s + x'_r)} \tag{3.46}$$

Re-arranging Equation 3.46 we obtain:

$$i_s(t) = \frac{V_m sin\omega_0 t}{Z_1} + \frac{V_m sin\omega_0 t(\omega_s - (\omega_a + V_c sin\omega_c t))}{(R_s(\omega_s - (\omega_a + V_c sin\omega_c t)) + j(x_s + x'_r)(\omega_s - (\omega_a + V_c sin\omega_c t))} \tag{3.47}$$

Equation 3.47 can be regarded as the sum of two terms, the first of which is not a function of slip, represents the steady state condition and so will not be affected fluctuations in the angular speed. The second term represents the effects of fluctuations in the angular speed and is a function of slip. The magnitude of the oscillation in angular speed is predicted to be very much less than the magnitude of the average rotational speed, $\omega_a$ Also the term $V_c sin\omega_c t$ in the denominator of the

second term in Equation 3.47 is considered negligible with respect to $\omega_a$ [75]. Hence $i_s(t)$ can be written as:

$$i_s(t) = \frac{V_m sin\omega_0 t}{Z_1} + \frac{V_m sin\omega_0 t(\omega_s - \omega_a - V_c sin\omega_c t)}{[(R_s(\omega_s - \omega_a) + R_r'(\omega_s)] + j(x_s + x_r')(\omega_s - \omega_a)} \quad (3.48)$$

For convenience let $Z' = [(R_s(\omega_s - \omega_a) + R_r'(\omega_s)] + j(x_s + x_r')(\omega_s - \omega_a)$

$$i_s(t) = \frac{V_m sin\omega_0 t}{Z_1} + \frac{(\omega_s - \omega_a) V_m sin\omega_0 t}{Z'} - \frac{V_m sin\omega_0 t(V_c sin\omega_c t)}{Z'} \quad (3.49)$$

### 3.7.4 .Spectral sidebands induced by angular speed oscillation

The third term in the expression for $i_s(t)$ (Equation 3.49) can be re-written using the trigonometric identity already used above. Also $\omega_0$ replacing by $2\pi f_0$ and $\omega_c$ by $2\pi f_c$ gives Equation 3.50 which shows location of sidebands in the frequency spectrum.

$$\frac{V_m sin\omega_0 t(V_c sin\omega_c t)}{Z'} = \frac{\frac{V_c V_m}{2}[cos2\pi(f_0 - f_c) - cos2\pi(f_0 + f_c)}{Z'} \quad (3.50)$$

It is clear from Equation 3.50 that sidebands are predicted at spectral locations $f_0 \pm f_c$, showing that the motor current is modulated at oscillation frequency $f_c$, due to the variation in the angular speed.

## 3.8 Summary

This chapter introduces the theory and illustrates the dynamic modelling for induction motor test rig vibration and current behaviour as well as different kinds of faults. The modelling includes a vibration generation from electric motor and output load as well. It provide the effect of vibration signal modulation on the motor current and how the phase current related and relation with vibration signal at specific frequency band. Based on this relationship the reconstruction of vibration signal from phase current of induction motor will full study in following chapters.

# CHAPTER 4

# EXPERIMENTAL TEST RIG, FAULT SIMULATION AND INSTRUMENTATION

*This chapter provides information about the test rig and three phase induction motor used in the experiment. It then briefly explains how the local faults were simulated. Finally, it describes the instrumentation for measuring both vibration and current signals and how the data was collected.*

## 4.1 Introduction

In order to establish a relationship between phase current and vibration signal, experimental work was conducted on the test rig as had originally been designed and used to monitor the health of a three phase induction motor using traditional techniques of vibration and phase current monitoring. The aim of the experiment was to introduce the seeding of known and controllable faults into a three phase induction motor under normal operating conditions in order to detect and correlate fault condition indices with realistic fault data.

## 4.2 Outline of the Test Facility

For the reasons given in Section 4.1, a low-voltage three phase induction motor test facility was constructed (Figures 4.1 and 4.2). It allowed the testing of 1.1 kW, three phase induction motor (Figure 4.1), which could be quickly and easily replaced as necessary, under repeatable and wholly realistic operating conditions. The mounted induction motor was directly coupled with a loading DC generator. The rotor of the generator was connected to an electrical loading bank so that the electrical energy generated could be dissipated as heat. The load could be set at 0%, 25%, 50%, 75% or 100% of the maximum rated load - based on the output torque – by switching-in different resistor combinations within the electrical loading bank whilst the rig was online

Figures 4.1 and 4.2 show the three-phase induction motor and a schematic diagram of the test facility. In the interest of safety, a detailed risk assessment on the use of the test facility was produced along with comprehensive operating instructions.

**Figure 4-1** Three-phase induction motor

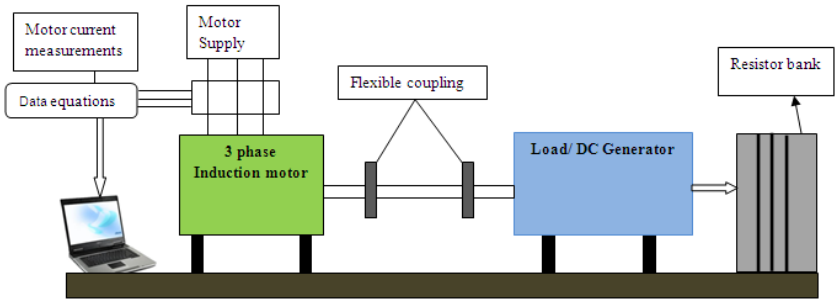


**Figure 4-2** Schematic of experimental set-up

Details of the induction motors placed into the test facility are presented in Table 4.1. Two motors was used one for healthy and other one was used to simulate rotor bar broken fault condition**.**

**Table 4-1** Test Motor Specification

| Parameter | Value |
|---|---|
| Number of phases | 3 |
| Number of poles | 4 Poles |
| Supply voltage | 220 V |
| Supply current (at full load) | 4.1 A |
| Rated power | 1.1 kW |
| Rated speed | 1475 rpm |
| Number of stator slots | 36 |
| Number of rotor bars | 28 |

### 4.3 Seeded Faults

Two fault conditions were seeded into the test facility. Each of the faults could be carefully controlled, varied in severity (for some faults this could be achieved online) and implemented over a range of load conditions.

#### 4.3.1 Seeded Phase Imbalance Faults

The first seeded fault condition was phase imbalance. In an ideal case, a three-phase balanced power supply can be represented by three equal magnitude voltage phasors spaced at exactly $120^0$. However, in practice, two main types of imbalance may be found in three-phase networks: structural and functional.

Pierrat and Morrison [76] state that, for economic reasons, the physical structure of transformers and especially power lines is not balanced. This leads to unbalanced voltage phasors even if the generator voltages and load currents are perfectly balanced. This type of imbalance is referred to as structural and its value is virtually constant (provided the network infrastructure does not change) and is referred to as quasi-deterministic. The amount of structural imbalance may be compounded by poor power management from the nearest substation. For example, the single-phase lighting in a large building may be powered unevenly from one phase, or power demands may not have been considered appropriately in the extension of a building.

Functional imbalance is due to fluctuations of consumer demand on the three-phase supply. This type of imbalance may have cyclic variation but is frequently random[76] . Large machines, such as a large motor or an arc welder, are particular causes of this type of imbalance because of their high current demands. In such instances, if the pull of current is more than the supply can provide, in an attempt to maintain power requirement, the voltage level will drop.

Alternatively, the increased resistance at a bad electrical connection, due to dirt, oxidation or even a loose connection, will result in increased voltage drop over that connection, and will correspondingly reduce the voltage over the motor windings. This is illustrated in Figure 4.3 by a bad connection of the red phase to the terminal block. Leakage current-to-earth faults in the local supply loop (ie between the machine and the nearest substation) may also lead to phase imbalance because of the loss of potential by the earth path.

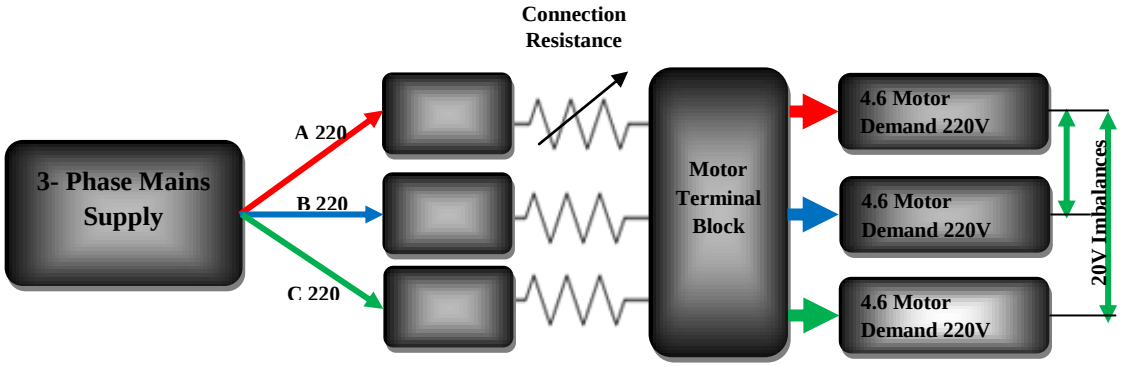


**Figure 4-3** Schematic of voltage imbalance due to a bad electrical connection

The motor test rig allowed for controlled imbalances to be induced by dropping the voltage on one phase by change the external resistance

The effect of power supply imbalance on a motor is to introduce negative sequence components (components of rotating magnetic field in the reverse direction to the main field [76]. Such components result in additional losses and overheating [76]. A small amount of imbalance will cause an increase in the winding temperature by a large amount. As a rule of thumb the temperature rises by 25% (in $^{0}$C) for every 3.5% voltage imbalance [77]. Several industrial maintenance engineers have reported to the author that phase imbalance is thus sometimes the cause of apparently random overheating of electric machines. Temperature rise causes thermal aging and makes the winding insulation, in particular, vulnerable to electrical, mechanical and

environmental stresses. It is estimated that for every $10^0$C rise in temperature the insulation life is halved [77].

Motors are designed in accordance with the NEMA standard MG 2-2001 to operate with a 10% voltage variation [10]. However, this design characteristic is based on no load operation; the introduction of shaft loading severely affects motor tolerance of imbalance. For example, a motor in the test rig will operate without noticeable impediment for an imbalance of 8.3% at zero-load, but when full load is applied the progressive heat build-up results in the motor tripping out (due to its inbuilt thermistor protection) after approximately 90 minutes of operation. In a critical industrial application and without adequate condition monitoring this would mean not only an unplanned stoppage but also that downtime would be incurred whilst the motor cooled sufficiently to recommence operation. Heat from the 3 kW motor in the test rig is dissipated only by natural convection and the motor requires longer than an hour before it can be operated following an overheat trip. The required cooling time could be much longer for larger motors and those which operate in hot and enclosed locations.

Voltage imbalance is compounded by the use of three-phase variable speed controllers, since some of the more common controllers on the market only have typical imbalance accuracies of 3% (7.2 V for the 240 V UK power supply) [10].

### 4.3.2 Seeded Broken Rotor Bar Faults

The second fault was seeded directly into the motor, this was a broken rotor bar. Induction motor failure through broken rotor bars, initiated by cracking in the rotor conductors, is common in many industrial applications. One of the reasons for this is that the large starting currents occur when the motor is relatively cold - this results in

thermal and mechanical stresses being a maximum. Therefore, the incidence of this failure mode is greatest when the start-up time is relatively long and when frequent starts are required as part of a heavy duty cycle. Figure 4.4 illustrates a typical squirrel cage rotor (from one of the 1.1 kW test motors). Figures 4.4 illustrates how a full broken bar were physically seeded by drilling through one of the aluminium conductors that make up the "squirrel cage".

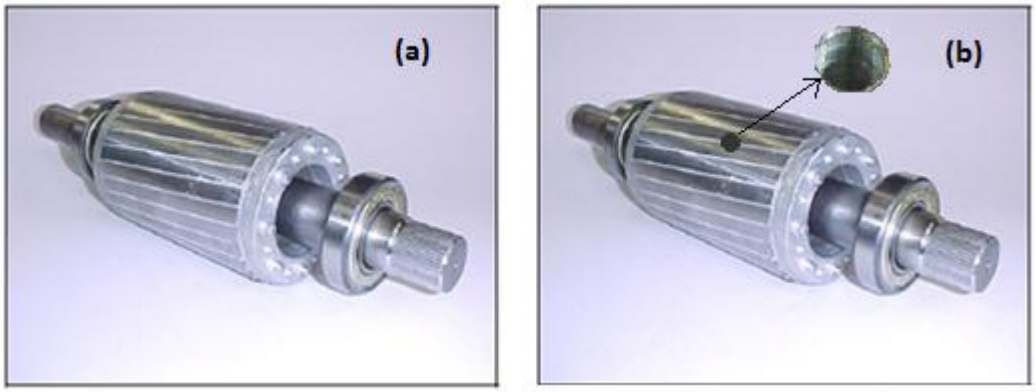


**Figure 4-4** Healthy and seeded broken rotor bar fault

## 4.4 Theories on Detection of Seeded Fault Conditions

This section provides the theory behind an initial approach to practical detection and diagnosis of the seeded faults detailed in Section 4.3.

### 4.4.1 Detection of Phase Imbalance Faults

In theory, electrical asymmetry (such as that caused by a voltage drop in one phase of power supply) may be detected and diagnosed through analysis of a frequency spectrum of recorded motor vibration. In particular, an increase of the frequency component at twice the electrical supply frequency is expected [78]. The following simple equations explain this characteristic.

The measured vibration is proportional to the force created by the electromagnetic forces within the motor. In generic form, the force (in newtons) experienced by between two magnetic poles is given by[10] :

$$F = \frac{B^2 A}{2\mu_0} \tag{4.1}$$

Where $B$ is the magnetic flux density (in Tesla, T), $A$ is the cross-sectional area ($m^2$) of the poles and $\mu$ is the permeability of the medium between the poles ($\mu_0$ specifically denotes the permeability of free space). It is well known that for constant cross-sectional area there is direct proportionality between flux density and current [10] , therefore:

$$B^2 \propto I^2 \tag{4.2}$$

Where $I$ is the alternating current which acts to magnetise a ferrous material and may be described as:

$$I = \hat{I}\sin(\omega t) \tag{4.3}$$

Where $\hat{I}$ is the magnitude of the alternating current, $t$ is time and $\omega$ is $2\pi f_1$ (where $f_1$ is the power supply frequency - 50Hz in the UK).

When Equation 4.3 is squared, the force relationship can be written as:

$$F \propto \frac{\hat{I}^2}{2}(1+\cos 2\omega t) \tag{4.4}$$

Thus changes in the 50Hz current supply should manifest themselves at 2×50 Hz (100 Hz) in the vibration signal.

### 4.4.2 Detection of Broken Rotor Bar Faults

Much of the work into the condition monitoring of induction machines has concentrated on the detection and diagnosis of broken rotor bars (see Section 3.1.2).

However, the focus has been on the detection and diagnosis of a relatively large number of broken bars, using the presence of sidebands around the electrical supply frequency of the current, or by sidebands around the shaft drive frequency in the vibration signal. The work described in this thesis extends the existing knowledge by investigating other means of measurement and by considering only very small fault severities (i.e. half and full single rotor bar breakage).

The sidebands previously mentioned are spaced at twice the slip frequency [10]. This feature may be understood by an analysis based on *sequence component theory* which is a mathematical means to simulate a three-phase unbalanced electrical power system by the phasor decomposition of positive, negative and zero rotating components [10]. The use of this method to explain the sideband spacing resulting from broken rotor bars has been demonstrated by several authors (for example Liang et. al. [78]) .

## 4.5 Parameter Measurement Transducers and Calibration

Three measurement parameters were routinely recorded from the induction motor test facility, so that their relative potential use in condition monitoring could be investigated. Each parameter was measured by a different type of transducer. Every transducer was connected to a data acquisition system (see Section 4.6) via high quality coaxial BNC cables which produce low noise levels, and a voltage output corresponding to the amplitude of the measured parameter was recorded. The transducers and associated calibration processes are discussed below.

### 4.5.1 Current Transducers

The current sensor module, PR30, made by LEM, is a Hall Effect sensor which could be interfaced with an oscilloscope or with an NI data acquisition card using LabVIEW software. It offers accurate and non-intrusive measurement of both AC and DC complex waveform currents.

### 4.5.2 Specification of current transducer

This type of current transducer was designed to gather electrical data with a measuring range from 0 to ±30 A. The normal current is 20 A RMS, output sensitivity is 100 mv/A, resolution ±1 mA, frequency range is from 10 - 100 kHz (0.5dB), conductor size 19mm diameter, jaw opening 20mm maximum and output cable with connector is 2 m long.

### 4.5.3 Accelerometers

An accelerometer is defined as an electromechanical device which converts a mechanical motion, vibration or shock to an electrical output. It is considered an inertial transducer which depends upon Newton's second law of motion. Accelerometers are widely employed devices because of their robustness, accuracy and sensitivity as well as being lighter, smaller and easier to mount than other kinds of vibration transducers. For the frequencies up to about 40 kHz, piezoelectric accelerometers are most suitable [79].

Piezoelectric accelerometers include two elements; a mass to generate an inertial force and a piezoelectric crystal to convert the force to electric charge, see Figure 4.5 [79].

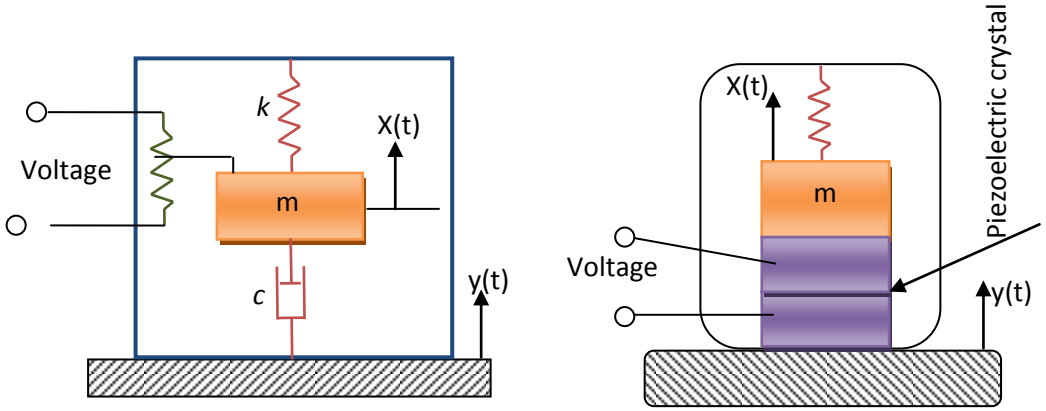


**Figure 4-5** Schematic of an accelerometer mounted on a structure

### 4.5.4 Accelerometer mounting techniques

It is essential to install an accelerometer correctly. There are four common mounting techniques used to attach transducers to accurately pick up vibration signals, see Figure 4.6. The main requirement is for close mechanical contact between the accelerometer base and the surface to which it is to be attached.

*Stud mounted* - this technique requires a stud to be mounted on the machine surface by drilling and screwing. The sensor is then screwed onto the stud, but not so tight as to generate stresses in the piezoelectric material. This is the best technique for permanent mounting and gives the best frequency response.

*Adhesive mounted* - in this method, accelerometers are glued using an appropriate adhesive material such as dental cement in a damp or wet environment or superglue or Araldite.

*Magnetic, beeswax or double sided adhesive tape* – These method are usually for temporary measurements and spot checks only. Their frequency responses, even when expertly attached are usually well below that of equivalent stud mounted accelerometers.

*Non-mounted systems* e.g. handheld probes are used for spot checks only and have a poor frequency response possibly only up to 5 kHz [1].

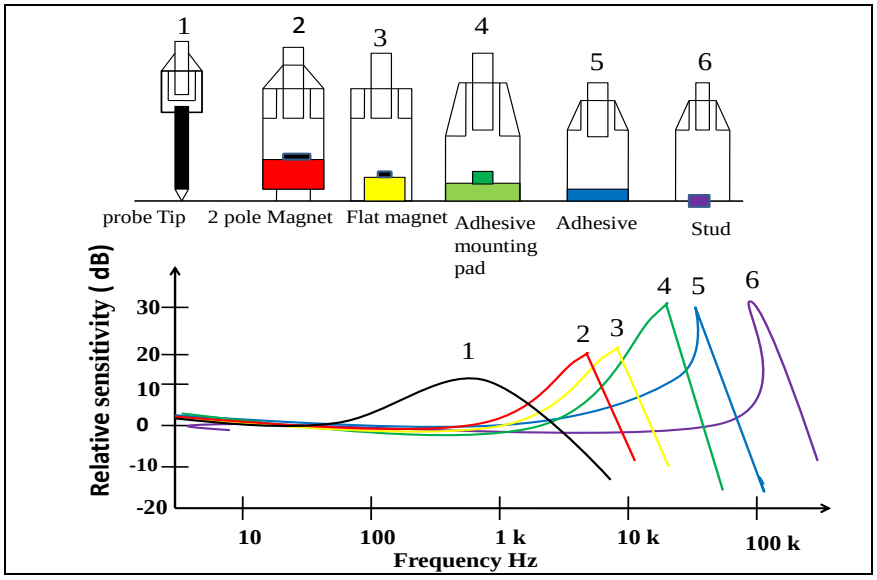


**Figure 4-6** Accelerometer mounting techniques [80]

Figure 4.6 is for expertly mounted accelerometers, and it can be seen that accelerometer mounting has a great effect on frequency range. Bad mounting of the accelerometer can seriously reduce the frequency ranges shown above.

The accelerometers used here were mounted using adhesive and each was connected to a PCB charge amplifier [model: 483A02] to fully utilise the full 16-bit resolution of the data acquisition cards (see Section 4.6). Calibration was by reference to charts provided on their last formal calibration (conducted by PCB Piezotronics in compliance with the recognised calibration standard: MIL-STD-45662A).

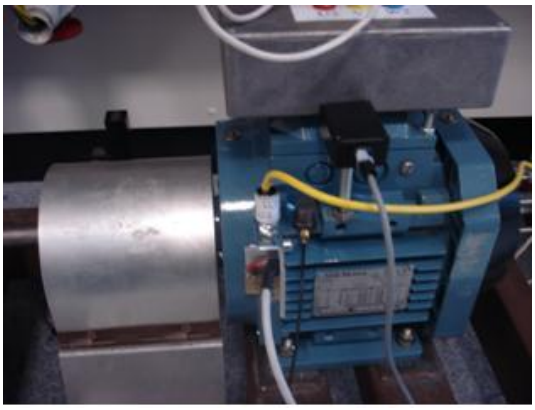

**Figure 4-7** Adhesive mounted accelerometer

### 4.5.5 Shaft Encoder

The measurement of instantaneous angular speed (IAS) was achieved by analysis of the data from a relatively cheap optical shaft encoder (approximately £80). The device produced a square pulse output for every angular degree (thus termed a 360 line encoder) and for every complete revolution. It was attached to a spindle adaptor on the non-drive end of the rotor shaft by a torsionally rigid rubber coupling (Figure 4.8). No calibration of the magnitude of the square wave pulse train was required as the calculation of IAS was based on the periodic spacing of the square waves and not their strength.

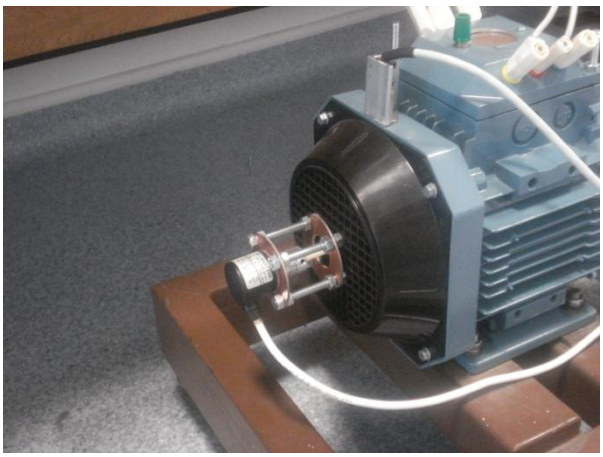

**Figure 4-8** 360 Line encoder with marker

## 4.6 Data Collection Hardware and Software

### 4.6.1 Hardware

The hardware includes the sensors, data acquisition (DAQ) card and PC. Here a National Instruments data acquisition card of type USB NI9233 was used, see Figure 4.9. This was used to transmit signals from the accelerometer to the PC. The card has the following features;

- 24-bit resolution,
- 102 dB dynamic range,
- 4 analogue inputs channel,
- ±5 V input range,
- Anti-aliasing filters, current excitation, and
- 50 kS/s maximum rate per channel


**Figure 4-9** Data acquisition card

The resolution and full scale supply voltage ($E_{FSR}$) of this DAQ card and the limit settings determine the smallest detectable change in the input voltage. This change in voltage represents 1 least significant bit (LSB) of the digital value and the resolution is calculated from the following formula [81]:

$$V_{cw} = \frac{E_{FSR}}{2^{24}} \quad (4.5)$$

For the DAQ, shown in Figure 4.9, the resolution is in the range of few microvolts.

A portable data acquisition system was used to allow data collection from the induction motor test facility.

### 4.6.2 Software

DAQ software was tailor-made using LabVIEW for control of the PCI boards, visualisation of recorded data and for saving collected data to the hard disk. The software was designed to be used on Windows® operating systems and the graphical user interface (GUI) developed is shown in Figure 4.10 .

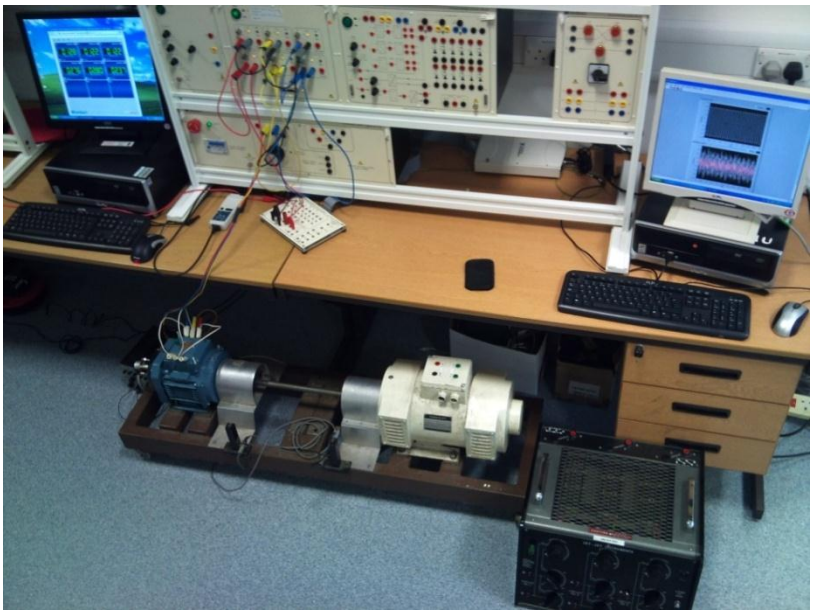

**Figure 4-10** Data Acquisition Graphical User Interface (GUI)

## 4.7 Experimental procedure

- The DAQ card, amplifier, accelerometers and cables were correctly connected and checked.

- The mounting locations for the transducers were cleaned of paint and the accelerometers were glued using an appropriate adhesive**.**
- The charge amplifier converts the accelerometer high impedance, low charge (in the range of Pico-coulombs) signal into a low impedance and high voltage (in the range of mV) signal.
- LabVIEW software was used to interface with the DAQ and to set the related parameters; signal input range, samples to read and sampling frequency.
- A suitable graphical user interface (GUI) was built in LabVIEW to monitor the test rig and to save the collected data for further analysis using MatLab.

### 4.8 Measurements Practice and data managements

A standard test procedure was developed to ensure good measurement practice. For consistency, measurement transducers were always connected to the same input connectors on the BNC input box. Similarly, each accelerometer was clearly labelled by colour coding to help ensure it was always used in the same orientation. Data was collected from all transducers in any acquisition, whether all these transducers were of immediate interest or not, as this did not alter the saved file size or the acquisition time.

Care was also taken to avoid unnecessary crossing of cables and hence minimise measurement error due to electromagnetic noise and power supply frequency pickup for data acquisition at a particular load and fault condition. This was often achieved over two separate days to ensure confidence in the repeatability of data collected. The first file in any data acquisition period was analysed, using the generic software described in Section 4.9, before further data was collected to ensure that sensible data had been recorded. A filename structure which included filter and amplifier settings

was established, from which the load and fault conditions and sequential file number could be identified.

### 4.9 Generic MatLab® Software for Data Manipulation

To enable fast analysis and manipulation of the raw data files recorded and to eliminate programming errors, a generically applicable user-friendly software program was written for use in MatLab. The program asked for the data filename(s) to be entered, offered the possibility of frequency averaging, automatically performed gain adjustments and calibration for each measurement channel, and allowed individual and multiple (superimposed) plotting of chosen channels in a variety of domains. It was this software that was used to produce most of the figures presented in this thesis.

A separate piece of software was also written to plot a spectrum of a chosen measurement channel (from a chosen data file) and then automatically overlay a series of windows to mark the positions of expected frequency components.

### 4.10 Summary

An induction motor test facility was developed in which 240 V, 1.1 kW, motor could be tested under varying shaft loads. The facility enabled a range of controlled faults to be seeded so that data could be recorded during operation at these conditions. The seeded faults were: power supply phase imbalance that created electrical asymmetry in the stator; and broken rotor bars that created electrical asymmetry in the rotor that resulted in an air gap eccentricity. Each of these faults was seeded at a variety of severities.

Theoretically, phase imbalance may be detected by changes in the 2×50 Hz component in the vibration signal and broken rotor bars may be detected by twice slip frequency sidebands.

Three types of measurement transducers were used in the motor test facility so that the information content provided by various machine parameters could be assessed and compared. Current transducers were used to measure electrically based parameters; accelerometers, and a shaft encoder were used to measure mechanically-based measurement parameters.

To enable simultaneous data collection from multiple measurement transducers, a 16- channel data acquisition system was purchased and software developed for user-friendly operation. Before data was collected, a structured approach to data management was established and a generic software program was written for fast analysis and manipulation of collected data.

# CHAPTER 5

# INDUCTION MOTOR MONITORING BASIC DATA ANALYSIS

*This chapter first reports the collection and recording the data for the healthy induction motor for a range of loads. This database is used to provide the baseline representing normal motor characteristics. The data is then analysed to provide a number of statistical parameters for the healthy induction motor for the purpose of detecting, diagnosing and assessing the severity of the seeded faults: phase imbalance, and damaged rotor bar. Results from time and frequency domain analysis, and the trending of individual frequency components are then presented.*

## 5.1 Introduction

There are many conventional techniques which are used to monitor the condition of rotating machinery. Most of these methods are easy to understand and are also simple to implement. Some of them will briefly be introduced here and applied to induction motor measured data in order to assess motor conditions. They are: Time domain analysis and frequency domain analysis

Some of these techniques extract diagnostic information directly from time domain signals whereas the others gather the information from the frequency domain.

## 5.2 Review of Basic Analysis Techniques

Time domain analysis and frequency domain analysis are the techniques most commonly used to process signals for CM.

### 5.2.1 Time Domain Analysis

Time domain analysis technique was introduced in section 1.7 and more explanation and mathematical analysis will be presented in this section.

Analogue measurements produce a continuous record of the amplitude of a signal; we will not use such a system here. The digital time domain signal is a record of the amplitude of the signal taken at specific time intervals. Sophisticated digital systems will increase the sampling rate with an increase in the high frequency content of the signal, and vice versa, but today it is common to sample at a fixed rate. Small changes in such parameters as motor speed are often clearly visible in the time domain signal, and valuable features such as transients show up. However, the raw time-domain signal is usually less useful than the corresponding frequency domain.

Statistical analysis is through parameters known as moments. These parameters have the advantage of being single-valued and so are relatively easy to interpret and use

for setting fault detection threshold levels. The first order moment (also called the first central moment) is the average value. The second central moment is the variance which provides a measure of the spread of the data. Parameters above the second order are termed "higher order". The third order moment is the skewness which is a measure of the asymmetry of the data distribution. The fourth order moment is the kurtosis which provides a measure on how sharp the peak is, and how spread out the "tails" are, of the data distribution. Higher orders do exist but require large data sample to evaluate and are rarely used. In CM the most commonly used statistical parameters for signal assessment are the Root Mean Square (RMS) a measure of the energy contained within the signal, Crest Factor (CF) the ratio of peak value to the RMS value, and Kurtosis (K).

The values of these parameters will change both with the presence of a fault and as the magnitude of the fault increases, and may be used as a measure of the deteriorating condition of the induction motor. For example, the observed value of the RMS of the vibration signal from a faulty induction motor should be significantly different from the value for a healthy one. Thus by comparing measured RMS values with values determined using vibrations from a healthy motor, the presence and severity of a fault may be detected. Typically RMS values are more useful when the fault has developed.

However, CF and K which reflect the "spikiness" of the measured signal are often more useful for incipient faults, and increase as the vibration increases. However, beyond a certain level with further increase in damage the vibration signal becomes more random in character and the values for CF and K fall to more normal levels. Thus, statistical analyses based on CF and K are generally not suitable to detect the later stages of motor defects.

#### 5.2.1.1 The Root Mean Square (RMS)

The RMS value of the time domain amplitude of a given signal is [28]:

$$RMS_x = \sqrt{\frac{1}{N}\sum_{n=1}^{N}\left(x(n)\right)^2} \tag{5.1}$$

Where

*N* is the number of samples taken,

*x(n)* is the amplitude of the nth sample.

RMS is a simple and common approach to the measurement of the overall intensity of a signal, and provides an averaging effect which reduces the influence of individual impulses in, say, a vibration signal.

#### 5.2.1.2 Crest Factor

CF gives an indication of significant changes in the envelope of the signal and is expressed as:

$$CF = \frac{\text{peak level}}{RMS_x} \tag{5.2}$$

#### 5.2.1.3 Kurtosis

Kurtosis is defined as:

$$K = \frac{\frac{1}{N}\sum_{n=1}^{N}\left(x(n)-\bar{x}\right)^4}{\left[\frac{1}{N}\sum_{i=1}^{N}\left(x(n)-\bar{x}\right)^2\right]^2} \tag{5.3}$$

As can be seen K depends on the fourth power of the difference between the sample values and the mean value, this makes it very sensitive to peaks in the signal. The higher the K value the sharper and higher the peaks and the more “stretched pout”

the tails. The lower the kurtosis the fewer and less pronounced the peaks. The above formula gives K = 3.0 for random noise following a Gaussian distribution.

The signals from healthy, motors have typical K values of 3.0 or lower. With the introduction of a fault the K value increases, which suggests the distribution of the measured signal samples is no longer Gaussian. This is because the presence of faults introduces impulses (isolated peaks with high amplitude) into the time domain signal.

### 5.2.2 Frequency Domain Analysis

It has been found that the frequency domain of the measured signal is more useful than the time domain for determining motor condition. Thus the time domain signal is transformed to the frequency domain; traditionally this has been done using the Fourier or Fast Fourier Transform (FFT). It has been found that defects such as misalignment, eccentricity and many other faults generate modulation sidebands in the spectrum. Indeed it will be shown in this thesis that phase imbalance and broken rotor bars cause the amplitude of particular frequencies, sidebands around the power supply frequency in the measured signal spectrum to change. The magnitude of these sidebands often provides useful information on the condition of the motor.

The sidebands cluster around the power supply frequency and the frequency of rotation of the motor. They are also found around the harmonics of these frequencies. Sidebands are generated by either frequency modulation or amplitude modulation or of the measured signal and so are often separated by integer multiples of the frequency of rotation of the motor. Thus, tracking the changes in amplitude of a sideband, or detecting eccentric sidebands in the signal, can provide a good indication of the presence of a fault and even possible motor failure.

In practice, however, there are problems with the spectrum as obtained using the FFT: the most important is in the detection of incipient faults when the signal to noise ratio (S/N) is low under which conditions the FFT can fail to detect the presence of peaks [82] ,secondly the spacing of the side bands depends on periodic variations in the load and in this situation it becomes difficult to extract meaningful information regarding individual peaks directly from FFT analysis of measured signal, thirdly when the complexity of the system generates a large number of frequency peaks it becomes almost impossible to distinguish the peaks from potential fault from peaks from other sources.

### 5.3 Baselining Healthy Motor Data

Essential for the CM of machinery is an appreciation of the baseline characteristics of the healthy machine. This section examines the baselining of the measurement parameters current and vibration.

#### 5.3.1 Baselining Current

Figure 5-1 shows the currents in each of the three phases of the supply. At 75% load the RMS current is about 5A (see Figure 5.5 for RMS currents at different loads). Theory predicts that for a two pole pair motor there should be two electrical periods for each revolution , and this is what is observed. The three phases are $120^0$ apart but are not perfectly sinusoidal, probably due to loading of the supply by other equipment in the building. Also, factors within the substation could influence the per-phase current profiles

.

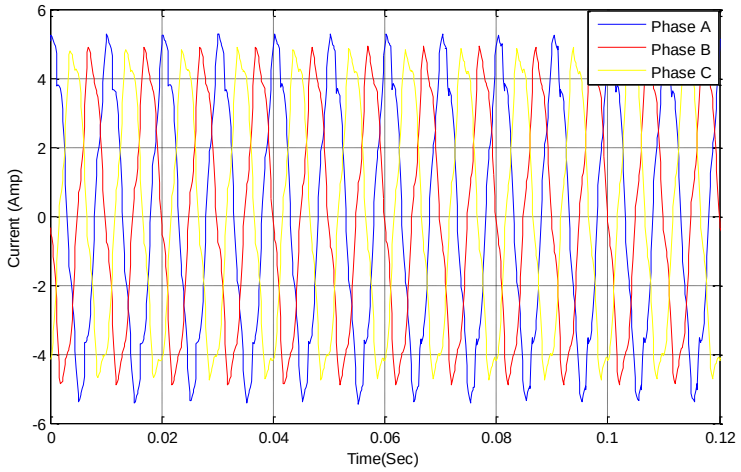


**Figure 5-1** Three-phase current at 100% load (healthy case)

Figure 5-2 shows current spectra for a single-phase, at 0% and 100% of the rated shaft load. It can be seen that the spectra from each phase overlay almost identically In both plots the 50 Hz supply frequency and its harmonics are clearly visible. However at 100% load some of the higher harmonics are less pronounced. At 0% load sidebands spaced at running speed around 50Hz are prominent; but are less prominent at 100% load because the running speed at 0% load is close to 25 Hz (because the slip is very small) so the sidebands of the harmonics of the supply frequency overlap and combine to be more visible. At higher loads the motor speed is less and therefore the sidebands of the harmonics do not overlap and can be separated. Of course separation of the different sidebands depends on the frequency resolution available, here it is 0.39 Hz.

At 100% load a number of additional peaks rise above the background noise level (in particular small sidebands around the 50 Hz peak representing twice the slip frequency) – these are considered in more detail in Section 5.6.3.

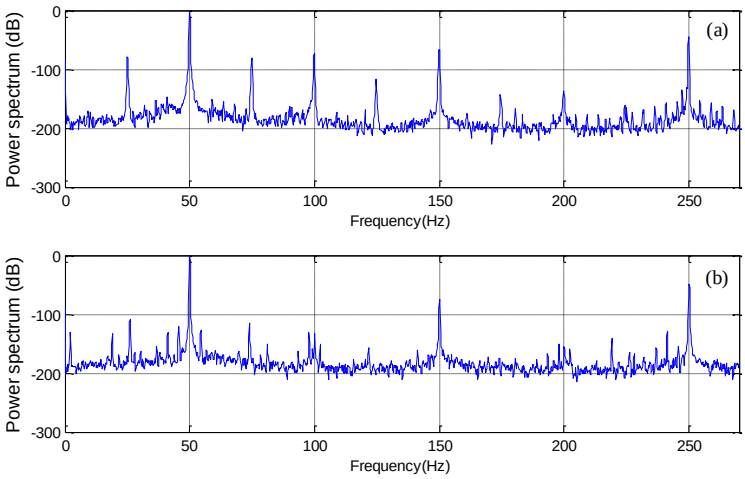


**Figure 5-2** Spectrum of single -phase current at 0% (a) and 100% (b) load (healthy motor)

### RMS Values of Current

Figure 5-3 shows average value of RMS values for the three-phases. The current at no-load is relatively high .Small motors are notorious for this feature which is caused by a relatively large air gap width in comparison to the rotor and stator dimensions (resulting in a relatively high magnetising current at all loads) [10]

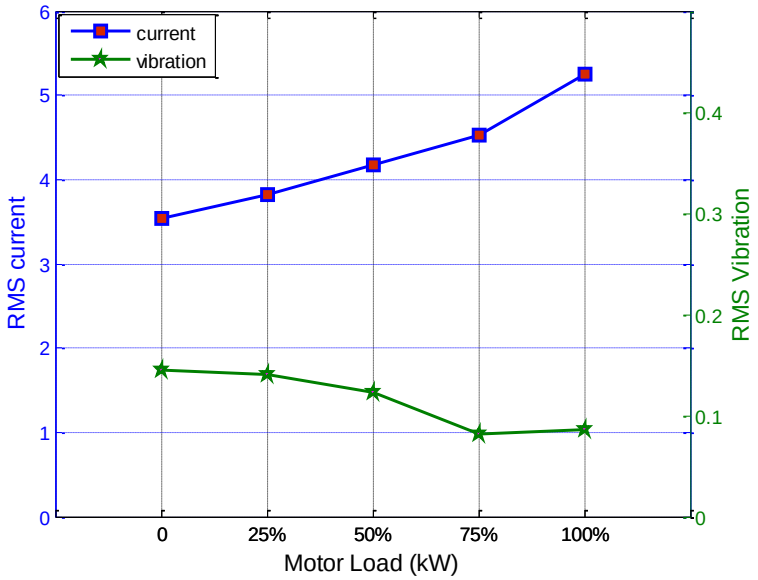


**Figure 5-3** Effect of load on RMS current and RMS vibration level (healthy motor)

### 5.3.2 Baselining of Vibration

The vibration parameter used in this research is acceleration. Figure 5-4 shows the vibration spectra at no-load and full-load conditions. It is obvious that there are greater differences between these two signals than there was between the current spectra. However, the measured acceleration will not be the same in all directions because the rotor/stator cross-section and mounting arrangements are not symmetrical. In addition, and importantly, different measurement positions will sum the vibrations reaching that point by different transmission paths[10].

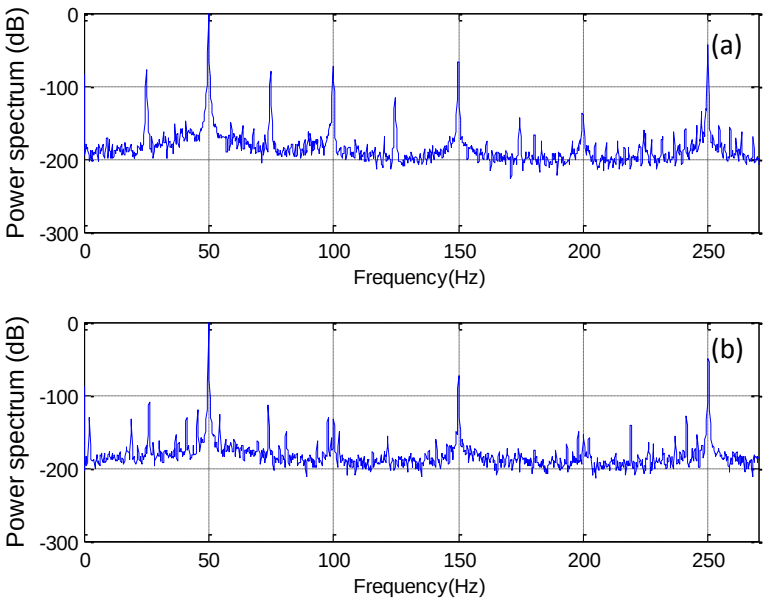


**Figure 5-4** vibration spectra at 0% (a) and 100% load (b) (healthy motor)

The 50 Hz supply frequency is seen in both spectra. However, at 0% load the running speed is very close to 25 Hz and its second harmonic is at 50 Hz the same as the mains pickup. The two components add. Similarly, the third harmonic of the running speed (3 x 25 = 75 Hz) overlaps with the lower running speed sideband of the 100Hz peak (100 – 25 = 75 Hz).

However, at higher loads, the running speed drops sufficiently so that these components may be distinguished separately.

**RMS Values of Vibration**

Figure 5-3 shows that the RMS acceleration as a function of load. Interestingly, load does not appear to have an effect on the overall signal.

## 5.4 Experimental results with basic techniques

### 5.4.1 Phase Imbalance Faults

The first fault condition seeded into the system was a phase imbalance; a decrease in the phase A voltage, as described in Section 4.3.1. Faults of three severities were seeded, first a drop of 20 V (8.3%), second a drop of 40 V (16.7%) and then one rotor bar broken

#### *5.4.1.1 Fault Detection by Current*

Figure 5-5 shows the RMS, CF and K values for the current signal for the motor under different load and fault condition. It can be seen from Figure 5-5, that while the three statistical parameters did vary with the induction motor fault and the load on the motor the changes in CF and K were not significant with either load or fault. Small changes can be seen in the RMS values for different faults and load, but no consistent pattern was observed. It was concluded that these features will not be effective indicators of these faults. More advanced signal processing techniques are necessary to determine required a robust feature able to diagnose induction motor faults.

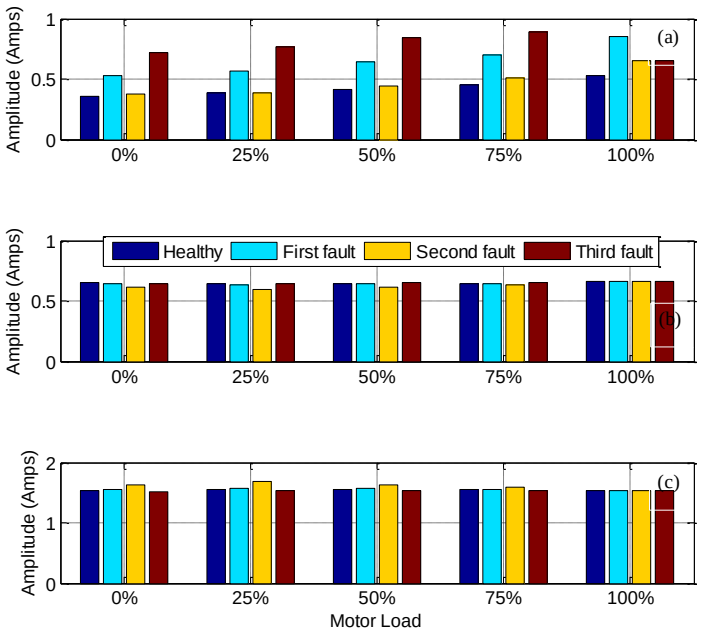


**Figure 5-5** Statistical parameters RMS (a), CF (b) and K (c) for the time-domain of the current signal

Figure 5-6 shows that the frequency domain of one phase of the supply current signal at 75% load, healthy and with voltage imbalances of 20 V and 40 V. Peak values corresponding to the power supply frequency and sidebands can be seen. It can also be seen that the spectral amplitude at power supply frequency and its sidebands change with the severity of the faults.

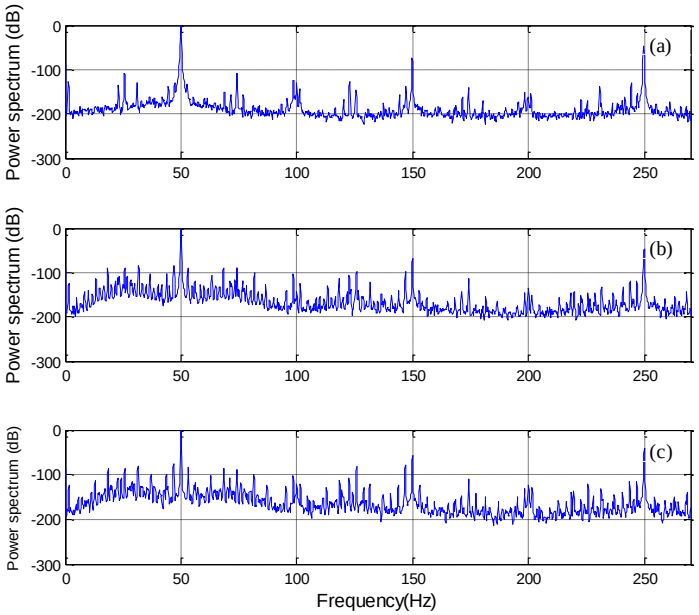


**Figure 5-6** Frequency domain of one phase of the supply current at 75 % load and with voltage imbalance (a)- Healthy (b)- 20 V drop (c) 40 V drop

Figure 5-7 shows trends the amplitude of the 50 Hz peak of the Phase A current with varying load, and voltage fault. The 50 Hz peak increases with load for all three voltage conditions, but the greater the voltage drop the greater the Phase A current as the motor attempted to maintain constant power.

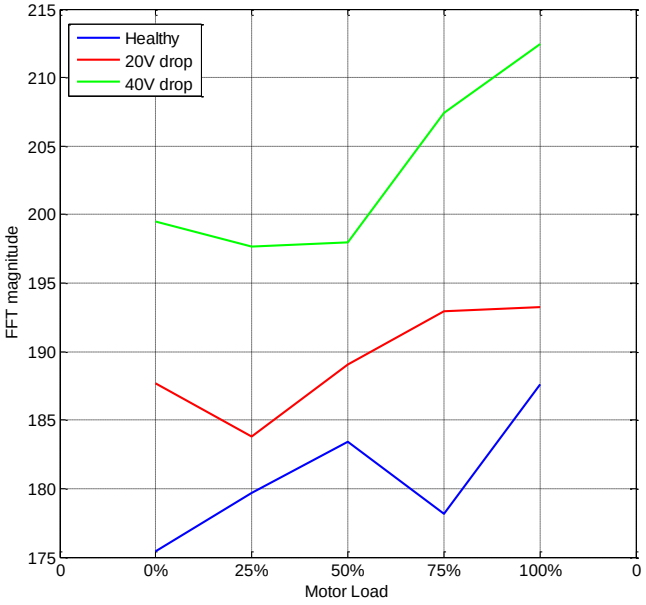


**Figure 5-7** Amplitude of peak at 50 Hz in Phase A

### *5.4.1.2 Fault Detection by Vibration.*

Figure 5-8 shows RMS, CF and K values of the time domain of the vibration signal for healthy motor and faulty motor operating under different conditions. It can be seen that the three parameters vary with type of fault and load. No significant changes were found for the CF and K values. The results did reveal some differences in the RMS values at 100% load for healthy and faulty conditions, there was no consistent pattern which would have allowed identification of which fault was which. These three statistical features are not able to detect the presence of a fault reliable nor identify it effectively. More advanced signal processing techniques are required for the robust identification of induction motor faults.

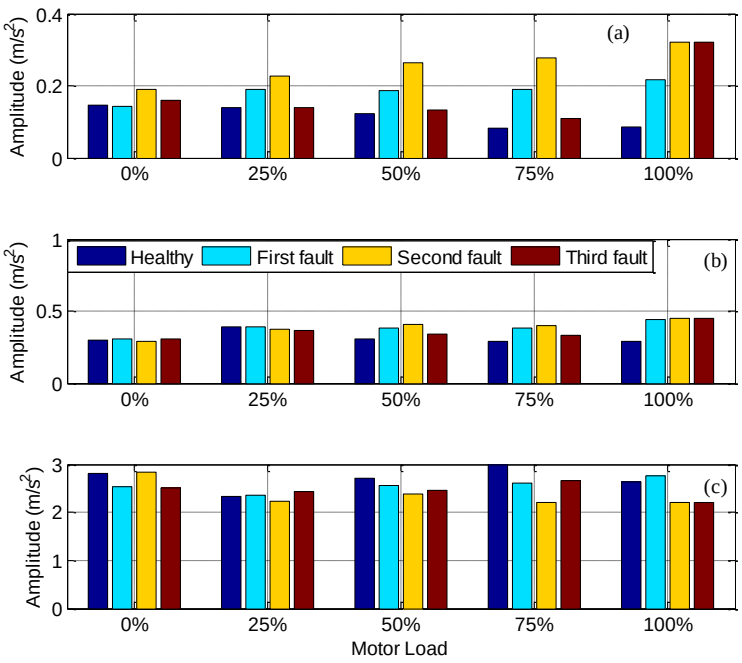


**Figure 5-8** Statistical parameters RMS (a), CF (b) and K (c)for the time-domain of the vibration signal

Figure 5-9 shows the vibration acceleration spectrum. It can be seen that the 100 Hz component increases in magnitude, as predicted in Section 4.4.1. The spectral

amplitude at twice power supply frequency and its sidebands change with the severity of the faults.

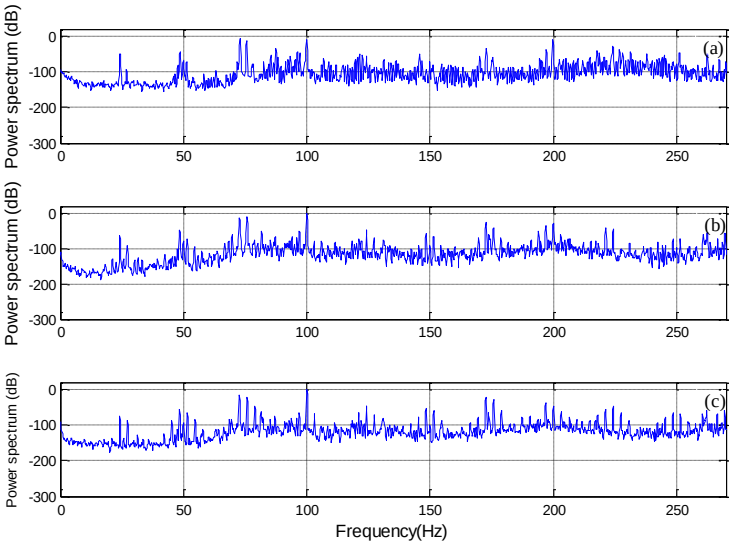


**Figure 5-9** Vibration acceleration spectrum, 75% load with voltage imbalance in one phase of the supply current (a) Healthy case (b)- 20 V drop (c)- 40V drop

Figure 5-10 shows the amplitude of the 100 Hz peak in the vibration acceleration spectrum for different loads and the two voltage imbalance faults. For the healthy motor it can be seen that the 100 Hz peak gradually rises to a maximum value at 50% load and then decreases gradually. Similar shapes are observed for each voltage fault, but the 100 Hz peak is larger the larger the voltage imbalance. With voltage imbalance the values of the 100 Hz peak appears to rise as the load is increased but not uniformly, this needs further investigation.

Although detection of the voltage imbalance fault based on change in amplitude of the 100 Hz component appears feasible, severity assessment may not always be possible.

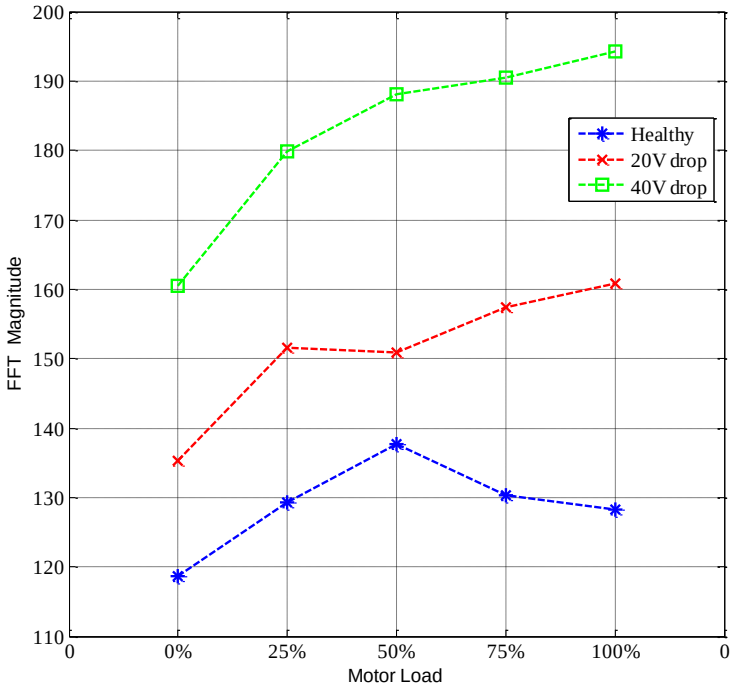


**Figure 5-10** Amplitude of the 100 Hz peak in the vibration acceleration spectrum with load and voltage imbalance in one phase of the supply current

### 5.4.2 Broken Rotor Bar Fault

A damaged (broken) rotor bar was the second fault to be considered. Section 4.3.2 describes how the damage was seeded by drilling into the conductor bars.

#### *5.4.2.1 Fault Detection by Inspection of Current Signal*

As predicted in Section 4.4.2, the seeded broken rotor bar generated sidebands in the spectrum of the current spaced at the twice slip frequency around the 100 Hz fundamental of the electrical current, see Figure 5-11 which shows the spectrum of the Phase A current for healthy motor operation, and operation with a fully broken bar. The fundamental frequency is labelled as are the location of the first and most visible of the lower and upper sidebands.

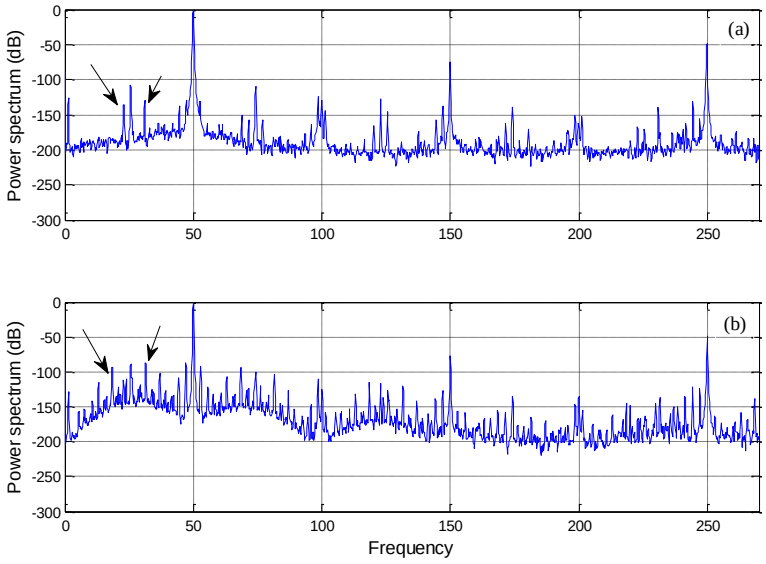


**Figure 5-11** Current spectrum at 75% load (healthy motor (a) and one fully broken rotor bar (b))

Figure 5-12 shows the amplitudes of the carrier frequency and the average of the first lower and upper sidebands for a healthy motor and motor with a broken rotor bar. The figure shows that the difference in amplitudes at each of the motor loads is sufficient to show the presence of a fault and is indicative of a broken bar fault. The results also show that detection of this fault appears to be heavily dependent on load – the indication of the fault is more pronounced at 100% load than at 75% load by approximately a factor of two

**Table 5-1** Slip and 1st and 2nd Sidebands

| Load percent (%) | Rotor speed | Slip | 1st sidebands | 2nd sidebands |
|---|---|---|---|---|
| 0% | 24.85 Hz | 0.006 | ±0.6 Hz | ±1.2 Hz |
| 25% | 24.60 Hz | 0.016 | ±1.6 Hz | ±3.2 Hz |
| 50% | 24.41 Hz | 0.0234 | ±2.34 Hz | ±4.68 Hz |
| 75% | 24.22 Hz | 0.0312 | ±3.12 Hz | ±6.24 Hz |
| 100% | 23.88 Hz | 0.0448 | ±4.48 Hz | ±8.96 Hz |

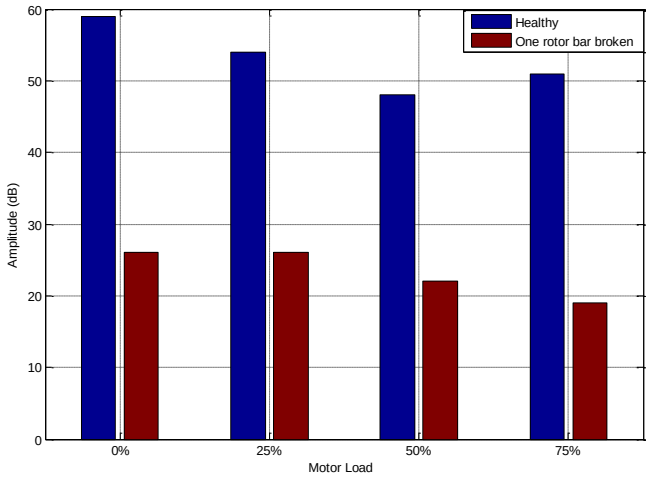


**Figure 5-12** Amplitudes of sidebands (50 Hz ± slip frequency) in current spectrum for healthy motor and one broken rotor bar.

### *5.4.2.2 Fault Detection by Inspection of Vibration Spectrum*

In theory, sidebands at twice the slip frequency should be found around the peak in the vibration spectrum at the motor speed. Figure 5-13 shows the vibration acceleration spectra for a healthy motor and motor with one broken rotor bar.

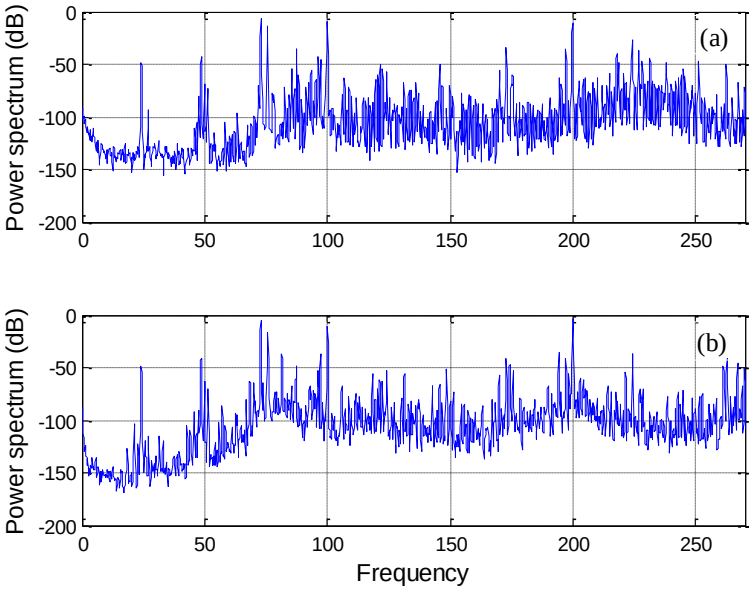


**Figure 5-13** Vibration spectrum at 75% load (healthy motor (a) and motor with one broken rotor bar (b))

Figure 5-14 is the corresponding figure to Figure 5-12. It shows the amplitudes of the sidebands immediately adjacent to the carrier (ie the first lower and upper sidebands) for healthy motor and motor with one broken rotor bar.

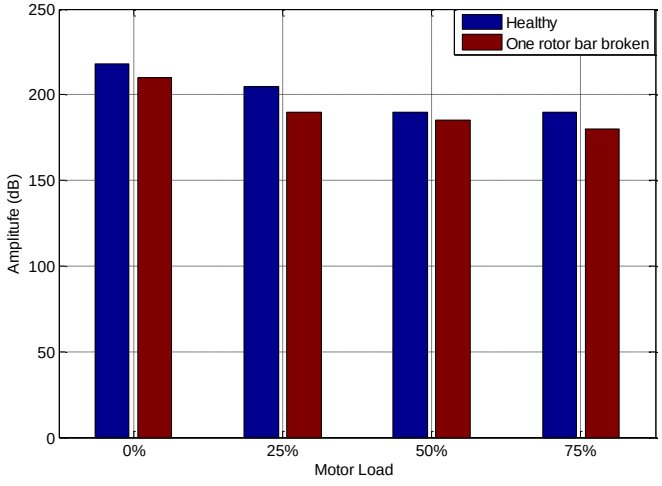


**Figure 5-14** Amplitudes of vibration acceleration peaks at 25 Hz ± slip frequency for healthy motor and motor with one broken rotor bar

## 5.7 Summary

This chapter has shown how data from current and vibration transducers attached to an induction motor system may be analysed in both the time and frequency domains to detect diagnose and assess the severity of two faults (phase voltage imbalance and rotor bar breakage). Faults of low severity have been successfully detected which paves the way for detection and diagnosis of incipient faults.

### 5.7.1 Baselining of Healthy Motor Data

The baselining procedure of Section 5.2 provided the basis for an investigation into the effect of load on healthy motor operation. It was shown that both RMS current and vibration signals varied. Furthermore, it was shown that two frequency components from two different sources could sometimes overlap at low slip speeds. Without prior understanding of this feature, this could have misled subsequent interpretation of the data recorded during faulty motor operation

### 5.7.2 Phase Imbalance Faults

Section 5.3.1 showed that phase voltage imbalances of 20V and 40V could be detected by examining changes in the 50 Hz component of the Phase A current. Section 5.3.4 showed the detection and diagnosis of voltage phase imbalance using the machine vibration by trending increases in the amplitude of the 100 Hz frequency component. The CM capabilities for this particular fault were found to be relatively consistent irrespective of the motor load.

### 5.7.3 Broken Rotor Bar Faults

Section 5.4.1 demonstrated that the broken rotor bar fault seeded into the motor could be detected, diagnosed and its severity assessed by examining the twice slip frequency sidebands around the 50 Hz power supply peak in the spectrum of the

current. The broken bar faults could also be detected by the presence of sidebands around the 25 Hz running speed component in vibration spectra (Section 5.4.2).

However neither the time nor frequency domains provide the instant of time at which the fault occurs and thus, in the next chapter time-frequency analysis will be used evaluates induction motor faults severity.

# CHAPTER 6

# TIME-FREQUENCY ANALYSIS TECHNIQUES

*This chapter compares the performance of the short time Fourier transform (STFT), the Wigner-Ville distribution (WVD), the continuous wavelet transform (CWT), the discrete wavelet transform (DWT) and wavelet multi-resolution analysis (MRA) using a simulated signal and measured data from an induction motor with seeded faults (phase voltage imbalance and broken rotor bar)*

*It is shown that there are limitations to STFT and WVD techniques which can be overcome using the CWT and DWT. However the DWT is found to be faster than the CWT.*

*Using higher level components of the DWT (d5 to d7) of the measured signal provided useful information on identification of the faults using the energy content in the frequency bands corresponding to mains supply frequency, twice the mains frequency and the shaft drive frequency The results of the experiment show wavelet decomposition is an appropriate technique for non- stationary signals representing faults in an induction motor.*

## 6.1 Introduction

Neither spectrum analysis nor time domain analysis alone can provide a complete picture of the time and frequency characteristics of a signal. For stationary signals this is not really a problem because, by definition, their behaviour is not changing; however, for non-stationary signals simultaneous time and frequency information is important. To characterise non-stationary signals, combined time-frequency techniques are used. Those which have gained popularity in recent years are: the short time Fourier transform (STFT), Wigner-Ville distribution (WVD) and the wavelet transform (WT).

## 6.2 Short Time Fourier Transform

The STFT can be used to describe the change of frequency content of a signal with time. The STFT uses a time window to separate the main signal into small parts, each part is then assumed to be a stationary signal and the Fourier transform (FT) is applied to each part individually [83], as shown in Figure 6.1. Because the main signal is divided into small time intervals the process is named the Short Time Fourier Transform. As a result, it can produce a different spectrum distribution for the different time windows[84] . A signal separated into such intervals is named a windowed signal as given in Equation 6.1

$$x_w(t) = x(t).w(t) \tag{6.1}$$

Where *x(t)* is a main signal, *w(t)* is a window function and $x_w(t)$ is a windowed signal.

Since a window function is applied at different locations of the whole time signal the windowed signal can be represented as a function of the time, t, and window location $\tau$ [83] as shown in Equation 6.2

$$x_w(t,\tau) = x(t).w(t-\tau) \quad (6.2)$$

The result of the Fourier Transform for each time interval can be called a windowed Fourier Transform and will be a function of window location. STFT can then be given as in Equation 6.3 [83] :

$$STFT(f,\tau) = \int_{-\infty}^{\infty} x(t)w(t-\tau)e^{-j2\pi ft}dt \quad (6.3)$$

Thus, for each location of the window, different spectra will be computed; the total number of these spectra is a function that represents a time frequency distribution [83]. The modulus of the STFT is called a spectrogram.

The procedure to calculate the STFT can be summarized in the following steps, also shown in Figure 6.1

- Compute a windowed signal $x_w(t)$, by multiplying the main signal $x(t)$ by the window function as in Equation 6.1
- Fast Fourier Transform is applied to each windowed signal.

When using very short window functions, the effectiveness of the STFT will decrease because as the time segments become very small and the amount of information decreases, so the content of the resulting spectrum decreases .

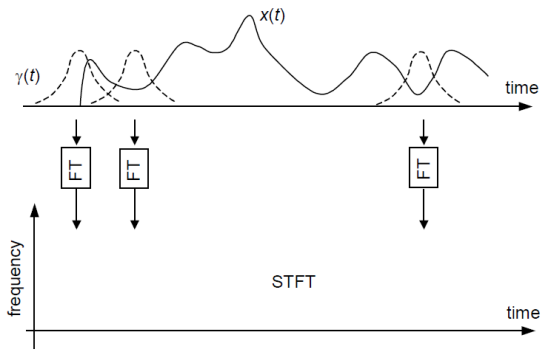


**Figure 6-1** Principle of operation of Short Time Fourier Transform [91]

### 6.3 Wigner-Ville Distribution

Another type of joint time-frequency analysis technique is the Wigner-Ville distribution (WVD). This was first presented in 1932 by Wigner for studying problems in quantum mechanics and 15 years later the French scientist (Ville) applied the Wigner distribution to signal processing. So that today it is generally called the Wigner-Ville Distribution [85].

To understand the WVD, the power spectrum, *PS(t, ω)*, is considered the Fourier Transform (FT) of the auto-correlation function, R(τ), which is defined as[85];

$$PS(t,\omega) = |X(\omega)|^2 = \int_{-\infty}^{+\infty} R(\tau) e^{-j\omega t} dt \qquad (6.4)$$

Where

$$R(\tau) = \int_{-\infty}^{+\infty} x(t) x^*(t-\tau) dt \qquad (6.5)$$

The Fourier Transform (FT) of the time-dependent auto-correlation function *R(t,τ)* with respect to the variable τ is a function of time and frequency:

$$PS(t,\omega) = \int_{-\infty}^{+\infty} R(t,\tau) e^{-j\omega\tau} d\tau \qquad (6.6)$$

Where the time-dependent auto-correlation function *R(t,τ)* is defined as:

$$R(t,\tau) = \frac{1}{2\pi} \int_{-\infty}^{+\infty} A_x(\nu,\tau) A_\gamma(\nu,\tau) e^{j\nu t} d\nu \qquad (6.7)$$

Where $A_x(\nu,\tau)$ represents the ambiguity function of signal *x(t)* and $A_\gamma(\nu,\tau)$ represents the ambiguity function of window function. The time-dependent auto-correlation function in the WVD is given as [[85], [86]]:

$$R(t,\tau) = x\left(t+\frac{\tau}{2}\right) x^*\left(t-\frac{\tau}{2}\right) \qquad (6.8)$$

Where *x(t)* is the analytical signal and $x^*(t)$ is the complex conjugate of the analytical signal *x(t)*.

From the above equations, the WVD can be written as:

$$WVD_{xx}(t,\omega) = \int_{-\infty}^{+\infty} x(t+\frac{\tau}{2})x^*\left(t-\frac{\tau}{2}\right)e^{-j\omega t}d\tau \qquad (6.9)$$

Where $WVD_{xx}\ (t,\ \omega)$ is the WVD of the complex continuous-time analytical signal $x(t)$.

### 6.4 The Continuous Wavelet Transform (CWT).

The CWT is an effective technique for the detection of faults in machinery and is widely recognized as useful for condition monitoring (CM). The CWT is suitable for the analysis of both stationary and transitory signals [87].

Time-frequency representations such as the STFT give a fixed resolution in the time and frequency domain once the window function is determined. Wavelet transforms (WTs) can analyse non-stationary signals. The WT of a time signal is an expansion of the signal in terms of a family of functions, which are generated from a single function called the wavelet kernel. The classical Fourier Transform moves data from a time to a frequency domain with sinusoids as the basis functions, which give the average characteristics of the signal. The WT translates data onto a scale, or time-frequency domain, with the wavelet as the basis function containing the localised features of the original signal. One of the important characteristics of the WT is that it can narrow or widen the time window depending on whether the frequency is high or low. This is an important difference between the WT and other time-frequency methods. As a result, the WT has the ability to resolve very short-lived transient phenomena in the time dimension, making it suitable for the analysis of non-stationary signals. Thus the WT is a technique which is potentially well suited to the detection of early failures from induction motors.

The CWT separates signals into a set of elementary functions, called wavelets. Wavelets come in sets or families of functions which define its basic shape and then each is defined by a *dilation*, which controls the scaling parameter, and *translation*, which controls the position of the wavelet in time. Mathematically, the CWT of the continuous signal *x(t)* is defined as [[5], [88],[89] ]:

$$CWT(a,b) = W_{\Psi}(a,b) = \frac{1}{\sqrt{a}}\int_{-\infty}^{\infty} x(t)\Psi^{*}\left(\frac{t-b}{a}\right)dt \qquad (6.10)$$

Where $\Psi(t)$ is the mother wavelet , b is the translation factor and a ($a > 0$) is the dilation factor. The factor $1/\sqrt{a}$ is used for energy normalisation. The continuous wavelet transform is extended by a family of kernel functions, which are translated and dilated versions of the mother wavelet, these are called daughter wavelets and expressed as:

$$\Psi_{ab}(t) = \frac{1}{\sqrt{a}}\Psi \qquad (6.11)$$

Where $\Psi_{ab}(t)$ represents the daughter wavelet and $\Psi(\frac{t-b}{a})$ is the translated and dilated mother wavelet. The scaling and shifting parameters *a* and *b* continuously change so that the size of wavelet function $\Psi_{ab}(t)$ is varying. This is in contrast with the STFT where the window size is fixed.

The CWT uses variable window size when analyzing different frequency components within a signal. When large scales are selected, the resulting $\Psi_{ab}(t)$ become a low frequency wavelet function and spreads out in time, and *vice versa* [5].

Comparison between STFT and CWT is illustrated in Figure 6.2. Once the elementary function has been selected for the STFT, the time-frequency resolution is fixed over the entire time-frequency domain, see Figure 6.2a. With the CWT, the

time resolution increases with the central frequency of the analysis filter, and the frequency resolution ($\Delta f$) is assumed to be proportional to $f$ [85] [90].

$$\frac{\Delta f}{f} = c \tag{6.12}$$

Where c is a constant. Figure 6.12b represents the CWT and shows that the frequency resolution is good at high frequencies, and the time resolution remains good at low frequencies [85].

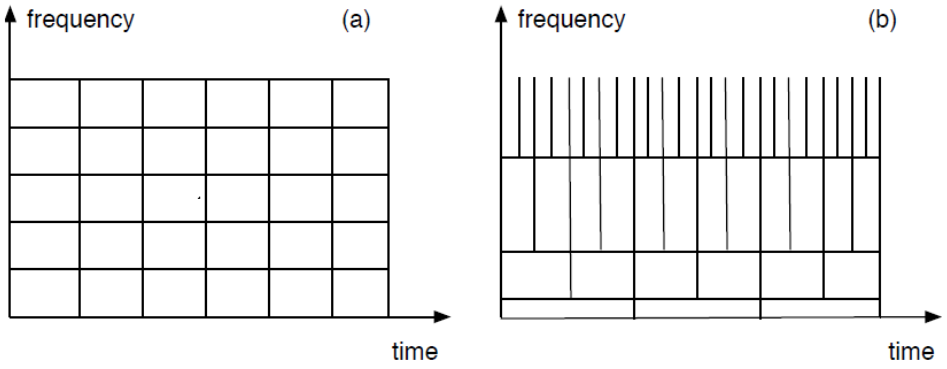


**Figure 6-2** Time-frequency resolution of (a) Short Time-Fourier Transform and (b) Continuous Wavelet Transform [85]

The explanation below describes the difference between the STFT and the CWT and helps us to understand the behaviour each.

The signal y*(t)* is assumed to carry two pulses in the time domain, $\emptyset(t - t_1)$ and $\emptyset(t - t_2)$, and two pulses in frequency domain, $e^{j\omega_1 t}$ and $e^{j\omega_2 t}$ as shown in Equation 6.13:

$$y(t) = \emptyset(t - t_1) + \emptyset(t - t_2) + e^{jw_1 t} + e^{jw_2 t} \tag{6.13}$$

The frequency domain for signal *y(t)* is expressed as in Equation 6.14:

$$Y(\omega) = e^{j\omega_1 t} + e^{j\omega_2 t} + 2\pi\emptyset(\omega - \omega_1) + 2\pi\emptyset(\omega - \omega_2) \quad (6.14)$$

The STFT and CWT for signal *y(t)* are plotted in Figure 6.3, which shows major differences between the two techniques. With the STFT; time and frequency resolution appear uniform over the time-frequency domain, see Figure 6.3a. But the resolution for both time and frequency changes when using the CWT, see Figure 6.3b. From Figure 6.3b it can be seen that at high frequencies, the CWT gives good time resolution as well as good frequency resolution at low frequency [91].

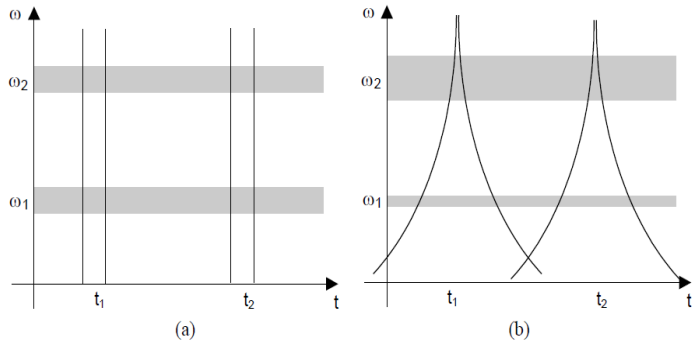


**Figure 6-3** Comparison of STFT and CWT (a) STFT time and frequency resolution (b) CWT time and frequency resolution

## 6.5 Discrete Wavelet Transform

Wavelet multi-resolution analysis (MRA) is a new and powerful method of signal analysis well suited to fault generated signals[91]. The windowing of the wavelet transform is adjusted automatically for low and high frequencies, i.e. it uses short time intervals for high frequency components and long time intervals for low frequency components and thus each frequency components gets treated appropriately without requiring any reinterpretation of the results.

This gives the wavelet transform much greater power in the analysis of the signals with localized transient components. The time frequency localization means that more energetic wavelet coefficients are localized. This is useful for feature extraction. Therefore, it is well suited for the fault location problem in, for example, electrical machines.

For the discrete wavelet transform (DWT) the main idea is the same as it is in the case of CWT, but it is considerably easier and faster to implement [91]. The wavelet is simply a sampled version of the continuous wavelet transform, and much of the information it provides is redundant as far as the reconstruction of the signal is concerned. But this redundancy requires a significant amount of computation time. Discrete wavelets overcomes this problem by providing sufficient information both for analysis and synthesis of the original signal with a significant reduction in the computation time.

A quick way to obtain the forward DWT coefficients is to use the filter bank structure shown in Figure 6.4. The approximation coefficients at a lower level are transferred through a high pass (h[n]) and a low-pass filter (g[n]), followed by a down sampling by two to compute both the detail (from the high-pass filter) and the approximation (from the low-pass filter) coefficients at a higher level. The two filters are linked to each other and they are known as quadrature mirror filters. High-pass and low-pass filters are derived from the mother wavelet and the scaling function, considered respectively in [91].

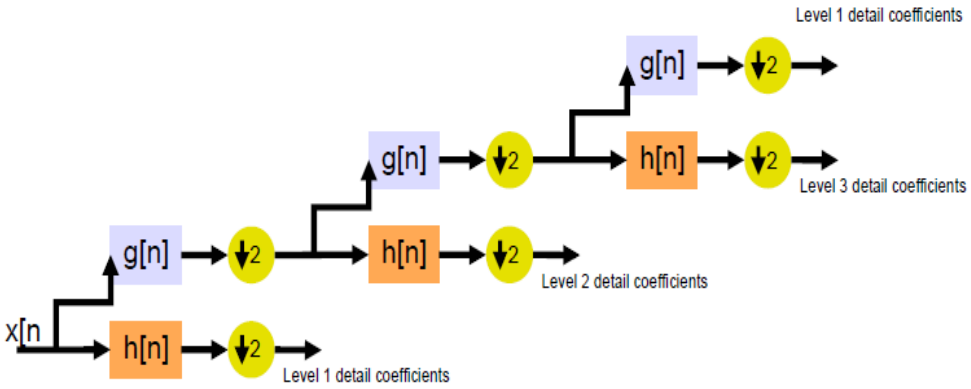


**Figure 6-4** Wavelet tree decomposition for three levels of detail

Figure 6.5 shows the frequency ranges covered and the final approximation for a three-level decomposition. These are directly related to the frequency bands where the analysis will be performed.

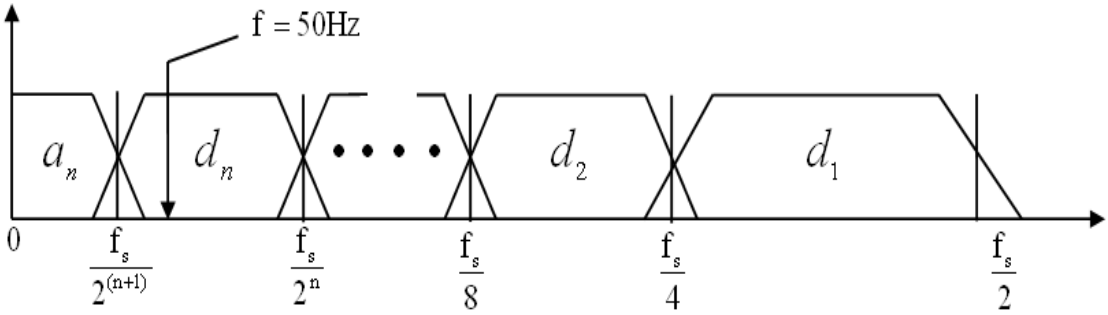


**Figure 6-5** Frequency ranges for details and final approximation

Figure 6.6 represents graphically the time-frequency window, which has better resolution in the time domain for high frequencies, and better frequency resolution for low frequencies, which means fewer resources for processing.

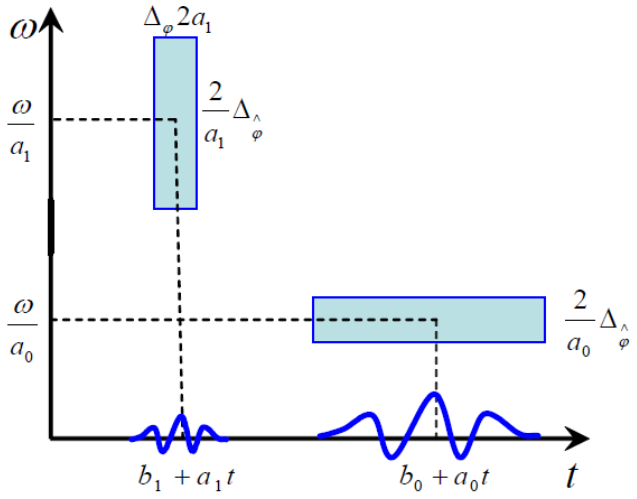


**Figure 6-6** Time-Frequency window for the wavelet transform

The shape of the frequency response for these filters depends on the type and the order of the mother wavelet used in the analysis. In order to avoid overlapping between two adjacent frequency bands, a high-order mother wavelet has to be used and that results in a high order frequency filter.

### 6.6 Numerical Simulation

With an induction motor operating at shaft frequency of 23.53 Hz, the power supply frequency at 50 Hz, twice power supply frequency 100 Hz, rotor oscillation frequency at 190.64 Hz with sidebands around the 1st shaft frequency at frequencies of 23.7066 Hz (23.83 - 2*slip) and 23.8934 Hz (23.83 + 2*slip), a simulated signal can be assumed to be

$x$ =0.2*sin(2*pi*23.83*t) + 0.1*sin(2*pi*1009.6*t) + 0.1*sin(2*pi*190.64*t)

+ 0.1*sin(2*pi*100*t) + 0.1*sin(2*pi*96*t) + 0.1*sin(2*pi*50*t) + 0.1*sin(2*pi *23.8934*t) + 0.1*sin(2*pi*23.7066*t). (6.15)

The vibration generated by mechnical damaged of an induction motor often exhibit the time domain pattern shown in Figure 6.7. The signal shown in Figure 6.8 is

artifically corrupted by Gaussian noise, and is used to compare the ability of the signal analysis techniques to extract weak spikes from vibration signals heavily contaminated with background noise and to choose the best which will then be used to detect induction motor faults from test rig data.

The time-domain and power spectrum of the simulated signal of Figure 6.8 with the addition of "spikes" to represent artificial faults are presented in Figures 6.9 and 6.10 respectively

The FFT simply identifies all frequencies in the signal, there is no information about when these spectral components occur. Therefore, the FFT is not a suitable method for non-stationary signals.

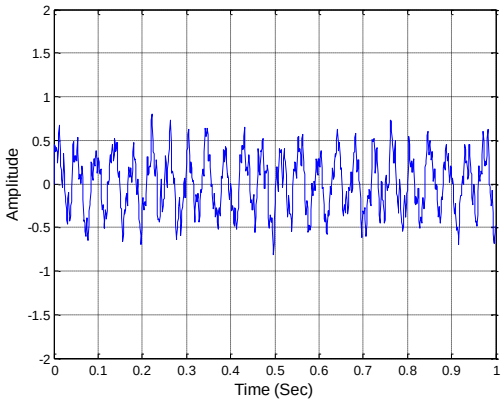


**Figure 6-7** Simulated signal

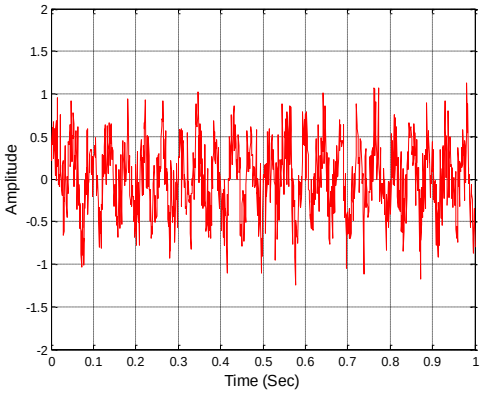


**Figure 6-8** Simulated signal with noise

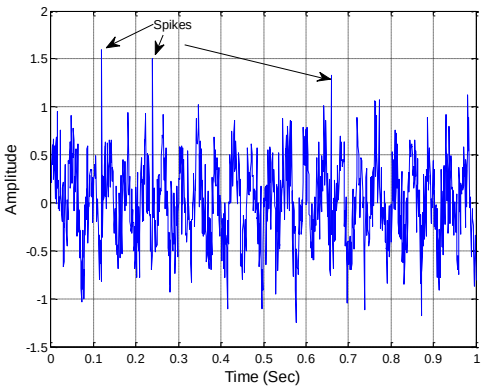


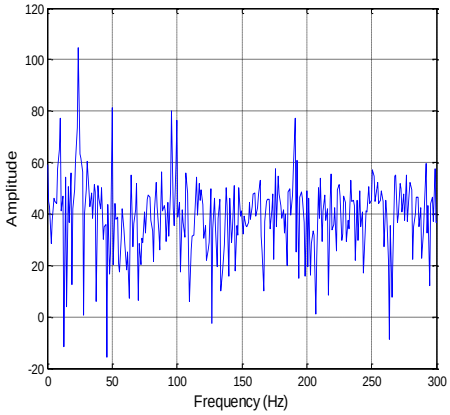


**Figure 6-9** Simulated signal with small spikes

**Figure 6-10** Power spectrum of simulated signal

Figures 6.11 and 6.12 show, respecrively, the STFT of the simulated signal articially corrupted by Gaussian noise and the same signal with "spikes" added. Both present the results using a spectrogram rectangle that gives a good description of the behaviour of each signal. However, a big diffenece in time-frquency localisation for the signal is apparent if the width of the window is changed. The bandwith limitation imposed by the window function mean that if, in the case of multi-component signals, we want to get better resolution in time we must sacrifice resolution in frequency and vice versa.

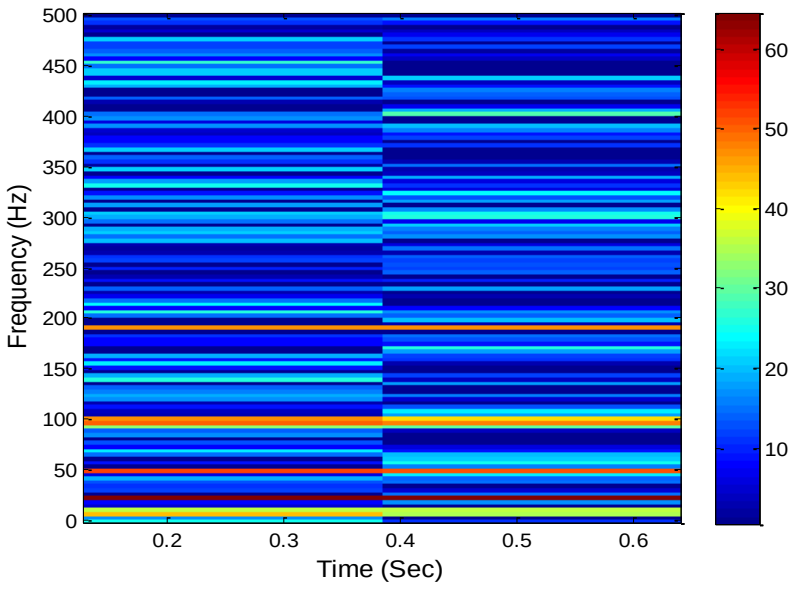


**Figure 6-11** STFT of simulated signal corrupted with Gaussian noise

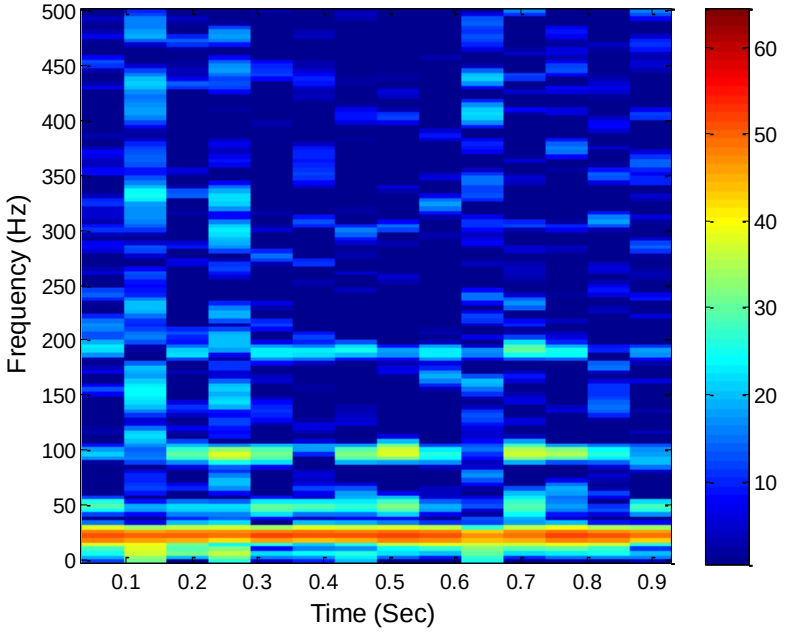


**Figure 6-12** STFT of simulated signal corrupted with Gaussian noise and with spikes

The following figures show the effect of "cross-terms" in the WVD. Figure 6.13 shows the WVD of the simulated signal, and Figure 6.14, the simulated signal corrupted with a few spikes.

Although it is a good representation of the two signals, the only advantage chosen the WVD over the STFT is better time-frequency resolution. Concentration of energy in some frequency bands also makes the WVD preferable to the STFT in many applications of signal processing

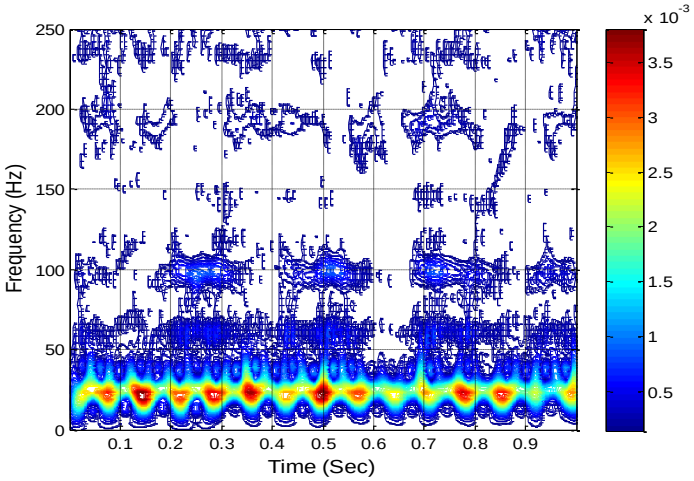


**Figure 6-13** WVD of simulated signal corrupted with Gaussian noise

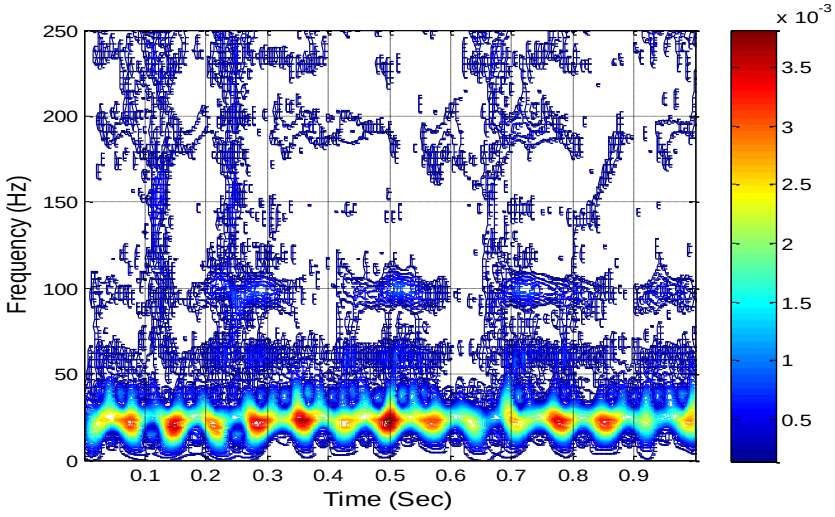


**Figure 6-14** WVD of simulated signal corrupted with Gaussian noise and with spike

In Figure 6.15, it is possible to see that, in the case of CWT, the characteristics of the time frequency signals are much clearer. The wavelet analysis highlights the exact time location of the transient spike as shown in Figure 6.16.

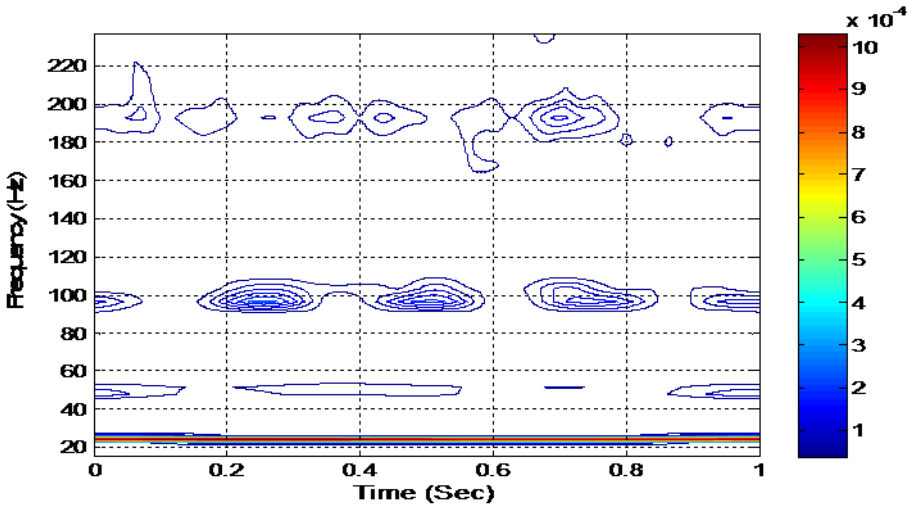


**Figure 6-15** CWT of simulated signal corrupted with Gaussian noise

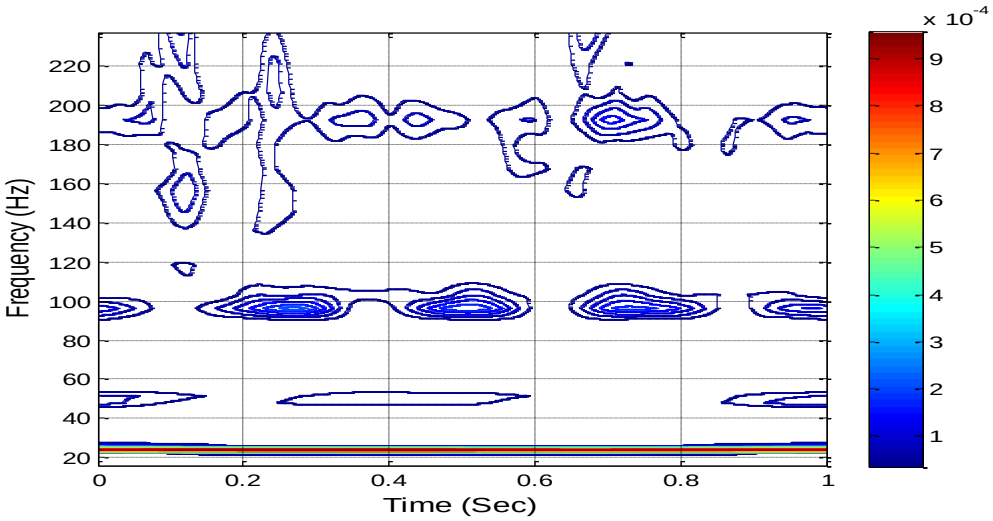


**Figure 6-16** CWT of simulated signal corrupted with Gaussian noise and with spikes

The DWT consists in sampling, scaling and shifting parameters, but neither the signal nor the transform. This leads to high-frequency resolution at low frequencies and high-time resolution for higher frequencies. Figures 6.17 and 6.18 illustrates the waveforms respectively of the simulated signal corrupted by Gaussian noise and the simulated signal corrupted by Gaussian noise and with peaks. Here the "db23" wavelet was used as the mother wavelet .The waveforms have clear spikes. Obvious periodic spikes can be seen in Figure 6.18 in subplot of scale 4 and in the subplot of scale 3. While no impulses exist in othe subplots.

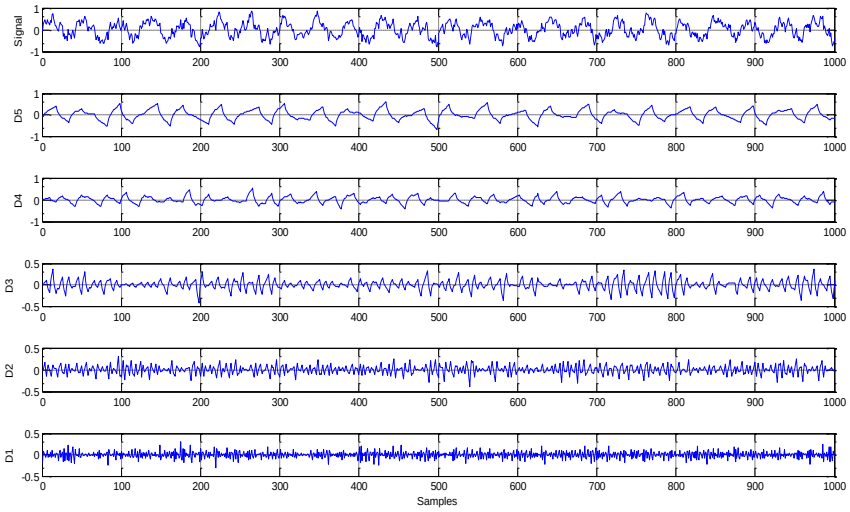


**Figure 6-17** DWT of simulated signal corrupted with Gaussian noise

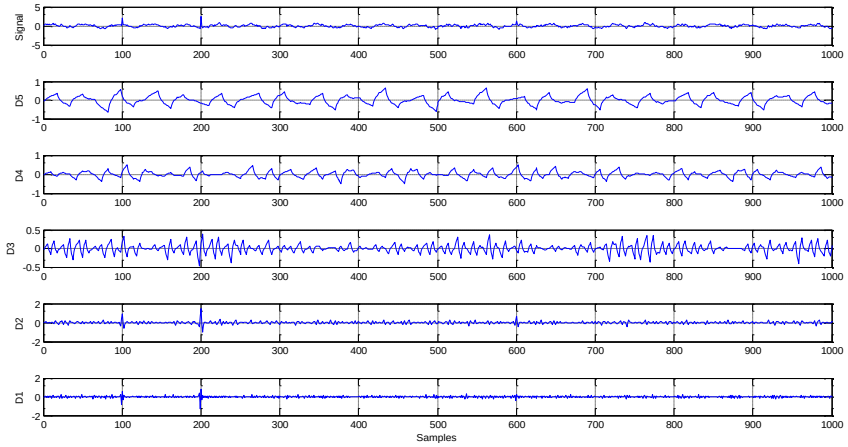


**Figure 6-18** DWT of simulated signal corrupted with Gaussian noise and with spikes

By comparing the results obtained from time-frequency analysis of simulated signal it can be seen that time-frequency analysis has advantages over time-domain or frequency-domain analysis, and these benefits make it a powerful tool in CM of machines. STFT can describe the frequency components of a signal at a specified time but a single window is used for all frequencies, so the the resolution of the STFT cannot vary for different frequencies.

The WT overcomes this problem by using a window length which is variable. However, the WDV is not capable of a satisfactory representation of multi-component signals due to the presence of cross terms. In practical applications the WVD requires smoothing to remove this cross contamination.

The DWT uses the same main idea as the CWT, but is considerably easier and faster to implement. Because of these benefits the DWT will be used for analysis of the induction motor data obtained in this research.

A brief assessment of the different signal processing techniques used above is given in Table 6.1. This summarizes the understanding of the applications and limitation of fault detection techniques gained in the simulation exercise performed here.

**Table 6-1** Comparison of techniques used for analysis of simulated signal representing vibration signal for induction motor with phase current fault

| Techniques Name | Advantage | Disadvantage |
|---|---|---|
| FFT | Suitable for high load condition<br>Easy to implement | Lost time information<br>Not effective at light load condition |
| STFT | Suitable for varying load condition Fast speed | Analyze signal with fixed sized window<br>Poor frequency resolution |
| WVD | Fine frequency resolution<br>Fast speed | Strong cross terms interferences |
| WT | Suitable for varying load and light load condition | Requires expertise |

## 6.7 Application of CWT to Induction Motor data

In this section, the WT transform is examined to see whether it is capable of detecting growing simulated local faults in the induction motor.

### 6.7.1 Detection of Phase Imbalance Faults

#### 6.7.1.1. Fault Detection by Current.

Figures from 6.19 to 6.22 illustrate the CWT of induction motor current signals for four loads on the healthy motor, motor with 20 V drop in one phase and motor with 40 V drop in one phase.

The fundamental and second power supply harmonics are visible, though the energy of the current signal is mainly concentrated around the fundamental power supply frequency. The wavelet transform results in good frequency resolution at low frequencies and gradually deteriorates when moving to higher frequencies as shown in Figure 6.19 – 6.22. This varying resolution on the time-frequency plane is due to the change in the size of the wavelet during the analysis. Low frequency characteristics of the current signal therefore can be captured and displayed more clearly when compared to higher frequency regions. For the healthy condition the wavelet does not change significantly and most of the signal energy remains around the fundamental power supply frequency region. However, the wavelet plot begins to show a small frequency activity (50 Hz) at 10 and 20 % fault level which is fault symptom.

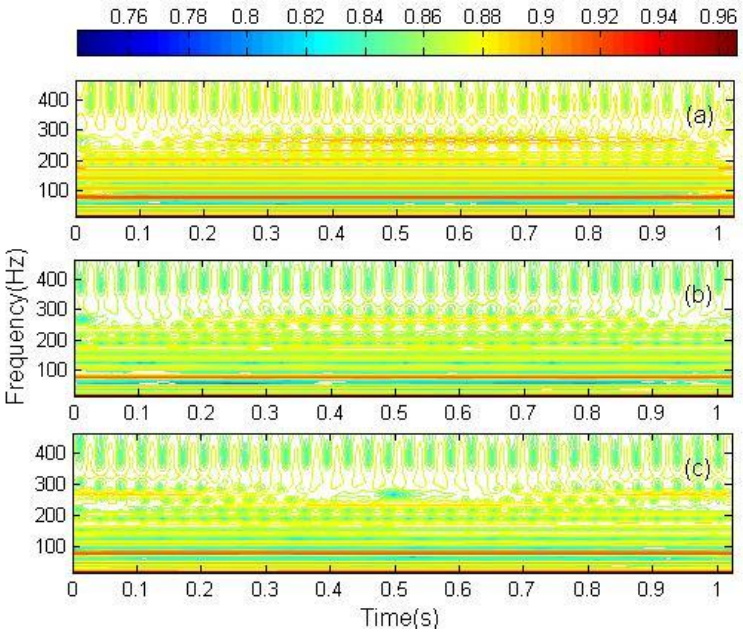


**Figure 6-19** cwt of current signal for different phase imbalance with 0% load

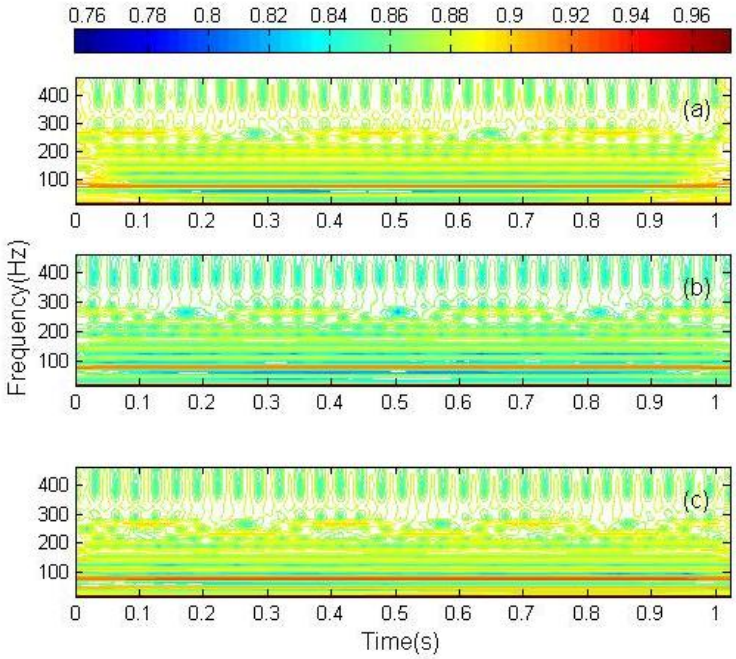


**Figure 6-20** cwt of current signal for different phase imbalance with 25% load

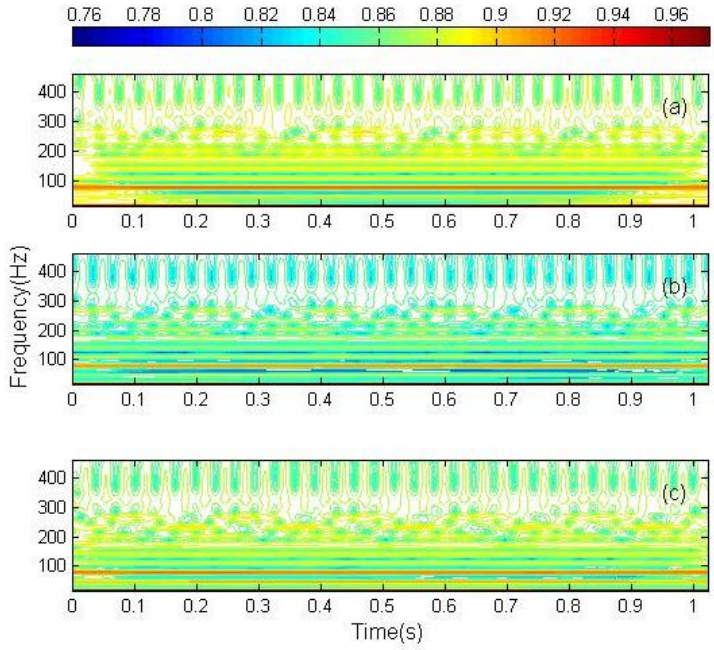


**Figure 6-21** cwt of current signal for different phase imbalance with 50% load

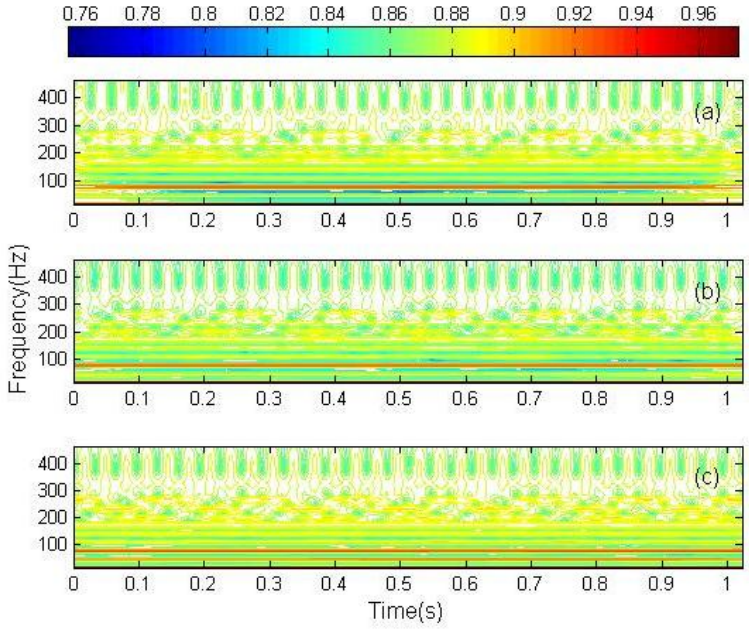


**Figure 6-22** cwt of current signal for different phase imbalance with 75% load

### 6.7.1.2. Fault Detection by Vibration

Figures 6.23 to 6.26 illustrate the use of the CWT for analysis of vibration signal collected from the induction motor housing. The operating conditions are as

described in Section 6.7.1.A above. The changes in amplitude and frequency distribution with time can be seen for every case which means the condition of the motor was varying. The energy of the signal remained close to twice the fundamental power supply frequency region (100 Hz) when the motor is in good condition or with very small faults (20 and 40 % voltage drop). However, when the local fault progresses energy in the vibration signal moves and concentrates in the frequency region around 150 Hz. But to classify the cases between healthy and faulty was difficult because there is no clear or known relationship between induction motor condition and amplitude/frequency distributions.

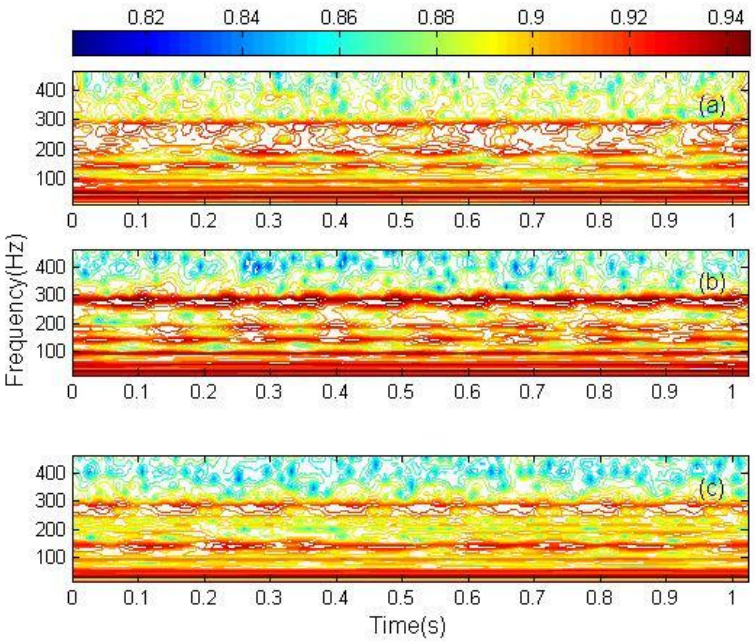


**Figure 6-23** cwt of vibration signal for different phase imbalance with 0% load

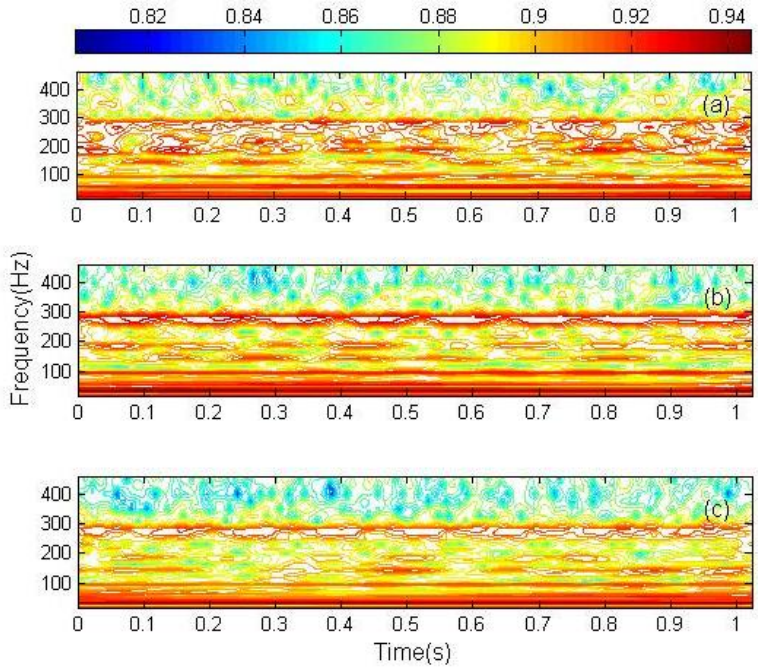


**Figure 6-24** cwt of vibration signal for different phase imbalance with 25% load

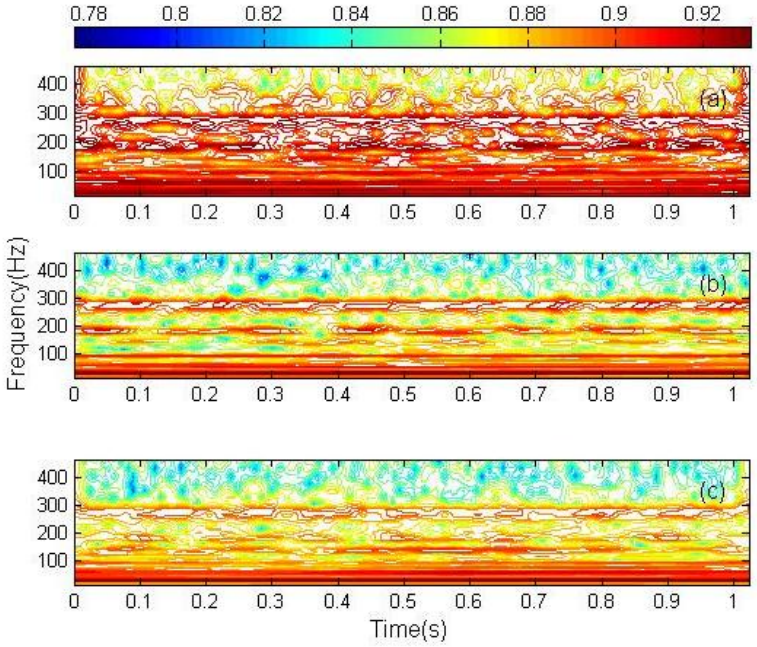


**Figure 6-25** cwt of vibration signal for different phase imbalance with 50% load

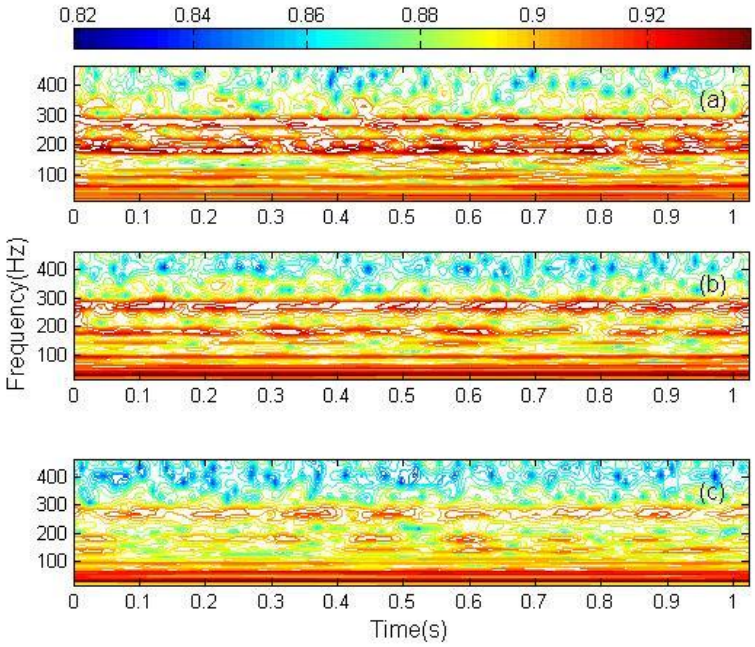


**Figure 6-26** cwt of vibration signal for different phase imbalance with 75% load

### 6.7.2 Detection of Broken Rotor Bar Fault

#### 6.7.2.1. Fault Detection by Current

Figures 6.27- 6.30 shows the WT of one phase of the motor current signal for a healthy motor and with one rotor bar broken, for four loads: no load, 25%, 50% and 75% full output load. Under healthy conditions, the wavelet plot shows a power supply frequency of about 50 Hz where the majority of the signal energy is concentrated. When one broken rotor bar was seeded into the motor there is no significant shift from normal condition.

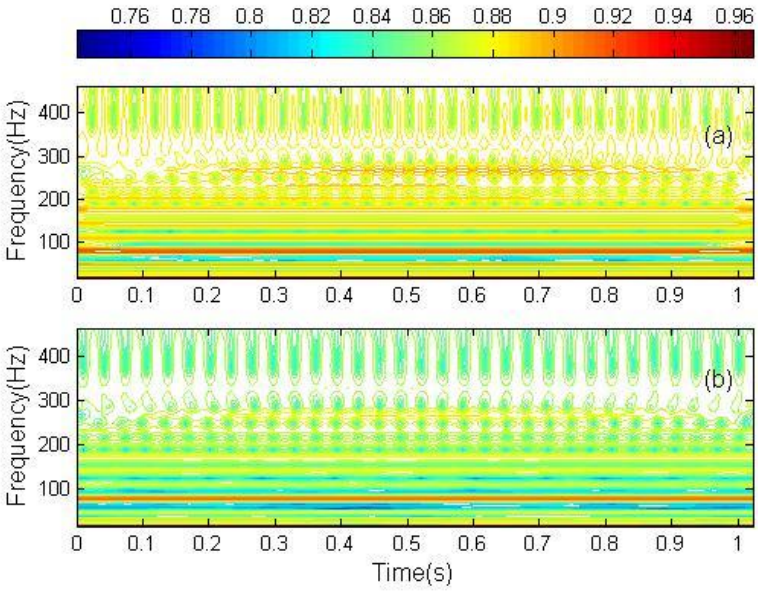


**Figure 6-27** CWT of current signal for healthy and one rotor bar broken with 0% Load

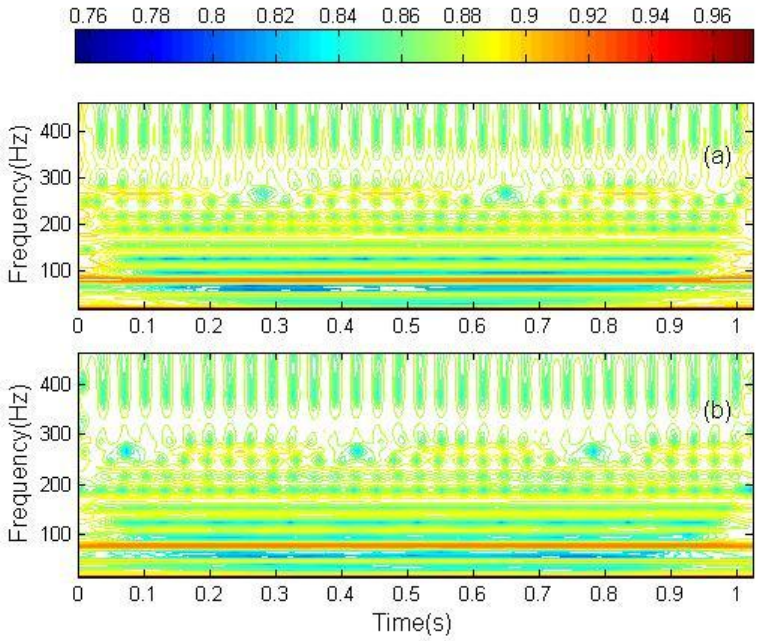


**Figure 6-28** CWT of current signal for healthy and one rotor bar broken with 25% Load

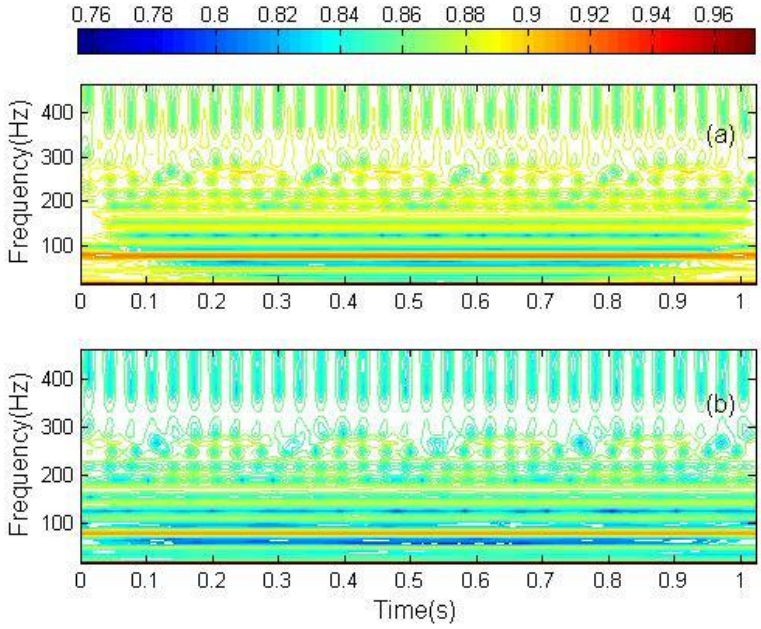


**Figure 6-29** CWT of current signal for healthy and one rotor bar broken with 50% Load

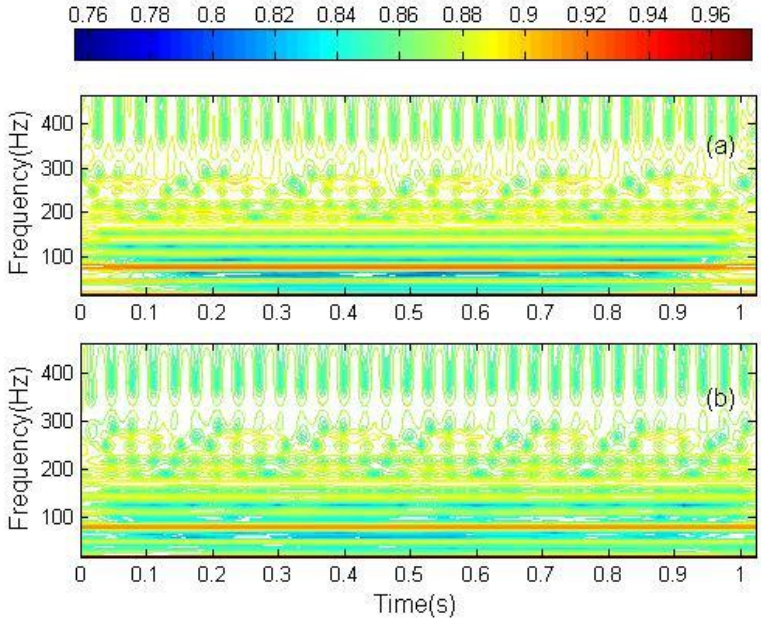


**Figure 6-30** CWT of current signal for healthy and one rotor bar broken with 75% Load

### 6.7.2.2. Fault Detection by Vibration Analysis

The WT for the healthy induction motor and motor with broken rotor bar are displayed in Figures 6.31 -6.34. The figure shows changes in amplitude and frequency distribution with time for every case which means the condition of the motor was varying. There is some change in the energy of the signal changes at the twice fundamental power supply frequency (100 Hz) when the broken rotor bar is seeded into the motor, however there is no significant difference between the normal and fault conditions of the wavelet plots.

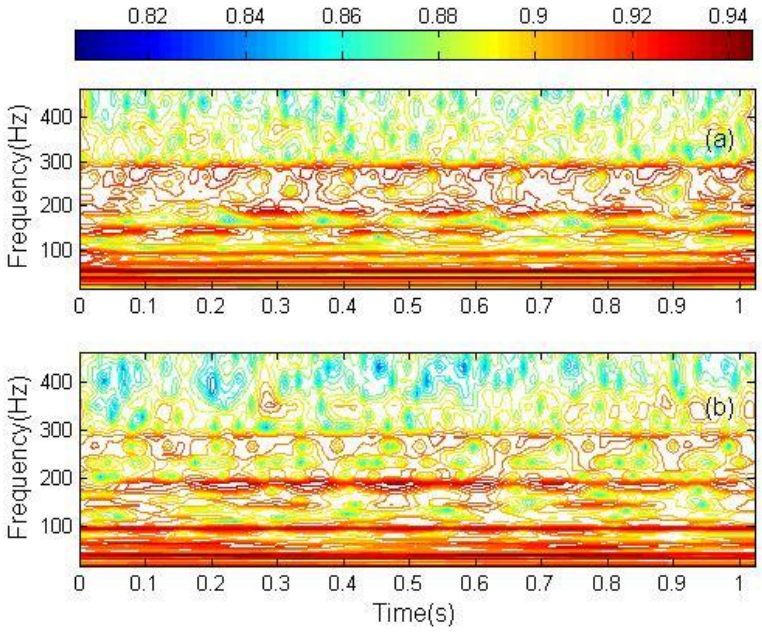


**Figure 6-31** CWT of vibration signal for healthy (a) and one rotor bar broken(b) with 0% Load

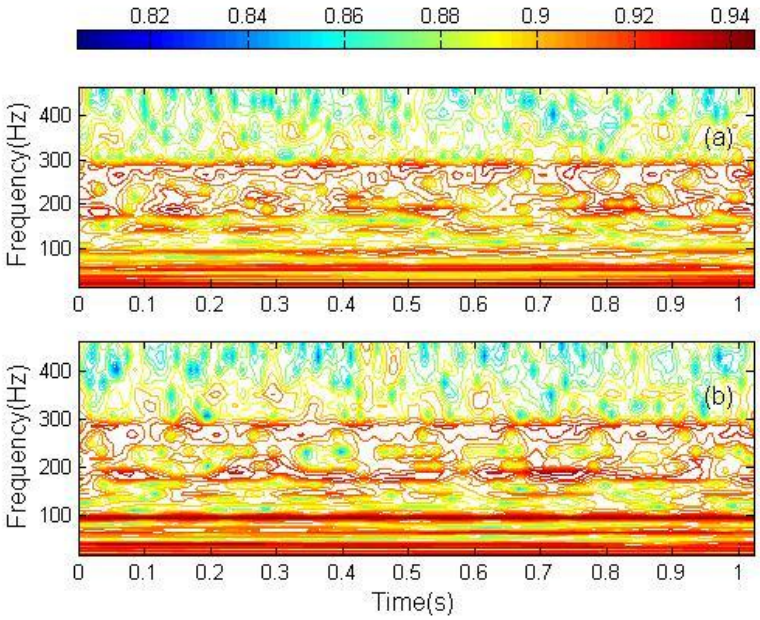


**Figure 6-32** CWT of vibration signal for healthy (a) and one rotor bar broken (b) with 25% Load

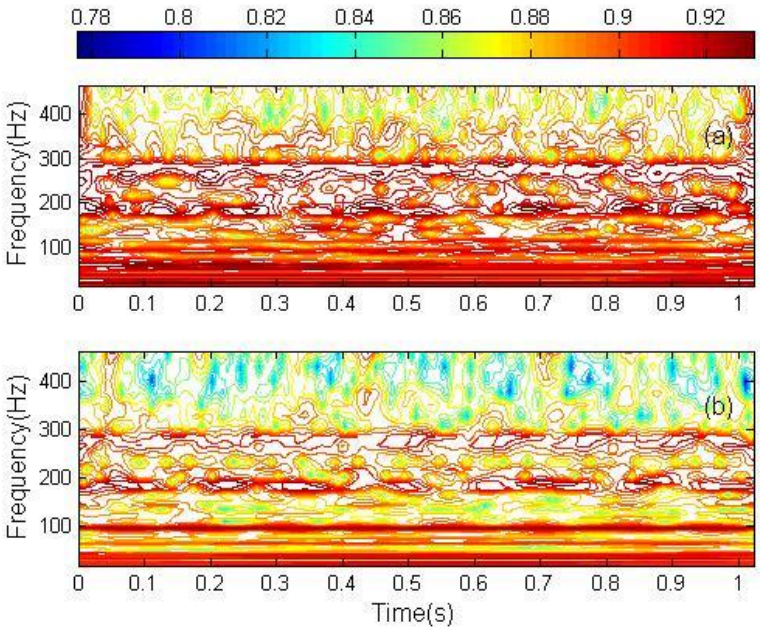


**Figure 6-33** CWT of vibration signal for healthy (a) and one rotor bar broken (b) with 50% Load

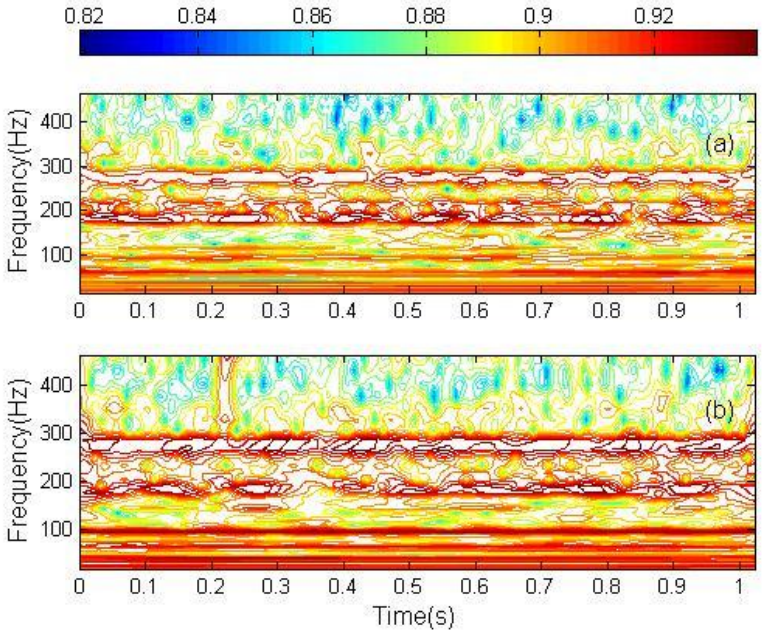


**Figure 6-34** CWT of vibration signal for healthy (a) and one rotor bar broken (b) with 75% Load

## 6.8 Application of DWT to Induction Motor Data

In this section, the DWT is examined to see whether it is capable of detecting simulated local faults in the induction motor. Figure 6-34 shows a flowchart with the steps that should be followed in order to apply the DWT for the diagnosis of faults in an induction motor.

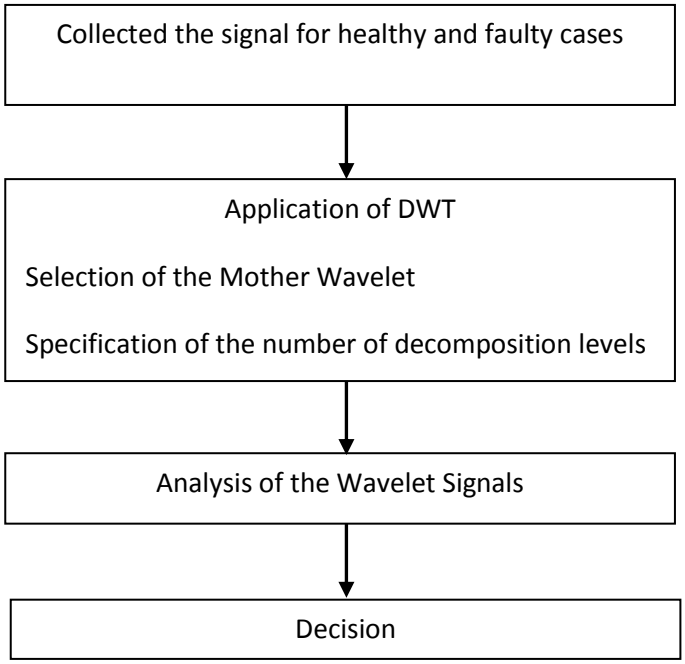


**Figure 6-35** Flowchart for the DWT-based diagnosis methodology

### 6.8.1 Selection of the Mother Wavelet

Before applying the DWT it is necessary to select the type of mother wavelet and the number of decomposition levels [91]. The selected mother wavelet is related to the coefficients of the filters used in the filtering process inherent in the DWT. Several wavelet families with different mathematical properties have been developed [91]. These wavelets may be classified into two general groups; the infinite supported wavelets such as the Gaussian, Mexican Hat, Morlet, Meyer, etc., and compact supported wavelets such as orthogonal wavelets (Daubechies or Coiflet) and bi-orthogonal wavelets, etc., [91]. In the field of fault diagnosis of an induction motor, some families have shown better results for particular applications. However, in the case of compactly supported wavelets, once the wavelet family is selected, it is advisable to carry out the DWT using a high-order wavelet (i.e. a wavelet with an associated filter with a large number of coefficients) as the mother wavelet. If a low order wavelet is used, the frequency response deteriorates and there may be overlap between adjacent frequency bands.

### 6.8.2 Specification of the Number of Decomposition Levels

The number of decomposition levels is determined by the low-frequency components to be traced. The extracted frequency band becomes lower if the number of decomposition levels of the DWT becomes higher as shown in Table 6.2. So, the evolution of these components will be reflected through the high-level signals resulting from the analysis

Typically, for the extraction of the frequency components caused by rotor asymmetries or even eccentricities, the number of decomposition levels should be equal or higher than that of the detail signal containing the fundamental frequency. This number of decomposition levels ($n_f$) is by given by [91].

$$n_f = integer\left[\frac{\log(^{f_s}/_{f})}{\log(2)}\right] \quad (6.16)$$

For data collection at a rate of *fs* = 5000 samples/s and f = 50 Hz, the application of Equation 6.16 leads to $n_f$ = 7. The frequency bands associated with each wavelet signal are shown in Table 6.2.

**Table 6-2** Frequency bands for the wavelet signal

| Level | Signal | Frequency band |
|---|---|---|
| D1 | Detail signal | 1250-2500 Hz |
| D2 | | 625-1250 Hz |
| D3 | | 312.5-625 Hz |
| D4 | | 156.25-312.5 Hz |
| D5 | | 78.12-156.25 Hz |
| D6 | | 39.06-78.12 Hz |
| D7 | | 19.53-39.062 Hz |

To perform the diagnosis, the energy factor need to be determined, this is defined as the estimation of the energy content of any decomposed detail. Energy is the percentage of energy corresponding to the details level**.**

### 6.8.3 Detection of Phase Imbalance Faults

#### 6.8.3.1. Fault Detection by Current Measurement

As predicted in Section 4.4.2, the induced faults in the current phase cause sidebands around the fundamental electrical supply frequency in the current signal. To obtain the components of the measured signal in a band near the fundamental harmonic of 50 Hz, a 7 levels one-dimensional discrete wavelet analysis was performed using the wavedec function. The db23 type wavelet from the Daubechies family was used.

As it will be seen the difference signal at the $6^{th}$ level of decomposition (d6) can be used for fault detection of the rotor induction motor phase imbalance faults, because its frequency band is between 39 and 78 Hz, where all the sideband components of interest can be found.

In Figures 6.36 to 6.39 the obtained d6 wavelet coefficient's variation with time are given for the healthy and faulty induction motor at different loads. For a better comparison in all the four cases the same axis scaling was applied.

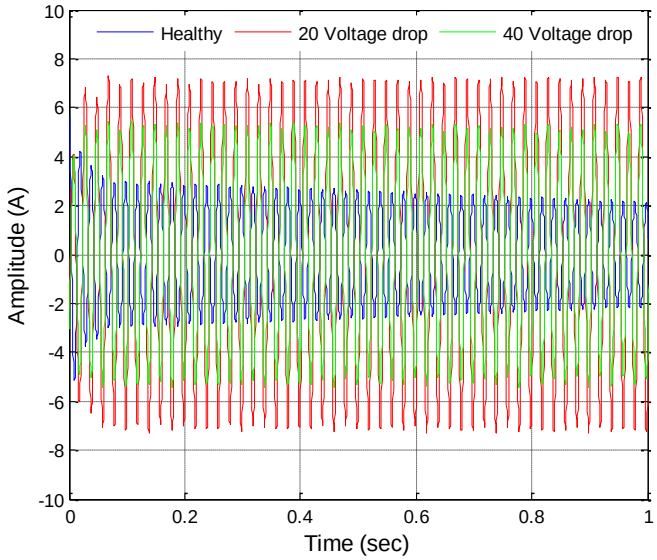


**Figure 6-36** Detail d6 level of current signal healthy and 20& 40 voltage drop with 0% Load

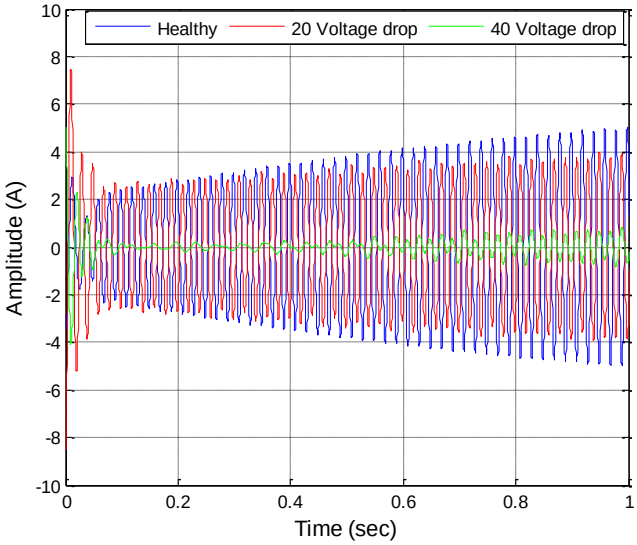


**Figure 6-37** Detail d6 level of current signal healthy and 20& 40 voltage drop with 25% Load

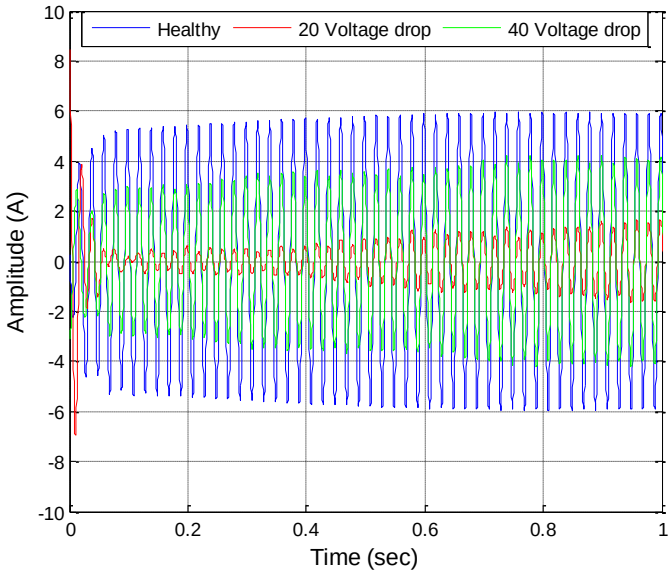


**Figure 6-38** Detail d6 level of current signal healthy and 20& 40 voltage drop with 50% Load

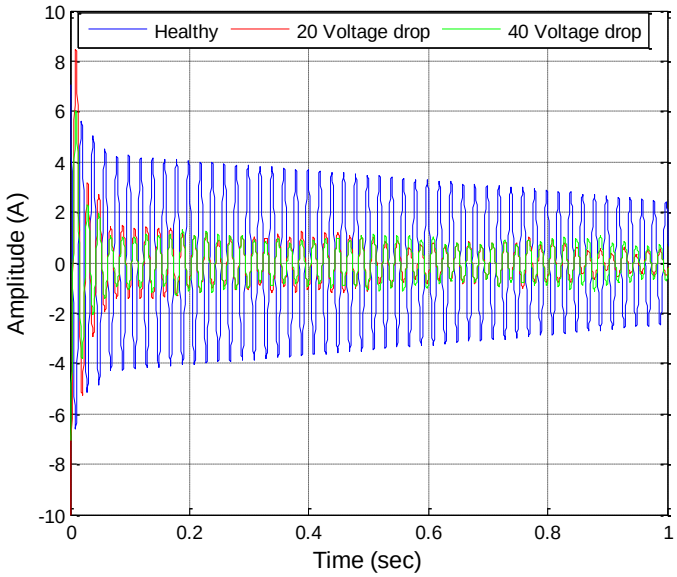


**Figure 6-39** Detail d6 level of current signal healthy and 20& 40 voltage drop with 75% Load

The fault can be detected by comparing d6 level of DWT of one phase of the motor current under healthy and fault conditions. It can be clearly seen that the amplitude at

level 6 significantly changes with the presence of as phase imbalance fault in the induction motor.

As a second step to improve comparison between healthy and faulty cases a classification method has been developed which represents the relative increase in amplitude of the energy level of a single branch of the decomposition tree to healthy condition values. In the Figures 6.36 -6.39 this method is applied to the $6^{th}$ level of the wavelet for the motor healthy and seeded with the phase voltage fault at different loads. It can be seen that the energy of the signal in the fundamental power supply frequency band (around 50 Hz) changes with the seeding of very small faults (20 and 40 voltage drop). It can be noticed that, using this method a clear detection of faults is observed at the $6^{th}$ level of composition as shown in figure 6.40

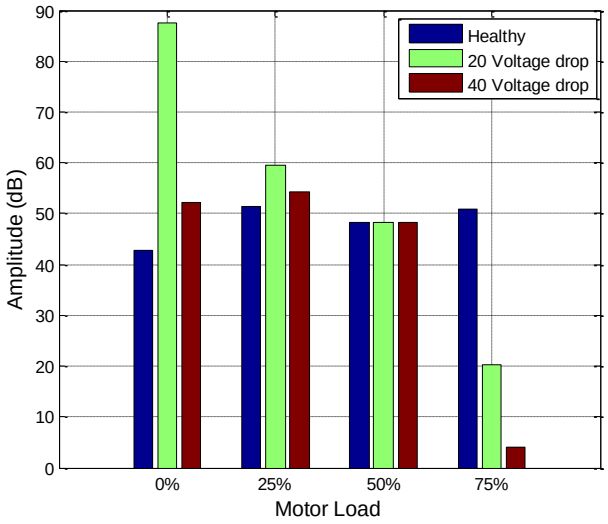


**Figure 6-40** Energy in $6^{th}$ level energy of stator current (frequency band between 39 and 78 Hz)

### 6.8.3.2. Fault Detection by Vibration Measurement

Theoretically, phase imbalance may be detected by changes in the 2×50Hz component in the measured vibration. As only a single branch of the decomposition

tree is required for the fault analysis of the phase imbalance fault of induction motor the d5 coefficient of the one-dimensional vibration signal was used because its frequency band is between 78 and 156 Hz, where all the sideband components of interest can be found [9]. The fault can be detected by comparing d5 level of DWT of vibration measured under healthy and fault conditions. It can be clearly shown that the amplitude at level 5 is significantly changed which indicates the presence of phase imbalance fault.

In Figures 6.41 – 6.45 the energy detection method is applied to the 5$^{th}$ level of the wavelet for the healthy motor and motor with seeded phase current faults at different loads. The energy of the signal changes at the twice fundamental power supply frequency band (100 Hz) when the motor is in good condition or with small faults (20 and 40 V drops). It can be noticed that, using this method a clear detection of faults is observed at the 5$^{th}$ level of composition.

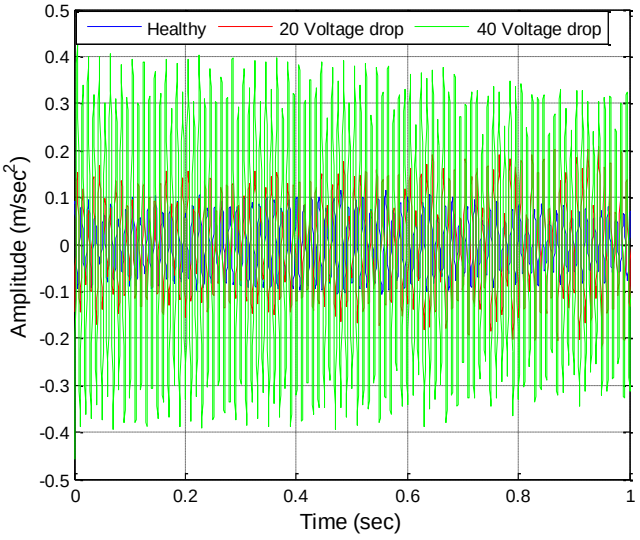


**Figure 6-41** Detail d5 level of vibration signal healthy and with 20 and 40 V drop 0% Load

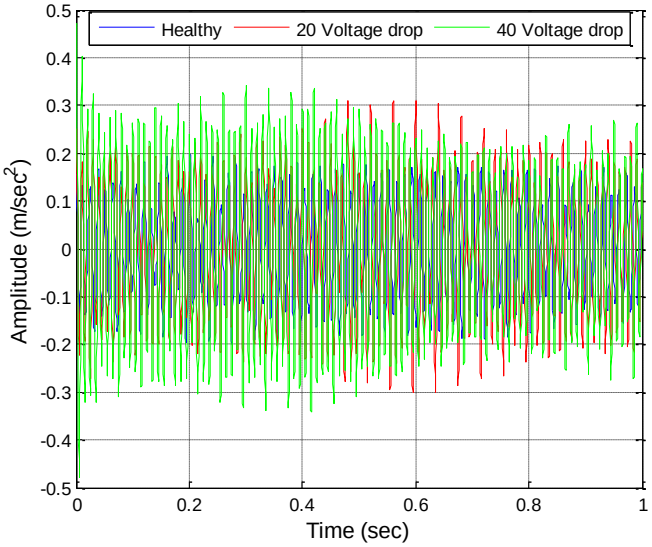


**Figure 6-42** Detail d5 level of vibration signal healthy and with 20 and 40 V drop with 25% Load

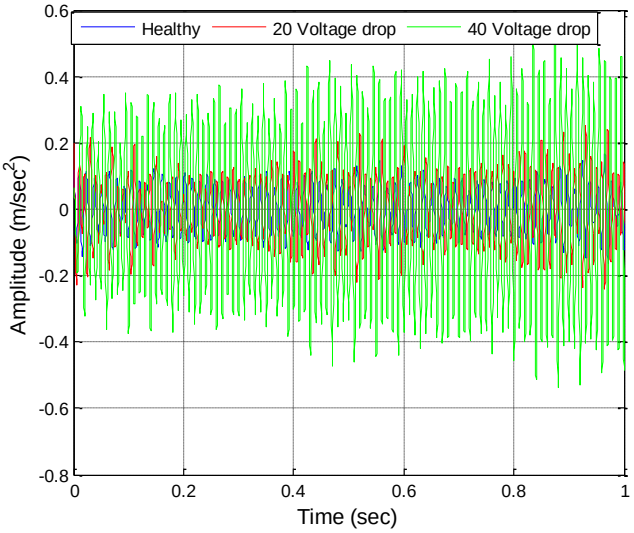


**Figure 6-43** Detail d5 level of vibration signal healthy and with 20 and 40 V drop with 50% Load

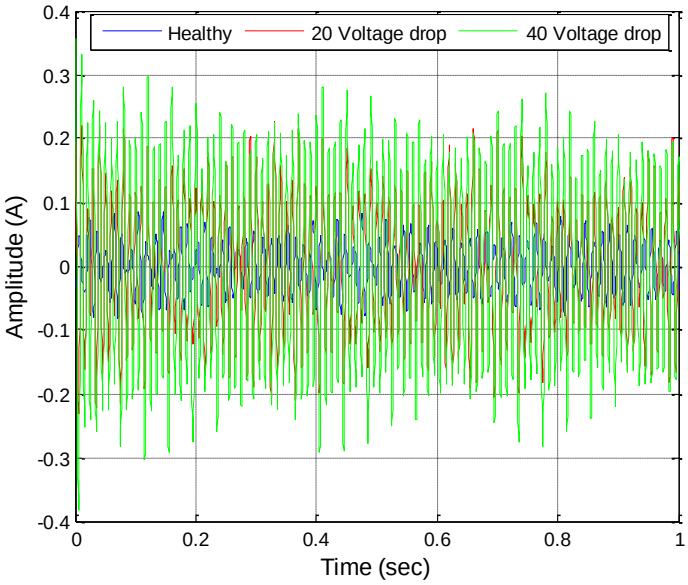


**Figure 6-44** Detail d5 level of vibration signal healthy and with 20 and 40 V drop with 75% Load

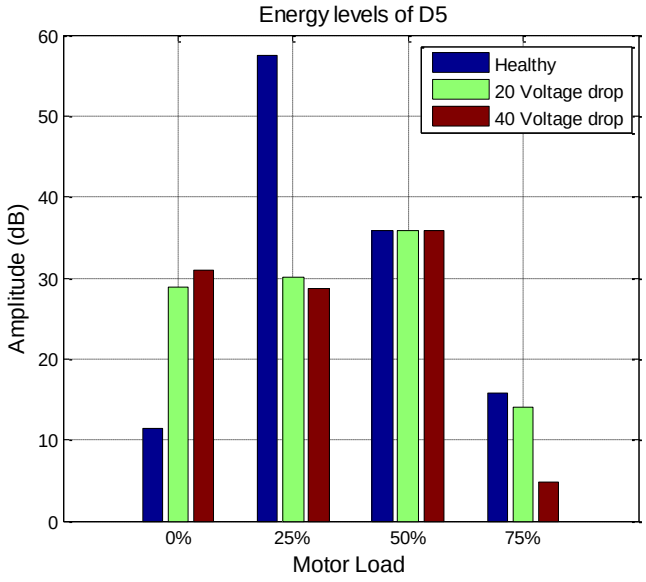


**Figure 6-45** Vibration energy in 5$^{th}$ level energy (frequency band between 78 and 156 Hz)

### 6.8.4 Detection of Broken Rotor Bar Faults

#### 6.8.4.1. Fault Detection by Current Measurement

As predicted in Section 4.4.2, the induced broken rotor bar faults caused sidebands spaced at twice the slip frequency around the fundamental electrical supply frequency. As mentioned in section 6.8.3, the sixth level of decomposition (d6) can be used for fault detection of a broken rotor bar in an induction motor.

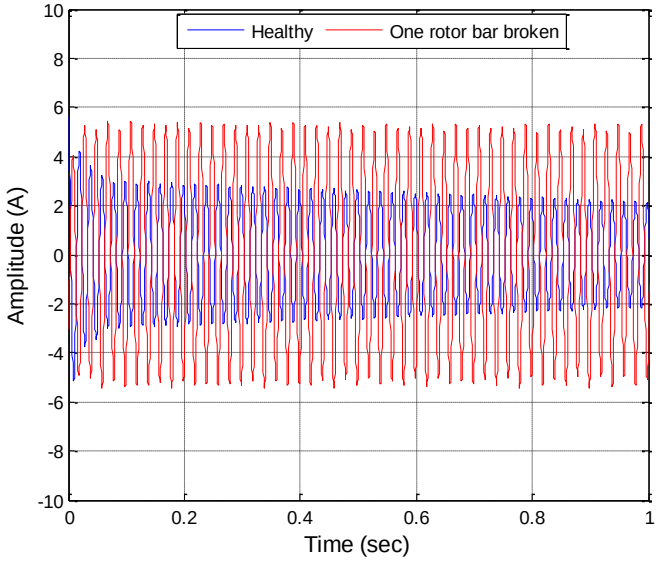


**Figure 6-46** Detail d6 level of current signal healthy and one broken rotor bar under 0% Load

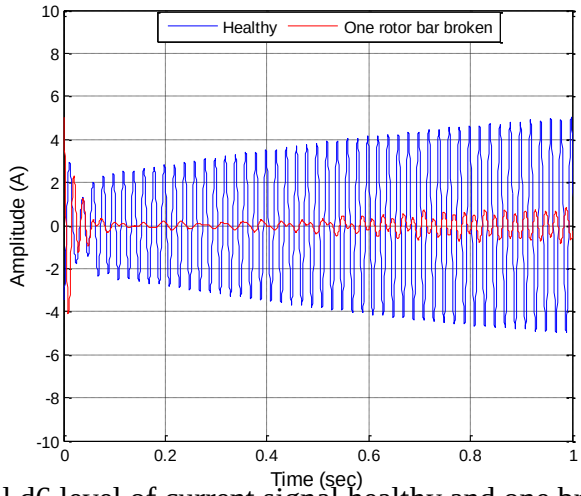


**Figure 6-47** Detail d6 level of current signal healthy and one broken rotor bar under 25% Load

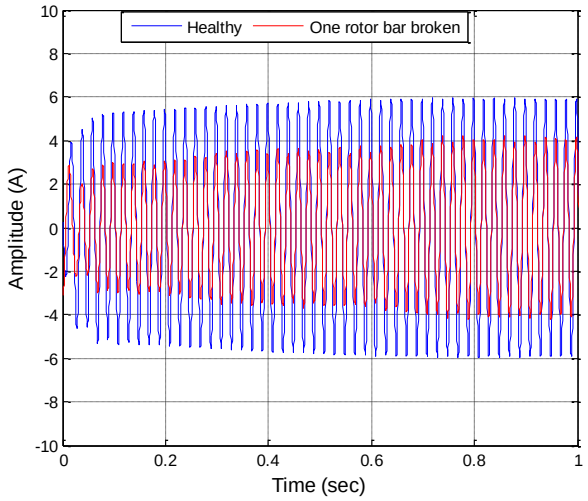


**Figure 6-48** Detail d6 level of current signal healthy and one broken rotor bar under 50% Load

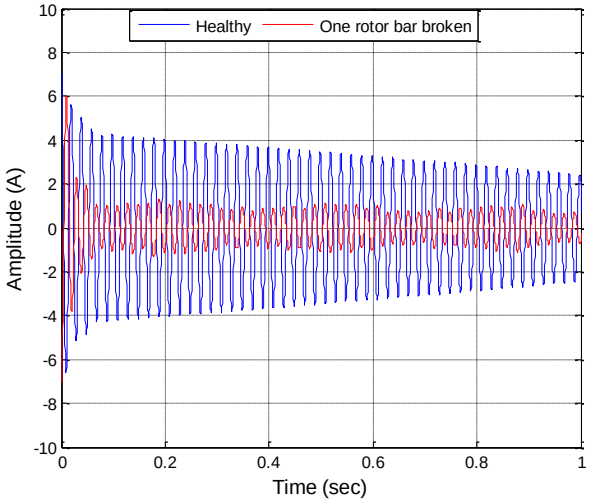


**Figure 6-49** Detail d6 level of current signal healthy and one broken rotor bar under 75% Load

The fault can be detected by comparing d6 level of DWT of one phase of the motor current for healthy motor and motor with one rotor bar broken. It can be clearly shown that the amplitude significantly changes which indicates the presence of the fault.

In Figure 6.50, the energy detection method is applied to the 6th level of the wavelet for healthy and faulty motor (broken rotor bar) for different loads. The energy of the signal around the fundamental power supply frequency (50 Hz) changes both with change in load and the seeding of the fault. It can be noticed that, using this method a clear detection of faults is observed at the 6$^{th}$ level of composition.

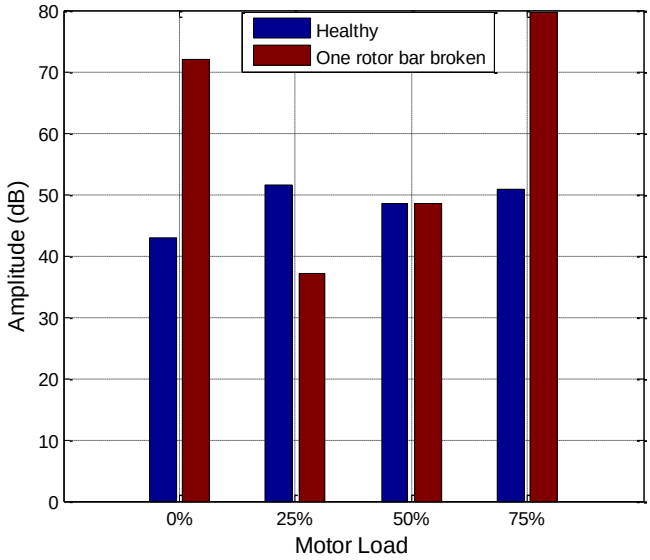


**Figure 6-50** Energy in 6$^{th}$ level energy of stator current (frequency band between 39 and 78 Hz)

### 6.8.4.2. Fault Detection by Vibration Measurement

Theoretically, broken rotor bars may be detected by the presence of sidebands around the running speed frequency in the vibration spectrum. In order to obtain the components of the measured signal in a band near the running speed frequency, 24.3 Hz, the 7$^{th}$ level of decomposition (d7) can be used for fault detection of the seeded rotor induction motor faults, because its frequency band is between 19 and 39 Hz, where all the sideband components of interest can be found [9].

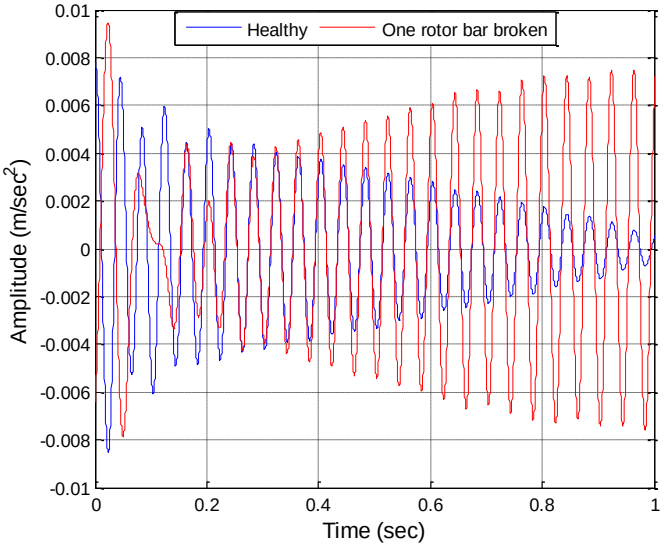


**Figure 6-51** Detail d7 level of vibration signal healthy and one rotor bar broken with 0% Load

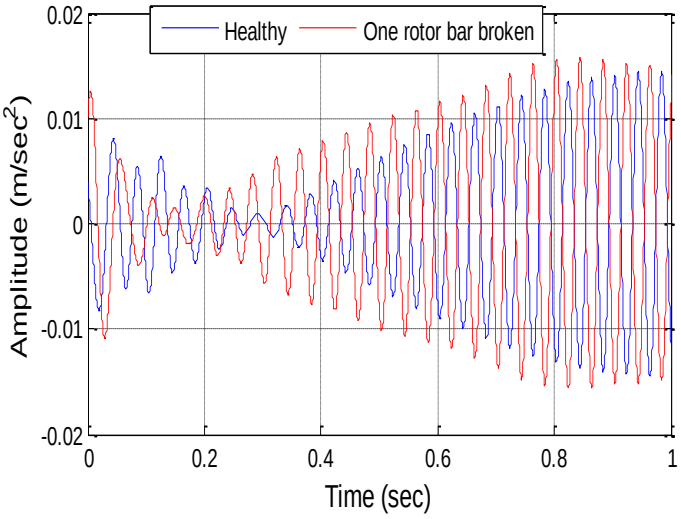


**Figure 6-52** Detail d7 level of vibration signal healthy and one rotor bar broken with 25% Load

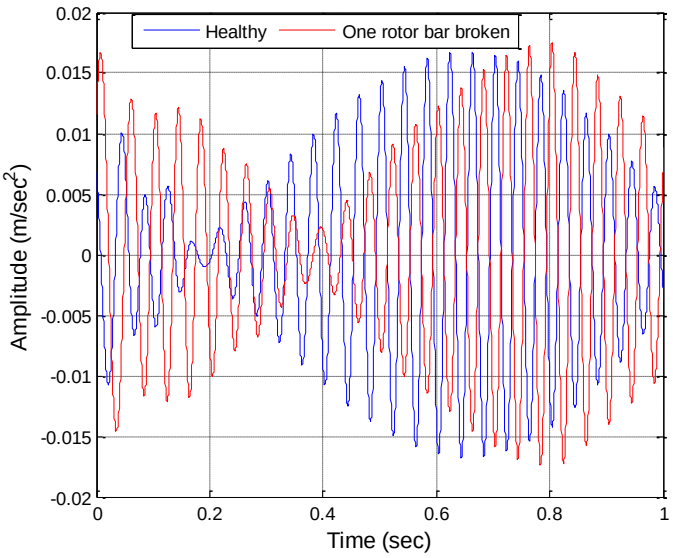


**Figure 6-53** Detail d7 level of vibration signal healthy and one rotor bar broken with 50% Load

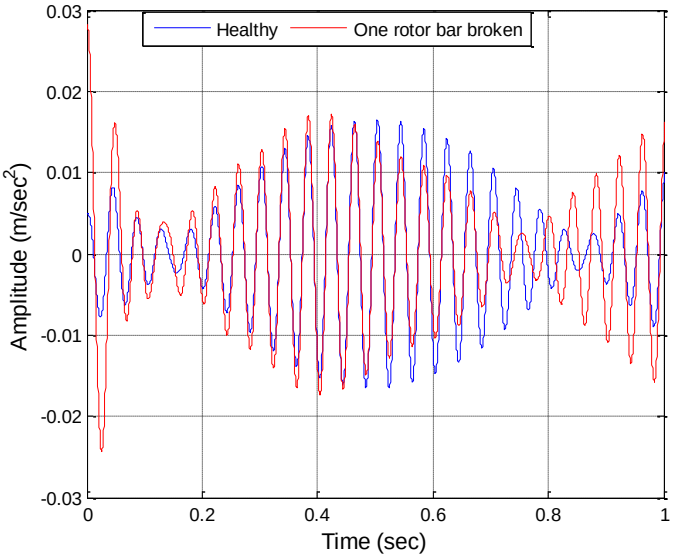


**Figure 6-54** Detail d7 level of vibration signal healthy and one rotor bar broken with 75% Load

The presence of the fault can be detected by comparing d7 level of DWT of vibration under healthy and faulty (one rotor bar broken) conditions. The energy of the signal in the fundamental running speed frequency band (24 Hz) changes when load on the

motor increases, whether the motor is healthy or with a rotor bar fault. However, there appears to be a significant difference between healthy and faulty condition only for low loads.

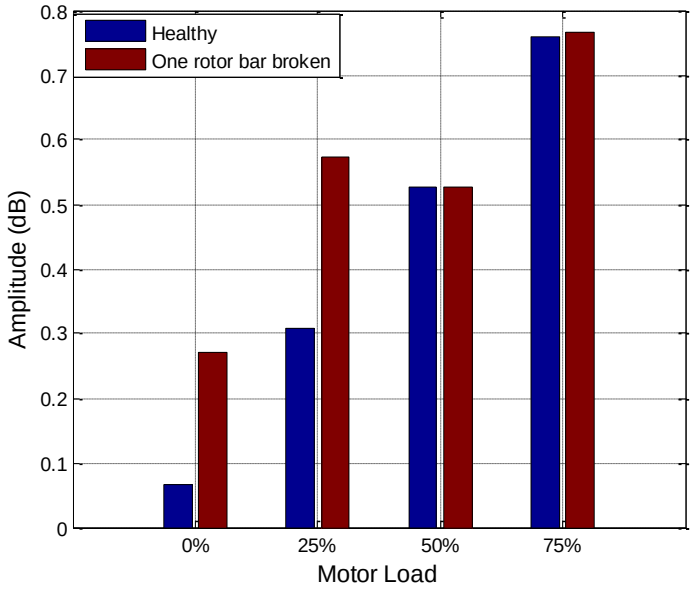


**Figure 6-55** Vibration energy in 7$^{th}$ level (frequency band between 19 and 38 Hz)

## 6.9 Summary

Chapter 5 showed that conventional statistical techniques and the FT of the time domain signals provide only limited information for fault detection and diagnosis, because non-stationary signals can be analysed more effectively by time-frequency analysis to provide a description of changes in frequencies of the measured signal with time. STFT, WVD, CWT and DWT are advanced signal processing time-frequency techniques that have been tested by numerical simulation signal to determine their effectiveness in diagnosing faults in an induction motor. The results showed that there are limitations when using STFT and WVD techniques to diagnose and classify the faults. To overcome these limitations WT was applied when the motor operated under various output loads and different degrees of faults. DWT has

also been used to diagnose faults in the induction motor under varying load conditions and was found faster than the CWT.

The higher level components DWT of the measured signal did not provide useful information. Low frequency details d5 to d7 are much more relevant for fault detection because they cover the frequency bands corresponding to the supply and the fault frequency. The results of experiment show the wavelet decomposition is an appropriate technique for non- stationary signals representing faults in an induction motor.

# CHAPTER 7

# RECONSTRUCTION OF VIBRATION SIGNAL FROM PHASE CURRENT SIGNAL IN INDUCTION MOTOR

*Many processes and systems using three phase induction motors are inherently non-linear. Thus they cannot be represented by simple and accurate models. A common example of a nonlinear process within the induction motor is the vibration signal measured in order to detect a fault or defect. Yet measurement and analysis of the vibration signal are important in improving motor performance and condition monitoring and this necessitates sophisticated analysis techniques that have yet to be proven in practice. An effective alternative to direct vibration measurement, preferably using easy-to-measure variables would be very attractive to industry, and in an attempt to meet this need this chapter applies radial basis function networks to the reconstruction of motor vibration using measurements of one phase of the motor current.*

## 7.1 Introduction

Vibration measurement is widely used for diagnosing the condition of rotating machinery; but sometimes direct measurement can be difficult and expensive in remote or locations that are challenging to access, in harsh environments and where it is expensive to install sensors close to the machine. These conditions apply to electrical submersible pumps (ESPs) in deep-well oil and gas extraction, or deep within nuclear power stations. The current driving the pump has a signature which has been shown to provide information on the condition of the pump without requiring direct access to the pump itself. But some faults, mechanical are better detected by vibration analysis.

This chapter investigates the relationship between driving current of a pump and pump vibration using coherence technique as a measure of the relationship. The relationship between driver's current signature (DCS) and its vibration signature (DVS) is found by calculating the magnitude of the square of the coherence and phase coherence parameters in a certain frequency band using a continuous wavelet transform (CWT). The secondary purpose was to develop a technique for detecting and locating faults (assessing condition and performance) in inaccessible equipment using radial basis function (RBF) networks to reconstruct the vibration waveform from the measured phase current.

Initially the relationship between phase current signals and vibration is investigated. This is done by using non-parametric mapping to establish a relationship between the motor phase current signal time series and the vibration time series by applying an RBF network.

The key parameters measured via the test rig were: one phase of the motor current signature (MCS) and the motor vibration signature (MVS). The phase current is an input parameter to the prediction model for predicting motor vibration, and the motor vibration is the output parameter.

Figure 7.1 shows how the RMS vibration varies with RMS stator current at different motor loads. It can be seen that RMS current and vibration are inversely related as the motor load increases.

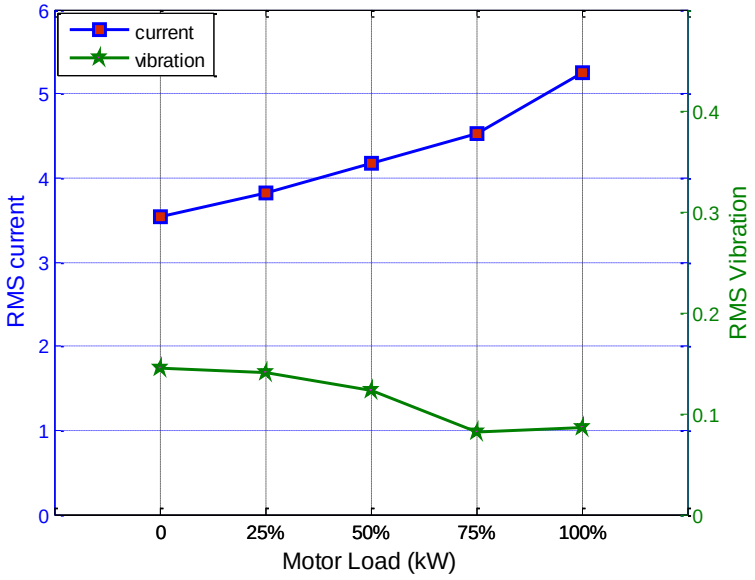


**Figure 7-1** Influence of load on the RMS current and vibration signals

### 7.1.1 Coherence

Coherence is a function of the power spectral densities (*Pxx* and *Pyy*) of *x* and *y* and the cross power spectral density (*Pxy*) of *x* and y and is given by:

$$C_{xy}(f) = \frac{|P_{xy}(f)|^2}{P_{xx}(f)P_{yy}(f)} \qquad (7.1)$$

Coherence is the function of frequency $f$ with $C_{xy}(f)$ lying in the range 0 to 1 and indicates how well the frequency components of signals *x* and *y* correspond. The

degree of synchronization in stator current signal and vibration signal it could be characterized by coherence phase and magnitude squared coherence.

Figure 7.2 shows the calculated coherence function between motor current and vibration signature. It can be seen that the largest values of coherence (where vibration signal and motor current are best correlated) are located at 50, 100 Hz , 400 Hz and 500 Hz.

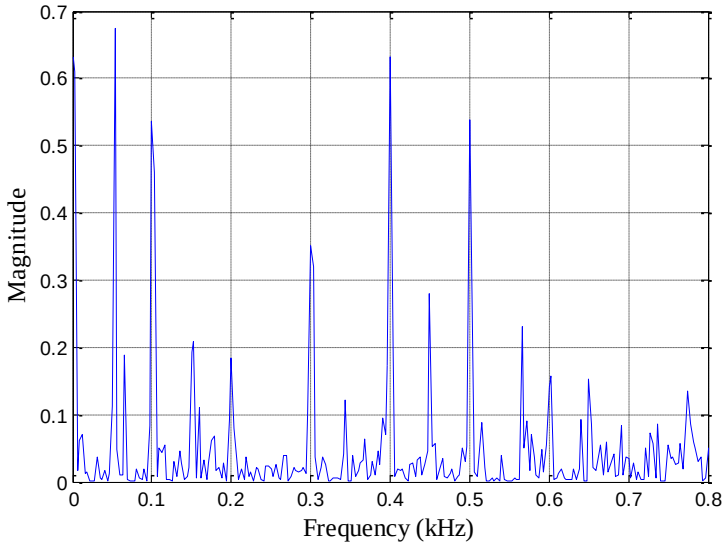


**Figure 7-2** Coherence between MCS and MVS signals

### 7.1.2 Wavelet coherence

Areas in the time-frequency plane where the two time series exhibit common power or consistent phase behaviour indicate a relationship between the signals.

The wavelet coherence of two time series x and y is:

$$\frac{S[C_x^*(a,b)C_y(a,b)]}{\sqrt{S(|C_x(a,b)|^2)}\ \sqrt{S(|C_y(a,b)|^2)}} \qquad (7.2)$$

Where *Cx(a,b)* and *Cy(a,b)* denote the continuous wavelet transforms of *x* and *y* at scale *a* and position *b*. The superscript * is the complex conjugate and *S* is a smoothing operator in time and scale.

Wavelet coherence is the square of the local correlation coefficient in the time-scale plane. Figure 7.3 displays wavelet coherence for the measured vibration and current signals. The common period of the signals at scale 192 is clearly detected. Note that this corresponds to a frequency of 50 Hz .The arrows in the figure represent the relative phase between the two signals as a function of scale and position.

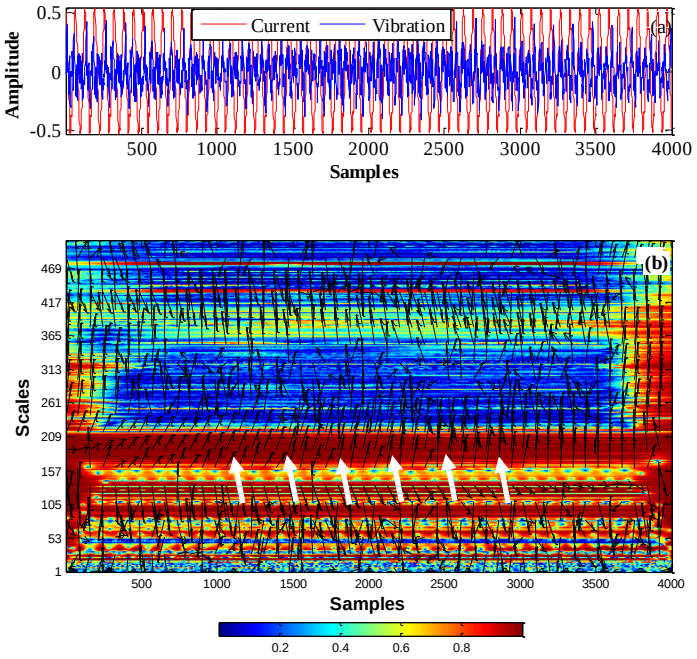


**Figure 7-3** Wavelet coherence of MCS and MVS signals (a) time domain (b) wavelet coherence

In conclusion the relationships between the input and output parameters (stator phase current and vibration respectively) had a non-linear correlation. Therefore, a suitable processing technique for modelling non-linear correlations had to be found.

Advances in computing technology and sensors, together with cost effective high performance signal processing have made advanced diagnostic systems readily

available including non-parametric models such as RBF neural networks. Such models are especially useful for obtaining connections between input and output variables where the operating conditions are known. Such an approach can be used for diagnostic purposes since a deviation from the expected output for a given input can be attributed to a specific defect or particular fault. For example, using simulation, reconstruction of an otherwise difficult to obtain vibration signal is possible from motor phase current. Such an approach could help in development of induction motor design.

## 7.2 Neural networks

### 7.2.1 A brief overview

Artificial neural networks (ANNs) are computer algorithms which attempt to simulate the working of the human brain [57]. Work in this field began mid-1940s inspired by interest in how the brain functions and today ANNs are widely used in application from engineering to finance, and from manufacturing to medicine.

Network architectures can be divided into fundamentally different groups[57]. The simplest is the single-layer feed-forward (F-F) neural network which consists of only an input and an output layer. Multi-layer F-F neural networks differ from the single-layer because they contain at least one hidden layer. A recurrent or feed-back neural network contains at least one feed-back loop.

An important feature of ANNs is their ability to improve their performance through learning making them respond differently to their environment because of what has been learned[57]. An ANN can learn from its environment and the manner it learns needs to be considered and integrated into the learning process. A learning paradigm relates to the process by which, or the environment in which an ANN learns: the two

generally considered most important are supervised learning (learning with a teacher) and unsupervised learning (learning without a teacher). This project uses supervised learning.

In supervised algorithms the learning is guided by specifying for each training input data sample, the class to which the pattern is supposed to belong. That is, the desired response of the network to each training input data sample is compared with the actual output of the network and the deviation between the both is used to adjust the weights so as to minimise it. Once the weights are adjusted (the deviation cannot be further minimised (significantly) the network is then capable of classifying input data samples.

In unsupervised learning the NN forms its own classification based on similarities (clustering).

An artificial neuron is a device with many inputs and one output. The neuron has two modes of operation; the training mode and the prediction/classification mode. In the training mode, the neuron can be trained to fire (or not), for particular input patterns. In the prediction mode, when a taught input pattern is detected at the input, its associated output becomes the current output.

If the input pattern does not belong in the taught list of input patterns, the activation function is used to determine whether to fire or not.

### 7.2.2 Neurons activation functions

The output of each particular neuron is determined by a non-linear activation function:

$$y = s(\sum_{j=1}^{P} w_j x_j + \theta) \qquad (7.3)$$

Where $\theta$ is the bias, which determines the values around which the output is most sensitive.

There are different activation functions, but the most popular functions are:

a) Linear

$$y = \sum_{j=1}^{P} w_j x_j + \theta \tag{7.4}$$

b) Threshold

$$y = \begin{cases} 1; \sum_{j=1}^{P} w_j x_j + \theta \geq 0 \\ 0; \sum_{j=1}^{P} w_j x_j + \theta < 0 \end{cases} \tag{7.5}$$

c) Sigmoid

$$y = \frac{1}{1+e^{-\beta \sum_{j=1}^{P} w_j x_j + \theta}} \tag{7.6}$$

d ) Gaussian

$$y = e^{-\beta \sum_{j=1}^{P} w_j x_j + \theta} \tag{7.7}$$

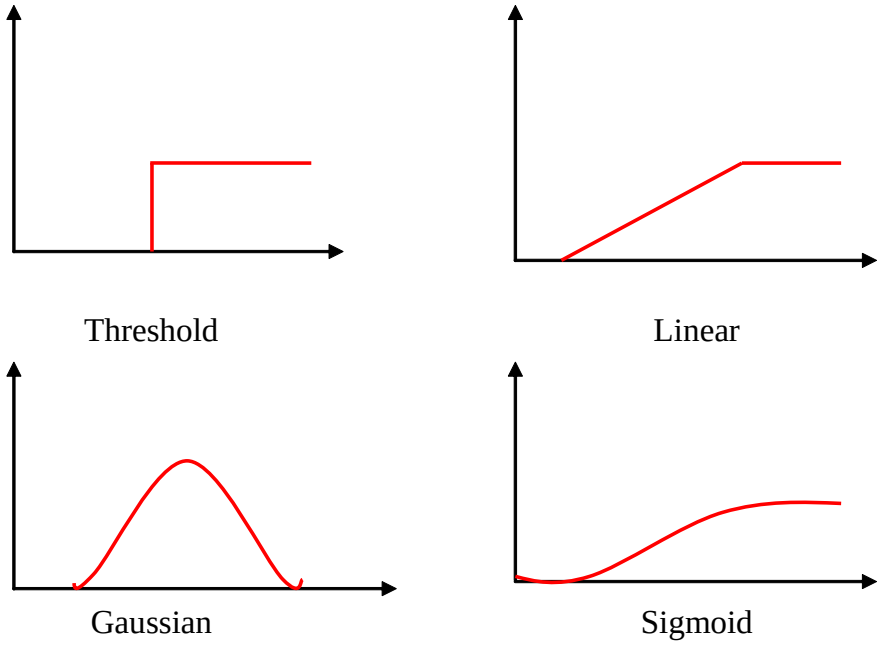


**Figure 7-4** Activation function

The most widely used are the last two because they are smooth (differentiable).

### 7.2.3 Motivation for use

ANNs are most commonly used in applications involving pattern recognition, and this is their use in this thesis. The inputs generate outputs according to patterns contained in the baseline data. The ANN has to reproduce that pattern so a given input produces the required output. Experience has demonstrated that the relationships between inputs and outputs are all non-linear using just one input. This means at least two inputs are necessary for the technique to produce the required output.

ANNs are able to model multi-input, non-linear relationships which make them very useful for real-world applications [92]. ANNs with a suitable design are able to learn rapidly from experience and, generally, the more data supplied the more accurate the

prediction [55]. Because ANNs appeared so well-matched to the system to be used in this project it was assumed they were a suitable prediction tool to use.

### 7.2.4 Specific types of neural network

When the activation functions in the *hidden layer* are *Gaussians* and the activation functions in the *output layer* are *linear* we have an interesting special type of NN called Radial basis function (RBF) .

Today many variations of ANNs are in use and here RBF neural networks will be used to provide an accurate fault diagnostic classification. RBF networks have two major advantages;

(i) a well-known and user friendly training algorithm determines the best possible network architecture according to the given input data with a minimum number of trials ( feature that is sought after in industry),

(ii) The radial basis function neural networks (RBFNN) has ability to model smooth non-linear function and;

(iii) The outputs of the ANN can not only provide fault detection and diagnosis but can also indicate the severity of the fault.

### 7.2.5 RBF Network Structure

In recent years, Radial Basis Function (RBF) networks have been enjoying greater and greater popularity as an alternative solution to the slowly convergent multi-layer perceptron. The radial basis function neural networks (RBFNN) has ability to model smooth non-linear function, and do not need many nodes to achieve the required approximating properties However, this kind of neural networks needs many nodes to achieve the required approximating properties [93]. This phenomenon is similar to the choice of the number of hidden layers and neurons in the multi-layer perceptron.

The RBFNN architecture is shown in Figure 7.4. Such a network has three layers: the input layer, non-linear hidden layer and the linear output layer, where x = [x1, . . . , xn]T , $x \in R^n$ is the input vector, h = [h1, . . . , hp]T , $h \in R^p$ is the hidden layer output vector, $W(k) \in R^{q \times p}$ is the weight matrix with entry $w_{ij}$ the weight linking the jth node in the hidden layer to the ith node in the output layer, and $\hat{y} = [\hat{y}_1, \hat{y}_2, \cdots, \hat{y}_p] \in R^p$ is the output vector of the RBFNN. The distance between the input vector x and the vector of the centers ci = [ci1, . . . , cin]T , is described by the following expression [93] :

$$z_i(k) = \left\| x(k) - c_i \right\| = \sqrt{([x(k) - c_i]^T [x(k) - c_i])} \tag{7.8}$$

$$h_i(k) = f[z_i(k)] \tag{7.9}$$

$$\hat{y}(k) = Wh(k) \tag{7.10}$$

where i=1….q , $q \in R$, ci is the ith center in the input space and $f[z_i(k)]$ is the nonlinear activation function in the hidden layer. Many different activation functions have been suggested. The most frequently used are Gaussian functions [93]

$$f[z_i(k), \sigma] = \exp(-\frac{z_i^{\,2}(k)}{\sigma_i^{\,2}}) \tag{7.11}$$

where $\sigma_i$ is a positive scalar width. The RBFNN model is used to estimate the compressor voltage input as an inverse model.

The fundamental operation in the RBF network is the selection of the function number, function centers and their position. a small a number of centers can result in weak approximating properties. On the other hand, the number of exact centers

increases exponentially with an increase in the input space size of the network. For training RBF neural network the K-means algorithm will be used.

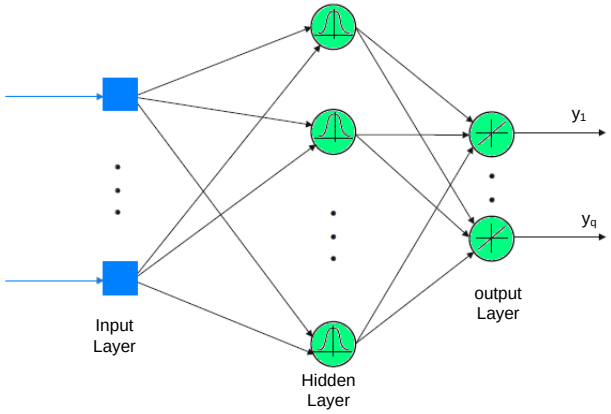


**7-5** Structure of the RBF Neural Network with N Inputs and Q Outputs

### 7.2.6 RBF Network off-line Training Algorithms

The training of RBF means optimizing the parameters of centers, widths and weights in the network to get the same desired output. For training RBF neural network the K-means algorithm is used to choose the centers, P-nearst algorithm decides the widths and the recursive training algorithm calculates weights for the output layer of RBF network. All this algorithms are discussed in brief below.

#### A. K-Means Algorithm

The aim of the K-means clustering method is to minimize the sum of the squared distance from each input data to its closest centre so that the data is adequately covered by the activation functions $f[z_i(k)]$. The k-means clustering method can be surmise as following:

1. Choose q inputs data randomly to be the initial centers c1(k), c2(k),…, cq(k). The number of the centers is designed according to the complexity of the problem.

2. Assume p(x) is the index of the best-matching centre for the input vector x. At the iteration t find p(x) by minimizing the sum squared distances:

$$p(x) = \arg\min \left\| x(k) - c_i(k) \right\|^2 \tag{7.12}$$

Where ci(k) is the centre of the ith activation at iteration k.

3. By using the following rule update the centers of the activation function:

$$c_i(k+1) = \begin{cases} c_i(k) + \alpha_C [x(k) - c_i(k)] & if \quad k = p(x) \\ c_i(k) & otherwise \end{cases} \tag{7.13}$$

Where $\alpha_C$ is the centre learning rate that lies in the range (0,1).

4. Increment k by 1 and repeat step 2 until $c_i$ (k+1) = $c_i$ (k).

**B. P-nearest Neighbour's Algorithm**

The width σ of the RBFNN for each center is determine by ρ – Nearest Neighbour's method as the square root of average squares of the distances from the center to nearest p centers is given by the following equation [93]

$$\sigma_i = \sqrt{\frac{1}{p} \sum_{j=1}^{p} \left\| c_i - c_j \right\|^2} \qquad i = 1, \ldots\ldots n_h \tag{7.14}$$

**C. Recursive Least Squares Algorithm**

The recursive least-squares algorithm is a recursive form of the least-squares algorithm. It is used here to find the RBF network weights W, which can be summarized as [23]:

$$y_p(k) = y_c(k) - W(k-1)h(k) \tag{7.15}$$

$$g_z(k) = \frac{P_z(k-1)h(k)}{\mu + h^T(k) P_z(k-1) h(k)} \tag{7.16}$$

$$P_z(k) = \mu^{-1} [P_z(k-1) - g_z(k) h^T(k) P_z(k-1) \tag{7.17}$$

$$W(k) = W(k-1) + g_z(k) y_p(k) \quad (7.18)$$

where W(k) and h(k) represent the RBF network weights and activation function outputs respectively at iteration k, yc(k) is the process output vector, and Pz and gz are middle terms. μ here is called the forgetting factor ranging from 0 to 1 and is chosen to be 1 for offline training. The parameters gz, W, and Pz are updated orderly for each sample with the change in the activation function output h(k)

### 7.3 Reconstructing of Vibration Signal

Neural networks are a powerful technique in modelling of non-linear dynamic processes. Moreover, RBF neural networks will be used to predict the motor vibration according to the one phase current demand in the feed-forward path.

#### a. Data collection

The first step in the reconstruction vibration based is the collect a suitable training data set. The accuracy of the neural network modelling performance will be influenced by the training data. In the three phase induction motor data collection, the training data must be representative motor behavior in order to analyze the performance of RBF reconstruction based in practical operating conditions. A set of phase current signal was collected to obtain a representative set of input data and a set of vibration signal was collected to obtain a representative set of target data

#### b. Data scaling

Before training or validating the neural network, all inputs and outputs data are scaled to the range of [-1, 1] using equation 7.19,

Z = (ymax-ymin)*(x-xmin)/(xmax-xmin) + ymin; (7.19)

Where y is the vibration measured signal and x is the phase current signal

**c. RBF neural network training**

In order to train this neural network model, This data were divided into two groups: the first 1024 data samples were used for training while the other 1024 data samples were used for validation. The raw data were scaled using equation 7.19.

## 7.4 Vibration waveform reconstruction

The intention of this research is to reproduce a vibration waveform from phase current data sets. To this end the training of the network required both current data for a variety of operating condition, and the corresponding vibration waveform. These vibration waveforms were collected using a vibration transducer. The use of this intrusive vibration sensor was necessary only to train the neural network, and once trained, such an intrusive measuring system was no longer necessary. Trained the neural network with the current signal as the ideal input and the correspondingly measured vibration as the ideal output, and with the induction motor operating under different loads was tested as shown in figure7-6.

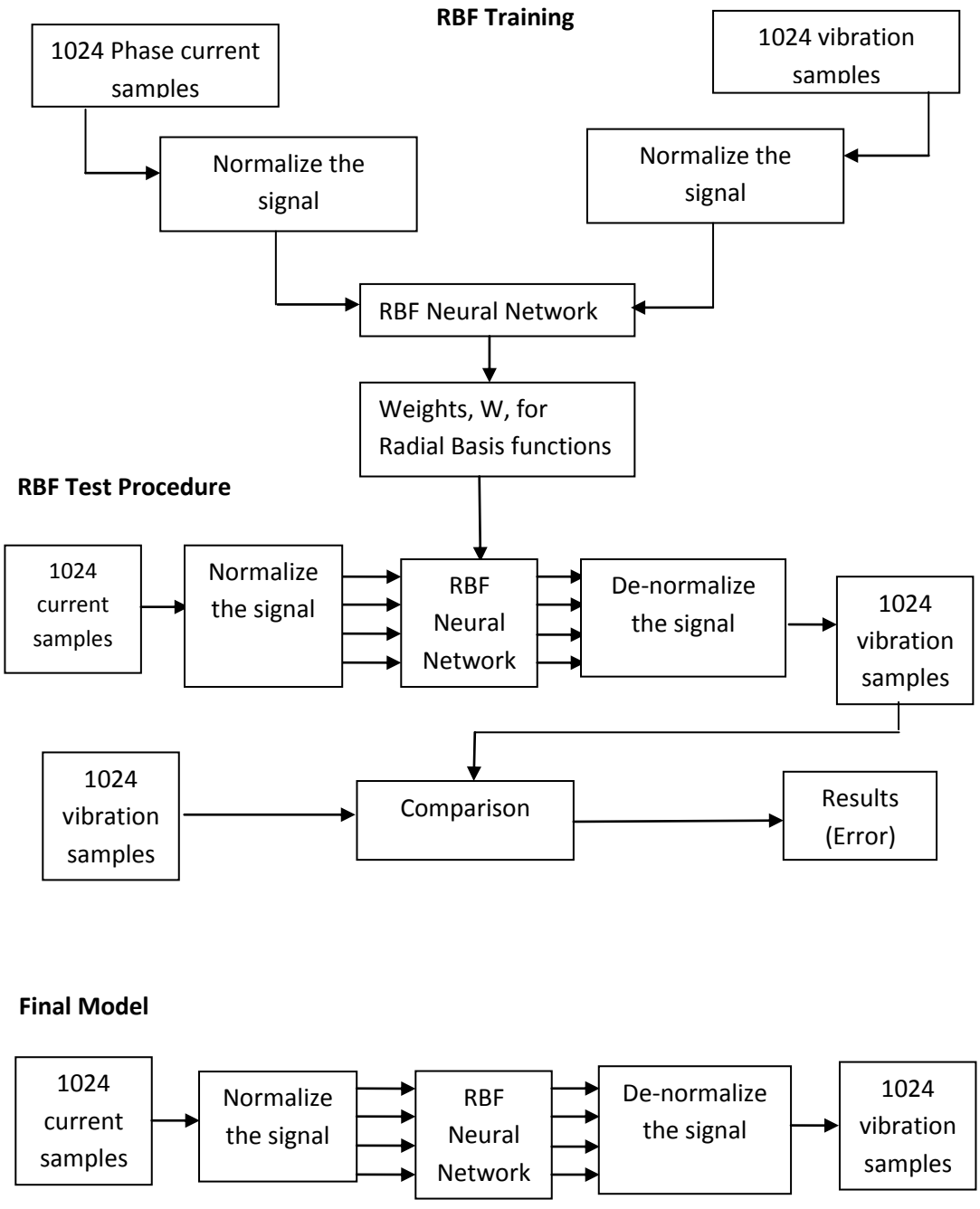


**Figure 7-6** flow chart of reconstruction signal

To make comparisons, the vibration signal was measured only once and used the target of the ANN and the output of network tested with untrained one phase current

are chosen to reconstruct motor vibration when the motor was subject to 0%, 50% and 100% loads.

The reconstructed vibration signals, both time and frequency domains, for different load conditions can be seen in Figures 7.6 to 7.9. To obtain a more accurate validation and to be able to extract additional information both measured and reconstruction signals were transformed to the frequency domain using the discrete Fourier transform (DFT). These three figures indicate that it is feasible to reconstruct induction motor vibration waveform with good accuracy from phase current signals by means of an ANN.

The Mean square error (E) is used to evaluate the method in this research, which is given by the following equations:

$$E_{rror} = {(y - a1)}/{(y)}$$

$e = y - a1$ % instantaneous error

$ec = e.^2$ % instantaneous squared predictive error

$$E = {sum(ec)}/{length(u)} \quad \text{\% Mean square error} \qquad (7.20)$$

Where y is the vibration measured signal and a1 is the reconstruction vibration signal

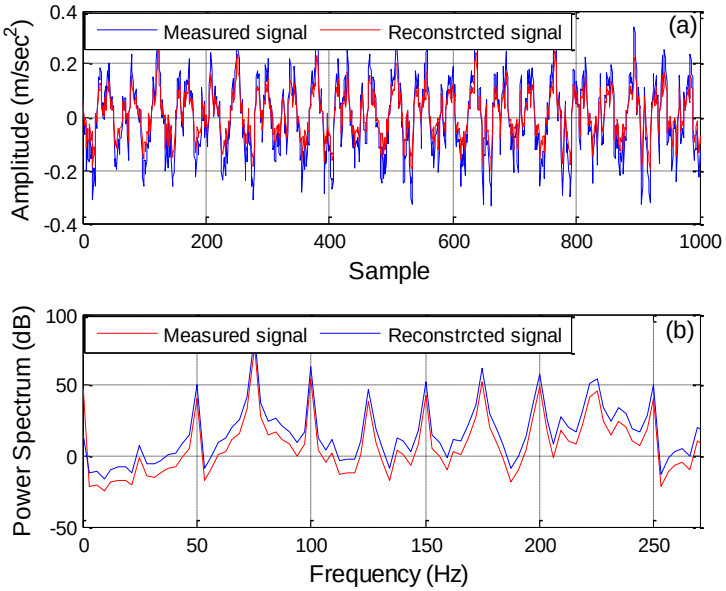


**Figure 7-7** Measured vibration signal and reconstructed signal at one trained data at 0% load (a) time domain (b) frequency domain

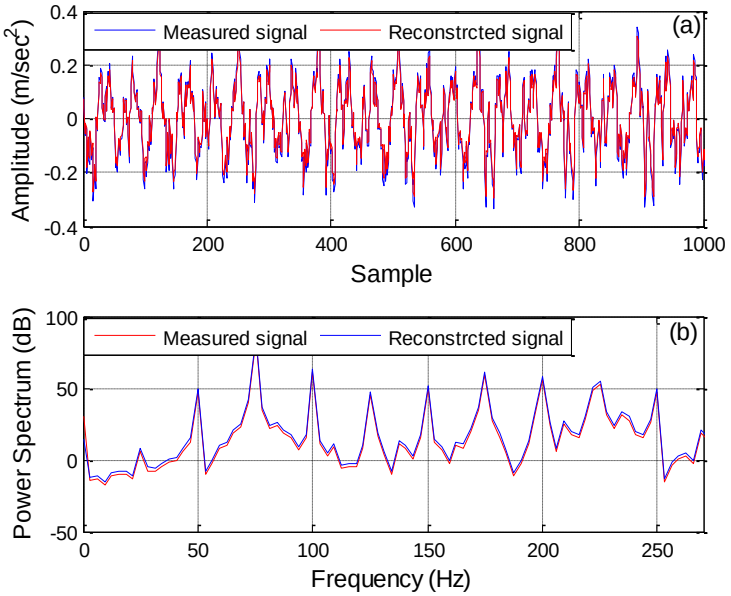


**Figure 7-8** Measured vibration signal and reconstructed signal at one trained data at 50% load (a) time domain (b) frequency domain

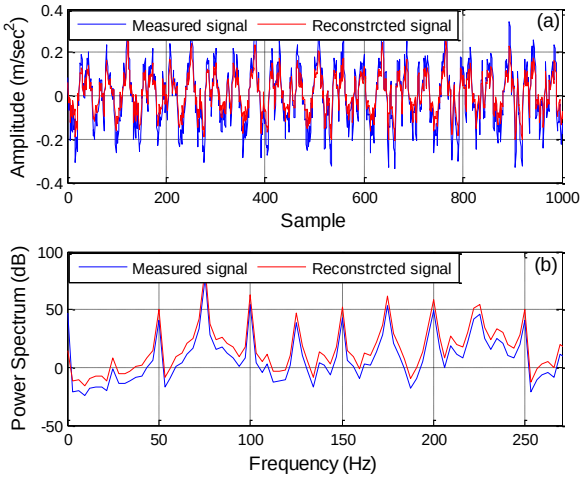


**Figure 7-9** Measured vibration signal and reconstructed signal at one trained data at 100% load (a) time domain (b) frequency domain

It can be seen from the measured and reconstructed results that although some errors do exist between the measured and predicted values (see Figures 7-10and 7-11)

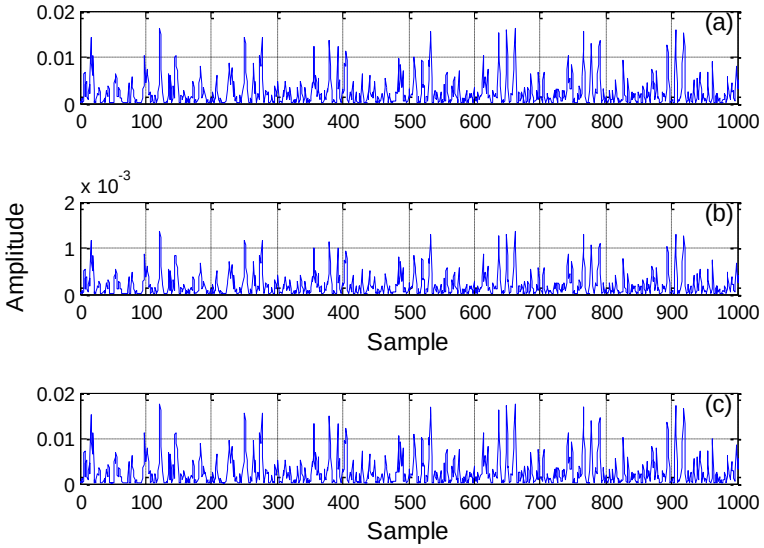


**Figure 7-10** Error between the measured and reconstructed signals A – Zero load, B - 50% load and C – 100% load

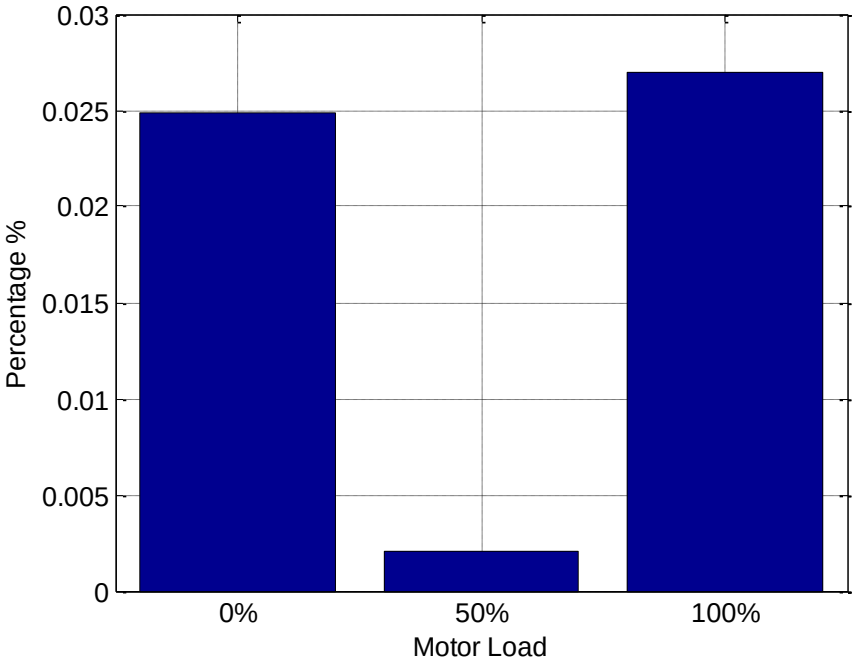


**Figure 7-11** Mean square error

### 7.5 Validation of the proposal method

The one phase current and vibration signals were recorded continually throughout the test. Since the model was to be validated across a wide range of load settings, data were collected with the motor running steadily at 0%, 50% and 100% load. The data set for each cycle was 1024 samples of each of the vibration and single phase current. At each motor operating setting, the data sets were divided into training data (which are used to set the free model parameters) and validating data (which are used to validate the trained network). After the RBF network had been trained using the input data and output data the weights were found and the RBF network was determined.

Figures 7-12, 7-13 and 7-14 show the measured and RBF reconstructed vibration waveforms for three different loads. It can be seen that the measured and predicted vibration traces correlate well. To show a more detailed comparison between

measured and predicted vibration signals the time domain signals were transformed to the frequency domain using the DFT.

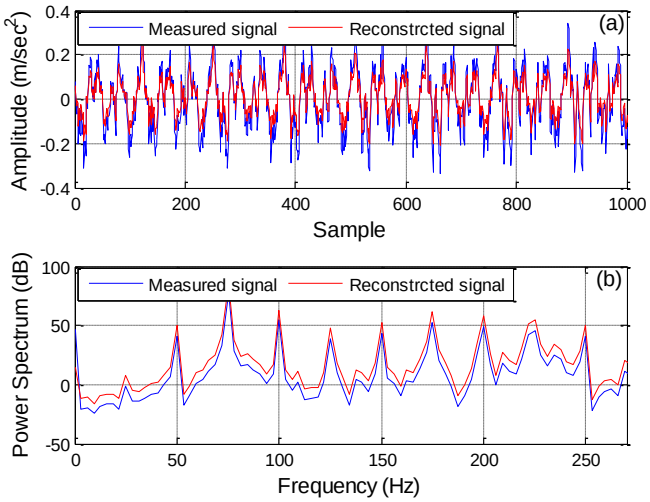


**Figure 7-12** Measured and predicted induction motor vibration waveforms at 0% load (a) time domain (b) frequency domain

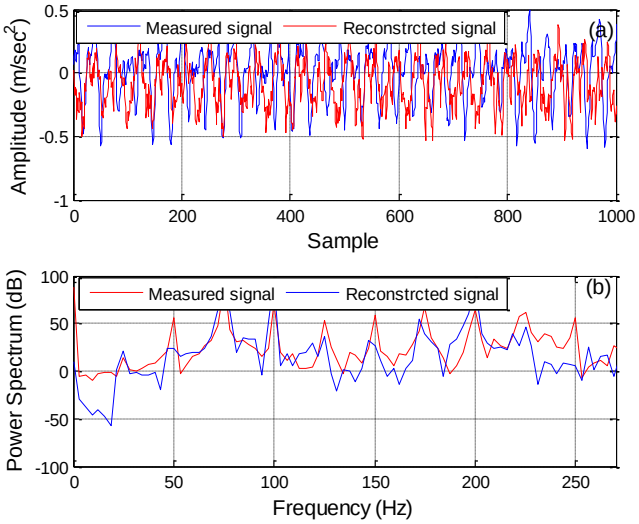


**Figure 7-13** Measured and predicted induction motor vibration waveforms at 50% load (a) time domain (b) frequency domain

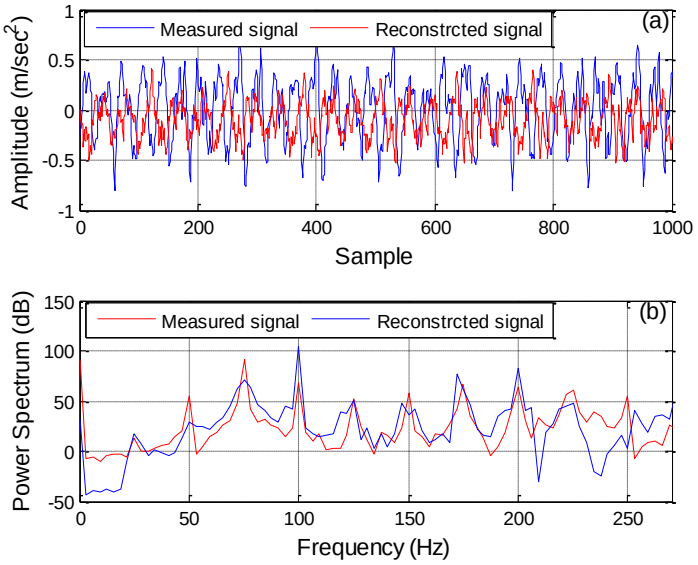


**Figure 7-14** Measured and predicted induction motor vibration waveforms at 100% load (a) time domain (b) frequency domain

It can be seen from the measured and reconstructed results that although some errors do exist between the measured and predicted values (see Figures 7-15 and 7-16) the consistency and accuracy of this approach are at acceptable level.

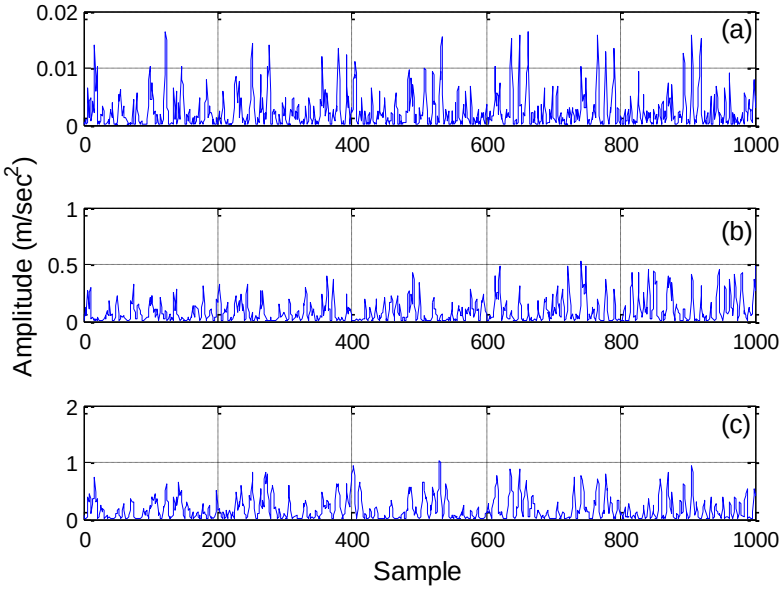


**Figure 7-15** Error between the measured and reconstructed signals A – Zero load, B - 50% load and C – 100% load

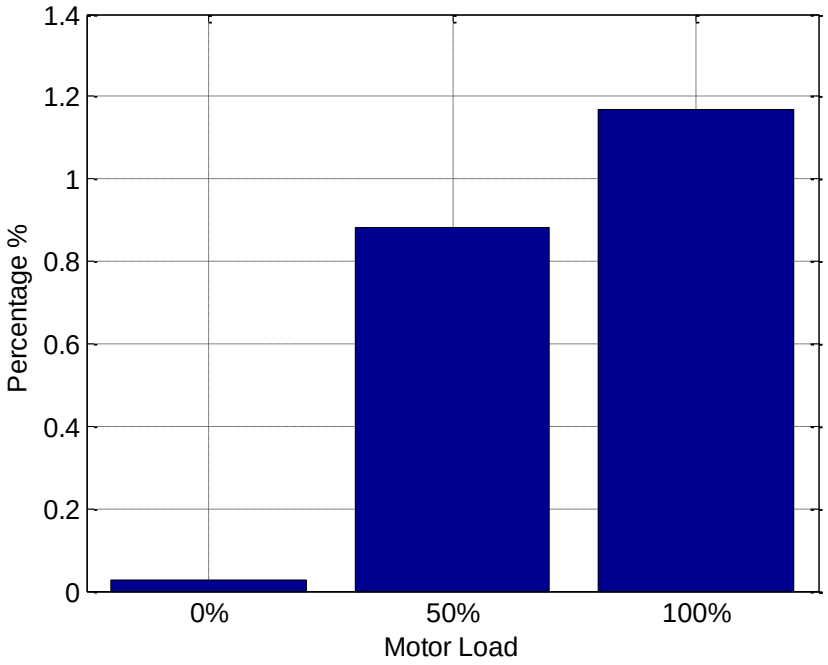


**Figure 7-16** Mean square error

### 7.6 Detection of the induction motor faults using reconstructed vibration signals

Measurement and analysis of motor vibration can yield considerable useful information about the induction motor conditions. The aim in this section is to determine if reconstructed motor vibration can be used for detection of faults in an induction motor. The method customarily used for this type of data capture involves recording motor vibration using vibration transducers mounted on the motor housing. This method has some obvious disadvantages; it is intrusive, is inappropriate for the more demanding on-board-conditions, and limited lifetime transducers are expensive when used in a harsh environment A simpler and easier method is the one proposed in the previous section i.e., a non-invasive method based on reconstructed vibration signals.

After the RBF network has been trained by the input data (one phase current) and output data (vibration), the network weights are obtained and the RBF network is fixed. To validate the RBF network, the validating one phase current data are used as

the input to the RBF network and the output, which is the predicted motor vibration, is obtained. By comparing the measured vibration values with the predicted vibration values, it is possible to decide whether the RBF network is performing satisfactorily.

Figures 7-17, 7-18, 7-19 and 7-20 present a selection of vibration waveforms, both time and frequency domain, generated from measured data and from RBF network model prediction for healthy motor and motor with and 20 and 40 voltage drop in one phase of the three phase supply, for the motor under different three loads. The amplitude of the signal changes at the twice fundamental power supply frequency band (100 Hz) when the motor is in good condition or with small faults (20 and 40 V drops). It can be seen that, using this method gives a clear indication of a fault. It can be seen that there is a reasonable degree of agreement between the measured and predicted vibration traces.

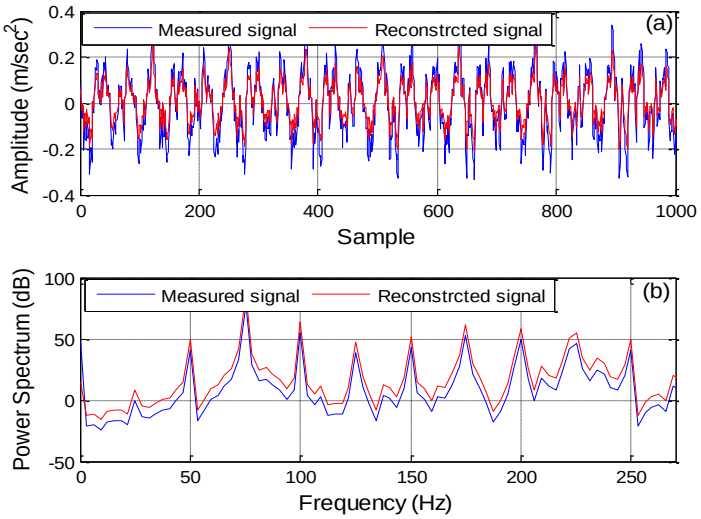


**Figure 7-17** Measured and reconstructed signal for healthy condition at 0% load (a) time domain (b) frequency domain

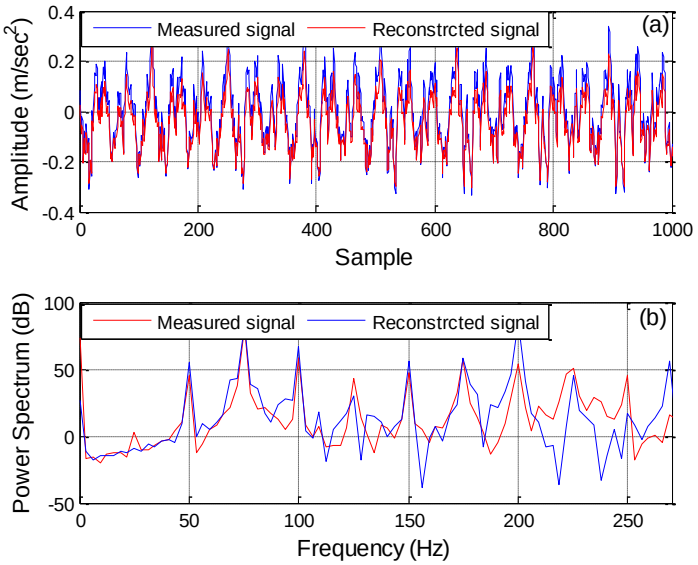


**Figure 7-18** Measured and reconstructed signal for 20 V drop at 0% load (a) time domain (b) frequency domain

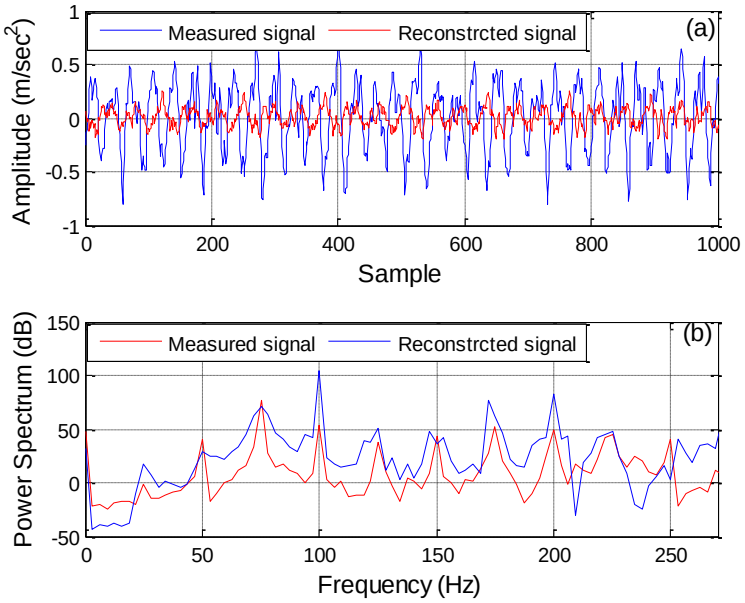


**Figure 7-19** Measured and reconstructed signal for 20 V drop at 0% load (a) time domain (b) frequency domain

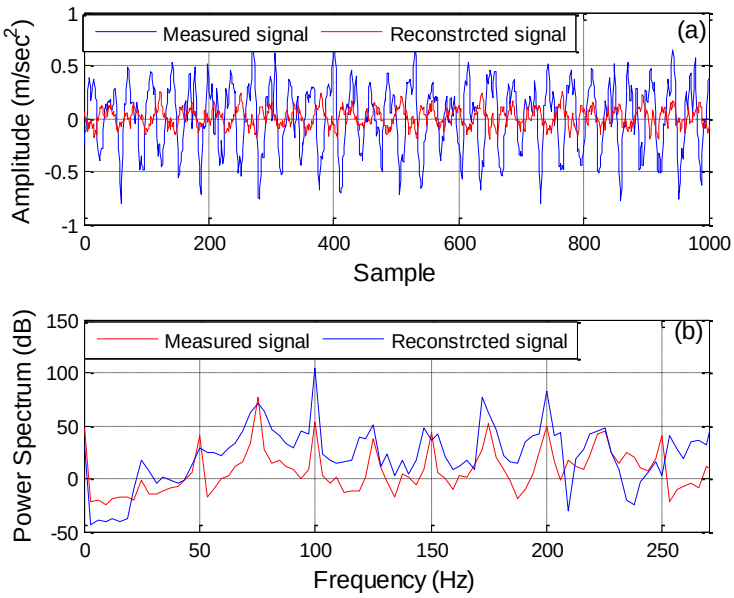


**Figure 7-20** Measured and reconstructed signal for 40 V drop at 0% load (a) time domain (b) frequency domain

Figure 7-21 clearly shows that the most accurate prediction (lowest MSE) was achieved at healthy case and under 0% load condition.

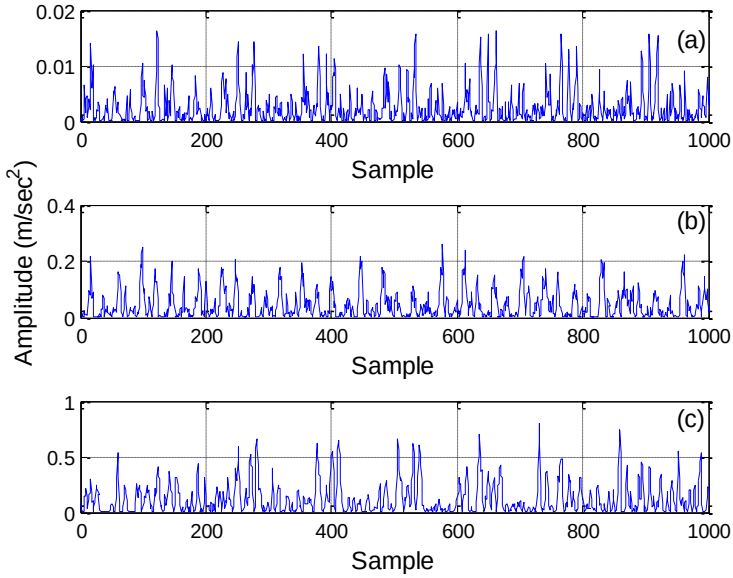

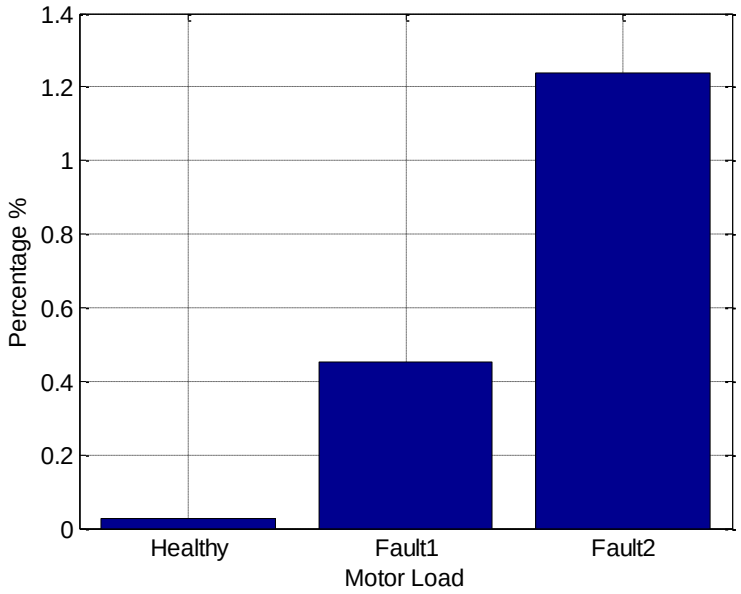


**Figure 7-21** Error between the measured and reconstructed signals. A – Healthy, B – 20 V voltage imbalance in one phase of motor current, and C – 40 V voltage imbalance in one phase of motor current

Theoretically, phase imbalance may be detected by changes in the 2×50Hz component in the measured vibration. The amplitude of this component changes when faults occurred as shown in figures 7-18, 7-19, and 7-20.

At 50% load the presence of the phase imbalance faults are more pronounced The presence of the fault can be detected by comparing the measured and reconstructed vibration signals for the healthy motor with those for the motor with a fault in one phase of the current (20 and 40 V drops) as shown in figures 7-22, 7-23, and 7-24. However, there appears to be a significant error between measured and reconstruction signals for faulty condition at 50% load, see Figure 7-25.

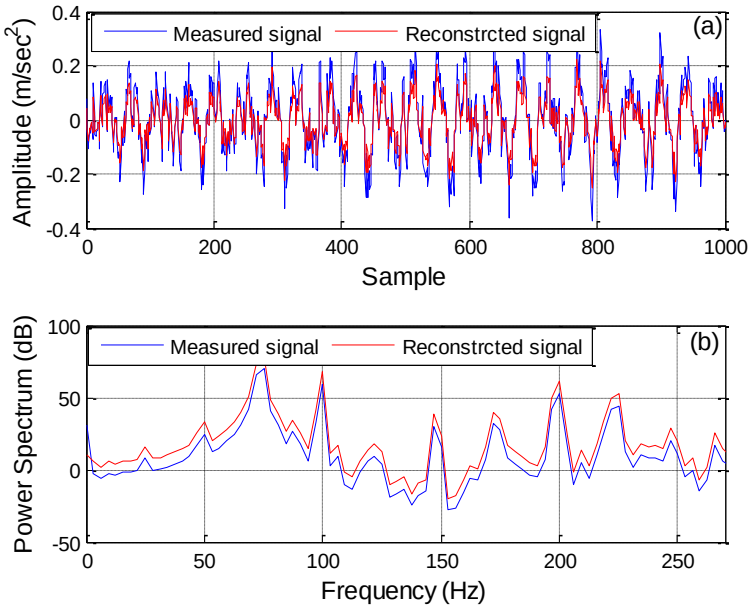


**Figure 7-22** Measured and reconstructed signal for healthy condition at 50% load (a) time domain (b) frequency domain

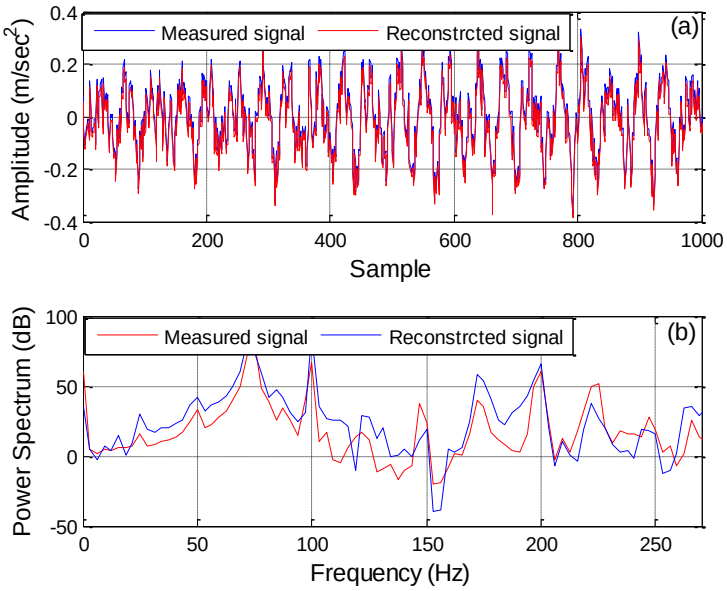


**Figure 7-23** Measured and reconstructed signal for 20 V drop at 50% load (a) time domain (b) frequency domain

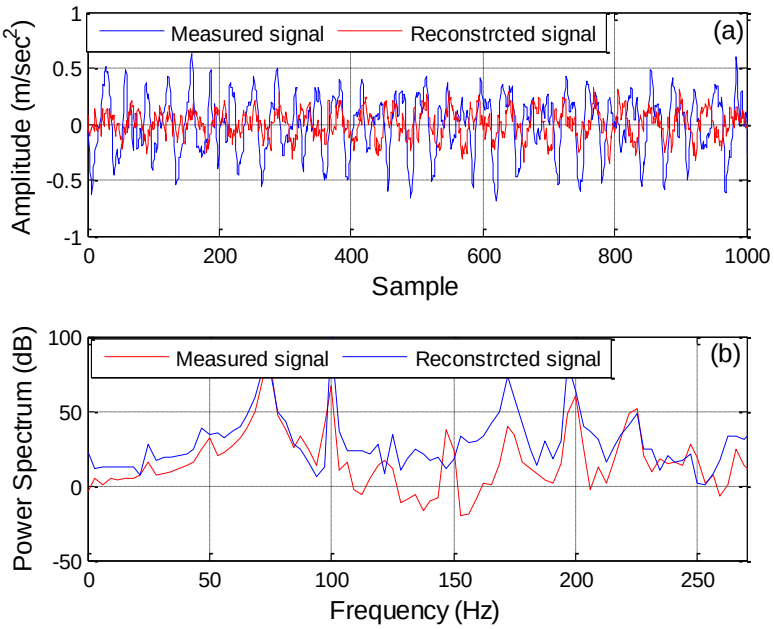


**Figure 7-24** Measured and reconstructed signal for 40 V drop at 50% load (a) time domain (b) frequency domain

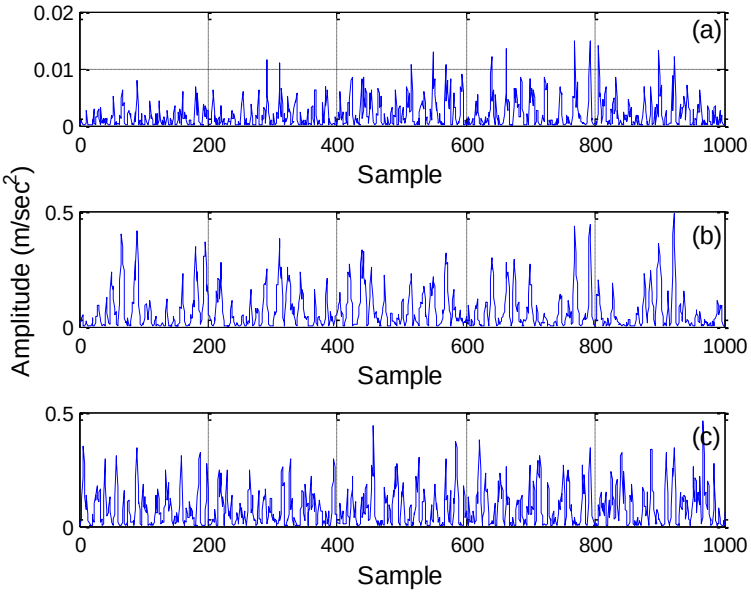

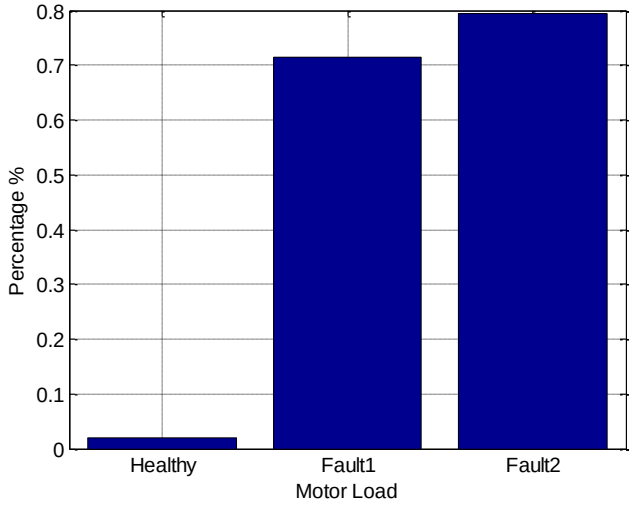


**Figure 7-25** Mean square error between the measured and reconstructed signals at 50% load. A – Healthy, B – 20 V voltage imbalance in one phase of motor current, and C – 40 V voltage imbalance in one phase of motor current

At 100% load the phase imbalance fault can again be detected by comparing measured and reconstructed motor vibration signals when the motor is in good condition or with small faults (20 and 40 V drops). It can be clearly seen that the amplitude of the signals significantly changes, particularly at 100 Hz, as shown in Figures 7-26, 7-27, and 7-28

However, there appears to be a significant error between measured and reconstructed signals for faulty conditions at 100 % load as shown in Figures 7-29.

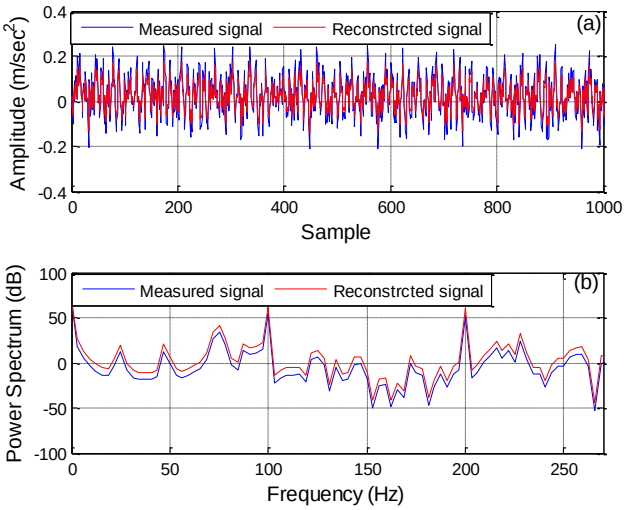


**Figure 7-26** Measured and reconstructed signal for healthy condition at 100% load (a) time domain (b) frequency domain

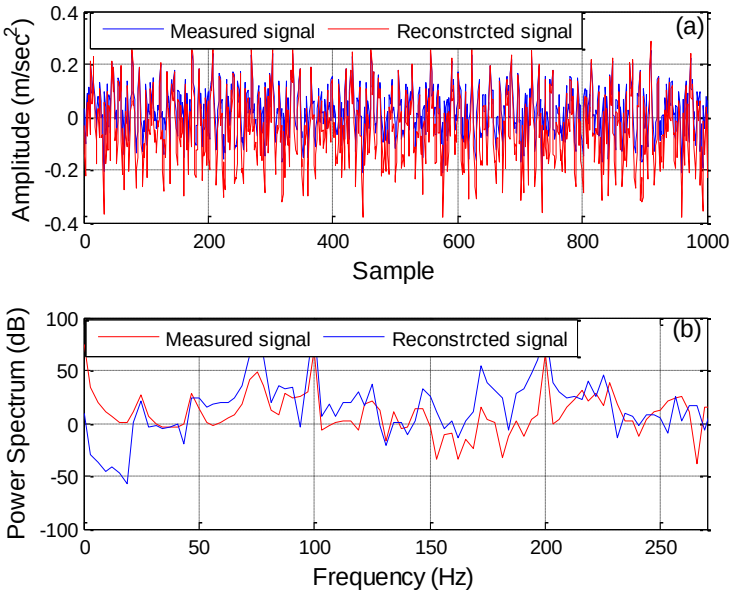


**Figure 7-27** Measured and reconstructed signal for 20 V drop at 100% load (a) time domain (b) frequency domain

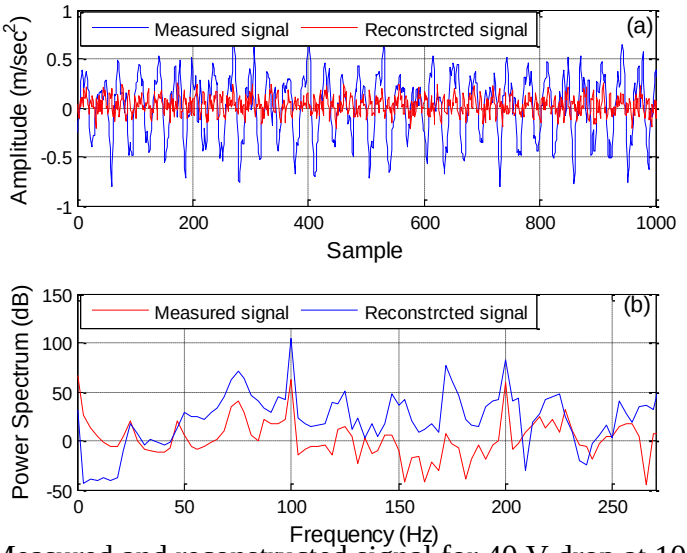


**Figure 7-28** Measured and reconstructed signal for 40 V drop at 100% load (a) time domain (b) frequency domain

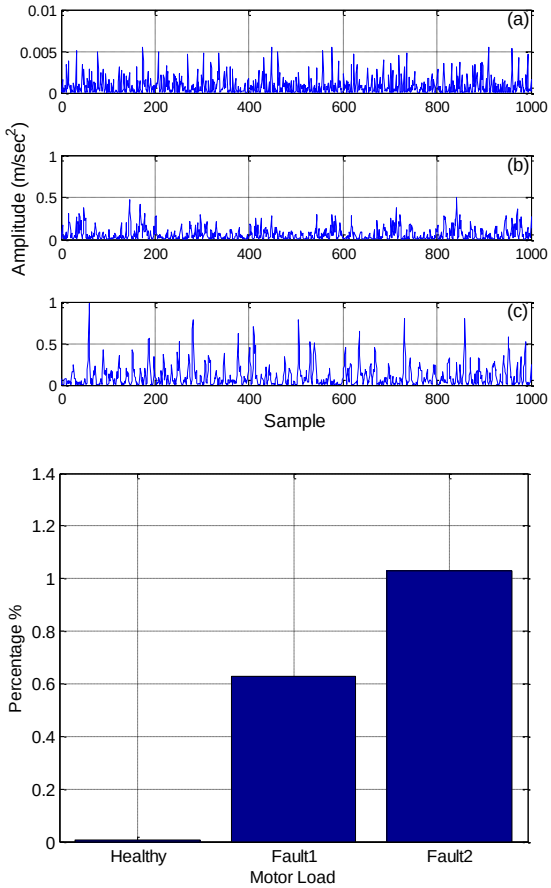


**Figure 7-29** Mean square error between the measured and reconstructed signals at 100% load. A – Healthy, B – 20 V voltage imbalance in one phase of motor current, and C – 40 V voltage imbalance in one phase of motor current

## 7.6 Summary

This study used spectral estimation to investigate the coherence between the DCS and the DVS signals at a particular frequency and in different frequency. Both signals are completely coherent if the magnitude squared coherence (MSC) is equal to 1, if MSC is equal to zero then the both signals are independent to each other. The results show the both signals are coherent at the frequencies at which the MSC is greater than 0.5 and both signals are less coherent if DSC is less than 0.5. Wavelet coherence analysis greatly facilitates the detection of the quasi-periodic component indicative of a system anomaly. Wavelet cross spectrum and wavelet coherence are useful to reveal localized similarities between DCS and DVS signals in the time-scale plane and to interpret the results. It may be possible to acquire the DVS signal information from the DCS signal

This research has demonstrated the possibility a condition monitoring method based on the motor current for reconstruction of motor vibration. It is proved feasible to reconstruct motor vibration effectively by using the current signal from one phase of the motor supply. This method is of high precision and good repeatability. This is a non-invasive technique which can open new possibilities for performing necessary diagnostics and making checks on induction motors without laborious and expensive investigations that are truly rigorous only in laboratory conditions. The method has been tested by statistical analysis and shows a good agreement with the widely used approach that entails making on-motor vibration measurements.

This application to motor modelling and motor vibration waveform reconstruction has utilized the ability of a RBF to classify a complicated nonlinear system in a succinct manner. Using the RBF network, the motor vibration process is described as a non-parametric model.

It is suggested that it is simpler and easier to reconstruct the vibration signal from the motor current than to use vibration sensors that may be intrusive, difficult to place, expensive and subject to attack when in corrosive environments. It has been demonstrated that the proposed method detects induction motor faults and the status of the induction motor can be estimated with a reasonable degree of accuracy.

# CHAPTER 8

# SMART TECHNIQUE FOR INDUCTION MOTOR DIAGNOSIS BY MONITORING THE POWER FACTOR USING ONLY THE MEASURED CURRENT

*This chapter presents a discussion on an innovative, non-intrusive, accurate and reliable method for the early detection and diagnosis of faults in an induction motor (IM) using an enhanced power parameter measurement technique. It is argued, and initial results suggest that it is more effective to monitor the operating power factor (PF) of the IM which provides better protection under-load than the motor current based approach. Traditionally, to estimate the PF would require both voltage and the current measurements in order to apply the displacement power factor method. This chapter determines the operating PF of the IM using only measured current and supplied manufacturer's data. Experimental results confirm that the PF can be used successfully for IM fault diagnosis and is promising also for assessing fault severity. The suggested method offers an inexpensive, reliable and non-intrusive and CM tool which can be used with real-time systems.* A significant portion of this chapter has been presented at the 25th Int. Cong. on Condition Monitoring and Diagnostic Engineering: *Smart Technique for Induction Motors Diagnosis by Monitoring the Power Factor Using Only the Measured Current* and published in Journal of Physics: Conference Series **364** (2012).

http://iopscience.iop.org/1742-6596/364/1/012062/pdf/1742-6596_364_1_012062.pdf

## 8.1 Introduction

Many techniques have been proposed for detection and diagnosis of faults in three-phase IM; including some which measure the current. Those that analyse the current using, for example, Fourier methods tend to be called "motor current signature analysis techniques[14]. Park's vector components derived from the three phases of the current through the IM have been used for diagnosing bearing faults and air-gap eccentricities. Coils sensing axial leakage flux have been successfully used for specific faults [94], [95]. Analysis of the instantaneous power of specific phases of the motor current has been used by the authors to effectively simulate and experimentally detect and diagnose mixed eccentricities in a squirrel cage IM [96]. Partial power as well as the total instantaneous power can be used for the detection of such faults. Complex apparent power (see Figure 8.1) has been suggested for the detection and diagnosis of air-gap eccentricities [97].

The PF (also known as cos φ) has been one of the IM parameters that has been used for CM of IMs. To use the displacement method to monitor the operating PF would normally require sensors to measure both current and voltage. PF calculations and derivations of basic equations are presented in ref [101], however, this work adopts the technique for monitoring the ESP induction motors condition by determining the PF using only measured current and manufacturer's data. Because no voltage measurements are required this method provides a relatively low-cost solution. In fact, for low load conditions, it is suggested that the PF is more reliable than motor current-based approaches and should be very useful for such applications as under-load protection of pumps with PF compensation for improving the power quality.

## 8.2 Static and dynamic air-gap eccentricities

Static eccentricity is when the rotor's axis of rotation is displaced and can be caused by stator ovality or by the incorrect positioning of the rotor or stator at the commissioning stage, e.g. the longitudinal axes of stator and rotor do not coincide. Since the rotor is not centred within the stator bore, the field distribution in the air-gap is no longer symmetrical. The non-uniform air-gap gives rise to a radial force of electromagnetic origin, which acts in the direction of minimum air-gap and which is called unbalanced magnetic pull (UMP). However, static eccentricity may cause dynamic eccentricity [14]. This kind of eccentricity may be caused by a bent shaft, mechanical resonances, bearing wear or misalignment or even static eccentricity as mentioned above. Therefore, the non-uniform air-gap of a certain spatial position is sinusoidally modulated and results in an asymmetric magnetic field. This, accordingly, gives rise to a revolving UMP [14]. Air-gap eccentricity in induction machines causes characteristic harmonic components in electrical, electromagnetic, and mechanical quantities. Therefore, either mechanical quantities such as vibrations or torque oscillations or electrical quantities such as currents or instantaneous power can be analyzed to detect eccentricity conditions[98].

### 8.2.1 Non-active power of an eccentric induction motor

When eccentricity takes place in an induction motor, the stator current, $I_{ecc}(t)$ is given by [96]:

$$i_{ecc}(t) = I_M cos\big((2\pi f)t - \varphi\big) + \sum_{m=1}^{\infty}\{I_{ec,m1}\cos[2\pi(f - mf_r)t - \alpha_{m1}] + I_{ec,m2}\cos[2\pi(f + mf_r)t - \alpha_{m2}]\} \quad (8.1)$$

Where $I_{ec,m1}$ and $\alpha_{m1}$ are the amplitude of the current component at a frequency $(f - mf_r)$ and its initial phase angle, respectively; $I_{ec,m2}$ and $\alpha_{m2}$ are the amplitude

of the current component at a frequency $(f + mf_r)$ and its initial phase angle, respectively. Clearly, in the current spectrum, two sideband components will appear around the fundamental component at frequencies $(f - f_r)$ and $(f + f_r)$ [96].

### 8.3. Unbalanced voltage

In this part the unbalance in the phase and the magnitude of the voltage are considered. To model the electrical motor symmetrical components can be used. A wide variety of research has been done on modelling of the unbalanced condition. For unbalanced voltage operation the torque can be written as [99]; [100]:

$$T = \frac{P}{\omega} = T_0 + T_2 \tag{8.2}$$

In which, $T_0$ is the DC torque. $T_2$ is the torque component whose frequency is twice the supply frequency. Assuming the IM can be considered as a RL load the torque can be written as:

$$T = \eta * E * I/\omega \tag{8.3}$$

In which E and I are input voltage and current of each phase respectively. Assuming sinusoidal waveforms for voltage and current, with a 50 Hz supply, this equation can be rewritten as:

$$T = Kcos(2\pi 50t + \alpha) * cos(2\pi 50t + \beta) \tag{8.4}$$

So,

$$T = K'[\cos(\alpha - \beta) + \cos(2\pi 100t + \alpha + \beta] \tag{8.5}$$

Based on Equation (8.5) the resulting torque would include a DC term and a term

whose frequency is twice the fundamental frequency of the applied voltage. In order to detect the unbalanced supply voltage this extra torque component can be used.

### 8.4 The effect of rotor bar fault on power factor

The input impedance of the induction motor, which shows the neglecting of the rotor leakage and stator impedance, can be written in the formula as follows:

$$Z_{in} = \frac{j\frac{R_2}{s}x_m}{\frac{R_2}{s}+jx_m} \tag{8.6}$$

The phase angle of the impedance will be;

$$\emptyset = \angle V_{in} = 90 - \tan^{1}\left(\frac{x_m}{R_2/_s}\right) \tag{8.7}$$

The steady state power factor of the IM is cos Ø.

Therefore, by increasing$R_2$, which might be due to a rotor bar fault, the phase angle of $V_{in}$ declines, and this in turn would give a higher power factor. It is evident that rotor bar faults can be detected using the analysis of the power factor.

### 8.5 The proposed method: current only power factor calculation

The power triangle shown in Figure 8.1 shows the basic principles of power measurement. If you have the values of three variables such as voltage, current and phase angle between current-voltage, the other parameters can be obtained.

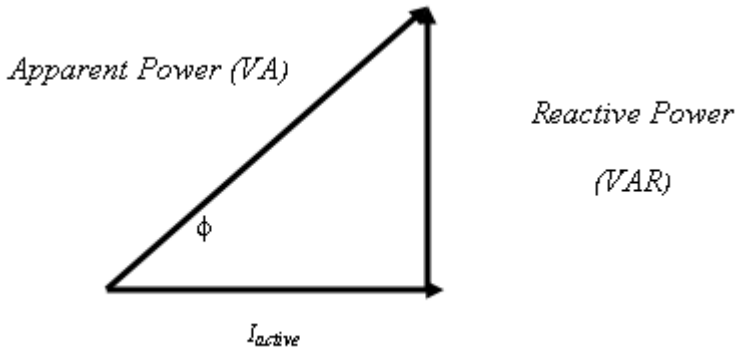


**Figure 8-1** the power triangle

The power factor defines what proportion of the power that is supplied would achieve useful work. The real power, true power, or resistive power is the power "drawn" by the electrical resistance, which performs useful work (Watts). Reactive power is the electrical power dissipated in the capacitances and inductances that are part of the system, and though this consumes energy it does not perform any useful work (VA). Useful work requires the voltage and current to be in the phase (=Apparent Power x cos Ø), while for Reactive power the current and voltage are 900 out of phase (=Apparent Power x sin Ø).

A mechanical way to represent power factor is to imagine a horse pulling a barge along a straight canal as shown in Figure 8.2. The horse pulls the barge from the tow-path and is thus pulling the barge at an acute angle to the direction of motion of the barge. Because the force exerted by the horse is at an angle, not all of the force moves the barge forward along the canal. Some force would pull the barge towards the side of the canal. So in this example we can conclude that:

- The force exerted by the horse is the total or apparent power
- The power used to move the barge is the working power or real power
- The force pulling the barge towards the side of the canal is nonworking power or reactive power.

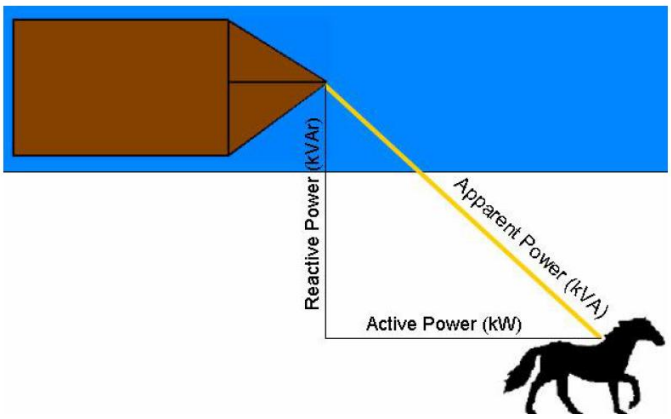


**Figure 8-2** Explanation of the differences in the power values

The apparent power ($P_{app}$) to the motor is given as [101]:

$$P_{app} = \sqrt{3}VI \tag{8.8}$$

Where $V$ and $I$ are the line voltage and current, respectively.

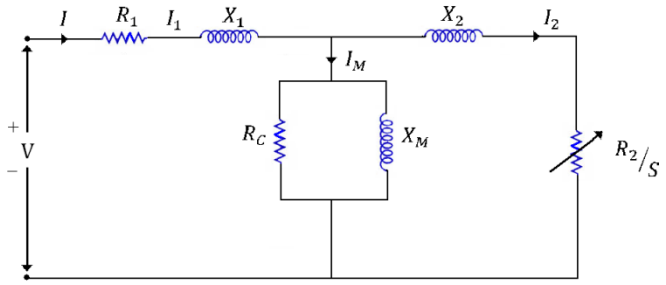


**Figure 8-3** IM equivalent circuit

The active power supplying the load is:

$$P_{act} = \sqrt{3}VIcos\emptyset \tag{8.9}$$

The power factor (PF) is

$$PF = \frac{P_{act}}{P_{app}} = cos\emptyset \tag{8.10}$$

The motor current, I, has two components, $I_{active}$ and $I_{reactive}$. The active part of the current ($I_{active}$) accounts for the torque, which changes according to the load (from no-load to full/over-load). The reactive part of the current ($I_{reactive}$ ) accounts for the magnetising current of the IM, and does not change much from the no-load to the full-load condition, staying practically constant [101].This is because for IM, the magnetising circuit, i.e. the stator coil inductances remain the same [101]:

$$I = \sqrt{I_{active}^2 + I_{reactive}^2} \tag{8.11}$$

$$I_{active} = I cos\emptyset \tag{8.12}$$

$$I_{reactive} = I sin\emptyset \tag{8.13}$$

Substituting Equation (8.10) in (8.13)

$$I_{reactive} = I sin(cos^{-1} PF) \tag{8.14}$$

Equation (8.10) can be rewritten using

$$PF = cos\emptyset = \sqrt{1 - sin^2\emptyset} = \sqrt{1 - \left(\frac{I_{reactive}}{I}\right)^2} \tag{8.15}$$

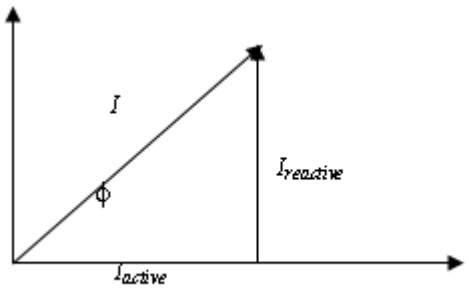


**Figure 8-4** Current presentation

As the reactive component remains constant, it can be estimated from the nominal condition given by the manufacturer data and/or nameplate data using (8.14). Now, as the motor load increases, the total motor current (I) in (8.15) would increase, while $I_{reactive}$ remains constant. Hence, the ratio ($I_{reactive}$/I) in Equation (8.15) decreases, causing the PF to increase and approach closer to unity. Theoretically, at no-load condition, there is no active current flow. So, at no-load, I = $I_{reactive}$, making $\emptyset = 90^0$ and PF = 0. Physically, at no-load, there is no mechanical resistance; therefore the entire circuit is almost wholly inductive due to the stator coils causing a low PF. A surge in motor load is essentially similar to adding resistance to the circuit, causing the PF to increase [101].

Therefore, in the current-only PF estimation approach, we would estimate the $I_{reactive}$ using (8.14) from the nominal PF from the nameplate data. So by using the measured motor current and assuming constant $I_{reactive}$, we can estimate the operating PF from Equation (8.15). Synchronized voltage and current measurement are not required as in displacement PF measurements.

**8.6 Economic issues**

The proposed PF method for determining motor faults measuring and analysing the current waveform has the following advantages:

- A non-invasive, on line monitoring technique,
- Uses the motor as sensor,
- Low cost, requires significantly less instrumentation than other methods,
- Low cost, the instrumentation required is relatively low cost, and
- Online monitoring with minimum computation complexity and remote accessibility.

**Table 8-1** Cost comparison of PF and vibration techniques

| **PF Method** | **Vibration analysis** |
|---|---|
| Cheap sensor (~£50) | Accelerometer (~£500)<br>Charge amplifier(~ £2 k) |
| Low data acquisition card specs,<br>10 bit, 10 kHz (~ £100) | High data acquisition card specs,<br>24 bit, 50 kHz (~ £900) |
| No accessibility problem | Possible accessibility problem |
| Total: ~ £150 | Total: ~ £3.5 k |

## 8.7 Experimental Results

The test rig consisted of a variable speed, 1.1 kW three-phase induction motor, attached to a DC-generator and a resister bank as load. The motor was tested at 1410 rpm and 100% load in a healthy condition and then under four different phase imbalance voltages of 10 V (fault1), 15 V (fault2), 20 V (fault3), and 25 V (fault4); these represented imbalances of 4%, 6%, 8% and 10% respectively, of the nominal main voltage level.

The measured current for the test motor at different loads and the corresponding calculated PFs using Equation (8.11) are shown in Figure 8.5. It can be seen that there is a direct relationship between the loads and the PF because the current motor increases when the load increases to maintain the same output power

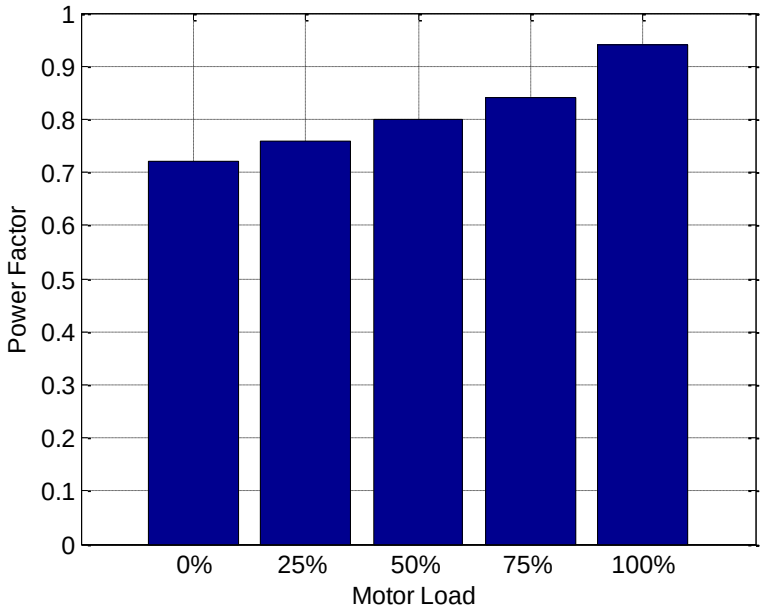


**Figure 8-5** Power factor for 1.1 kW 3 phase induction motor for healthy condition at various loads

The PF values were calculated for the motor running under various fault conditions and at different loads. Figures 8.6 and 8.7 show the PF values for all the cases tested. It can be seen that there is a direct relationship between the fault severity and the PF.

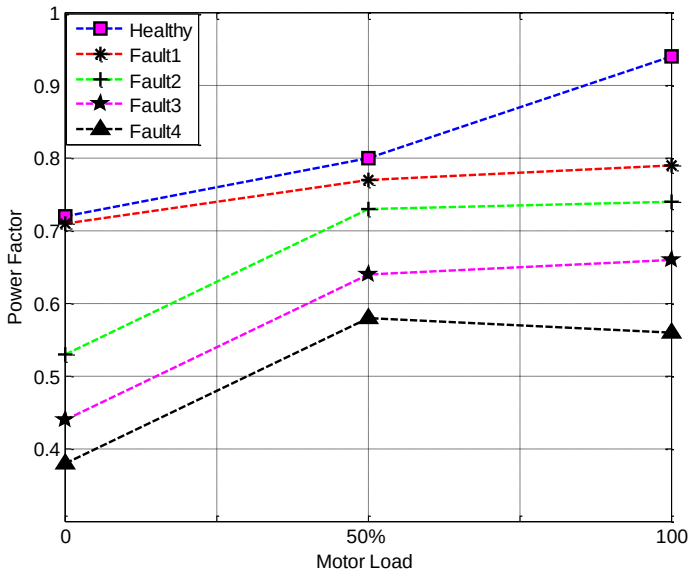


**Figure 8-6** Calculated power factor for 1.1 kW three phase induction motor at three loads, healthy and with various imbalance phase faults

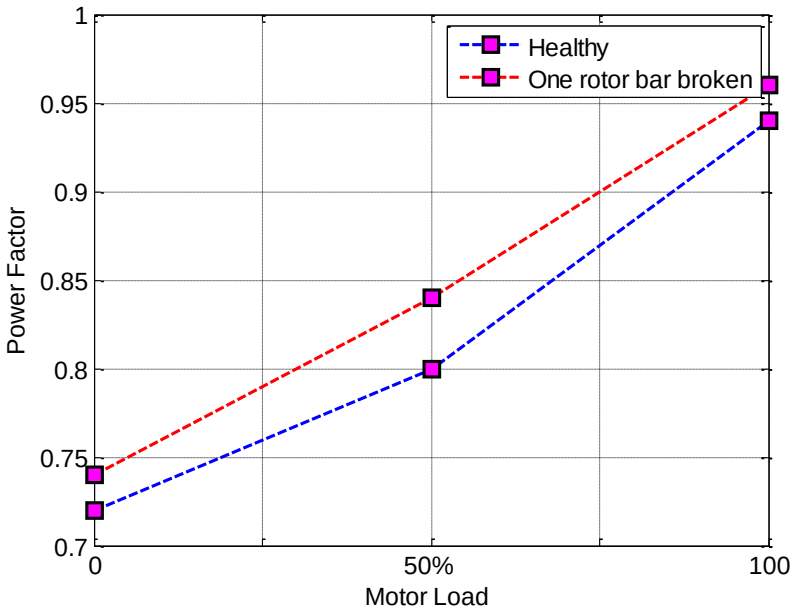


**Figure 8-7** Calculated power factors for 1.1 kW 3 phase induction motor at three loads, healthy and with one rotor bar broken

## 8.8 Summary

For the IM, the operating PF can provide better CM than motor current-based approaches. Traditionally, PF estimation would require both voltage and the current measurement to use the ZC displacement method. In this chapter, a method of determining the operating PF of the IM using only the measured current and the manufacturer's data available from the nameplate and/or datasheet has been presented. From the nameplate data the reactive component of the motor current is estimated, and this remains constant for different load conditions, as per the IM principle. Then, using the measured total motor current and the estimated constant reactive part, the PF can be found for different loads and motor conditions. Experimental results are shown for a realistic test setup the potential of the proposed method is very promising when compared to other state of the art methods (power rating, pole pairs**,** etc.,) for the class of motor used. Using the operating PF, a method

which does not require voltage measurement would provide a cheaper solution to monitoring IM, e.g., in pump applications. Operational PF can also be used for PF compensation to improve the power quality.

# CHAPTER 9

# CONTRIBUTION TO KNOWLEDGE, ACHIEVEMENTS, CONCLUSIONS AND FUTURE WORK

*This chapter illustrates contribution to knowledge. It summarises the achievements of the research project and explains how the objectives stated in Section 1.10 were achieved. The chapter concludes the study and suggests some steps for further work.*

## 9.1 Contribution to knowledge

The research work carried out in this thesis included a number of important aspects that were novel and not previously implemented by other researchers or practitioners in a similar manner. These aspects of novelty are summarized below:

**• Novelty one:**

An effective alternative to direct vibration measurement, preferably using easy-to-measure variables would be very attractive to industry, and in an attempt to meet this need to apply Radial Basis Function networks to the reconstruction of motor vibration using measurements of one phase of the motor current.

**• Novelty two:**

Apply a method of determining the operating PF of the IM using only the measured current and the manufacturer's data available from the nameplate and/or datasheet to detect, diagnose and assess the relative fault severity of the seeded faults

## 9.2 Review of objectives and achievements

The main achievements of this work are described below and correlated with the original objectives set out in Section 1.10.

**Objective 1:**

Explore induction motors failure modes and understand condition monitoring techniques e.g. vibration and motor current signature analysis.

**Achievement 1:**

Static Techniques include motor current measurement, temperature of the motor, electrical resistance of the winding, observation of the state of the lubricating oil and Dynamic techniques include Motor Vibration Signature and Motor Current Signature

Analysis were outlined in chapter one. Also in Chapter one motor failure mode and the data processing to detect and diagnosis the faults is introduced.

**Objective 2:**

Develop a mathematical model for induction motor operations and effect of faults on the measured performance

Build and develop a mathematical model of the electromechanical system under investigation (motor, coupling and load), to gain a better understanding of how a three phase induction motor interacts with a faults. Moreover, to use the model to gain a better understanding of how effect of faults on the measured performance and to compare the experimental results with those obtained from the model to assess the effectiveness of MCSA in a qualitative manner.

**Achievement 2:**

This objective was delivered in chapters three. The developed model includes not only the dynamics of a motor but also the behaviour of phase imbalance faults and rotor bar breakage faults. Numerical simulation of the Equations forming the model show that the current spectrum of a faulty motor is dominated by the main supply frequency 50Hz but also with a number of pronounced sidebands that spread around

50Hz. These sidebands are largely determined by the primary shaft speed and slip. Moreover, when a local fault is introduced into the motor, the model predicts the amplitude of these sidebands will increase, and more sideband components will appear at higher order harmonics of the primary shaft speed. These features, which form the basis of a possible detection mechanism, have been confirmed through test investigation. A detailed model for the motor load driving system has been deduced and explained. The developed model can be used to simulate different operational

conditions with the correct selection of parameters. It was found that this simulation is an inexpensive and useful method for gaining an insight into the dynamic behaviour of motor faults using the induction motor as the only transducer.

**Objective 3:**

Design and construct a test rig with associated instrumentation for fault simulation, data collection and subsequent data analysis.

**Achievement 3:**

Chapter four described the test rig used in research, see Figure 4.2. It comprises a 1.1 kW three-phase induction motor and connected to a D.C generator and adjacent resistor banks. The seeded faults were: power supply phase imbalance and broken rotor bars. Each of these faults was seeded at a variety of severities. Three types of measurement transducers were used in the motor test facility so that the information content provided by various machine parameters could be assessed and compared. Current transducers were used to measure electrically based parameters; accelerometers, and a shaft encoder were used to measure mechanically-based measurement parameters.

**Objective 4:**

To investigate and apply basic monitoring techniques e.g. time-domain and frequency-domain analysis to collected data and attempt to detect, diagnose and assess the relative fault severity of the seeded faults, and determine the practical implications of doing this.

**Achievement 4:**

Time and frequency domain signal processing methods were applied to the collected data from the different measurement transducers. Each of the processing methods

was evaluated based upon its usefulness in the fault detection, diagnosis and severity assessment levels of condition monitoring. Attention was also focused on the practical implications of using the various methods.

Although initial emphasis was focused upon spectral analysis, data was also examined in the time domains. These two methods are presented throughout Chapter 5. For the frequency analyses, trending of individual components was also performed.

**Objective 5:**

Apply advanced signal processing methods such as time-frequency domain analysis using the short- time Fourier transform, Wigner Ville distribution and continuous wavelet transform (CWT) and discrete wavelet transform (DWT) for detecting and diagnosing quantified faults.

**Achievement 5:**

This objective was delivered in chapter six. The performance of the short time Fourier transform (STFT), the Wigner-Ville distribution (WVD), the continuous wavelet transform (CWT), the discrete wavelet transform (DWT) and wavelet multi-resolution analysis (MRA) are compared using a simulated signal and measured data from an induction motor with seeded faults (phase voltage imbalance and broken rotor bar)

It is shown that there are limitations to STFT and WVD techniques which can be overcome using the CWT and DWT. However the DWT is found to be faster than the CWT.

Using higher level components of the DWT (d5 to d7) of the measured signal provided useful information on identification of the faults using the energy content in

the frequency bands corresponding mains supply frequency, twice the mains frequency and the shaft drive frequency The results of the experiment show wavelet decomposition is an appropriate technique for non- stationary signals representing faults in an induction

**Objective 6:**

Measurement and analysis of the vibration signal are important in improving motor performance and condition monitoring and this necessitates sophisticated analysis techniques that have yet to be proven in practice. An effective alternative to direct vibration measurement, preferably using easy-to-measure variables would be very attractive to industry, and in an attempt to meet this need to apply Radial Basis Function networks to the reconstruction of motor vibration using measurements of one phase of the motor current.

**Achievement 6:**

Demonstrated the possibility a condition monitoring method based on the motor current for reconstruction of motor vibration was delivered in chapter seven. It is proved feasible to reconstruct motor vibration effectively by using the current signal from one phase of the motor supply. This method is of high precision and good repeatability. This is a non-invasive technique which can open new possibilities for performing necessary diagnostics and making checks on induction motors without laborious and expensive investigations that are truly rigorous only in laboratory conditions. The method has been tested by statistical analysis and shows a good agreement with the widely used approach that entails making on-motor vibration measurements.

This application to motor modelling and motor vibration waveform reconstruction has utilized the ability of a RBF to classify a complicated nonlinear system in a succinct manner. Using the RBF network, the motor vibration process is described as a non-parametric model.

It is suggested that it is simpler and easier to reconstruct the vibration signal from the motor current than to use vibration sensors that may be intrusive, difficult to place, expensive and subject to attack when in corrosive environments. It has been demonstrated that the proposed method detects induction motor faults and the status of the induction motor can be estimated with a reasonable degree of accuracy.

**Objective 7:**

Apply a method of determining the operating PF of the IM using only the measured current and the manufacturer's data available from the nameplate and/or datasheet to detect, diagnose and assess the relative fault severity of the seeded faults

**Achievement 7:**

An innovative, non-intrusive, accurate and reliable method for the early detection and diagnosis of faults in an induction motor (IM) using an enhanced power parameter measurement technique was presented in chapter eight. It is argued, and initial results suggest that it is more effective to monitor the operating power factor (PF) of the IM which provides better protection under-load. Traditionally, to estimate the PF would require both voltage and the current measurements in order to apply the displacement power factor method. The novelty method determines the operating PF of the IM using only measured current and supplied manufacturer's data. Experimental results confirm that the PF can be used successfully for IM fault diagnosis and is promising also for assessing fault severity. The suggested method

offers an inexpensive, reliable and non-intrusive and CM tool which can be used with real-time systems.

## 9.3 Conclusions

### 9.3.1 Basic techniques

Most fault diagnostic techniques are intended to identify early faults in three phase induction motor. This study presents one phase current and vibration based fault detection and diagnosis techniques for an induction motor using statistical parameters. Both modelling of the induction motor and implementation of a practical vibration measurement system were employed. Advanced signal processing methods were used to extract features from the experimental data collected.

Statistical parameters may be used on their own for fault detection; however, their sensitivity has been shown to be poor for small fault conditions. They did not change or create a trend that would indicate failure in the early stages of faults. A rising trend was observed though in severe faults with larger fault (Chapter 5).

The statistical parameters were unable to provide any reliable diagnostic information when the failure modes were a cracked tooth and local wear. This suggests that they are not very sensitive to these types of faults (Chapter 5).

Comparatively, the spectrum can be used in fault detections more reliably than time statistical parameters with respect to fault sensitivity. However, it too was also unable to indicate fault symptoms sufficiently early (Chapter 5).

### 9.3.2 Joint time-frequency techniques

In terms of sensitivity and early fault revelation, all time-frequency methods were more reliable and descriptive to indicate the fault symptoms. Due to the joint ability of illustrating both time and frequency information together with time-frequency

localisation capability, there was enhancement of the sensitivity of these techniques to the early detection of faults. For instance, all two different faults were detected by the time-frequency methods in earlier stages than with conventional techniques (Chapter 6). The short- time Fourier transform (STFT), Wigner Ville distribution (WVD) and wavelet transform (WT) and were applied to the measurement data.

The limitation of these techniques can be summarized as:

1. With the STFT the smaller the window the less information it contains, there comes a limit below which the information is so diminished the STFT becomes ineffective.
2. The WVD is nonlinear because the time-shifted analytical signal is multiplied by its complex conjugate. The consequent uncertainties can make interpretation of WVD results difficult.

Amongst the time-frequency methods, the discrete wavelet transform was not only computationally less time consuming, but it was also more capable of revealing fault symptoms at an earlier stage than the STFT and the WVD

### 9.3.3 Validation of the proposed processing techniques

Vibration measurement is widely used for diagnosing the condition of rotating machinery; but sometimes direct measurement can be difficult and expensive in remote or locations that are challenging to access, in harsh environments and where it is expensive to install sensors close to the machine Therefore, selected alternative approaches were investigated by the author to obtain a method to reconstruction vibration waveform from easy parameter measurement as phase current.

The relationship between driver's current signature (DCS) and its vibration signature (DVS) is found by calculating the magnitude of the square of the coherence and

phase coherence parameters in a certain frequency band using a continuous wavelet transform (CWT). Using a non-parametric approach to performing reconstruction signal based on the true data obtained. The ability to predict without relaying on assumptions such as those on system physics properties avoids the potentially large errors brought about by making incorrect assumptions about those properties,

The radial base function was used to reconstruction vibration waveform from current measure. This method is of high precision and good repeatability. This is a non-invasive technique which can open new possibilities for performing necessary diagnostics and making checks on induction motors without laborious and expensive investigations that are truly rigorous only in laboratory conditions. The method has been tested by statistical analysis and shows a good agreement

Based on the above observations and findings, it is concluded that the proposed method detects induction motor faults and the status of the induction motor can be estimated with a reasonable degree of accuracy.

### 9.4 Future work

The results presented in this work have shown the effectiveness of various techniques in study of an induction motor. The author thinks further investigations should be performed in the different fields of motor diagnostics. Future work can be carried out in two aspects of induction motor condition monitoring. One is improving and exploiting further in the fields of diagnostic methods which include both the signal and model based techniques. The other one is to perform more tests and experiments in motors. Suggestions for future research directions are summarised below:

### 9.4.1 Investigation in Experimental Aspects*:*

a. Use a different size of motors.

b. Simulate and seed other types of common failure modes; e.g. bearing, stator fault, air gap eccentricity. In this work, each fault was simulated individually (one fault at a time) .Future work can explore simultaneous faults and faults combining e.g. phase imbalance and broken rotor bar together.

### 9.4.2 Diagnostic Techniques related

c. In most advanced diagnostic techniques, time averaged signals are usually used instead of raw signals. Although the time averaging technique is well established and straightforward, the quality of results from advance diagnostic techniques depends upon the accuracy of the time averaged signals. There is a need for more study in this field.

d. In using a wavelet transform, different wavelets have different impacts in revealing fault features. It would be more complementary if some criteria could be established with regard to which types of wavelets are more suitable for certain types of non-stationary events. One type wavelet have been studied in this work. Therefore, enhancement of fault features in wavelet analysis should be investigated by using different wavelets.

e. Apply empirical mode decomposition based techniques for different types of induction motor faults.

f. Investigate the effectiveness of a smoothed pseudo Wigner-Ville distribution based technique for other condition monitoring applications. .

g. The analysis carried out in this research was based upon visual observation. Further work should concentrate on automatic recognition and identification of faults, such as neural network and data clustering techniques.

h. In this work, the detection of a fault has been reported. Other fault related issues, such as quantification of the severity of the fault, estimation of the remaining life also has a practical importance in an induction motor applications. Therefore, future research should focus on this aspect of motor studies.

### 9.4.3 Reconstruction signal method related

i. In this work motor vibration waveform reconstruction has exemplified the ability of a RBF to typify a complicated nonlinear system in a succinct manner. Using an other types of neural network should be investigated

j. Develop other type signal-based condition monitoring and fault diagnosis method for induction motor. The mathematical relationships between the current and the voltage harmonics have to be studied. Both these harmonics are complementary, in the sense that, in voltage source drives, the current harmonics dominate and in current source drives, voltage harmonics may dominate. Hence, diagnostic schemes that utilise the fault information in both the current and voltage may provide a more reliable indication of motor fault and should be investigated further.

### 9.4.5 Power factor Diagnostic Technique related

k. In this work, the detection of two faults namely phase imbalance and rotor bar broken; by PF method has been reported. Other faults to be seeded to investigated their effect on power factor.

**References**


1. P.Girdhar, C.S.a. ed. ( 2004). Practical machinery vibration analysis and predictive maintenance. UK

2. A.Davies ed. (1998) Handbook of condition monitoring techniques and methodology. UK. Chapman&Hall.

3. Barron. ed. (1996) Engineering condition monitoring practice;methods and application. USA: Addison Wesley Longman Inc.

4. Albarbar, A., Pietruszkiewicz, R., and Starr., a.A. ( 2007) Towards the implementation of integrated multi-measurand wireless monitoring system. In: 2nd World Congress on Engineering Asset Management (WCEAM) Harrogate.

5. Naim., B. The vibro-acoustic monitoring of gearboxes. PhD thesis , The University of Manchester.

6. Payne, B.S., Liang, B, and Ball, A D (1999) Modern Condition Monitoring Techniques for Electric Machines. In: Integration of Dynamics, Monitoring and Control (DYMAC), pp. 325-330.

7. Thomson, W.T., and Fenger, M. (2001) Current signature analysis to detect induction motor faults. Industry Applications Magazine, IEEE 7, 26-34.

8. Rao, B.K.N. ed. (1996) Handbook of condition monitoring

9. Yung, C., and Bonnett, A.H. (2004) Repair or replace? Industry Applications Magazine, IEEE 10, 48-58.

10. Payne, B.S. (2003) Condition monitoring of electric motors for improved asset management. PhD thesis , The University of Manchester

11. Jacob, P.J. (1998) Non-parametric Models and Statistical Techniques in Composite Materials Testing and Condition Monitoring. PhD thesis , The University of Manchester

12. Filippetti, F., Franceschini, G., and Tassoni, C. (1993) Neural networks aided on-line diagnostics of induction motor rotor faults. In: Industry Applications Society Annual Meeting, 1993., Conference Record of the 1993 IEEE, pp. 316-323 vol.311.

13. Paya, B.A., Esat, I.I., and Badi, M.N.M. (1997) Artificial neural network based fault diagnostics of rotating machinery using wavelet transforms as a preprocessor. Mechanical Systems and Signal Processing 11, 751-765.

14. Nandi, S., Toliyat, H.A., and Xiaodong, L. (2005) Condition monitoring and fault diagnosis of electrical motors-a review. Energy Conversion, IEEE Transactions on 20, 719-729.

15. Nandi, S., and Toliyat, H.A. (1999) Condition monitoring and fault diagnosis of electrical machines-a review. In: Industry Applications Conference, 1999. Thirty-Fourth IAS Annual Meeting. Conference Record of the 1999 IEEE, pp. 197-204 vol.191.

16. Bonnett, A.H., and Yung, C. (2008) Increased Efficiency Versus Increased Reliability. Industry Applications Magazine, IEEE 14, 29-36.

17. Toliyat, H.A., Arefeen, M.S., and Parlos, A.G. (1996) A method for dynamic simulation of air-gap eccentricity in induction machines. Industry Applications, IEEE Transactions on 32, 910-918.

18. Henao, H., Martis, C., and Capolino, G.A. (2004) An equivalent internal circuit of the induction machine for advanced spectral analysis. Industry Applications, IEEE Transactions on 40, 726-734.

19. Negrea, M., Jover, P., and Arkkio, A. (2005) Electromagnetic flux-based condition monitoring for electrical machines. In: Diagnostics for Electric Machines, Power Electronics and Drives, 2005. SDEMPED 2005. 5th IEEE International Symposium on, pp. 1-6.

20. Legowski, S.F., Sadrul Ula, A.H.M., and Trzynadlowski, A.M. (1996) Instantaneous power as a medium for the signature analysis of induction motors. Industry Applications, IEEE Transactions on 32, 904-909.

21. Ellison, A.J., and Yang, S.J. (1971) Effects of rotor eccentricity on acoustic noise from induction machines. Electrical Engineers, Proceedings of the Institution of 118, 174-184.

22. Thomson, W.T., and Fenger, M. (2000) Industrial application of current signature analysis to diagnose faults in 3-phase squirrel cage induction motors. In: Pulp and Paper Industry Technical Conference, 2000. Conference Record of 2000 Annual, pp. 205-211.

23. Cameron, J.R., Thomson, W.T., and Dow, A.B. (1986) Vibration and current monitoring for detecting airgap eccentricity in large induction motors. Electric Power Applications, IEEE Proceedings B 133, 155-163.

24. Hsu, J.S. (1995) Monitoring of defects in induction motors through air-gap torque observation. Industry Applications, IEEE Transactions on 31, 1016-1021.

25. Hsu, J.S., Woodson, H.H., and Weldon, W.F. (1992) Possible errors in measurement of air-gap torque pulsations of induction motors. Energy Conversion, IEEE Transactions on 7, 202-208.

26. Xianghui, H., Habetler, T.G., Harley, R.G., and Wiedenbrug, E. (2005) The effect of induction motor rotor eccentricity on surge test data. In: Electric Machines and Drives, 2005 IEEE International Conference on, pp. 1878-1880.

27. Trutt, F.C., Sottile, J., and Kohler, J.L. (2002) Condition monitoring of induction motor stator windings using electrically excited vibrations. In: Industry Applications Conference, 2002. 37th IAS Annual Meeting. Conference Record of the, pp. 2301-2305 vol.2304.

28. Dorrell, D.G., and Smith, A.C. (1996) Calculation and measurement of unbalanced magnetic pull in cage induction motors with eccentric rotors. II. Experimental investigation. Electric Power Applications, IEEE Proceedings - 143, 202-210.

29. Finley, W.R., Hodowanec, M.M., and Holter, W.G. (2000) An analytical approach to solving motor vibration problems. Industry Applications, IEEE Transactions on 36, 1467-1480.

30. Trutt, F.C., Sottile, J., and Kohler, J.L. (2001) Detection of AC machine winding deterioration using electrically excited vibrations. Industry Applications, IEEE Transactions on 37, 10-14.

31. Muller, G.H., and Landy, C.F. (2003) A novel method to detect broken rotor bars in squirrel cage induction motors when interbar currents are present. Energy Conversion, IEEE Transactions on 18, 71-79.

32. Villada, F., Cadavid, D., Munoz, N., Valencia, D., and Parra, D. (2003) Fault diagnosis in induction motors fed by PWM inverters. In: Diagnostics for Electric Machines, Power Electronics and Drives, 2003. SDEMPED 2003. 4th IEEE International Symposium on, pp. 229-234.

33. Vandevelde, L., and Melkebeek, J.A.A. (2001) Numerical analysis of vibrations of squirrel-cage induction motors based on magnetic equivalent circuits and structural finite element models. In: Industry Applications Conference, 2001. Thirty-Sixth IAS Annual Meeting. Conference Record of the 2001 IEEE, pp. 2288-2295 vol.2284.

34. Ishibashi, F., Kamimoto, K., Noda, S., and Itomi, K. (2003) Small induction motor noise calculation. Energy Conversion, IEEE Transactions on 18, 357-361.

35. Jang, G.H., and Park, S.J. (2003) Simulation of the electromechanical faults in a single-phase squirrel cage induction motor. Magnetics, IEEE Transactions on 39, 2618-2620.

36. Mori, D., and Ishikawa, T. (2005) Force and vibration analysis of induction motors. Magnetics, IEEE Transactions on 41, 1948-1951.

37. Schoen, R.R., Habetler, T.G., Kamran, F., and Bartheld, R.G. (1994) Motor bearing damage detection using stator current monitoring. In: Industry Applications Society Annual Meeting, 1994., Conference Record of the 1994 IEEE, pp. 110-116 vol.111.

38. Schoen, R.R., and Habetler, T.G. (1993) Effects of time-varying loads on rotor fault detection in induction machines. In: Industry Applications Society Annual Meeting, 1993., Conference Record of the 1993 IEEE, pp. 324-330 vol.321.

39. El Hachemi Benbouzid, M. (2000) A review of induction motors signature analysis as a medium for faults detection. Industrial Electronics, IEEE Transactions on 47, 984-993.

40. Thomson, W.T. (2001) On-line MCSA to diagnose shorted turns in low voltage stator windings of 3-phase induction motors prior to failure. In: Electric Machines and Drives Conference, 2001. IEMDC 2001. IEEE International, pp. 891-898.

41. Benbouzid, M.E.H., and Kliman, G.B. (2002) What Stator Current Processing Based Technique to Use for Induction Motor Rotor Faults Diagnosis. Power Engineering Review, IEEE 22, 62-62.

42. Dimitrov, L.V., and Chobanov, V.J. (2004) Diagnosis of rotor faults of induction motors, operated in non-rated conditions. In: Electronics Technology:

Meeting the Challenges of Electronics Technology Progress, 2004. 27th International Spring Seminar on, pp. 110-113 vol.111.

43. Frosini, L., and Bassi, E. (2010) Stator Current and Motor Efficiency as Indicators for Different Types of Bearing Faults in Induction Motors. Industrial Electronics, IEEE Transactions on 57, 244-251.

44. Faiz, J., Ebrahimi, B.M., Akin, B., and Toliyat, H.A. (2010) Dynamic analysis of mixed eccentricity signatures at various operating points and scrutiny of related indices for induction motors. Electric Power Applications, IET 4, 1-16.

45. Yi-Ching, S., Kuo-Lung, L., and Hsueh-Hsien, C. Feature Selection of Non-intrusive Load Monitoring System Using STFT and Wavelet Transform. In: e-Business Engineering (ICEBE), 2011 IEEE 8th International Conference on, pp. 293-298.

46. Eren, L., and Devaney, M.J. (2004) Bearing damage detection via wavelet packet decomposition of the stator current. Instrumentation and Measurement, IEEE Transactions on 53, 431-436.

47. Antonino-Daviu, J.A., Riera-Guasp, M., Folch, J.R., and Palomares, M.P.M. (2006) Validation of a new method for the diagnosis of rotor bar failures via wavelet transform in industrial induction machines. Industry Applications, IEEE Transactions on 42, 990-996.

48. Patel, R.K., Agrawal, S., and Joshi, N.C. (2012) Induction motor bearing fault identification using vibration measurement. In: Engineering and Systems (SCES), 2012 Students Conference on, pp. 1-5.

49. Obaid, R.R., Habetler, T.G., and Stack, J.R. (2003) Stator current analysis for bearing damage detection in induction motors. In: Diagnostics for Electric Machines,

Power Electronics and Drives, 2003. SDEMPED 2003. 4th IEEE International Symposium on, pp. 182-187.

50. Gritli, Y., Rossi, C., Zarri, L., Filippetti, F., Chatti, A., Casadei, D., and Stefani, A. Advanced diagnosis of broken bar fault in induction machines by using Discrete Wavelet Transform under time-varying condition. In: Electric Machines & Drives Conference (IEMDC), 2011 IEEE International, pp. 424-429.

51. Cusido, J., Romeral, L., Ortega, J.A., Rosero, J.A., and Garcia Espinosa, A. (2008) Fault Detection in Induction Machines Using Power Spectral Density in Wavelet Decomposition. Industrial Electronics, IEEE Transactions on 55, 633-643.

52. Filippetti, F., Franceschini, G., Tassoni, C., and Vas, P. (2000) Recent developments of induction motor drives fault diagnosis using. Industrial Electronics, IEEE Transactions on 47, 994-1004.

53. Awadallah, M.A., and Morcos, M.M. (2003) Application of AI tools in fault diagnosis of electrical machines and drives-an overview. Energy Conversion, IEEE Transactions on 18, 245-251.

54. Chow, M.Y., Sharpe, R.N., and Hung, J.C. (1993) On the application and design of artificial neural networks for motor fault detection. II. Industrial Electronics, IEEE Transactions on 40, 189-196.

55. Merwe, N., and Hoffman, A. (2002) The application of neural networks to vibration diagnostics for multiple fault conditions. Elsevier: Computer Standards Interfaces, 24, 139-149.

56. Penman, J., and Yin, C.M. (1994) Feasibility of using unsupervised learning, artificial neural networks for the condition monitoring of electrical machines. Electric Power Applications, IEEE Proceedings - 141, 317-322.

57. Du, T., and Wolfe, P. (1997) Implementation of fuzzy logic systems and neural networks in industry. Elsevier: Computers in Industry 32, 261-272.

58. Martins, J.F., Pires, V.F., and Pires, A.J. (2007) Unsupervised Neural-Network-Based Algorithm for an On-Line Diagnosis of Three-Phase Induction Motor Stator Fault. Industrial Electronics, IEEE Transactions on 54, 259-264.

59. Nejjari, H., and Benbouzid, M.E.H. (2000) Monitoring and diagnosis of induction motors electrical faults using a current Park's vector pattern learning approach. Industry Applications, IEEE Transactions on 36, 730-735.

60. Abiyev, R.H., and Kaynak, O. (2008) Fuzzy Wavelet Neural Networks for Identification and Control of Dynamic Plants 2014; A Novel Structure and a Comparative Study. Industrial Electronics, IEEE Transactions on 55, 3133-3140.

61. Bouzid, M., Champenois, G., Bellaaj, N.M., Signac, L., and Jelassi, K. (2008) An Effective Neural Approach for the Automatic Location of Stator Interturn Faults in Induction Motor. Industrial Electronics, IEEE Transactions on 55, 4277-4289.

62. Hua, S., and Kil To, C. (2007) Induction Machine Condition Monitoring Using Neural Network Modeling. Industrial Electronics, IEEE Transactions on 54, 241-249.

63. Li, B., Chow, M.Y., Tipsuwan, Y., and Hung, J.C. (2000) Neural-network-based motor rolling bearing fault diagnosis. Industrial Electronics, IEEE Transactions on 47, 1060-1069.

64. Jack, L.B., and Nandi, A.K. (2000) Genetic algorithms for feature selection in machine condition monitoring with vibration signals. Vision, Image and Signal Processing, IEEE Proceedings - 147, 205-212.

65. Wu, S., and Chow, T.W.S. (2004) Induction machine fault detection using SOM-based RBF neural networks. Industrial Electronics, IEEE Transactions on 51, 183-194.

66. Kaminski, M., Kowalski, C.T., and Orlowska-Kowalska, T. Application of radial basis neural networks for the rotor fault detection of the induction motor. In: EUROCON - International Conference on Computer as a Tool (EUROCON), 2011 IEEE, pp. 1-4.

67. Matic, x, D., Kulic, F., Climente, A., n, V., and Puche-Panadero, R. Artificial neural networks broken rotor bars induction motor fault detection. In: Neural Network Applications in Electrical Engineering (NEUREL), 2010 10th Symposium on, pp. 49-53.

68. Bouzid, M., Champenois, G., Bellaaj, N., and Jelassi, K. Automatic and robust diagnosis of broken rotor bars fault in induction motor. In: Electrical Machines (ICEM), 2010 XIX International Conference on, pp. 1-7.

69. Santos, S.P., and Costa, J.A.F. (2008) Application of multiple decision trees for condition monitoring in induction motors. In: Neural Networks, 2008. IJCNN 2008. (IEEE World Congress on Computational Intelligence). IEEE International Joint Conference on, pp. 3736-3741.

70. Dash, R.N., Subudhi, B., and Das, S. A comparison between MLP NN and RBF NN techniques for the detection of stator inter-turn fault of an induction motor. In: Industrial Electronics, Control & Robotics (IECR), 2010 International Conference on, pp. 251-256.

71. Xianjiang, S., Junpeng, S., Junshan, S., and Baonian, L. (2008) Experiment and simulation of rotor's torsional vibration based on sensorless detection

technology. In: Automation and Logistics, 2008. ICAL 2008. IEEE International Conference on, pp. 2673-2678.

72. Riley, C.M., Lin, B.K., Habetler, T.G., and Kliman, G.B. (1997) Stator current-based sensorless vibration monitoring of induction motors. In: Applied Power Electronics Conference and Exposition, 1997. APEC '97 Conference Proceedings 1997., Twelfth Annual, pp. 142-147 vol.141.

73. Riley, C.M., Lin, B.K., Habetler, T.G., and Schoen, R.R. (1998) A method for sensorless on-line vibration monitoring of induction machines. Industry Applications, IEEE Transactions on 34, 1240-1245.

74. Ong, C.-M. ed. (1998) Dynamic Simulation of Electrical Machinery Using Matlab / Simulink. New Jersey.: Prentice Hall PTR.

75. Rgeai, M.N. (2007) Helical gearbox fault detection using motor current signature analysis. PhD thesis , The University of Manchester.

76. Pierrat, L., and Morrison, R.E. (1995) Probabilistic modeling of voltage asymmetry. Power Delivery, IEEE Transactions on 10, 1614-1620.

77. Bonnett, A.H., and Soukup, G.C. (1992) Cause and analysis of stator and rotor failures in three-phase squirrel-cage induction motors. Industry Applications, IEEE Transactions on 28, 921-937.

78. Liang, B., Payne, B.S., Ball, A.D., and Iwnicki, S.D. (2002) Simulation and fault detection of three-phase induction motors. Mathematics and Computers in Simulation 61, 1-15.

79. J. Dally, W.R.a.K.M. ed. (1984) Instrumentation for engineering measurements. USA: John Wiley &Sons,Inc.

80.http://literature.rockwellautomation.com/idc/groups/literature/documents/at/enacc-at984_-en-e.pdf

81. Measurements Manual Report

http://www.engr.sjsu.edu/bjfurman/courses/ME120/me120pdf/DAQslides.pdf

82. Schmidc, H. ( May 13, 2009) How to use the FFT for signal and noise simulations and measurements. [IME Report].

83. Belsak A. and Flasker J. (2006) Method for detecting fatigue crack in gears. Theoretical and Applied Fracture Mechanics 46, 105–113.

84. Nagarajaiah S, Varadarajan N. (2005) Short time Fourier transform algorithm for wind response control of buildings with variable stiffness. TMD. Engineering Structures, 27, 431-441.

85. Gianluca D'Elia "Fault detection in rotating machines by vibration signal processing techniques". PhD Thesis. University of Bologna

http://diem1.ing.unibo.it/dottorato/meccanica/elia.pdf, Accessed July 2011.

86. Chen Dapang, and Qian Shine. (1996). Joint time-frequency analysis: methods and applications. Prentice Hall Inc.

87. Jian-Da Wa and Jien Chen., J.W.A.J. (2006) Continuous wavelet transform technique for fault signal diagnosis of internal combustion engines. NDT&E International, 39, 304–311.

88. Chui, C. ed. (1992) Wavelet analysis and its applications. Academic Press.

89. Rioul, O., and Duhamel, P. (1992) Fast algorithms for discrete and continuous wavelet transforms. Information Theory, IEEE Transactions on 38, 569-586.

90. Rioul, O., and Vetterli, M. (1991) Wavelets and signal processing. Signal Processing Magazine, IEEE 8, 14-38.

91. Dash, R.N. (2010) Fault Diagnosis in Induction Motor Using Soft Computing Techniques. Mater thesis. National Institute Of Technology India.

92. Şeker, S., Ayaz, E., and Türkcan, E. (2003) Elman's recurrent neural network applications to condition monitoring in nuclear power plant and rotating machinery, Engineering Applications of Artificial Intelligence. 16, 647-656.

93. Zhai, Y.J., and Yu, D. L (2008) Radial-basis-function-based feedforwar-feedback control for air-fuel ratio of spark ignition engines. Automobile Engineering 222, 415-428.

94. Devanneaux, V; Dagues, B.; Faucher, J. . (2001) An accurate model of squirrel cage induction machines under static, dynamic or mixed eccentricity,. Proc. IEEE SDEM-PED'01, 121-126.

95. I. Hirotsuka, K., and Ueda F. (2006) New Calculation Method and Characteristics for the Induction Motor under Unbalanced Voltage Condition. Institute of Electrical Installation Engineers of Japan **26**, 215-219.

96. Liu Xianggen; Zhang, Z.; Chen, D (Sept. 2004. :) Online rotor mixed fault diagnosis way based on spectrum analysis of instantaneous power in squirrel cage induction motors. IEEE Trans. on Energy Conversion, 485-490.

97. Drif, M.C., Marqnes A. (March 2008) Air-gap eccentricity fault diagnosis, in three-phase induction motors, by the complex apparent power signature analysis,. IEEE Trans. on Ind. Elec. **55**, 1404-1410.

98. Kral Pirker; Pascoli G. (1999) Rotor eccentricity detection of induction machines by means of torque estimation-measurement results, IEEE SDEMPED'99, 283-287.

99. Lie Xu, Wang Yi. (2007) Dynamic modelling and control of DFIG-Based wind turbines under unbalanced network conditions. IEEE trans. on Power Systems, 314 - 323.

100. Ted K. A. Brekken, Ned Mohan. (2007) Control of a doubly fed Induction wind generator under unbalanced grid voltage conditions. IEEE trans. on Energy Conversion, 129 - 135.

101. Abhisek Ukil, Richard Bloch, and Andrea Andenna. (2011) Estimation of Induction Motor Operating Power Factor From Measured Current and Manufacturer Data. IEEE transactions on energy conversion.